Kinetic and mechanistic studies of reactive intermediates in photochemical and transition metal-assisted oxidation, decarboxylation and alkyl transfer reactions

by

Jack McCaslin Carraher

A dissertation submitted to the graduate faculty

in partial fulfillment of the requirements for the degree of

DOCTOR OF PHILOSOPHY

Major: Inorganic Chemistry
Specialization: Industrial Chemistry

Program of Study Committee:
Andreja Bakac, Co-Major Professor
Aaron Sadow, Co-Major Professor
William Jenks
Javier Vela
Keith Woo

Iowa State University

Ames, Iowa

2014

DEDICATION

To my wife Sarah (Lovebug);

It's been a long hard road, and we made it through all our ups and downs together. Today we write an end to this chapter, and begin looking forward to the steps that await us.

TABLE OF CONTENTS

ABSTRACT

Reactive species like high-valent metal-oxo complexes and carbon and oxygen centered radicals are important intermediates in enzymatic systems, atmospheric chemistry, and industrial processes. Understanding the pathways by which these intermediates form, their relative reactivity, and their fate after reactions is of the utmost importance. Herein are described the mechanistic detail for the generation of several reactive intermediates, synthesis of precursors, characterization of precursors, and methods to direct the chemistry to more desirable outcomes yielding 'greener' sources of commodity chemicals and fuels.

High-valent Chromium from Hydroperoxido-Chromium(III)

The decomposition of pentaaquahydroperoxido chromium(III) ion (hereafter $Cr_{aq}OOH^{2+}$) in acidic aqueous solutions is kinetically complex and generates mixtures of products (Cr_{aq}^{3+}, $HCrO_4^-$, H_2O_2, and O_2). The yield of high-valent chromium products (known carcinogens) increased from a few percent at pH 1 to 70 % at pH 5.5 (near biological pH). Yields of H_2O_2 increased with acid concentration. The reproducibility of the kinetic data was poor, but became simplified in the presence of H_2O_2 or 2,2′-azinobis(3-ethylbenzothiazoline-6-sulfonate) dianion ($ABTS^{2-}$). Both are capable of scavenging strongly oxidizing intermediates). The observed rate constants (pH 1, $[O_2] \leq 0.03$ mM) in the presence of these scavengers are independent of [scavenger] and within the error are the same ($k_{ABTS2-} = (4.9 \pm 0.2) \times 10^{-4}$ s^{-1} and $k_{H2O2} = (5.3 \pm 0.7) \times 10^{-4}$ s^{-1}); indicating involvement of the scavengers in post-rate determining steps. In the presence

of either scavenger, decomposition of $CrOOH^{2+}$ obeyed a two-term rate law, k_{obs} / s^{-1} = $(6.7 \pm 0.7) \times 10^{-4} + (7.6 \pm 1.1) \times 10^{-4}$ $[H^+]$. Effect of $[H^+]$ on the kinetics and the product distribution, cleaner kinetics in the presence of scavengers, and independence of k_{obs} on [scavenger] suggest a dual-pathway mechanism for the decay of $Cr_{aq}OOH^{2+}$. The H^+-catalyzed path leads to the dissociation of H_2O_2 from Cr(III), while in the H^+-independent reaction, $Cr_{aq}OOH^{2+}$ is transformed to Cr(V). Both scavengers rapidly remove Cr(V) and simplify both the kinetics and products by impeding formation of Cr(IV, V, VI).

Syntheses, Reactivity, and Thermodynamic Considerations $LRhR^{2+}$

Macrocyclic rhodium(II) complexes $LRh(H_2O)^{2+}$ (L = L^1= cyclam and L^2 = *meso*-Me_6-cyclam) react with alkyl hydroperoxides $R(CH_3)_2COOH$ to generate the corresponding rhodium(III) alkyls $L(H_2O)RhR^{2+}$ (R = CH_3, C_2H_5, $PhCH_2$). Methyl and benzyl complexes can also be prepared by bimolecular group transfer from alkyl cobaloximes $(dmgX)_2(H_2O)CoR$ (where R = CH_3, CH_2Ph and dmgX is either dimethylglyoxime or a BF_2-capped derivative of dmg) to $LRh(H_2O)^{2+}$. When R = C_2H_5, C_3H_7 or C_4H_9, the mechanism changes from group transfer to hydrogen atom abstraction from the coordinated alkyl and produces $L(H_2O)RhH^{2+}$ and an α-olefin. The new $LRhR^{2+}$ complexes were characterized by solution NMR and by crystal structure analysis. They exhibit great stability in aqueous solution at room temperature, but undergo efficient Rh-C bond cleavage upon photolysis.

'Green' Model for Decarboxylation of Biomass Derived Acids via Photolysis of in situ formed Metal-Carboxylate Complexes

Photolysis of aqueous solutions containing propionic acid and Fe^{3+}_{aq} in the absence of oxygen generates a mixture of hydrocarbons (ethane, ethylene and butane), carbon

dioxide, and Fe^{2+}. Photolysis in the presence of O_2 yields catalytic amounts of hydrocarbon products. When halide ions are present during photolysis; nearly quantitative yields of ethyl halides are produced *via* extraction of a halide atom from FeX^{2+} by ethyl radical. The rate constants for ethyl radical reactions with $FeCl^{2+}$ ($k = 4.0 (\pm 0.5) \times 10^6\ M^{-1}s^{-1}$) and with $FeBr^{2+}$ ($k = 3.0 (\pm 0.5) \times 10^7\ M^{-1}s^{-1}$) were determined *via* competition reactions. Irradiation of solutions containing aqueous Cu^{2+} salts and linear carboxylic acids yield α-olefins selectively. This process is made catalytic by the introduction of O_2. Photochemical decarboxylation of propionic acid in the presence of Cu^{2+} generates ethylene and Cu^{+}. Longer-chain acids also yield alpha olefins as exclusive products. In the absence of continued purging with O_2 to aid removal of olefin, Cu^{+}(olefin) complexes accumulate and catalytic activity slows dramatically due to depletion of Cu^{2+}. The results underscore the profound effect that the choice of metal ions, the medium, and reaction conditions exert on the photochemistry of carboxylic acids.

Free Oxygen Atom in Solution from 4-Benzoylpyridine N-Oxide Excited Singlet

Photolysis of 4-benzoylpyridine N-oxide (BPyO) in the presence of quenchers of the triplet excited state produces up to 41% $O(^3P)$ (as determined by generation of ethylene upon scavenging with cyclopentene). In the absence of ^{3}BPyO* quenchers a maximum of 13% $O(^3P)$ relative to consumed BPyO is obtained. The remaining products are hydroxylated-4-benzoylpyridine and 4-benzoylpyridine. Additionally, the rate of BPyO consumption (as determined by UV-vis) decreases in the presence of ^{3}BPyO* quenching agents. Second order rate constants for ^{3}BPyO* quenching were determined. A mechanism for photochemical deoxygenation of BPyO is proposed on the basis of

kinetic data and product distribution under various conditions. Additionally, comparisons are made between the observed intermediates and similar triplet excited states and radical anions.

GENERAL INTRODUCTION

Reactive Intermediates in Industry and Biology

Several industrially and biologically relevant processes involve oxidations with molecule oxygen or hydrogen peroxide and transition metal complexes. For instance industrial scale production of propylene oxide utilizes a Mo, V, or Ti catalyst and O_2.[1] Molecular oxygen is utilized to regenerate catalytically active Cu^{2+} in the production of vinyl chlorides.[1] Biologically, the enzymatic systems cytochrome P450,[2] methane monooxygenase,[3] bleomycin,[4] and vanadium haloperoxidases[5] utilize transition metal centers and O_2 or H_2O_2. During these conversions peroxo-metal, hydroperoxo-metal, metal-oxo complexes, and oxygen and/or organic radicals are proposed reactive intermediates. Small inorganic and organometallic molecules have reactivity similar to their enzymatic counterparts,[6-13] and study of their chemistry offers insight into the mechanistic details in enzyme chemistry. For instance, insight into the chemistry of some high-valent metalloenzymes was gained in studies of N_4 macrocyclic rhodium complexes with O_2 and NO.[14,15] Superoxo-chromium(III) ($CrOO^{2+}$), hydroperoxido-chromium(III) ($CrOOH^{2+}$), chromium(IV)oxo (CrO^{2+}), and chromium(V)oxo species are known to participate in redox reactions, hydrogen atom and hydride transfer, and oxygen atom transfer reactions, all of which have been observed in enzymatic systems.[12]

High-Valent Chromium in Biological Systems

Understanding the chemistry of such small inorganic molecules is beneficial for understanding active sites of enzymes. Other metal complexes are present in biological systems as dissolved inorganic salts. Low concentrations of Cr(III) are thought to be

necessary for glucose and lipid metabolism in mammals.[16,17] Ingestion or inhalation of Cr(VI), on the other hand, has been linked to growth of cancer cells.[18] Cr(IV) and Cr(V) (products of intracellular reduction of Cr(VI)) have been identified as the species responsible for the majority of the biological damage resulting from exposure to Cr(VI). These species have been found to oxidize DNA bases and sugars, inhibit enzyme activity through formation of Cr-DNA adducts, crosslink DNA and proteins, and cause DNA strand scission.[19] Chromium(III) compounds are generally thought to be safe, and 1000 mg tablets of chromium(III) picolinate are available over-the-counter at pharmacies.

The inherent safety of Cr(III) compounds is thought to be due to their inertness. However, redox reactions involving Cr(III) have been observed under biologically relevant conditions.[17,20,21] Additionally, our own work has shown that aqueous Cr(III) can be made substitutionally labile by coordinated nitrate, sulfate, and acetate. $CrOOH^{2+}$ was generated directly from H_2O_2 and Cr_{aq}^{3+} as a result of this rapid ligand exchange.[22] Other studies indicate formation of Cr(VI) *via* decomposition of $CrOOH^{2+}$.[10,23] It is therefore plausible that Cr(III), while being widely considered as safe, is a carcinogenic Trojan horse. An in-depth mechanistic study of $CrOOH^{2+}$ decomposition was therefore warranted because of the widespread use of Cr(III) compounds as dietary supplements.

Radical Reactivity

Radicals are another class of reactive intermediate that have been linked to adverse health effects (*e.g.*, cardiovascular diseases, stroke, and atherosclerosis).[24] Radicals are common in transition metal reactions with oxygen, and they are proposed intermediates in atmospheric photochemistry,[24] industrial refinement of crude oil (in thermal cracking),[1] and the above mentioned enzymatic processes.[19,24] The unpaired

electron in radical species facilitate reactivity through pathways which would be otherwise inaccessible. Typically, these reactions exhibit large second order rate constants ($\geq 10^7$ M^{-1} s^{-1} in aqueous solutions).[25,26] The large redox potentials (typically greater than 1 volt) associated with radicals makes them excellent candidates for degradation of atmospheric and aqueous pollutants.[24] In addition, radical chemistry can be tuned by the chemical environment; facilitating abstraction of H atoms, initiating radical chain reactions, oxidizing or reducing substrates, transferring groups from M-X (where X = CN, SCN, halides, etc…), adding to metal centers, increasing chain length by dimerization,[25,26] and producing acyl radicals by adding CO.[27] Utilization of radicals in synthetic chemistry can reduce the number of steps (*i.e.*, time and cost) in the synthesis of complex molecules. For instance, radical addition to C≡C bonds results cyclization to products that maintain the stereochemistry of the parent alkyne.[28,29]

Radical Sources

'Clean' sources of radicals are required to study the above mentioned reactions. Methods for thermal generation of radicals include hydrogen atom abstraction,[30,31] thermal homolysis of organometallic complexes,[29,32,33] and Fenton-like chemistry involving reduced metals and hydroperoxides,[27,31,34] Figure 1. Radical generation *via* photochemical methods include direct photolysis of molecules like benzoyl ketones,[35-38] cobaloximes,[39-42] and metal carboxylate complexes.[43-49] Radicals can also be generated by photolysis of a sensitizing agent like benzophenone in the presence of 2-propanol,[38,50] Figure 2.

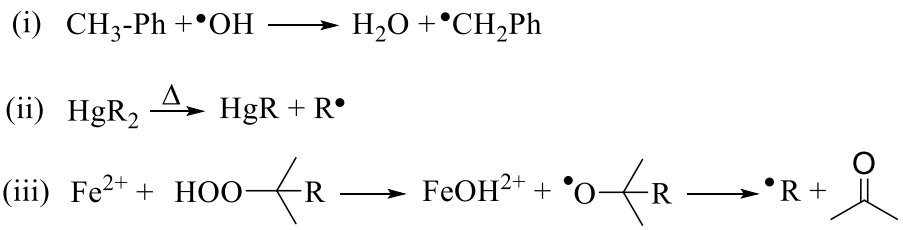

Figure 1. Examples of radical generation from thermochemical sources through H-atom abstraction (i), Thermal homolysis (ii), and Fenton-like chemistry between a reduced metal and a hydroperoxide (iii)

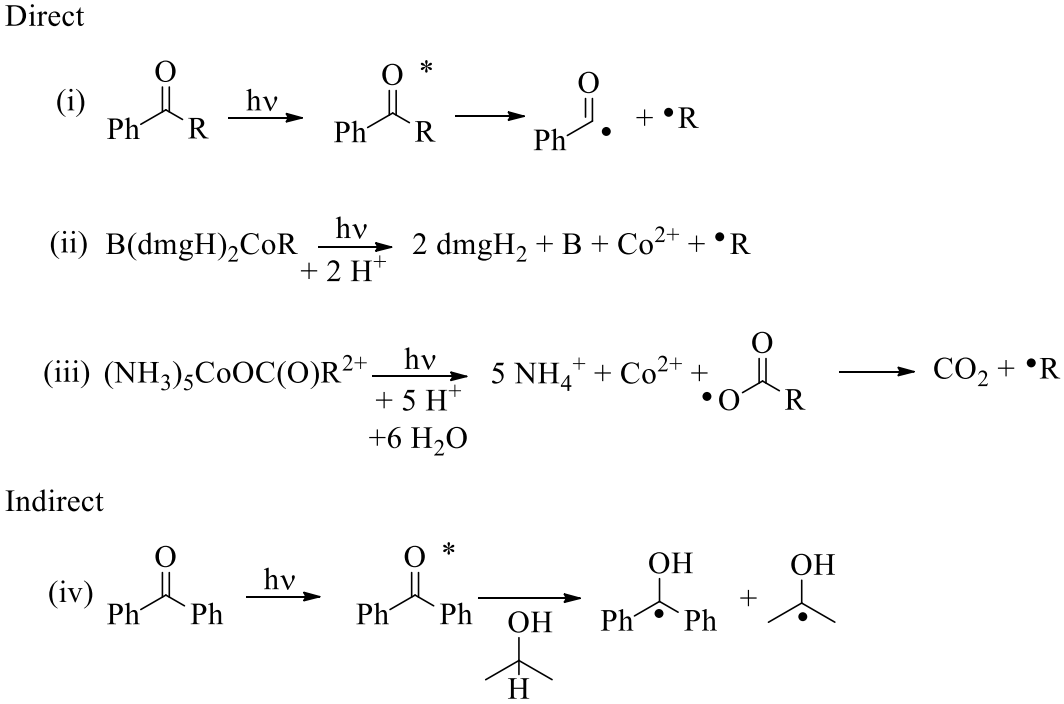

Figure 2. Examples of radical generation from photochemical sources. Excitation of phenyl ketones and intramolecular homolysis of C-C bond (i), homolytic cleavage of Co-C bond upon photolysis of alkyl cobaloximes (ii), homolytic cleave of Co-O bond followed by rearrangement to CO_2 and $^{\bullet}R$ (iii), and indirect photochemical generation of 2-hydroxy-2-propyl radical via hydrogen atom abstraction from 2-propanol by triplet excited benzophenone (iv).

Photochemistry and Synthesis of Metal-Alkyl Complexes

Unfortunately, many photochemical sources of radicals are not free of undesirable side reactions. For instance, alkyl cobaloximes as precursors to photochemical generation of alkyl radicals are complicated by side reactions in which free $dmgH_2$ can participate. Additionally, $dmgH_2$ precipitates from acidic aqueous solutions, complicating spectroscopic studies. Alkyl cobaloximes are also known to decompose *via* thermal homolysis of the Co-C bond at elevated temperatures,[51,52] and undergo group transfer with other metal complexes, eq 1.[53,54] Alkyl cobalt complexes with N_4 macrocycles ($LCoR^{2+}$) are free of any $dmgH_2$ side reactions, and homolytically cleave the Co-C bond upon irradiation with visible light.[55] Unfortunately, $LCoR^{2+}$ complexes with bulkier R groups, like the benzyl[56] or 2-propyl and 2-butyl[57] readily homolyze or are not isolable. Electronic and steric factors are less important in Rh complexes than Co complexes,[58] but rhodoximes are still affected by side reactions of free $dmgH_2$ in solution.[59,60] We therefore set out to synthesize and characterize a novel series of N_4 macrocyclic $LRhR^{2+}$ complexes through radical addition to LRh^{2+}, eq 2, and group transfer from other alkyl metal complexes, eq 3. Group transfer to LRh^{2+} (Rh : M-R = 1 : 1) is theoretically more atom economical than the radical addition method (Rh : HOOR = 2 : 1). However, the group transfer method for $LRhR^{2+}$ synthesis must take into account the relative stability of Rh-hydride and Rh-alkyl complexes,[61,62] and the relative stability of Rh-H and Rh-R complexes. The combination of the relative stability of Rh-H to Rh-R and the known retarding effect that sterics have on the rates of group transfer reactions[63-65] was expected to provide ideal conditions for the observation of a mechanistic switch between alkyl transfer and hydrogen atom abstraction. Therefore, an in-depth investigation (kinetics and

products analysis) was carried out for reactions between LRh^{2+} and coordinatively saturated alkyl metal complexes.

$$B(dmgH)_2CoR + Cr^{2+}_{aq} \rightarrow B(dmgH)_2Co + CrR^{2+} \qquad (B = H_2O \text{ or } Py) \qquad (1)$$

$$LRh^{2+} + {}^{\bullet}R \rightarrow LRhR^{2+} \qquad (2)$$

$$LRh^{2+} + M\text{-}R^{n+} \rightarrow LRhR^{2+} + M^{n+} \qquad (3)$$

Photochemistry of Metal-Carboxylate Complexes

Another photochemical method for generation of radical species is the photolysis of metal-carboxylate complexes. Photolysis of Fe(III)-O_2CR^{n+} is known to cleave the Fe-O bond yielding a carboxyl radical (${}^{\bullet}O_2CR$). Carboxyl radicals readily undergo C-R bond homolysis generating CO_2 and ${}^{\bullet}R$.[44-46,66,67] Transition-metal assisted photochemical decarboxylation offers a route to 'green' production of high performance fuels and functionalization of fatty acids to commodity chemicals, utilizing biomass sources.

Biodiesel (typically a fatty acid methyl ester) is less attractive than petroleum based diesel due to higher viscosity in cold weather, excessive engine wear, and accelerated decomposition in storage; all of which is attributed to higher oxygen content.[68] Many of the current processes for deoxygenation of biofuels utilize gaseous hydrogen at elevated temperature and pressure in the presence of various metal-based catalysts.[69-71] Methods that utilize cheap metal salts (Fe(III) or Cu(II)) as catalysts, sun-light, and do not require heating or potentially explosive gases would enhance the economy and safety of such conversions. Metal-assisted photochemical decarboxylation provides economical and ecological incentives as well. Decarboxylation *via* photolysis of *in situ* generated carboxylato-metal complexes offers an array of products due to the

known tunability of radical chemistry (*i.e.*, allows for multiple products from one feedstock through changes in the environment). Consider the production of long-chain α-olefins from biomass *via* metal-assisted photochemical decarboxylation versus industrial refinement of crude oil. Photolysis of a copper(II) fatty acid carboxylate complex (with direct sunlight) is expected to generate alkyl radicals, eq 4. Alkyl radicals are known to react with Cu^{2+}, eq 5.[72] Cu^{2+} can then be regenerated by introduction of atmospheric O_2, eq 6. Current industrial methods for α-olefin production from crude oil require energy intensive thermal cracking to generate small olefins (ethene, propene, butene), separation, and oligomerization through the Ziegler process (yielding a range of α-olefins from C_6 to larger than C_{20}).[1] Successful exploration of this type of chemistry would prove beneficial to the development of more environmentally friendly processes for mass production of fine chemicals and fuels. An investigation utilizing iron(III) and copper(II) salts was therefore undertaken.

$$\text{Cu-O}_2\text{CCH}_2\text{CH}_2\text{R}^+ \xrightarrow[-Cu^+]{h\nu} {}^\bullet\text{O}_2\text{CCH}_2\text{CH}_2\text{R} \xrightarrow[-CO_2]{} {}^\bullet\text{CH}_2\text{CH}_2\text{R} \qquad (4)$$

$${}^\bullet\text{CH}_2\text{CH}_2\text{R} + \text{Cu}^{2+} \rightarrow \text{CH}_2\text{=CHR} + \text{Cu}^+ + \text{H}^+ \qquad (5)$$

$$4\text{Cu}^+ + \text{O}_2 + 4\text{H}^+ \rightarrow 4\text{Cu}^+ + 2\text{H}_2\text{O} \qquad (6)$$

Generation and Reactivity of Oxygen Atoms in Solution

Photochemical generation of triplet oxygen atoms ($O(^3P)$) has been studied extensively in the gas phase.[73-82] $O(^3P)$ is a diradical that exhibits unique reactivity that other reactive oxygen species do not. For instance, $O(^3P)$ adds to olefins yielding epoxides.[76,81-86] Hydroxyl and superoxide radicals initiate radical chain reactions, and ozone over-oxidizes olefins to aldehydes or ketones and carboxylic acid. Unfortunately,

selective sources of free O(^{3}P) with high yields are relatively unknown in solution. Microwave discharge[84] is reported to generate O(^{1}D), $^1O_2$, and O_3 in addition to O(^{3}P),[83] and the highest yield of O(^{3}P) reported from photolysis of a pyridine N-oxide is ~ 5 %.[87-90] Several photochemical studies utilizing compounds with N-oxide and S-oxide functionality offer no direct evidence for free O(^{3}P) formation. Instead, O(^{3}P) is implied based on the observation of deoxygenated reactant and oxidized solvent.[91,92]

Mechanistically, photochemical deoxygenation of N-oxides and S-oxides is not well understood. It has been suggest that excited triplet state of heterocyclic N-oxides is responsible for photo-deoxygenation (*i.e.*, release of O(^{3}P)), and that the excited singlet is responsible for O migration and ring cleavage.[89,93,94] This hypothesis is supported by an apparent correlation between the degree to which the triplet is formed in substituted pyridine N-oxides, and the extent of deoxygenation.[87,89,92,95] In addition, introduction of the known triplet quencher, O_2,[96-98] results in a decrease in the efficiency of deoxygenation.[93,95] Contrary reports by de Lucas et al. found that deoxygenation of a thiophene S-oxide did not occur when the triplet excited state was generated by indirect photolysis (energy transfer from triplet excited benzophenone).[99] Similarly, recent calculations by Jenks also suggest that the observed excited triplet of thiophene S-oxide is too low in energy for deoxygenation.[100] Others suggest that free O(^{3}P) is never formed, and that an oxaziradine intermediate is responsible for the observed chemistry.[101-103] For example, the cleavage of DNA resulting from photolysis of 3-amino-1,2,4-benzotriazine 1,4-dioxide is attributed to an oxaziridine intermediate, that is believed to have been trapped by photolysis in the presence of *p*-anisidine.[101] A time-resolved study in which

excited states can be observed, and products that more directly implicate generation of $O(^3P)$ would prove very beneficial to this field of study.

Therefore, 4-benzoylpyridine N-oxide (BPyO) was chosen for time resolved study by laser flash photolysis. An 80 % yield of 4-benzoylpyridine (deoxygenated BPyO) was reported after irradiation for short time periods.[92] The efficiency of deoxygenation was attributed to the fast intersystem crossing, $k_{isc} \sim 10^{11}$ s^{-1}, which was expected to convert the majority of the excited singlet to the triplet (minimizing the reactivity of the excited singlet).[92] The benzophenone-like character was also expected to contribute to a long lifetime of the triplet excited state (^{3}BPyO*), and exhibit spectral features similar to the excited triplet of benzophenone. Direct observation and manipulation of ^{3}BPyO* in tandem with product analysis offers a great deal of insight into the photochemical deoxygenation process of BPyO.

Dissertation Organization

This dissertation consists of five chapters. Chapters one through four have been published in *Chemical Research in Toxicology, Inorganica Chimica Acta, Chemical Communications*, and *Dalton Transactions*, respectively. Chapter five corresponds to a manuscript in preparation. Each chapter is self-contained with its own equations, figures, tables, and references. Following the last manuscript is general conclusions. With the exception of ICP-MS analysis (Chapter 1) performed by Dr. Travis Witte, and collection and manipulation of crystallographic data (Chapter 2) which were performed by Dr. Arkady Ellern, and insightful discussions with Dr. Oleg Pestovsky (Chapter 4) all the work performed in this dissertation was performed by the author of this thesis.

References

(1) *Industrial Organic Chemistry*; 3rd ed.; Weissermel, K.; Arpe, H.-J., Eds.; VCH Publishers, Inc.: New York, NY, 1997.
(2) Metelitsa, D. I. *Russian Chemical Reviews* **1981**, *50*.
(3) Shteinman, A. A. *FEBS Lett.* **1995**, *362*, 5.
(4) Decker, A.; Chow, M. S.; Kemsley, J. N.; Lehnert, N.; Solomon, E. I. *J. Am. Chem. Soc.* **2006**, *128*, 4719.
(5) Butler, A. *Coord. Chem. Rev.* **1999**, *187*, 17.
(6) Crabtree, R. H. *J. Am. Chem. Soc.* **1996**, *118*, 6806.
(7) Pestovsky, O. *Preprints of extended abstracts - American Chemical Society. Division of Environmental Chemistry* **2006**, *46*, 573.
(8) Bakac, A. *Inorg. Chem.* **2010**, *49*, 3584.
(9) Bakac, A. *Dalton Trans.* **2006**, 1589.
(10) Bakac, A. *Coord. Chem. Rev.* **2006**, *250*, 2046.
(11) Bakac, A. *Adv. Inorg. Chem.* **2004**, *55*, 1.
(12) Bakac, A.; Espenson, J. H. *Acc. Chem. Res.* **1993**, *26*, 519.
(13) Denisov, I. G.; John Wiley & Sons, Inc.: 2010, p 109.
(14) Kristian, K. E.; Song, W.; Ellern, A.; Guzei, I. A.; Bakac, A. *Inorg. Chem.* **2010**, *49*, 7182.
(15) Szajna-Fuller, E.; Bakac, A. *Inorg. Chem.* **2007**, *46*, 10907.
(16) Kotaś, J.; Stasicka, Z. *Environ. Pollut.* **2000**, *107*, 263.
(17) Vincent, J. B. *Acc. Chem. Res.* **2000**, *33*, 503.
(18) Norseth, T. *Environ. Health Perspect.* **1981**, *40*, 121.
(19) Little, L. G.; Sugden, K. D. In *Metal Complex–DNA Interactions*; John Wiley & Sons, Ltd: 2009, p 463.
(20) Levina, A.; Lay, P. A. *Coord. Chem. Rev.* **2005**, *249*, 281.
(21) Codd, R.; Dillon, C. T.; Levina, A.; Lay, P. A. *Coord. Chem. Rev.* **2001**, *216–217*, 537.
(22) Song, W.; Bakac, A. *Inorg. Chem.* **2009**, *49*, 150.
(23) Wang, W. D.; Bakac, A.; Espenson, J. H. *Inorg. Chem.* **1993**, *32*, 5034.
(24) *Free radicals in biology and environment*; Minisci, F., Ed.; Kluwer Academic Publishers: Dordrecht / Boston / London, 1997; Vol. 27.
(25) Neta, P.; Grodkowski, J.; Ross, A. B. *J. Phys. Chem. Ref. Data* **1996**, *25*.
(26) Buxton, G. V.; Greenstock, C. L.; Helman, W. P.; Ross, A. B. *J. Phys. Chem. Ref. Data* **1988**, *17*, 513.
(27) Bakac, A. *Croat. Chem. Acta* **2001**, *74*, 633.
(28) Rowlands, G. J. *Tetrahedron* **2010**, *66*, 1593.
(29) *Carbon-Centered Free Radicals and Radical Cations : Structure, Reactivity, and Dynamics*; Forbes, M. D. E., Ed.; Wiley: Hoboken, NJ, USA, 2010.
(30) Tully, F. P.; Ravishankara, A. R.; Thompson, R. L.; Nicovich, J. M.; Shah, R. C.; Kreutter, N. M.; Wine, P. H. *J. Phys. Chem* **1981**, *85*, 2262.
(31) Bakac, A.; Wang, W.-D. *Inorg. React. Mech.* **1998**, *1*, 65.
(32) Suggs, J. W.; Jun, C. H. *J. Am. Chem. Soc.* **1986**, *108*, 4679.
(33) Mancuso, C.; Halpern, J. *J. Organomet. Chem.* **1992**, *428*, C8.

(34) Wang, W. D.; Bakac, A.; Espenson, J. H. *Inorg. Chem.* **1993**, *32*, 2005.
(35) Seidl, B.; Liska, R.; Grabner, G. *Journal of Photochemistry and Photobiology A: Chemistry* **2006**, *180*, 109.
(36) Colley, C. S.; Grills, D. C.; Besley, N. A.; Jockusch, S.; Matousek, P.; Parker, A. W.; Towrie, M.; Turro, N. J.; Gill, P. M. W.; George, M. W. *J. Am. Chem. Soc.* **2002**, *124*, 14952.
(37) Morlet-Savary, F.; Fouassier, J. P.; Tomioka, H. *Polymer* **1992**, *33*, 4202.
(38) Turro, N. J. *Modern Molecular Photochemistry*; University Science Books, 1991.
(39) Rangel, M.; Pereira, E.; Oliveira, C.; de Castro, B. *J. Organomet. Chem.* **2001**, *632*, 85.
(40) Giannotti, C.; Bolton, J. R. *J. Organomet. Chem.* **1974**, *80*, 379.
(41) Giannotti, C.; Merle, G.; Bolton, J. R. *J. Organomet. Chem.* **1975**, *99*, 145.
(42) Rao, D. N. R.; Symons, M. C. R. *Journal of the Chemical Society, Faraday Transactions 1: Physical Chemistry in Condensed Phases* **1984**, *80*, 423.
(43) Glebov, E. M.; Pozdnyakov, I. P.; Grivin, V. P.; Plyusnin, V. F.; Zhang, X.; Wu, F.; Deng, N. *Photochemical & Photobiological Sciences* **2011**, *10*, 425.
(44) Bideau, M.; Claudel, B.; Faure, L.; Rachimoellah, M. *Journal of Photochemistry* **1987**, *39*, 107.
(45) Gilbert, B. C.; Hodges, G. R.; Lindsay, S. J. R.; MacFaul, P.; Taylor, P. *J. Chem. Soc., Perkin Trans. 2* **1996**, 519.
(46) Gilbert, B. C.; Lindsay, S. J. R.; Parsons, A. F.; Setchell, P. K. *J. Chem. Soc., Perkin Trans. 2* **1997**, 1065.
(47) Kuhnle, J. A.; Lundin, R. E.; Waiss, A. C., Jr. *J. Chem. Soc., Chem. Commun.* **1972**, 287.
(48) Bideau, M.; Claudel, B.; Faure, L.; Kazouan, H. *Journal of Photochemistry and Photobiology A: Chemistry* **1992**, *67*, 337.
(49) Pozdnyakov, I. P.; Glebov, E. M.; Plyusnin, V. F.; Grivin, V. P.; Bunduki, E.; Goryacheva, N. V.; Gladki, V.; Duka, G. G. *High Energy Chem.* **2009**, *43*, 406.
(50) Beckett, A.; Porter, G. *Transactions of the Faraday Society* **1963**, *59*, 2038.
(51) Brown, T.; Dronsfield, A.; Jablonski, A.; Wilkinson, A.-S. *Tetrahedron Lett.* **1996**, *37*, 5413.
(52) Brown, K. L.; Jang, G.-w.; Segal, R.; Rajeshwar, K. *Inorg. Chim. Acta* **1987**, *128*, 197.
(53) Stolzenberg, A. M.; Cao, Y. *J. Am. Chem. Soc.* **2001**, *123*, 9078.
(54) Bakac, A.; Espenson, J. H. *J. Am. Chem. Soc.* **1984**, *106*, 5197.
(55) Bakac, A.; Espenson, J. H. *Inorg. Chem.* **1989**, *28*, 3901.
(56) Bakac, A.; Espenson, J. H. *Inorg. Chem.* **1987**, *26*, 4305.
(57) Bakac, A.; Espenson, J. H. *Inorg. Chem.* **1987**, *26*, 4353.
(58) Geremia, S.; Dreos, R.; Randaccio, L.; Tauzher, G.; Antolini, L. *Inorg. Chim. Acta* **1994**, *216*, 125.
(59) Asaro, F.; Costa, G.; Dreos, R.; Pellizer, G.; von Philipsborn, W. *J. Organomet. Chem.* **1996**, *513*, 193.
(60) Giese, B.; Kesselheim, C.; Hartung, J.; Lindner, H. J.; Svoboda, I. *Chem. Ber.* **1993**, *126*, 1193.
(61) Fu, X.; Wayland, B. B. *J. Am. Chem. Soc.* **2005**, *127*, 16460.

(62) Feng, M.; Chan, K. S. *J. Organomet. Chem.* **1999**, *584*, 235.
(63) Johnson, M. D. *Acc. Chem. Res.* **1983**, *16*, 343.
(64) Dodd, D.; Johnson, M. D.; Lockman, B. L. *J. Am. Chem. Soc.* **1977**, *99*, 3664.
(65) Espenson, J. H.; Shveima, J. S. *J. Am. Chem. Soc.* **1973**, *95*, 4468.
(66) Boddien, A.; Gärtner, F.; Federsel, C.; Sponholz, P.; Mellmann, D.; Jackstell, R.; Junge, H.; Beller, M. *Angew. Chem. Int. Ed.* **2011**, *50*, 6411.
(67) Boddien, A.; Mellmann, D.; Gärtner, F.; Jackstell, R.; Junge, H.; Dyson, P. J.; Laurenczy, G.; Ludwig, R.; Beller, M. *Science* **2011**, *333*, 1733.
(68) Hofman, V. W., D.; Webster, J. **2006**.
(69) Han, J.; Sun, H.; Duan, J.; Ding, Y.; Lou, H.; Zheng, X. *Adv. Synth. Catal.* **2010**, *352*, 1805.
(70) Kunkes, E. L.; Simonetti, D. A.; West, R. M.; Serrano-Ruiz, J. C.; Gärtner, C. A.; Dumesic, J. A. *Science* **2008**, *322*, 417.
(71) Yakovlev, V. A.; Khromova, S. A.; Sherstyuk, O. V.; Dundich, V. O.; Ermakov, D. Y.; Novopashina, V. M.; Lebedev, M. Y.; Bulavchenko, O.; Parmon, V. N. *Catal. Today* **2009**, *144*, 362.
(72) Buxton, G. V.; Green, J. C. *Journal of the Chemical Society, Faraday Transactions 1: Physical Chemistry in Condensed Phases* **1978**, *74*, 697.
(73) Cvetanovic, R. J.; Ring, D. F.; Doyle, L. C. *J. Phys. Chem* **1971**, *75*, 3056.
(74) Nicovich, J. M.; Gump, C. A.; Ravishankara, A. R. *J. Phys. Chem* **1982**, *86*, 1684.
(75) Nicovich, J. M.; Gump, C. A.; Ravishankara, A. R. *J. Phys. Chem* **1982**, *86*, 1690.
(76) Gaffney, J. S.; Atkinson, R.; Pitts, J. N. *J. Am. Chem. Soc.* **1975**, *97*, 5049.
(77) Hewitt, C. N.; Harrison, R. M. *Atmospheric Environment (1967)* **1985**, *19*, 545.
(78) Blanco, M. B.; Taccone, R. A.; Lane, S. I.; Teruel, M. A. *The Journal of Physical Chemistry A* **2006**, *110*, 11091.
(79) Garton, D. J.; Minton, T. K.; Troya, D.; Pascual, R.; Schatz, G. C. *The Journal of Physical Chemistry A* **2003**, *107*, 4583.
(80) Cvetanović, R. J. *J. Phys. Chem. Ref. Data* **1987**, *16*, 261.
(81) Upadhyaya, H. P.; Naik, P. D.; Pavanaja, U. B.; Kumar, A.; Vatsa, R. K.; Sapre, A. V.; Mittal, J. P. *Chem. Phys. Lett.* **1997**, *274*, 383.
(82) Sun Young, L.; Hee Soo, Y.; Wee Kyung, K.; Jung, K.-H. *Chem. Phys. Lett.* **1996**, *257*, 415.
(83) Zadok, E.; Rubinraut, S.; Mazur, Y. *The Journal of Organic Chemistry* **1987**, *52*, 385.
(84) Tanner, D. D.; Kandanarachchi, P.; Das, N. C.; Brausen, M.; Vo, C. T.; Camaioni, D. M.; Franz, J. A. *The Journal of Organic Chemistry* **1998**, *63*, 4587.
(85) Thomas, K. B.; Greer, A. *The Journal of Organic Chemistry* **2003**, *68*, 1886.
(86) Gibson, K. D.; Sibener, S. J. *Surf. Sci.* **2006**, *600*, L76.
(87) Bucher, G.; Scaiano, J. C. *J. Phys. Chem* **1994**, *98*, 12471.
(88) Scaiano, J. C.; Bucher, G.; Barra, M.; Weldon, D.; Sinta, R. *Journal of Photochemistry and Photobiology A: Chemistry* **1996**, *102*, 7.
(89) Albini, A.; Alpegiani, M. *Chem. Rev.* **1984**, *84*, 43.
(90) Kurasawa, Y.; Takada, A.; Kim, H. S. *J. Heterocycl. Chem.* **1995**, *32*, 1085.
(91) McCulla, R. D.; Jenks, W. S. *J. Am. Chem. Soc.* **2004**, *126*, 16058.
(92) Albini, A.; Fasani, E.; Frattini, V. *Journal of Photochemistry* **1987**, *37*, 355.

(93) Lin, S.-K. *Journal of Photochemistry* **1987**, *37*, 363.
(94) Tokumura, K.; Matsushita, Y. *Journal of Photochemistry and Photobiology A: Chemistry* **2001**, *140*, 27.
(95) Bellamy, F.; Barragan, L. G. R.; Streith, J. *Journal of the Chemical Society D: Chemical Communications* **1971**, 456.
(96) Foote, C. S. *Photochem. Photobiol.* **1991**, *54*, 659.
(97) Grewer, C.; Brauer, H.-D. *J. Phys. Chem* **1994**, *98*, 4230.
(98) Ledger, M. B.; Porter, G. *Journal of the Chemical Society, Faraday Transactions 1: Physical Chemistry in Condensed Phases* **1972**, *68*, 539.
(99) de Lucas, N. C.; Albuquerque, A. C. C.; Santos, A. C. A. S.; Garden, S. J.; Nicodem, D. E. *Journal of Photochemistry and Photobiology A: Chemistry* **2007**, *188*, 293.
(100) Stoffregen, S. A.; Lee, S. Y.; Dickerson, P.; Jenks, W. S. *Photochemical & Photobiological Sciences* **2014**, *13*, 431.
(101) Daniels, J. S.; Chatterji, T.; MacGillivray, L. R.; Gates, K. S. *The Journal of Organic Chemistry* **1998**, *63*, 10027.
(102) Cordes, T.; Regner, N.; Heinz, B.; Borysova, E.; Ryseck, G.; Gilch, P. *Journal of Photochemistry and Photobiology A: Chemistry* **2009**, *206*, 10.
(103) Orf, H. W.; Dolphin, D. *Proceedings of the National Academy of Sciences* **1974**, *71*, 2646.

CHAPTER 1

INTRAMOLECULAR CONVERSION OF PENTAAQUA-HYDROPEROXIDO-CHROMIUM(III) ION TO AQUEOUS CHROMIUM(V)

POTENTIAL SOURCE OF CARCINOGENIC FORMS OF CHROMIUM IN AEROBIC ORGANISMS

Jack M. Carraher and Andreja Bakac

A paper published in *Chemical Research in Toxicology*[*]

Abstract

The decomposition of the title compound $(H_2O)_5CrOOH^{2+}$ (hereafter $Cr_{aq}OOH^{2+}$) in acidic aqueous solutions is kinetically complex and generates mixtures of products (Cr_{aq}^{3+}, $HCrO_4^-$, H_2O_2, and O_2). Relative yields of individual products vary greatly with reaction conditions and initial concentrations of $Cr_{aq}OOH^{2+}$. At pH 5.5 in the presence of O_2, the reaction was complete in less than a minute and generated chromate in about 70 % yield. These findings, in addition to poor reproducibility of kinetic data, are indicative of the involvement of one or more reactive intermediates that consume additional amounts of $Cr_{aq}OOH^{2+}$ in post-rate-determining steps. The kinetics were simplified in the

[*] Carraher, Jack M.; Bakac, Andreja *Chem. Res. Toxicol.* **2010**, *23* 1735 - 1742

presence of H_2O_2 or $ABTS^{2-}$, both of which are capable of scavenging strongly oxidizing intermediates. The measured rate constant in 0.10 M $HClO_4$ at low O_2 concentrations ($\leq$ 0.03 mM) was independent of the concentration of the scavengers and was, within error, the same for $ABTS^{2-}$, k = 4.9 ($\pm$ 0.2) $\times 10^{-4}$ s^{-1}, and H_2O_2, k = 5.3 ($\pm$ 0.7) $\times 10^{-4}$ s^{-1}. At a constant ionic strength of 1.0 M, the reaction in the presence of either H_2O_2 or $ABTS^{2-}$ obeyed a two-term rate law, $k_{obs} / s^{-1} = 6.7 (\pm 0.7) \times 10^{-4} + 7.6 (\pm 1.1) \times 10^{-4} [H^+]$. Both in the presence and absence of $ABTS^{2-}$ as the scavenger, the yields of H_2O_2 increased with increasing $[H^+]$. These results are discussed in terms of a dual-pathway mechanism for the decay of $Cr_{aq}OOH^{2+}$. The H^+-catalyzed path leads to the dissociation of H_2O_2 from Cr(III), while in the H^+-independent reaction, $Cr_{aq}OOH^{2+}$ is transformed to Cr(V). Both scavengers rapidly remove Cr(V) and simplify both the kinetics and products.

Introduction

Hydroperoxido complexes of transition metals have been observed or postulated as intermediates in the reduction and activation of molecular oxygen in both nature and the laboratory. In some cases, hydroperoxido complexes are directly involved in substrate oxidation, but in others, they serve only as precursors to active oxidants. In the mechanism of action of bleomycin, the hydroperoxidoiron species is the active oxidant that attacks the DNA.[1] In the case of Cytochrome P450, the most intensely studied oxygenase in the literature, the debate regarding the role of the hydroperoxido intermediates[2-5] is still not settled after several decades of research. Hydroperoxides are also involved as intermediates in a number of other enzymes that reduce oxygen or utilize hydrogen peroxide,[6] including oxygenases, peroxidases, catalases, nitric oxide synthases, and others.

The ubiquity of hydroperoxides in biological chemistry as well as in industrial and laboratory oxidations with O_2 and H_2O_2 has prompted intense synthetic efforts and mechanistic studies of the chemistry of transition metal hydroperoxido complexes as both models for active sites in biomolecules and intermediates in catalytic oxidations.[7-17]

Some of our own research has focused on reactive intermediates involved in the activation of oxygen with chromium,[17-19] even though this metal is not believed to be present at the active sites of enzymes involved in oxidations with O_2 or H_2O_2. Chromium is also quite unattractive as an industrial catalyst, and much of the industrial research deals with the removal of chromium from products and byproducts. Nonetheless, mechanistic studies of oxygen activation by chromium have great biological significance in the context of the carcinogenicity of chromate. There is growing evidence that the interaction of O_2 and/or H_2O_2 with low-valent chromium may generate some of the intermediates believed responsible for the carcinogenic action of chromate. There is thus a reasonable possibility that even those chromium compounds that are currently considered safe for human consumption as food additives may be hazardous to human health.

In our earlier studies[17,18] of the reactivity of $Cr_{aq}OOH^{2+}$, we have focused on reactions with oxygen-atom acceptors,[20] 1-e reductants,[21] and coordinating anions.[22,23] In every instance, the self-decomposition of $Cr_{aq}OOH^{2+}$ was much slower than the reaction of interest, but several observations suggested that high-valent chromium species were involved as intermediates[18] in the slow background decay. In the absence of added substrates, the decay traces were exponential, but the observed rate constant appeared to increase with increasing $[Cr_{aq}OOH^{2+}]_0$.[21] The reaction yielded a mixture of products

($HCrO_4^-$, $Cr(H_2O)_6^{3+}$ (hereafter Cr_{aq}^{3+}), O_2, and H_2O_2) in proportions that were sensitive to concentrations and reaction conditions.[21] An unusual kinetic stabilization of $Cr_{aq}OOH^{2+}$ by H_2O_2 was also observed.[23] In view of the substitutional inertness of Cr_{aq}^{3+}, this stabilization could not be explained by a simple coordination/dissociation equilibrium of eq 1 because the reverse step is much too slow to contribute on the time scales involved (less than an hour).

$$(H_2O)_5CrOOH^{2+} + H^+ \overset{H_2O}{\rightleftharpoons} Cr(H_2O)_6^{3+} + H_2O_2 \qquad (1)$$

The unusual behavior of $Cr_{aq}OOH^{2+}$ described above has prompted us to carry out a detailed investigation of this reaction, especially in view of our work with N_4 macrocyclic hydroperoxido chromium complexes, $(H_2O)LCr^{III}OOH^{2+}$ (L = L^1 = 1,4,8,11-[14]aneN_4, and L^2 = meso-Me_6-1,4,8,11-[14]aneN_4)[24-27] which were shown to undergo an intramolecular electron transfer to form Cr(V). The persistence of these Cr(V) complexes and our ability to observe them directly by UV-Vis and ESR spectroscopies was believed to be a result of the stabilization of the high oxidation state by electron-rich N_4 macrocyclic ligands. Our recent study of the formation and decay of $Cr_{aq}OOH^{2+}$ in the presence of simple inorganic oxoanions suggested, however, that even in this case the decay may involve Cr(V) despite the absence of macrocyclic amine ligands.

All of our observations can be combined in a plausible scenario whereby inorganic chromium(III) in a biological milieu and in the presence of H_2O_2 leads directly to high-oxidation states of chromium believed to be responsible for the carcinogenicity of chromate. We have demonstrated the rapid formation of $Cr_{aq}OOH^{2+}$ from Cr(III) and H_2O_2 in acidic aqueous solutions when simple oxyanions, such as acetate, are coordinated to Cr(III).[23] This reaction is likely to be even more facile in biological solutions owing to

an abundance of carboxylato groups in biological fluids and increased kinetic lability of Cr(III) at higher pH. If, as it seems, the hydroperoxidochromium ions are indeed converted to Cr(IV), Cr(V), and/or Cr(VI), then a facile mechanism exists for the oxidation of Cr(III) by H_2O_2 to carcinogenic forms of chromium.

To provide more insight into this possibility, we carried out a mechanistic study of the decomposition of $Cr_{aq}OOH^{2+}$ under a range of conditions. The results, presented here, lead to a consistent mechanistic picture and provide strong evidence for a major path involving the transformation of $Cr_{aq}OOH^{2+}$ to Cr(V).

Experimental

Materials and Methods

Hexammineruthenium(III) chloride, chromium(III) perchlorate, 2,2′-azinobis(3-ethylbenzothiazoline-6-sulfonate) ammonium salt ($(NH_4)_2$ABTS), and titanium oxysulfate were purchased from Sigma-Aldrich. Methanol, zinc, hydrochloric acid, perchloric acid, 30% hydrogen peroxide, sodium iodide, and mercuric chloride were obtained from Fisher Scientific. The buffer piperazine-N,N′-bis(2-ethanesulfonic acid) (PIPES) was obtained from Sigma-Aldrich. Aqueous stock solutions of the buffer (pH 6.83) were prepared by sonication of an appropriate mass of PIPES in a solution of sodium hydroxide. Solutions of Cr_{aq}^{2+} and $Ru(NH_3)_6^{2+}$ were prepared by reduction of Cr_{aq}^{3+} and $Ru(NH_3)_6^{3+}$ solutions, respectively, with zinc amalgam under air-free conditions.

Aqueous solutions of $(H_2O)_5CrOO^{2+}$ (hereafter $Cr_{aq}OO^{2+}$) were prepared from Cr_{aq}^{2+} and O_2 in 0.10 M $HClO_4$ containing 0.10 M methanol as the stabilizer as described previously.[28] For the preparation of $Cr_{aq}OOH^{2+}$, the desired volume of the superoxido

complex was thermostatted for 10 min in a spectrophotometric cell at 25.0 ± 0.5 °C, followed by a brief (2 min) purge with a brisk stream of argon to remove most of dissolved O_2. Longer purging times were avoided to minimize the decomposition of $Cr_{aq}OO^{2+}$ under conditions of limited [O_2]. At that point, a slight (5 - 10 %) excess of $Ru(NH_3)_6^{2+}$ was injected to generate the hydroperoxido complex for work at low [O_2]. Such solutions contained $\leq 3 \times 10^{-5}$ M O_2, as measured with an oxygen electrode. The decay of $Cr_{aq}OOH^{2+}$ was monitored at 270 nm, where the change in molar absorptivity ($\Delta\varepsilon_{270}$) was 900 ± 100 M^{-1} cm^{-1}. For work at high [O_2], the freshly generated solutions of $Cr_{aq}OOH^{2+}$ were resaturated with O_2 for 1 min and diluted with appropriate amounts of O_2-saturated 0.10 M $HClO_4$. The final O_2 concentration was approximately 0.82 mM (μ = 0.10 M, T = 25 °C). In experiments utilizing air-stable $ABTS^{2-}$ as a reductant for $Cr_{aq}OO^{2+}$, the purging with argon prior to the reduction was omitted, and the final oxygen concentration was 1.26 mM. These solutions were deaerated with a stream of argon for work under low [O_2]. Some experiments were conducted at higher ionic strength (up to 1.0 M) adjusted with $LiClO_4$. Water was purified with a Barnstead EASYpure III UV UF system.

Concentrations of H_2O_2 in spent reaction solutions were determined by adding a known excess of iodide and monitoring the growth of I_3^- at 355 nm under air-free conditions. The kinetics[29] agreed well with those determined independently with genuine H_2O_2. The yield of H_2O_2 was calculated from the overall absorbance change taking ε (I_3^-) = 2.6×10^4 M^{-1} cm^{-1}.[30] In some experiments, notably those that yielded larger concentrations of H_2O_2, the $[Ti^{IV}O]SO_4$ method[31] was used. Chromate yields were determined from the absorbance at the 352 nm maximum ($\varepsilon = 2.6 \times 10^3$ M^{-1} cm^{-1} in

acidic solutions) and independently in the reaction with iodide.[32] When both chromate and H_2O_2 were produced, the total oxidizing equivalents were determined in the reaction with iodide. The concentration of $HCrO_4^-$ was obtained spectrophotometrically and that of H_2O_2 was calculated from the difference. The calculations took into account the correct stoichiometric ratios, *i.e.*, ($[I_2]_\infty$ / $[HCrO_4^-]_0$ = 1.5 and $[I_2]_\infty$ / $[H_2O_2]_0$ = 1.0).

Instrumentation

UV-Vis spectra and kinetic traces were obtained with a Shimadzu UV-3101PC spectrophotometer at 25.0 ± 0.2 °C. Elemental analyses of chromium precipitates were performed with a high-resolution double focusing ICP-MS Element 1 by Thermo Finnigan. Oxygen concentrations were determined with a YSI 5331 oxygen probe manufactured by Yellow Springs Instrument Co., Inc.

Results

Preliminary Observations

Kinetic traces for the disappearance of $Cr_{aq}OOH^{2+}$ at 270 nm at low [O_2] (≤ 0.03 mM; see Experimental Procedures) were exponential, but the rate constants exhibited large scatter and increased with increasing initial concentrations of $Cr_{aq}OOH^{2+}$, as shown in Figure 1. The line drawn through the points has an intercept of 4.6 (± 2.5) × 10^{-4} s^{-1} and a slope of 7.2 (± 1.1) M^{-1} s^{-1}. The poor reproducibility made it difficult to determine the kinetic dependence on [H^+], but the rate constants at comparable concentrations of $Cr_{aq}OOH^{2+}$ in Table 1 do appear to increase with increasing [H^+] and ionic strength. The yields of H_2O_2 exhibit a clear dependence on [H^+], Figure 2, in agreement with qualitative observations in our previous report.[21] Increasing methanol concentration from 0.10 to 2.6 M had no effect on the kinetics or products within our precision limits. Spent

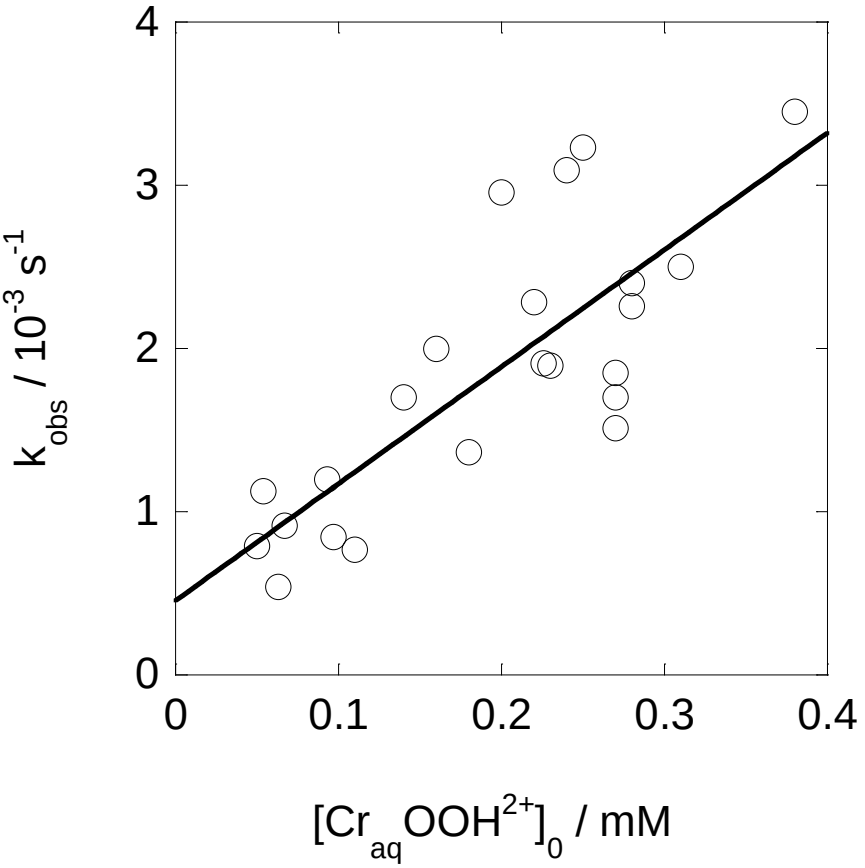

Figure 1. Plot of k_{obs} vs. $[Cr_{aq}OOH^{2+}]_0$ for the decomposition of $Cr_{aq}OOH^{2+}$ at **low [O_2]** ($\leq 3 \times 10^{-5}$ M). [MeOH] = 0.1 M, [H^+] = 0.10 M, 25.0 °C.

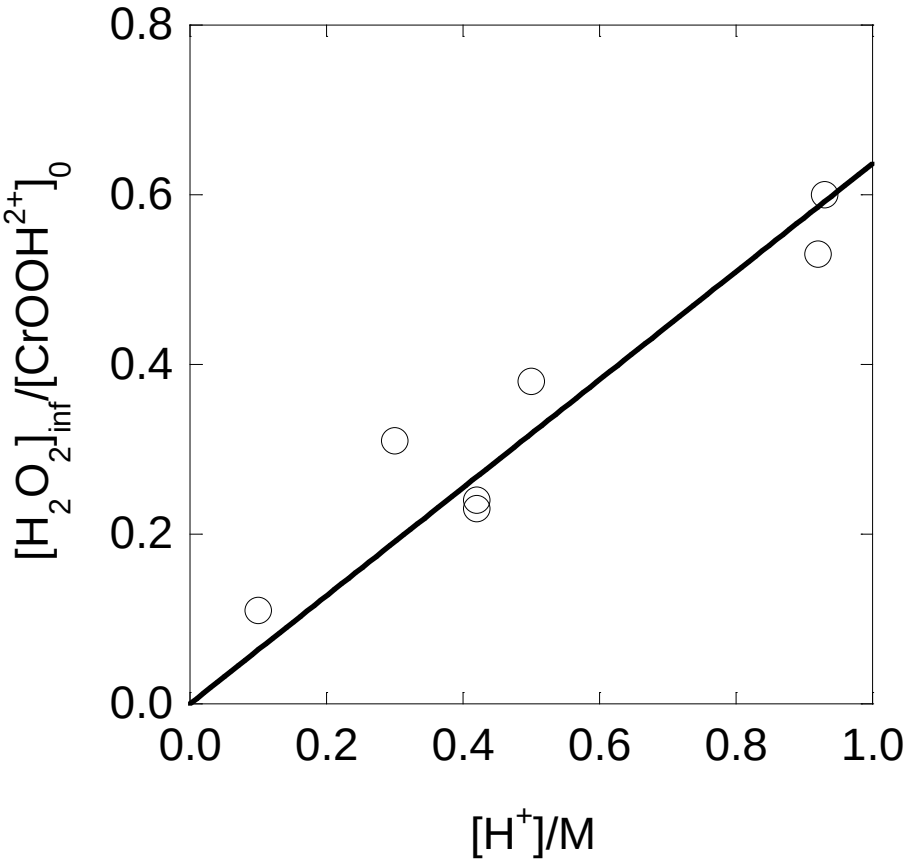

Figure 2. Yields of H_2O_2 as a function of $[H^+]$. Data from **Table 1**.

Table 1. Kinetics and Products of $Cr_{aq}OOH^{2+}$ Decomposition at **Low $[O_2]$**[a]

Entry No	$[Cr_{aq}OOH^{2+}]_0$ / 10^{-5} M	$[H^+]$ / M	k_{obs} / 10^{-3} s^{-1}	$[H_2O_2]_\infty$ / $[Cr_{aq}OOH^{2+}]_0$	$[O_2]_\infty$ / $[Cr_{aq}OOH^{2+}]_0$
1	8.9	0.10	1.32	0.11	
2	14	0.10[b]	1.74	0.11	[c]
3	8.4	0.30	1.01	0.31	
4	17	0.10[b]		[d]	0.35
5	14[e]	0.42	0.80		
6	21[e]	0.42	1.4	0.24	0.24
7	25[e]	0.42	-	0.23	
8	7.3	0.50	1.76	0.38	
9	9.0	0.93[f]	1.55	0.60	
10	9.8	0.92[f]	2.68	0.53	

[a] $[O_2] \leq 3 \times 10^{-5}$ M, μ = 0.50 M, [MeOH] = 0.10 M, 25.0 °C. [b] 0.10 M ionic strength. [c] None detected. [d] 9.6 mM externally added H_2O_2. [e] Data from ref. 21. [f] 0.93 M ionic strength.

reaction solutions exhibited a weak UV-Vis spectrum of Cr_{aq}^{3+} and showed no indication of $HCrO_4^-$ (λ_{max} = 352 nm).

The decomposition of $Cr_{aq}OOH^{2+}$ at high $[O_2]$ (0.82 mM O_2; see Experimental Procedures) was slower than that observed under low $[O_2]$, but kinetic traces were complicated by an initial absorbance increase followed by a decrease. The reproducibility and duration of the initial phase were highly dependent on concentrations of both $Cr_{aq}OOH^{2+}$ and H^+. Precise kinetic data were not obtained, but successive spectral scans showed that small amounts of the superoxidochromium(III) ion, $Cr_{aq}OO^{2+}$, which also absorbs at 270 nm, were responsible for the observed absorbance changes in this phase.

Spent reaction solutions contained Cr_{aq}^{3+}, H_2O_2, and $HCrO_4^-$. The latter two were identified and quantified as described in Experimental Procedures. The results are shown in Table 2 and can be summarized as follows. The sum of oxidizing equivalents in the products, H_2O_2 and $HCrO_4^-$, is less than that in the initially present $Cr_{aq}OOH^{2+}$. Also, the

relative yields of H_2O_2 increase, and those of chromate decrease as the acid concentration is raised. No chromate was detected at 1 M H^+.

Table 2. Products of Decomposition of $Cr_{aq}OOH^{2+}$ at High $[O_2]$[a]

$[Cr_{aq}OOH^{2+}]_0$ / 10^{-4} M	$[H^+]$ / M	$[HCrO_4^-]_\infty$ / $[Cr_{aq}OOH^{2+}]_0$	$[H_2O_2]_\infty$ / $[Cr_{aq}OOH^{2+}]_0$
1.0	0.1	0.18	0.16
1.8	0.1	0.14	0.13
2.5	0.1	0.11	0.15
0.55	0.93	[b]	0.45
0.78	0.93	[b]	0.42

[a] $[O_2]$ ~ 0.82 mM, [MeOH] = 0.1 M, 25.0 °C, ionic strength = $[H^+]$. [b] $HCrO_4^-$ not detected (≤ 0.002 mM). [c] Data from reference 21.

Effect of H_2O_2

The complex kinetic behavior and the effect of reaction conditions on the nature of products suggest that at least two processes are involved in the decay of $Cr_{aq}OOH^{2+}$. One is an H^+-induced acidolysis to Cr_{aq}^{3+} and H_2O_2. The other has to account for the formation of chromate and some O_2, implying that $Cr^{IV}{}_{aq}O^{2+}$ and/or $Cr^{V}{}_{aq}$ are involved as intermediates. The chemistry of the former has been studied in some depth,[17,33] but little is known about the reactivity of aqueous Cr(V) except that it disproportionates to $Cr_{aq}O^{2+}$ and $HCrO_4^-$ with inverse $[H^+]$ dependence in acidic solutions.[34] A related macrocyclic complex, $L^1Cr(V)$, rapidly oxidizes H_2O_2, $k > 5\times 10^3$ M^{-1} s^{-1}.[35] To explore the possibility that Cr(V) is involved in the decay of $Cr_{aq}OOH^{2+}$ and that the Cr(V) / H_2O_2 reaction may be the source of O_2 observed under some conditions, we examined the effect of externally added H_2O_2 on the kinetics and products of $Cr_{aq}OOH^{2+}$ decomposition.

In the presence of H_2O_2 at low O_2, the decay of $Cr_{aq}OOH^{2+}$ became slower and kinetically well behaved at both low and high $[H^+]$. Occasionally, some tailing was observed at the end of the reaction as shown in Figure 3b. This is caused by the slow

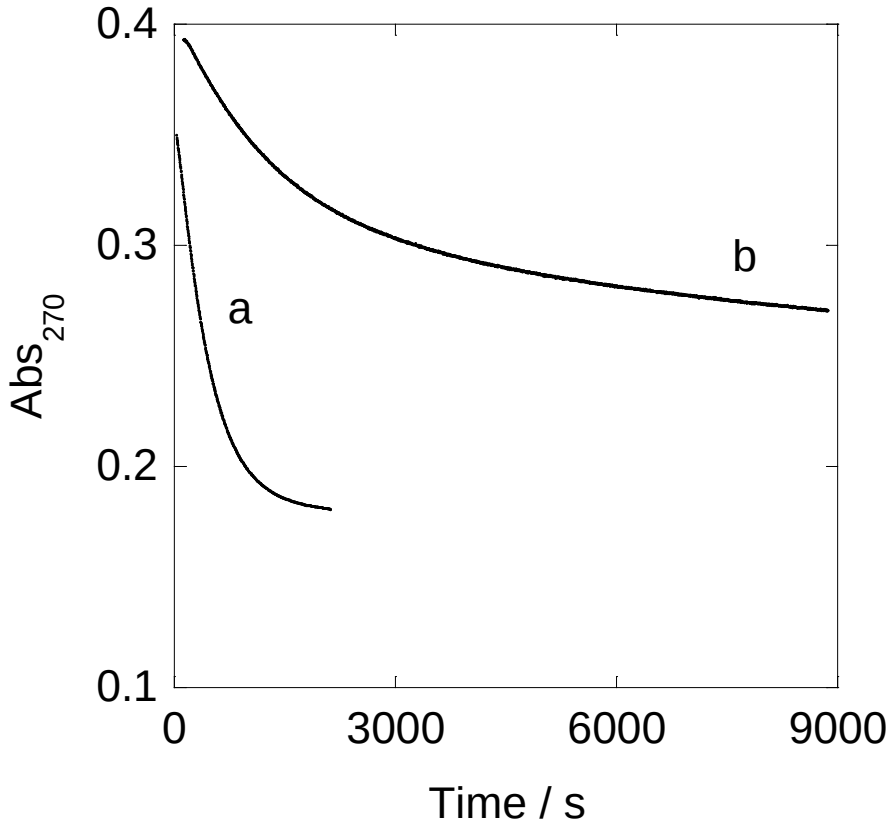

Figure 3. Kinetic traces for the decomposition of $Cr_{aq}OOH^{2+}$ in the absence (a) and presence (b) of added H_2O_2. Conditions: $[H^+] = 0.10$ M, $[O_2] \leq 3 \times 10^{-5}$ M, [MeOH] = 0.10 M, 25.0 °C. (a) $[Cr_{aq}OOH^{2+}] = 0.17$ mM. (b) $[Cr_{aq}OOH^{2+}] = 0.13$ mM, $[H_2O_2] = 9.3$ mM. The upward displacement of trace *b* relative to *a* is caused by the background absorbance by H_2O_2.

decay of traces of remaining $Cr_{aq}OO^{2+}$ (see Experimental Procedures). In such cases, the data were fit with an equation for (exponential + linear) kinetics. The rate constant obtained from the major, exponential component, 5.3 (± 0.7) × 10^{-4} s^{-1} in 0.10 M $HClO_4$, was independent of the concentration of H_2O_2 in the range 10 mM ≥ [H_2O_2] ≥ 1.0 mM. Figure 3 shows kinetic traces for two runs that were obtained under identical conditions except that 9.3 mM H_2O_2 was added to one of the solutions (top trace). *tert*-BuOOH (1 - 5 mM) had no effect on the kinetics of decomposition of $Cr_{aq}OOH^{2+}$.

In several experiments, O_2 was quantified after the completion of the run and corrected for the amount initially present (Table 1). No O_2 was detected at low [H^+], but significant amounts were found when the reaction was run in the presence of H_2O_2: entries 2 and 4. At 0.42 M H^+, O_2 was generated even in the absence of added H_2O_2. These findings support our notion that the reaction generates an oxidizing intermediate, such as Cr(V), which is intercepted with H_2O_2 to produce Cr(III) and O_2.

We next searched for another reagent that could scavenge the putative Cr(V) without reacting directly with $Cr_{aq}OOH^{2+}$. Among several possibilities, $ABTS^{2-}$ worked the best, as described below. In addition to its effect on the kinetics, this reductant also facilitated the monitoring of the reaction progress owing to strong light absorption by the reaction product, $ABTS^{\bullet-}$ (ε_{650} = 1.35 × 10^4 M^{-1} cm^{-1}).[36] Also, $ABTS^{2-}$ rapidly reduces[35] $Cr_{aq}OO^{2+}$ to $Cr_{aq}OOH^{2+}$, which simplified the overall scheme and eliminated the need for air-sensitive $Ru(NH_3)_6^{2+}$ as reducing agent.

Effect of $ABTS^{2-}$ at Low [O_2]

The addition of $ABTS^{2-}$ to $Cr_{aq}OO^{2+}$ caused a sudden increase in absorbance at 650 nm corresponding to one equivalent of $ABTS^{\bullet-}$ per mol of $Cr_{aq}OO^{2+}$ as in eq 2.[24, 35]

$$Cr_{aq}OO^{2+} + ABTS^{2-} (+ H^{+}) \rightarrow Cr_{aq}OOH^{2+} + ABTS^{\bullet-} \quad (2)$$

This step was followed by a slower, exponential absorbance increase. The rate constant for the exponential phase was independent of [$ABTS^{2-}$], [$Cr_{aq}OOH^{2+}$], and [MeOH], as shown in Table 3 and Figure 4. (In a single experiment with an exceptionally small concentration of $Cr_{aq}OOH^{2+}$ (0.017 mM), the rate constant was much smaller, 3.1 × 10^{-4} s^{-1}. Under these conditions, the concentration of residual O_2 (≤ 0.03 mM) is significant relative to the concentrations of other potential scavengers for Cr_{aq}^{2+}, which brings about the formation of $Cr_{aq}OO^{2+}$ and regeneration of $Cr_{aq}OOH^{2+}$, as in Scheme 2.) The value of the rate constant in 0.10 M $HClO_4$, k = 4.9 (± 0.2) × 10^{-4} s^{-1}, is similar to that obtained in the presence of added H_2O_2, k = 5.3 (± 0.7) × 10^{-4} s^{-1}, and both are close to the value of the intercept in Figure 1, 4.6 (± 2.5) × 10^{-4} s^{-1}, but with smaller standard deviations. All of the kinetic data are summarized in Table 4.

Table 3. Effect of $ABTS^{2-}$ on Decomposition of $Cr_{aq}OOH^{2+}$ at Low [O_2][a]

[$Cr_{aq}OO^{2+}$] / 10^{-5} M [b]	[$ABTS^{2-}$] / 10^{-4} M	k_{obs} / 10^{-4} s^{-1}	[$ABTS^{\bullet-}$]$_\infty$ / [$Cr_{aq}OO^{2+}$]$_0$
2.8	2.3	5.2	2.0
3.7	5.0	4.5	2.0
4.7	5.0	4.8	2.0
5.9	1.6	5.4[c]	1.7[c]
6.2	6.7	4.8	1.7
6.3	5.0	4.8	1.7
6.3	5.0	5.0[d]	1.7[d]
6.5	3.3	4.9	1.7
6.6	5.0	4.4[c]	1.9[c]
7.3	3.3	5.1	1.5

[a] [O_2] ≤ 3 × 10^{-5} M, [H^+] = 0.10 M, [MeOH] = 0.10 M, 25.0 °C. [b] Reduced *in situ* to $Cr_{aq}OOH^{2+}$ with $ABTS^{2-}$, see text. [c] [MeOH] = 1.0 M. [d] [MeOH] = 0.5 M.

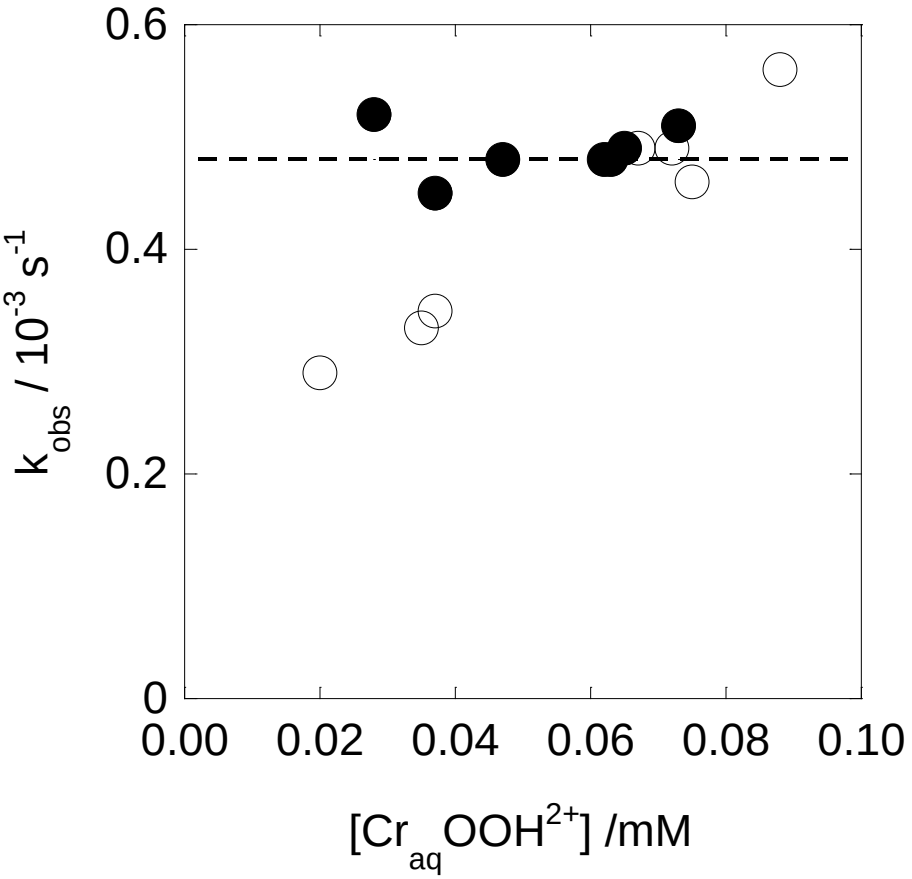

Figure 4. Plot of k_{obs} against the concentration of $Cr_{aq}OOH^{2+}$ for the decay of $Cr_{aq}OOH^{2+}$ in the presence of 0.2 - 0.7 mM $ABTS^{2-}$ in O_2-saturated (open circles, $[O_2]_0$ = 1.26 mM) and Ar purged (filled circles, $[O_2]_0 \leq 3 \times 10^{-5}$ M) solutions.

Table 4. Summary of Kinetic Data for the Decay of $Cr_{aq}OOH^{2+}$ [a]

Scavenger	$[H^+]$/M	k_{obs}/s^{-1}
None	0.10	$5 (\pm 3) \times 10^{-4} + 7 (\pm 1) [Cr_{aq}OOH^{2+}]$
$ABTS^{2-}$ [b]	0.10	$4.9 (\pm 0.2) \times 10^{-4}$
H_2O_2 [c]	0.10	$5.3 (\pm 0.7) \times 10^{-4}$
$ABTS^{2-}$ [b] or H_2O_2 [c]	0.10 - 1.0 [d]	$6.7 (\pm 0.7) \times 10^{-4} + 8 (\pm 1) \times 10^{-4} [H^+]$
$ABTS^{2-}$ [e]	0.10	$2.0 (\pm 0.3) \times 10^{-4} + 3.9 (\pm 0.4) [Cr_{aq}OOH^{2+}]$

[a] Aqueous solutions, 25.0 °C, 7.3×10^{-5} M $\leq [Cr_{aq}OOH^{2+}] \leq 2.7 \times 10^{-4}$ M, μ = 0.10 M, $[CH_3OH]$ = 0.10 M, $[O_2] \leq 3 \times 10^{-5}$ M. [b] 0.16 - 0.67 mM $ABTS^{2-}$. [c] 1-10 mM H_2O_2. [d] μ = 0.50 - 1.0 M. [e] $[O_2]$ = 1.26 mM.

The yield of $ABTS^{\bullet-}$, expressed as the ratio $[ABTS^{\bullet-}]_\infty$ / $[Cr_{aq}OO^{2+}]_0$, never reached the theoretical value of 3, expected on the basis of eq 2 followed by eq 3. Moreover, the yield tended to decrease as the initial concentration of $Cr_{aq}OOH^{2+}$ increased. As shown later, this result can be rationalized by the increased importance of a side reaction between Cr_{aq}^{2+} and $ABTS^{\bullet-}$ at higher $[ABTS^{\bullet-}]$.

$$Cr_{aq}OOH^{2+} + 2ABTS^{2-} (+ 3H^+) \rightarrow Cr_{aq}(H_2O)^{3+} + 2ABTS^{\bullet-} + H_2O \qquad (3)$$

In an attempt to examine the competition between $ABTS^{2-}$ and H_2O_2 for Cr(V), several experiments utilized mixtures of these reductants. Low concentrations of H_2O_2 (0.77 mM to 7.7 mM) had no effect on the yield of $ABTS^{\bullet-}$ ($[ABTS^{2-}]_0$ = 0.25 mM), which allows us to place a limit on the ratio, $k_{ABTS} / k_{H2O2} \geq 10^2$. Under a reasonable assumption that k_{H2O2} for this Cr(V) complex is at least as large as that for a related macrocyclic species $L^1Cr(V)$,[35] we obtain $k_{ABTS} \geq 5 \times 10^5$ M^{-1} s^{-1}. Experiments at higher concentrations of H_2O_2, which would provide a better estimate for k_{ABTS} / k_{H2O2}, were not informative because of the direct reaction between $ABTS^{2-}$ and H_2O_2 under those conditions.

Effect of $ABTS^{2-}$ in O_2-Saturated Solutions ($[O_2]$ = 1.26 mM)

An initial jump in absorbance (corresponding to reduction of $Cr_{aq}OO^{2+}$) was followed by exponential kinetics yielding rate constants that were independent of the concentration of $ABTS^{2-}$, but increased steadily as the initial concentration of $Cr_{aq}OOH^{2+}$ increased (Table 5 and Figure 4). Remarkably, the reaction at the lowest concentrations of $Cr_{aq}OOH^{2+}$ was slower than that at more standard concentrations of $Cr_{aq}OOH^{2+}$ under any conditions in this work. The yield of $ABTS^{\bullet-}$ showed no dependence on the concentration of either reactant, $[ABTS^{\bullet-}]_\infty$ / $[Cr_{aq}OO^{2+}]_0$ = 2.2 ± 0.1 (Table 5).

Table 5. Effect of $ABTS^{2-}$ on Decomposition of $Cr_{aq}OOH^{2+}$ in O_2-Saturated Solutions [a]

$[Cr_{aq}OO^{2+}]$ / 10^{-5} M[b]	$[ABTS^{2-}]$ / 10^{-4} M	k_{obs}/ 10^{-4} s^{-1}	$[ABTS^{\bullet-}]_\infty$/ $[Cr_{aq}OO^{2+}]_0$
2.0	4.0	2.9	2.1
3.7	4.0	3.3	2.1
6.7	6.0	4.9	2.2
7.2	4.0	4.9	2.1
7.5	3.3	4.6	2.2
8.8	4.0	5.6	2.3

[a] $[O_2]$ = 1.26 mM, [MeOH] = 0.1 M, 25.0 °C. [b] Reduced in situ to $Cr_{aq}OOH^{2+}$ with $ABTS^{2-}$, see text.

At $[Cr_{aq}OOH^{2+}] \geq 0.10$ mM, the addition of $ABTS^{2-}$ generated a precipitate. After filtration, the precipitate was washed with 0.10 M $HClO_4$ and redissolved in 0.10 M HNO_3. The UV-Vis spectrum showed that both $ABTS^{2-}$ and $ABTS^{\bullet-}$ were present. The precipitate also contained chromium as shown by inductively coupled plasma-mass spectrometry (ICP-MS). Kinetic experiments with added $ABTS^{2-}$ were therefore limited to low concentrations of $Cr_{aq}OOH^{2+}$.

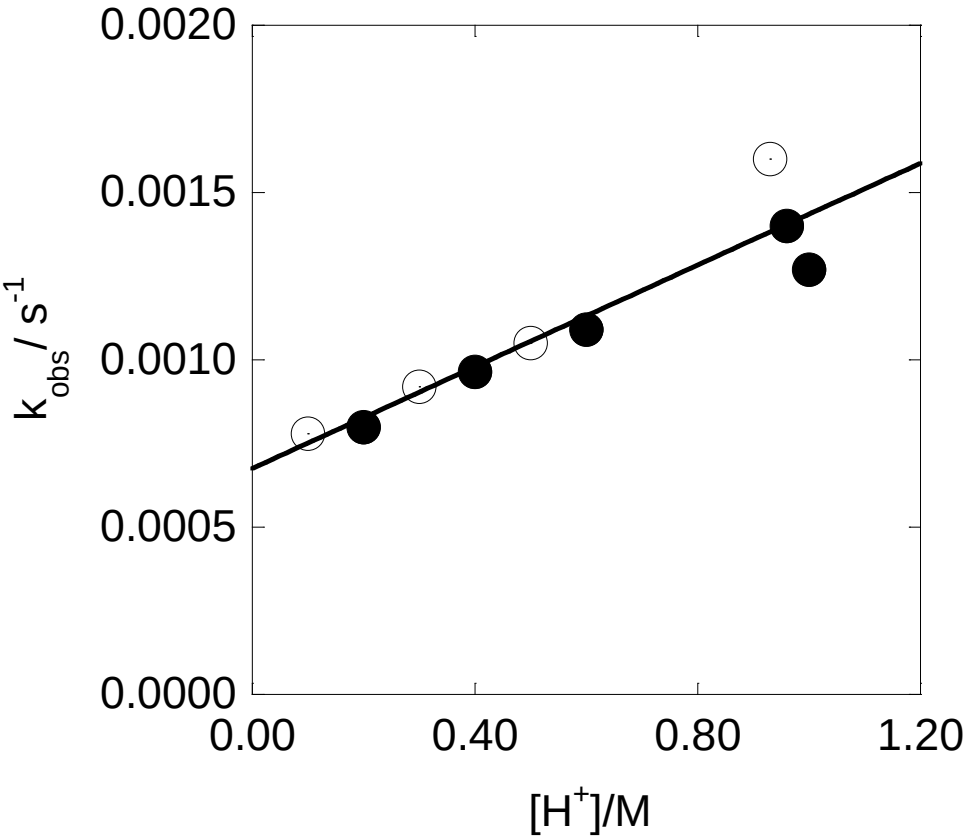

Figure 5. Dependence of k_{obs} on $[H^+]$ for the decomposition of $Cr_{aq}OOH^{2+}$ at low $[O_2]$ in the presence of 10 mM H_2O_2 (●) or 5 mM $ABTS^{2-}$ (○). Conditions: $[Cr_{aq}OOH^{2+}]$ = 0.04 - 0.10 mM, 25 °C, μ = 0.50 - 1.0 M.

Effect of H^+

At low O_2 in the presence of added H_2O_2 or $ABTS^{2-}$, the kinetics exhibited a clear dependence on $[H^+]$. In the range 1.0 M $\geq [H^+] \geq$ 0.10 M at 1.0 M ionic strength, both sets of data define a single line with a slope of 7.6 (± 1.1) × 10^{-4} M^{-1} s^{-1} and an intercept of 6.7 (± 0.7) × 10^{-4} s^{-1}, as shown in Figure 5.

Attempts to detect Cr(V) by EPR were not successful, probably because the signal caused by Cr_{aq}^{3+} obscured the weak signal from the low steady-state concentrations of Cr(V). Efforts to scavenge Cr(V) by complexing it with bis(2-hydroxy-2-methylbutyrate) (37) did not succeed either, as the acidic pH made the complexation reaction inefficient.

Discussion

An acceptable mechanism for the decomposition of $Cr_{aq}OOH^{2+}$ must account for the following observations. (1) In addition to Cr(III) and H_2O_2, the reaction generates $HCrO_4^-$ and O_2. (2) Relative yields of these products are highly sensitive to initial concentrations of $Cr_{aq}OOH^{2+}$, O_2, and H^+. (3) In the absence of O_2, the kinetics are exponential, but first-order rate constants increase with the initial concentration of $Cr_{aq}OOH^{2+}$. (4) The reproducibility of kinetic data is poor, as shown by the significant scatter in the plot of k_{obs} against $[Cr_{aq}OOH^{2+}]$ (Figure 1). (5) Externally added reductants that do not react directly with $Cr_{aq}OOH^{2+}$, such as H_2O_2 and $ABTS^{2-}$, simplify the kinetics and slow down the decay of $Cr_{aq}OOH^{2+}$. In the presence of these reductants, the kinetics are well-behaved and exhibit direct dependence on $[H^+]$ (Figure 5).

The accelerating effect of H^+ on the kinetics and increasing yields of H_2O_2 at higher $[H^+]$ are attributed to the acidolysis of eq 1. In the range 1.0 M $\geq [H^+] \geq$ 0.10 M, the kinetic contribution from the $[H^+]$-dependent term increases from 10 % to about 50

%. The yields of H_2O_2 follow the same trend and increase from trace amounts to about 60 %. Within the experimental error, the two values are comparable and demonstrate the internal consistency of the data. The intercept in Figure 5, 6.7 (± 0.7) × 10^{-4} s^{-1}, is somewhat larger than the value at 0.10 M ionic strength, 5.3 (± 0.7) × 10^{-4} s^{-1} (see Table 4).

The remaining products ($HCrO_4^-$ and O_2) and complex kinetics observed in the absence of scavengers must be associated with another pathway(s). We propose an intramolecular transformation of the hydroperoxido Cr(III) complex to Cr(V), followed by the chemistry of Cr(V) depicted in Scheme 1 for low [O_2] conditions. As discussed below, this mechanism can account for all of the observations made in this work.

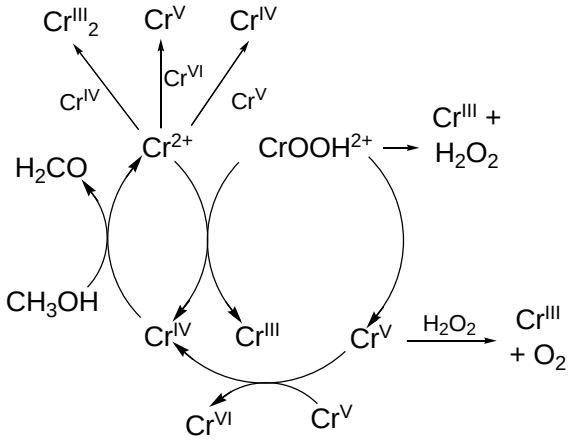

Scheme 1. Mechanism of decomposition of $Cr_{aq}OOH^{2+}$ at low concentrations of O_2

The main path for the disappearance of Cr(V) is the disproportionation to $Cr^{IV}{}_{aq}O^{2+}$ and $HCrO_4^-$. On the basis of the reported data for this reaction in formate-containing solutions,[34] we estimate k = 5 × 10^5 M^{-1} s^{-1} in 0.10 M $HClO_4$ and 5 × 10^4 M^{-1} s^{-1} in 1.0 M $HClO_4$.

The $Cr^{IV}_{aq}O^{2+}$ so generated reacts with methanol in a single two-electron step[19] and produces Cr_{aq}^{2+} which reacts with either the starting $Cr_{aq}OOH^{2+}$ or any of the three high-oxidation-state chromium species in Scheme 1. The reaction with $Cr_{aq}OOH^{2+}$ is written in analogy with the Fe_{aq}^{2+} / $Cr_{aq}OOH^{2+}$ reaction which produces $Cr^{IV}_{aq}O^{2+}$ with a rate constant comparable to that for the Fe_{aq}^{2+} / H_2O_2 reaction.[38] On the basis of this precedent, we surmise that the Cr_{aq}^{2+} / $Cr_{aq}OOH^{2+}$ reaction has a rate constant comparable to that for Cr_{aq}^{2+} / H_2O_2 (7×10^4 M^{-1} s^{-1})[39] and that it generates one equivalent of $Cr^{IV}_{aq}O^{2+}$. Reactions with $HCrO_4^-$ ($k = 10^9$ M^{-1} s^{-1}),[17] $Cr^{IV}_{aq}O^{2+}$ (10^8 M^{-1} s^{-1}),[40] and (presumably) Cr(V) have much greater rate constants, but this advantage is offset by the lower concentrations of these transients. As a result, Cr_{aq}^{2+} reacts in several competing pathways, some of which produce stable products (*e.g.*, Cr(III) dimer), while others regenerate $Cr^{IV}_{aq}O^{2+}$ and/or Cr(V) and re-enter various cycles with or without the additional consumption of $Cr_{aq}OOH^{2+}$, as shown in Scheme 1. Also, under conditions that generate substantial amounts of H_2O_2, the Cr_{aq}^{2+} / H_2O_2 reaction may become competitive and generate hydroxyl radicals. These would be rapidly scavenged by CH_3OH and produce the strongly reducing $^{\bullet}CH_2OH$.

The observed rate constant depends critically on the fate of Cr_{aq}^{2+}. The most important competition is that between $Cr_{aq}OOH^{2+}$ and all the remaining reactive chromium species. As shown in Scheme 1, the $Cr_{aq}OOH^{2+}$ / Cr_{aq}^{2+} reaction in the presence of methanol is one of two propagating steps in a chain reaction that converts $Cr_{aq}OOH^{2+}$ to Cr_{aq}^{3+}, *i.e.*, eqs 4 and 5. This is the main reason for the faster kinetics at higher concentrations of $Cr_{aq}OOH^{2+}$ in Figure 1.

$$Cr_{aq}OOH^{2+} + Cr_{aq}^{2+} (+H^+) \rightarrow Cr_{aq}O^{2+} + Cr_{aq}^{3+} + H_2O \qquad (4)$$

$$Cr_{aq}O^{2+} + CH_3OH \rightarrow Cr_{aq}^{2+} + CH_2O + H_2O \quad (5)$$

In the presence of large concentrations of O_2, the steps leading to the formation of Cr_{aq}^{2+} are the same as those in air-free solutions, but the fate of Cr_{aq}^{2+} is different. In the early stages, Cr_{aq}^{2+} reacts exclusively with O_2 ($k = 1.6 \times 10^8$ M^{-1} s^{-1}) and generates $Cr_{aq}OO^{2+}$, which causes the observed absorbance increase at 270 nm. Once a sufficient amount of $Cr_{aq}OO^{2+}$ is built up, a competition is established between $Cr_{aq}OO^{2+}$ and O_2 for Cr_{aq}^{2+}, $k(Cr_{aq}^{2+} / Cr_{aq}OO^{2+}) = 8 \times 10^8$ M^{-1} s^{-1},[17] as shown in eqs 6, 7, and 5.

$$Cr_{aq}^{2+} + O_2 \rightarrow Cr_{aq}OO^{2+} \quad (6)$$

$$Cr_{aq}OO^{2+} + Cr_{aq}^{2+} \rightarrow nCr_{aq}O^{2+} \quad \text{where } (n < 2) \text{ is from ref 18} \quad (7)$$

The chemistry in eqs 4 and 5 also explains the observation of chromate as a reaction product in O_2-saturated solutions. Chromate is formed by disproportionation of Cr(V) as in Scheme 1. Under low $[O_2]$ conditions, it is reduced by Cr_{aq}^{2+} (formed in eq 5) and/or $^{\bullet}CH_2OH$ to Cr(III). At high $[O_2]$, both Cr_{aq}^{2+} and $^{\bullet}CH_2OH$ are rapidly removed in reactions with O_2 and $Cr_{aq}OO^{2+}$, allowing chromate to accumulate.

In principle, the complex chemistry of Scheme 1 could be greatly simplified by either enhancing the acidolysis to such an extent that the Cr(V)-forming path becomes negligible or removing Cr(V) with a scavenger that generates stable products. The former option is not feasible because the acidolysis contributes only 50 – 60 % even at 1 M H^+; see Results. The use of H_2O_2 as a scavenger for Cr(V), however, had the desired effect, which we attribute to the reaction in eq 8. The dependence of the first-order rate constant on $Cr_{aq}OOH^{2+}$ disappeared, and the measured rate constant assumed the same value as the intercept in the plot of k_{obs} vs. $Cr_{aq}OOH^{2+}$ in the absence of H_2O_2 (Figure 1). The

removal of Cr(V) efficiently eliminated steps such as those in eqs 4 and 5 that were responsible for the additional consumption of $Cr_{aq}OOH^{2+}$ in Scheme 1.

$$Cr(V) + H_2O_2 (+ H^+) \rightarrow Cr_{aq}^{3+} + O_2 \quad (8)$$

Another argument in support of eq 8 is the detection of O_2 when H_2O_2 was added to reaction solutions. As shown in Table 1, the reaction that generated no O_2 in the absence of H_2O_2 produced 0.35 equivalents of O_2 in the presence of 10 mM H_2O_2. It is not clear why the yields were not closer to the theoretically predicted 0.9 equivalents, although some losses of $Cr_{aq}OO^{2+}$ (and thus $Cr_{aq}OOH^{2+}$) almost certainly occurred during the degassing and thermostatting procedures. The yields of H_2O_2 in Table 1 would be much less affected by such losses because this product accumulates throughout the experiment.

At 0.4 M H^+ and high initial [$Cr_{aq}OOH^{2+}$] (Table 1, entry 6), the reaction generated substantial amounts of O_2 in the absence of externally added H_2O_2. It appears that these conditions had generated sufficient amounts of H_2O_2 to serve as an internal scavenger for Cr(V).

Experiments with added $ABTS^{2-}$ provided additional insight into the chemistry in Scheme 1. This reductant was shown in the past to be an efficient scavenger for N_4-macrocyclic Cr(V) complexes.[24,35] In the absence of O_2, the kinetic effect of $ABTS^{2-}$ on the decay of $Cr_{aq}OOH^{2+}$ was the same as the effect of H_2O_2, *i.e.*, kinetic traces were exponential, and the rate constant was independent of [$Cr_{aq}OOH^{2+}$] and [$ABTS^{2-}$] (Table 3).

The reaction yielded $ABTS^{\bullet-}$ as a product, a result that would be expected regardless of whether the oxidation took place in 1-e or 2-e steps. In the latter case, the

initially formed $ABTS^{0}$ would rapidly react with excess $ABTS^{2-}$ and yield two equivalents of $ABTS^{\bullet-}$. A mechanistic clue comes from the observed substoichiometric yields of $ABTS^{\bullet-}$, especially at higher initial [$Cr_{aq}OOH^{2+}$]. This result suggests that the Cr(V) / $ABTS^{2-}$ reaction takes place in 1-e steps and involves $Cr^{IV}{}_{aq}O^{2+}$ as an intermediate. The reduction of $Cr^{IV}{}_{aq}O^{2+}$ with methanol in the next step generates $Cr_{aq}{}^{2+}$, as in Scheme 1, which will rapidly reduce $ABTS^{\bullet-}$ back to $ABTS^{2-}$. The higher the initial concentration of $Cr_{aq}OOH^{2+}$, the greater the concentration advantage of $ABTS^{\bullet-}$ over other competitors for $Cr_{aq}{}^{2+}$. Note that $ABTS^{\bullet-}$ is generated in both the preparative reaction in eq 2 and in the Cr(V) / $ABTS^{2-}$ reaction. The rate constant for the $Cr_{aq}{}^{2+}$ / $ABTS^{\bullet-}$ reaction was too fast for a direct measurement even at 0.010 mM concentrations, which places a limit of $k \geq 10^{5}\ M^{-1}\ s^{-1}$.

In the presence of O_2 and $ABTS^{2-}$, the kinetics of $Cr_{aq}OOH^{2+}$ decomposition were independent of [$ABTS^{2-}$]. The rate constant at low [$Cr_{aq}OOH^{2+}$] was smaller than that under any other conditions in this work but increased as the initial concentration of $Cr_{aq}OOH^{2+}$ increased. This behavior is qualitatively consistent with the chemistry described so far and the ability of $ABTS^{2-}$ to reduce $Cr_{aq}OO^{2+}$ to $Cr_{aq}OOH^{2+}$, as shown in Scheme 2. At 0.02 mM $Cr_{aq}OOH^{2+}$, the value of the rate constant ($2.9 \times 10^{-4}\ s^{-1}$) is slightly more than half of that measured at more standard [$Cr_{aq}OOH^{2+}$] under argon, ($4.9 \times 10^{-4}\ s^{-1}$), *i.e.*, the reaction completed less than two full cycles in Scheme 2. Both the inefficiency of that chemistry and small yields of $ABTS^{\bullet-}$ result from fast competing reactions between the various intermediates shown in Scheme 1.

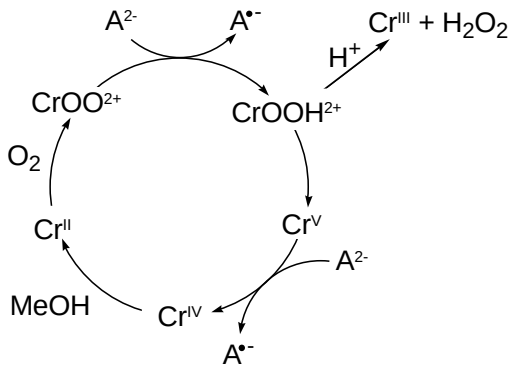

Scheme 2. Decomposition of $Cr_{aq}OOH^{2+}$ in the presence of O_2 and $ABTS^{2-}$ (Abbreviated as A^{2-})

The ready oxidation of H_2O_2 (2-e E° for O_2 / H_2O_2 = 0.78 V)[41] and $ABTS^{2-}$ (E° for $ABTS^{\bullet-}$ / $HABTS^{-}$ = 0.81 V)[36] by Cr(V) in acidic solutions defines the respective limits/estimates for 1-e and 2-e reduction potentials of Cr(V) as well.

The majority of work in this study was performed in acidic solutions where chromium reactants, products, and many of the intermediates are well characterized species. By extrapolating the results to higher, biologically relevant pH, one would predict that Cr(V) formation should be even more dominant as a decomposition route for $Cr_{aq}OOH^{2+}$. This was confirmed in an experiment at pH 5.5 (see Table 2), where a 0.10 mM solution of $Cr_{aq}OOH^{2+}$ decomposed in under a minute to yield 0.045 mM $HCrO_4^-$, *i.e.*, close to 70 % of the maximum amount possible on the basis of 1.5 : 1 stoichiometry ($[Cr_{aq}OOH^{2+}]_0$ / $[HCrO_4^-]_\infty$). The faster kinetics than that predicted by linear extrapolation from acidic pH are easily understood in terms of the greater reactivity of various hydrolytic forms of chromium at higher pH.

The chemistry of Scheme 1 thus appears inevitable under biological conditions, provided reductants are present that could play a role similar to that of methanol (E° (CH_3OH/CH_2O) = 0.232 V)[42] in our study. It is our contention that a number of

biological 2-electron reductants should be able to reduce $Cr_{aq}O^{2+}$ in the equivalent of eq 5. The most obvious candidate is NADH, which has a 2-electron reduction potential of -0.320 V at pH 7.[43] In fact, an analogue of this compound, 10-methyl-9,10-dihydroacridine, has been shown in our earlier work to reduce $Cr_{aq}O^{2+}$ to Cr_{aq}^{2+}.[44]

Conclusions

This work provides a consistent mechanistic picture for the decomposition of $Cr_{aq}OOH^{2+}$ and strong evidence for the involvement of Cr(V) as a key intermediate. The parallel acidolysis path yields Cr_{aq}^{3+} and H_2O_2. The observed kinetic $[H^+]$ dependence in Figure 4 in conjunction with yields of H_2O_2 in Figure 2 clearly identify acidolysis as a source of acid dependence. The kinetics of formation of Cr(V) are independent of $[H^+]$ and are represented by the intercept in Figure 4. Similar findings were obtained in our earlier studies of the conversion of N_4-macrocyclic complexes, $L(H_2O)CrOOH^{2+}$ (L = L^1 and L^2) to $L(OH)Cr^{V}O^{2+}$.[26] In that work, the lack of $[H^+]$ dependence was interpreted by the cancellation of two opposing effects: protonation of the hydroperoxide to generate water as the leaving group and deprotonation of *trans*-H_2O to stabilize the high-oxidation-state metal complex. These arguments are also applicable in the present case, although the exact chemical formula of aqueous Cr(V) initially formed under our conditions is less certain. Pulse radiolysis studies in the presence of formate provided support for an octahedral $H_3Cr^{V}O_4$ as the dominant form of Cr(V) in strongly acidic solutions.[34] The lack of acid dependence on the kinetics requires that the initial product carry the same charge as the starting hydroperoxido complex, *i.e.*, 2+. Different charges in the two studies can be reconciled if the initial product of the $Cr_{aq}OOH^{2+}$ reaction, presumably $(H_2O)_4Cr(O)(OH)^{2+}$, rapidly loses two more protons.

The decomposition of $Cr_{aq}OOH^{2+}$ at pH 5.5 is even faster than that in acidic solutions and generates higher amounts (close to 70 %) of chromate. Stabilizing macrocyclic ligands are clearly not required for this type of transformation. Thus, chromium in oxidation states 4+ and 5+, believed to be involved in the mechanism of carcinogenicity of chromate,[45-47] can be formed from aqueous Cr(III), an oxidation state traditionally assumed to be inert and safe for human consumption as a food supplement. The rapid formation of $Cr_{aq}OOH^{2+}$ from inorganic Cr(III) and H_2O_2, established in our earlier work,[23] followed by the facile decay of $Cr_{aq}OOH^{2+}$ to Cr(V) demonstrated here provide a feasible mechanism for the formation of Cr(V) from Cr(III) and H_2O_2, the latter being present naturally in aerobic organisms. We believe that this work adds substantial new evidence to that already available[46,48] in the literature questioning the safety of Cr(III) supplementation.

Acknowledgment

We are thankful to Drs. Pestovsky and Szajna-Fuller for insightful discussions and assistance with experimental work, and to Mr. Travis Witte and Dr. Houk's research group for help with ICP-MS analysis. This work was supported by a grant from National Science Foundation, CHE 0602183. Some of the work was conducted with the use of facilities at the Ames Laboratory.

References

(1) Burger, R. M. (2000) Nature of activated bleomycin. *Struct. Bonding (Berlin, Ger.)* 97, 287–303.
(2) Ogliaro, F., de Visser, S. P., Cohen, S., Sharma, P. K., and Shaik, S. *J. Am. Chem. Soc.* **2002**, *124*, 2806–2817
(3) Jin, S., Bryson, T. A., and Dawson, J. H. *J. Biol. Inorg. Chem.* **2004**, *9*, 644–653
(4) Ortiz de Montellano, P. R., and De Voss, J. J. *Nat. Prod. Rep.* **2002**, *19*, 477–493

(5) Denisov, I. G., Mak, P. J., Makris, T. M., Sligar, S. G., and Kincaid, J. R. *J. Phys. Chem. A* **2008**, *112*, 13172–13179
(6) Denisov, I. G., Dawson, J. H., Hager, L. P., and Sligar, S. G. *Biochem. Biophys. Res. Commun.* **2007**, *363*, 954–958
(7) Mairata i Payeras, A., Ho, R. Y. N., Fujita, M., and Que, L., Jr. *Chem. Eur. J.* **2004**, *10*, 4944–4953
(8) Koehntop, K. D., Rohde, J.-U., Costas, M., and Que, L., Jr. *Dalton Trans.* **2004**, 3191–3198
(9) Lehnert, N., Ho, R. Y. N., Que, L., Jr., and Solomon, E. I. *J. Am. Chem. Soc.* **2001**, *123*, 12802–12816
(10) Lehnert, N., Neese, F., Ho, R. Y. N., Que, L., Jr., and Solomon, E. I. *J. Am. Chem. Soc.* **2002**, *124*, 10810–10822
(11) Maiti, D., Narducci Sarjeant, A. A., and Karlin, K. D. *Inorg. Chem.* **2008**, *47*, 8736–8747
(12) Li, L., Narducci Sarjeant, A. A., and Karlin, K. D. *Inorg. Chem.* **2006**, *45*, 7160–7172
(13) Park, M. J., Lee, J., Suh, Y., Kim, J., and Nam, W. *J. Am. Chem. Soc.* **2006**, *128*, 2630–2634
(14) Denney, M. C., Smythe, N. A., Cetto, K. L., Kemp, R. A., and Goldberg, K. I. *J. Am. Chem. Soc.* **2006**, *128*, 2508–2509
(15) Szajna-Fuller, E., and Bakac, A. *Inorg. Chem.* **2010**, *49*, 781–785
(16) Rybak-Akimova, E. V. (2010) Mechanism of Oxygen Binding and Activation at Transition Metal Centers, in *Physical Inorganic Chemistry: Reactions, Processes, and Applications* (Bakac, A., Ed.) pp 109 - 188, Wiley, Hoboken, NJ
(17) Bakac, A. *Prog. Inorg. Chem.* **1995**, *43*, 267–351
(18) Bakac, A. *Coord. Chem. Rev.* **2006**, *250*, 2046–2058
(19) Bakac, A. *Inorg. Chem.* **2010**, *49*, 3584–3593
(20) Bakac, A., Assink, B., Espenson, J. H., and Wang, W.-D. *Inorg. Chem.* **1996**, *35*, 788–790
(21) Wang, W.-D., Bakac, A., and Espenson, J. H. *Inorg. Chem.* **1993**, *32*, 5034–5039
(22) Cheng, M., Song, W., and Bakac, A. *Eur. J. Inorg. Chem.* **2008**, 4687–4689
(23) Song, W., and Bakac, A. *Inorg. Chem.* **2010**, *49*, 150–156
(24) Bakac, A., and Wang, W.-D. *J. Am. Chem. Soc.* **1996**, *118*, 10325–10326
(25) Pestovsky, O., and Bakac, A. *J. Am. Chem. Soc.* **2003**, *125*, 14714–14715
(26) Pestovsky, O., and Bakac, A. *Dalton Trans.* **2005**, 556–560
(27) Lemma, K., Ellern, A., and Bakac, A. *Dalton Trans.* **2006**, 58–63
(28) Bakac, A. *J. Am. Chem. Soc.* **2000**, *122*, 1092–1097
(29) Liebhafsky, H. A., and Mohammed, A. *J. Am. Chem. Soc.* **1933**, *55*, 3977–3986
(30) Awtrey, A. D., and Connick, R. E. *J. Am. Chem. Soc.* **1951**, *73*, 1842–1843
(31) Pestovsky, O., and Bakac, A. *J. Am. Chem. Soc.* **2004**, *126*, 13757–13764
(32) Gaswick, D. C., and Krueger, J. H. *J. Am. Chem. Soc.* **1969**, *91*, 2240–2244
(33) Bakac, A. *Adv. Inorg. Chem.* **2004**, *55*, 1–59
(34) Buxton, G. V., and Djouider, F. *J. Chem. Soc., Faraday Trans.* **1996**, *92*, 4173–4176
(35) Bakac, A., and Wang, W. D. *Inorg. Chim. Acta* **2000**, *297*, 27–35

(36) Scott, S. L., Chen, W. -J., Bakac, A., and Espenson, J. H. *J. Phys. Chem.* **1993**, *97*, 6710–6714
(37) Krumpolc, M., DeBoer, B. G., and Rocek, J. *J. Am. Chem. Soc.* **1978**, *100*, 145–153
(38) Wang, W. -D., Bakac, A., and Espenson, J. H. *Inorg. Chem.* **1993**, *32*, 2005–2009
(39) Bakac, A., and Espenson, J. H. *Inorg. Chem.* **1983**, *22*, 779–783
(40) Nemes, A., and Bakac, A. *Inorg. Chem.* **2001**, *40*, 2720–2724
(41) Sawyer, D. T. (1988) The Chemistry and Activation of Dioxygen Species (O_2, O_2^-, and HOOH) in Biology, in *Oxygen Complexes and Oxygen Activation by Transition Metals* (Martell, A. E., and Sawyer, D. T., Eds.) pp 131-148, Plenum Press, New York
(42) Bard, A. J., Parsons, R., and Jordan, J. (1985) *Standard Potentials in Aqueous Solution*, p 196, Marcel Dekker, New York
(43) Stryer, L. (1988) *Biochemistry*, 3rd ed., p 401, W. H. Freeman and Company, New York
(44) Pestovsky, O., Bakac, A., and Espenson, J. H. *J. Am. Chem. Soc.* **1998**, *120*, 13422–13428
(45) Farrell, R. P., Judd, R. J., Lay, P. A., Dixon, N. E., Baker, R. S. U., and Bonin, A. M. *Chem. Res. Toxicol.* **1989**, *2*, 227–229
(46) Levina, A., and Lay, P. A. *Coord. Chem. Rev.* **2005**, *249*, 281– 298
(47) Bose, R. N., Fonkeng, B. S., Moghaddas, S., and Stroup, D. *Nucleic Acids Res.* **1998**, *26*, 1588–1596
(48) Vincent, J. B. *Acc. Chem. Res.* **2000**, *33*, 503–510

CHAPTER 2

PREPARATION AND REACTIVITY OF MACROCYCLIC RHODIUM(III) ALKYL COMPLEXES

Jack M. Carraher, Arkady Ellern, and Andreja Bakac

A paper published in *Inorganica Chimica Acta*[*]

Abstract

Macrocyclic rhodium(II) complexes $LRh(H_2O)^{2+}$ (L = L^1= cyclam and L^2 = *meso*-Me_6-cyclam) react with alkyl hydroperoxides $RC(CH_3)_2OOH$ to generate the corresponding rhodium(III) alkyls $L(H_2O)RhR^{2+}$ (R = CH_3, C_2H_5, $PhCH_2$). Methyl and benzyl complexes can also be prepared by bimolecular group transfer from alkyl cobaloximes $(dmgH)_2(H_2O)CoR$ and $(dmgBF_2)_2(H_2O)CoR$ (R = CH_3, $PhCH_2$) to $LRh(H_2O)^{2+}$. The new complexes were characterized by solution NMR and by crystal structure analysis. They exhibit great stability in aqueous solution at room temperature, but undergo efficient Rh-C bond cleavage upon photolysis.

Introduction

Spectroscopic and crystallographic characterization of rhodium(III) complexes is, in general, greatly facilitated by substitutional and redox inertness of Rh(III). Inorganic complexes of saturated N_4 macrocycles[1] clearly belong in this category and are considered especially robust. Recent work has shown, however, that this platform in

[*] Carraher, Jack M.; Ellern, Arkady; Bakac, Andreja *Inorg. Chim. Acta*, **2014**, *409*, 254-258

combination with small molecules (O_2 and $^{\bullet}NO$) can be used to generate and stabilize complexes in nonstandard oxidation states. For example, the nitrosyl $L^2(H_2O)RhNO^{2+}$, formally a Rh(III) complex of NO^-, is oxidized by $Ru(bpy)_3^{3+}$ to $L^2(H_2O)RhNO^{3+}$, a $\{MNO\}^7$ species in Enemark-Feltham notation.[2] This compound is highly oxidizing (E^0 = 1.31 V)[3] and persists in acidic aqueous solutions for over a minute. The dioxygen analog, $L^2(H_2O)RhOO^{3+}$, was not observed directly, but its presence was inferred from the kinetics and products of the $L^2(H_2O)RhOOH^{2+}$ / I^- reaction.[4] It was concluded that $L^2(H_2O)RhOO^{3+}$ has a sufficiently long lifetime in aqueous solutions to engage in bimolecular reactions with reducing substrates.[4]

We have now extended our work with macrocyclic rhodium(III) to alkyl complexes. The goal is to prepare and characterize such compounds, and examine their reactivity in thermal reactions, especially those involving redox transformations, and as potential photochemical sources of alkyl radicals. Despite the abundance of alkylmetal complexes that release radicals upon photolysis, none of them are problem-free. Alkylcobaloximes, for example, release free $dmgH_2$ that precipitates from aqueous solutions and complicates spectroscopic studies. Also, $dmgH_2$ is not chemically inert and will engage in substitution and redox reactions with various substrates. Clearly, alkylrhodoximes[5,6] suffer from the same downsides as their cobalt analogs.

A series of macrocyclic cobalt complexes $L^1(H_2O)CoR^{2+}$ (L^1 = cyclam) produce alkyl radicals efficiently upon photolysis with visible light.[7] Unfortunately, the benzyl complex is unstable and decays by thermal Co-C bond homolysis in seconds,[8] and branched alkyls (2-propyl, 2-butyl) were too unstable to isolate.[9] As part of our mechanistic studies on alkyl group transfer to Rh(II),[10] we have now prepared several

alkylrhodium complexes of saturated macrocycles L^1 and L^2, and found them to be good photochemical sources of alkyl radicals. These complexes are thermally more stable than the cobalt analogs, and the use of saturated macrocyclic equatorial ligands eliminates problems encountered previously with $dmgH_2$. The results are described herein.

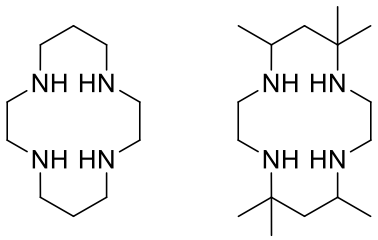

L^1 L^2

Experimental

Materials

Acidic aqueous solutions of $L(H_2O)Rh^{2+}$ complexes (L = L^1, L^2) were generated by photolysis of the corresponding hydrides $L(H_2O)RhH^{2+}$.[11] Solid perchlorate and trifluoromethanesulfonate salts of $L(H_2O)RhH^{2+}$ were prepared as described previously.[11] Alkyl cobalt complexes $(dmgH)_2(H_2O)CoR$ ($dmgH_2$ = dimethylglyoxime) and $(dmgBF_2)_2(H_2O)CoR$ were prepared by published procedures.[12] The hydroperoxides $C_2H_5C(CH_3)_2OOH$ and $PhCH_2C(CH_3)_2OOH$ were synthesized from the corresponding alcohols,[13] and $CH_3C(CH_3)_2OOH$ (70 % in H_2O) was purchased from Sigma-Aldrich. D_2O (99.9 % D) and $Cr(ClO_4)_3$,6 H_2O (both Sigma-Aldrich), $NaClO_4$, and 70 % $HClO_4$ (both Fisher) were used as received. Water was purified with a Barnstead EASYpure III UV UF system.

Methods and Instrumentation

Photolyses were performed in standard 1-cm square fluorescence quartz cells in Luzchem LZC-5 photoreactor at 313 nm. Gaseous products were analyzed with an Agilent Technologies 7890A gas chromatograph equipped with an FID detector and a 0.320 mm I.D. capillary column (GS-GASPRO 113-4312, 15 m). Nitrogen flow rate was 25 cm^3/s. The split injector (1 : 40) was kept at 200 $^{\circ}C$ and FID detector at 350 $^{\circ}C$. Initial oven temperature was 40 $^{\circ}C$, increased by 10 $^{\circ}C$ / min, and held at a final temperature of 200 $^{\circ}C$ for 1 min. Prior to injection of the gas samples, the solutions were shaken vigorously to expel gases into the headspace. Standard mixtures of ethane, ethylene and butane in aqueous solution for GC calibration were prepared by the reaction of *tert*-amyl hydroperoxide and excess $Fe(H_2O)_6^{2+}$ as described previously.[14] UV-Vis spectra and kinetic data were collected with a Shimadzu UV-3101PC spectrophotometer. Kinetic data were fitted with KaleidaGraph 4.0 software.

^1H NMR spectra were collected with a Bruker 600 MHz NMR (AVIII600). Heteronuclear Single Quantum Coherence (HSQC) spectra were acquired with 256 slices at 8 scans per slice for a total acquisition time of 5.1 ms. Elemental (C, H, N) analysis used a PE 2100 Series II combustion analyzer (Perkin Elmer Inc., Waltham, MA) with acetanilide standard (Perkin Elmer). Combustion and reduction temperatures were 925 $^{\circ}C$ and 640 $^{\circ}C$. The precision for each element is ± 0.3 %. Rhodium concentrations for the determination of molar absorptivities were obtained by ICP-MS Element 1 by Thermo Finnigan.

Preparation of $L(H_2O)RhR^{2+}$ Complexes by Hydroperoxide Method

Solutions of $L(H_2O)RhR^{2+}$ (L = L^1, L^2) were generated from $RC(CH_3)_2OOH$ (R = CH_3, C_2H_5, $PhCH_2$) and two equivalents of $L(H_2O)Rh^{2+}$ in 1 - 2 mM concentration range. Alkylrhodium products were purified by cation exchange on Sephadex C-25 and eluted with 0.4 M $HClO_4$ or 0.4 M CF_3SO_3H. The yields were typically 30 - 40 %, but increased up to 70% in spectrophotometric titrations with more dilute solutions.

*$L^1(H_2O)RhCH_3^{2+}$ (*solution*)* UV λ_{max} / nm (ε / M^{-1} cm^{-1}): 260 (300), 297 (310). ^{1}H NMR (600 MHz, 298 K, D_2O, pH 6.8): δ 4.46 (br s N*H*), 4.17 (br s N*H*), 3.34 (m), 3.20 (m), 2.99 (m), 2.86 (m), 2.65 (m), 2.19 (m), 1.69 (q), 1.18 (d, ^{2}J[Rh,H] = 2.4 Hz, Rh-*CH_3*). Two minor isomeric methyl rhodium species are also present, with Rh-*CH_3* resonances at 1.14 (d) and 1.08 (d), see later.

*$L^1(H_2O)RhCH_2CH_3^{2+}$ (*solution*)* UV λ_{max} / nm (ε / M^{-1} cm^{-1}): 261 (440), 301 (sh, 290), Figure S1. ^{1}H NMR (600 MHz, 298 K, D_2O): δ 3.36 – 2.68 (m), 2.32 (m), 2.21 (m), 1.98 (br, Rh-*CH_2*-CH_3), 1.82 (m), 0.73 (t, ^{3}J[H,H] = 7.4 Hz, Rh-CH_2-*CH_3*), Figure S2. The triplet at 0.68 ppm is assigned to Rh-CH_2-*CH_3* of an isomeric ethyl rhodium species, see later.

$[L^1(H_2O)RhCH_2Ph](ClO_4)_2$ Anal. Calcd for $C_{17}H_{33}N_4RhCl_2O_9$: C, 33.40; H, 5.44; N, 9.17. Found: C, 33.28; H, 4.95; N, 8.92. UV (0.1 M $HClO_4$) λ_{max} / nm (ε / M^{-1} cm^{-1}): 258 (14000), Figure S3. ^{1}H NMR (600 MHz, 298 K, D_2O): δ 7.45 – 7.35 (m, Rh-CH_2-*C_6H_5*), 4.99 (s, N*H*), 4.34 (s, N*H*), 3.98 (s, N*H*), 3.41 (dd, 1H, ^{2}J[Rh,H] = 3.6 Hz, ^{2}J[H,H] = 9 Hz, Rh-*CH_2*-Ph), 3.33 (dd, 1H, Rh-*CH_2*-Ph), 3.24 (d), 3.09 (m), 3.00 (m), 2.94 (m), 2.66 (m), 2.22 (br s), 2.12 (m), 1.94 (d), 1.72 (m), 1.24 (q), Figure 5. ^{13}C NMR (600

MHz, 298 K, D_2O, pH 6.8: δ 130.31, 128.20, and 126.46 (Rh-CH_2-C_6H_5), 52.96, 51.11, 46.75, 42.71, 28.97, 24.79 (macrocyclic ligand), 18.45 (Rh-CH_2-Ph). The cross peaks in HSQC spectra of $L^1(H_2O)RhCH_2Ph^{2+}$ and $L^1(H_2O)RhH^{2+}$, Figure S4, clearly identify chemical shifts of the benzyl group and the cyclam ligand in the aliphatic range. More detailed discussion of the NMR spectra is presented later.

$[L^2(H_2O)RhCH_3](ClO_4)_2$ Anal. Calcd for ($RhC_{17}H_{41}N_4Cl_2O_9$): C, 33.02; H, 6.52; N, 9.06. Found: C, 32.69; H, 6.46; N, 8.96. UV λ_{max} / nm (ε / □M^{-1} cm^{-1}): 268 (360), 301 (360). ^{1}H NMR (600 MHz, 298 K, D_2O): δ 4.05 (br s, N*H*), 3.97 (br s, N*H*), 3.66 (d), 3.21 (m), 3.13 (m), 2.99 (m), 2.20 – 2.60 (m), 1.82 (dd), 1.62 (m), 1.54 (m), 1.33 (s, 6H Rh-CH_3 and L^2-CH_3), 1.31 (s, 3H), 1.27 (s, 3H), 1.26 (s, 3H), 1.21 (d, 3H), 1.19 (s, 3H), Figure S5. The spectrum of $L^2(H_2O)RhH^{2+}$ is shown for comparison in Figure S6.

Preparation of $L(H_2O)RhR^{2+}$ by Alkyl Group Transfer

A solution of $L^1(H_2O)RhCH_2Ph^{2+}$ was prepared by addition of 100 mL of 2 mM $L(H_2O)Rh^{2+}$ to 0.1 g (ca 3 mmol) of solid $(dmgH)_2(H_2O)CoCH_2Ph$ or $(dmgBF_2)_2(H_2O)CoCH_2Ph$. The mixture was allowed to react for 18 hours in the dark under argon, followed by filtration to remove solid $dmgH_2$ or $Co(dmgBF_2)_2$, respectively. The product $L^1(H_2O)RhCH_2Ph^{2+}$ was purified by cation exchange on Sephadex C25, eluted with 0.4 M $HClO_4$ and concentrated by rotary evaporation. Addition of solid $NaClO_4$ yielded the white solid of $[L^1(H_2O)RhCH_2Ph](ClO_4)_2$ which was filtered and air-dried. Yield: 17%.

Solutions of $L^1(H_2O)RhCH_3^{2+}$ and $L^2(H_2O)RhCH_3^{2+}$ were prepared by a method analogous to that used for $L^1(H_2O)RhCH_2Ph^{2+}$ except that methyl transfer from $(dmgH)_2(H_2O)CoCH_3$ was complete as soon as all of the alkyl cobaloxime was dissolved.

The yield of methylrhodium complexes was 80 %. Perchlorate and trifluoromethane sulfonate salts of $L^1(H_2O)RhCH_3^{2+}$ were too soluble in water to be isolated as solids, but $[L^2(H_2O)RhCH_3](CF_3SO_3)_2$ precipitated upon addition of solid $LiCF_3SO_3$ to a solution that was first concentrated by rotary evaporation. The white crystals were washed with CH_2Cl_2, hexanes and ice-cold water, and air-dried. The UV-Vis and ^1H NMR spectra were identical to those given above for the compounds obtained by the hydroperoxide method.

Crystal Growth and Structure Determination

A solid sample of $[L^2(H_2O)RhCH_3](CF_3SO_3)_2$ (20 mg) was dissolved in warm 1 mM $HClO_4$. The solution was cooled, filtered, and transferred to an NMR tube. Good quality crystals of $[L^2(H_2O)RhCH_3](ClO_4)_2$ grew in a refrigerator in four days. Similarly, solid $[L^1(H_2O)RhCH_2Ph](ClO_4)_2$ was dissolved in a minimum amount of warm water (~ 30 °C) and allowed to crystallize in a refrigerator.

A crystal suitable for X-Ray analysis was selected under the microscope and covered with PARATONE oil. The sample was mounted in a diffractometer under the stream of cold nitrogen. The full sphere X-ray intensity data were measured till resolution 0.71 Å (0.5 deg. width ω-scan, 15 sec per frame) using a BRUKER APEX2 CCD diffractometer. The frames were integrated using a narrow-frame algorithm. Data were corrected for absorption effects using the multi-scan method (SADABS).[15,16] Structures were solved by direct methods. All non-hydrogen atoms were refined in full-matrix anisotropic approximation based on F^2. All expected hydrogen atoms were placed at calculated positions and were refined in isotropic approximation using the "riding" model. The $U_{iso}(H)$ values were set at 1.2 - 1.5 times the U_{eq} value of the carrier atom. All

calculations were performed using APEX II software suite.[17] CCDC 938294-938295 contains the supplementary crystallographic data for this paper. These data can be obtained free of charge from The Cambridge Crystallographic Data Centre via www.ccdc.cam.ac.uk/data_request/cif.

X-ray crystal structures for the cations *trans*-$[L^2(H_2O)RhCH_3]^{2+}$ and *trans*-$[L^1(H_2O)RhCH_2Ph]^{2+}$ are shown in Figures 1 and 2, respectively.

Results and Discussion

Reactions of $L(H_2O)Rh^{2+}$ with Alkyl Hydroperoxides

The reactions between submillimolar concentrations of $CH_3C(CH_3)_2OOH$ and $L(H_2O)Rh^{2+}$ (L = L^1, L^2) were nearly complete in mixing time and too fast for kinetic measurements by UV-Vis. All of the observations are consistent with the sequence in eq 1 - 2 written in analogy with reactions of other reduced transition metal complexes[18,19] but encumbered with side reactions owing to the low concentrations of photochemically generated $L(H_2O)Rh^{2+}$. Slightly more than two equivalents of $L(H_2O)Rh^{2+}$ per mole of hydroperoxide were consumed, as determined from the UV-Vis spectra acquired during stepwise addition of hydroperoxide to $L(H_2O)Rh^{2+}$. UV-Vis spectra of purified solutions of $L(H_2O)RhCH_3^{2+}$ (L = L^1 and L^2) are shown in Figure 3, and ^{1}H NMR in Figure 4.

$$L(H_2O)Rh^{2+} + CH_3C(CH_3)_2OOH + H^+ \rightarrow LRh(H_2O)_2^{3+} + {}^{\bullet}CH_3 + (CH_3)_2CO \quad (1)$$

$$L(H_2O)Rh^{2+} + {}^{\bullet}CH_3 \rightarrow L(H_2O)RhCH_3^{2+} \qquad \text{fast} \qquad (2)$$

As already commented in the Experimental, the yields of $L(H_2O)RhCH_3^{2+}$ were smaller than expected for the ideal 2 : 1 stoichiometry of eq 1 - 2. Also, methane and ethane were identified by GC immediately after completion of the reaction. The ratio of

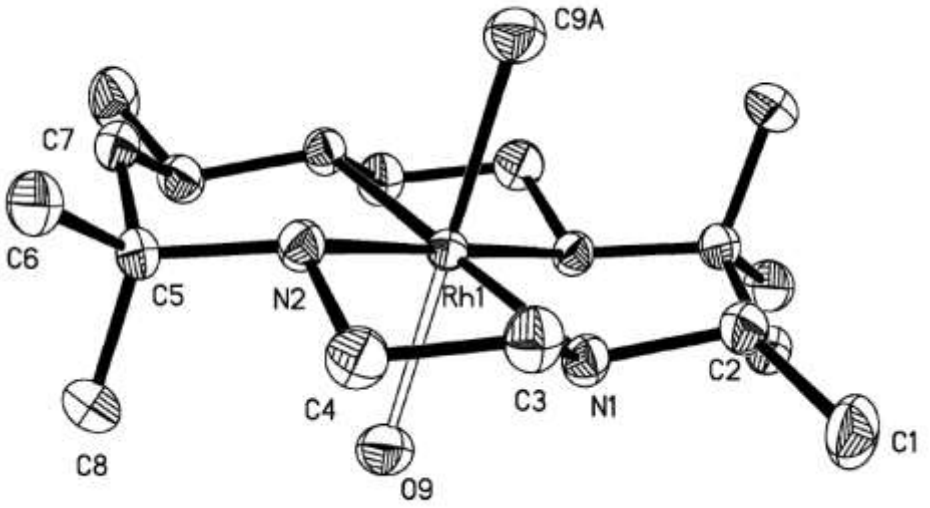

Figure 1. ORTEP drawing of the cation *trans*-$[L^2(H_2O)RhCH_3]^{2+}$ at 50 % probability level. Hydrogen atoms are not shown. Bond lengths/Å: Rh1-N1, 2.073(2); Rh1-N2, 2.090(2); Rh1-C9A, 2.216(3); Rh1-O9, 2.216(3). Angles/deg: N1-Rh1-N2, 84.62(9); N1-Rh1-O9, 93.57(10); N1-Rh1-C9A, 86.43(10); N2-Rh1-O9, 84.96(10); N2-Rh1-C9A, 95.04(10).

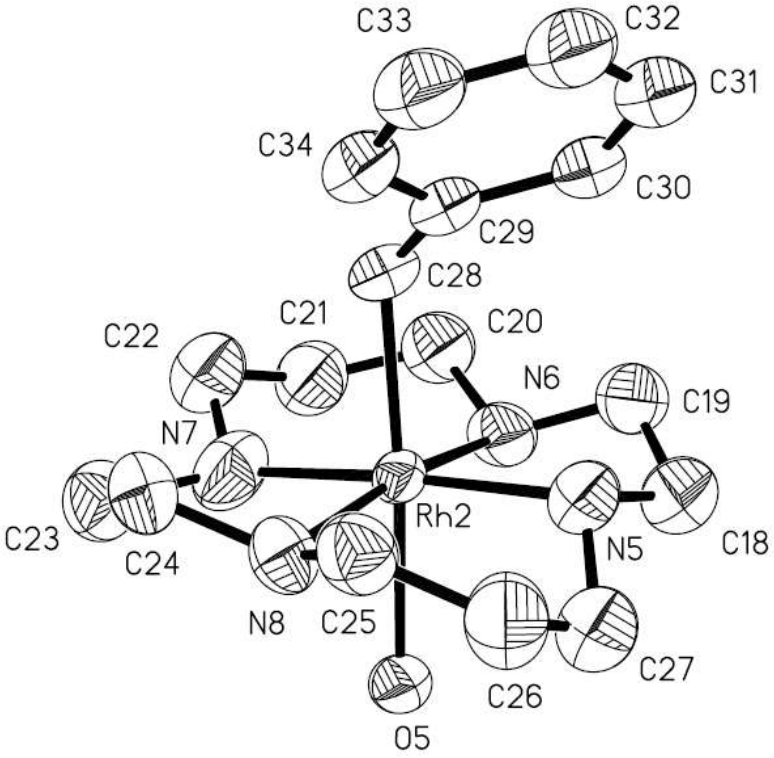

Figure 2. ORTEP drawing of the cation *trans*-$[L^1(H_2O)RhCH_2Ph]^{2+}$ at 50 % probability level. Hydrogen atoms are not shown. Bond lengths/Å: Rh2-N5, 2.055(7); Rh2-N6, 2.057(6); Rh2-N7, 2.045(8); Rh2-N8 2.050(6); Rh2-C28, 2.106(7); Rh2-O5, 2.299(5); C28-C29, 1.472(12). Angles/deg: N5-Rh2-N7, 176.0(3); N5-Rh2-N8, 94.5(3); N6-Rh2-N7, 93.8(3); N5-Rh2-C28, 91.7(3); O5-Rh2-C28, 173.7(3); Rh2-C28-C29, 122.9(5).

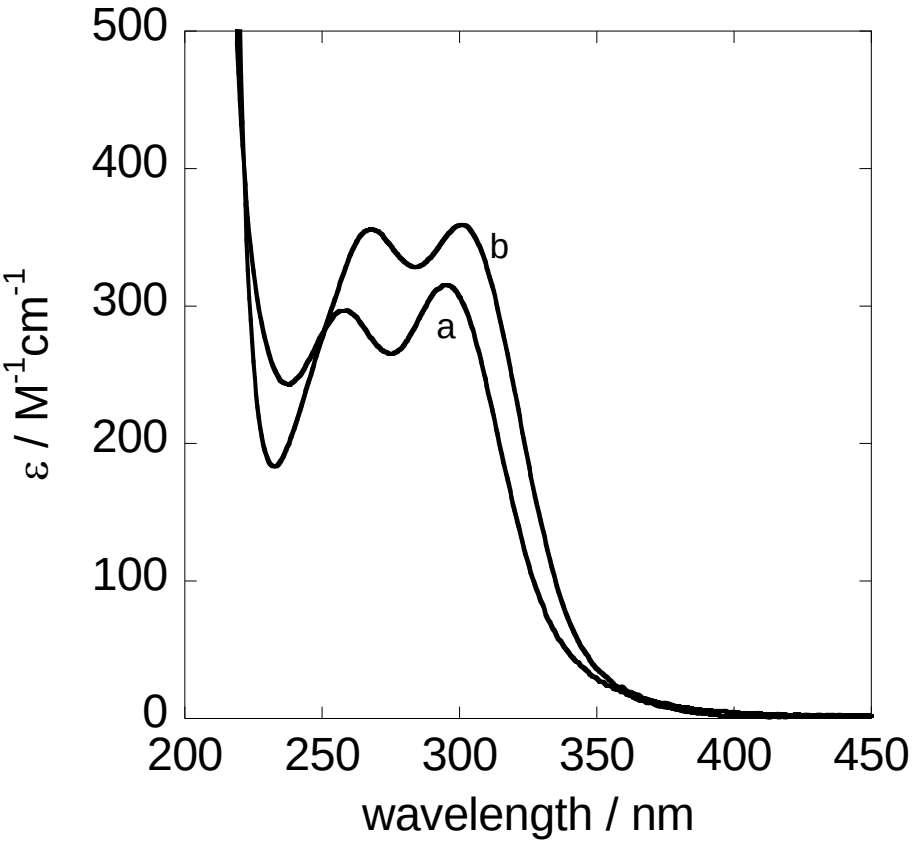

Figure 3. UV spectra of $L^1(H_2O)RhCH_3^{2+}$ (a) and $L^2(H_2O)RhCH_3^{2+}$ (b) in acidic aqueous solution.

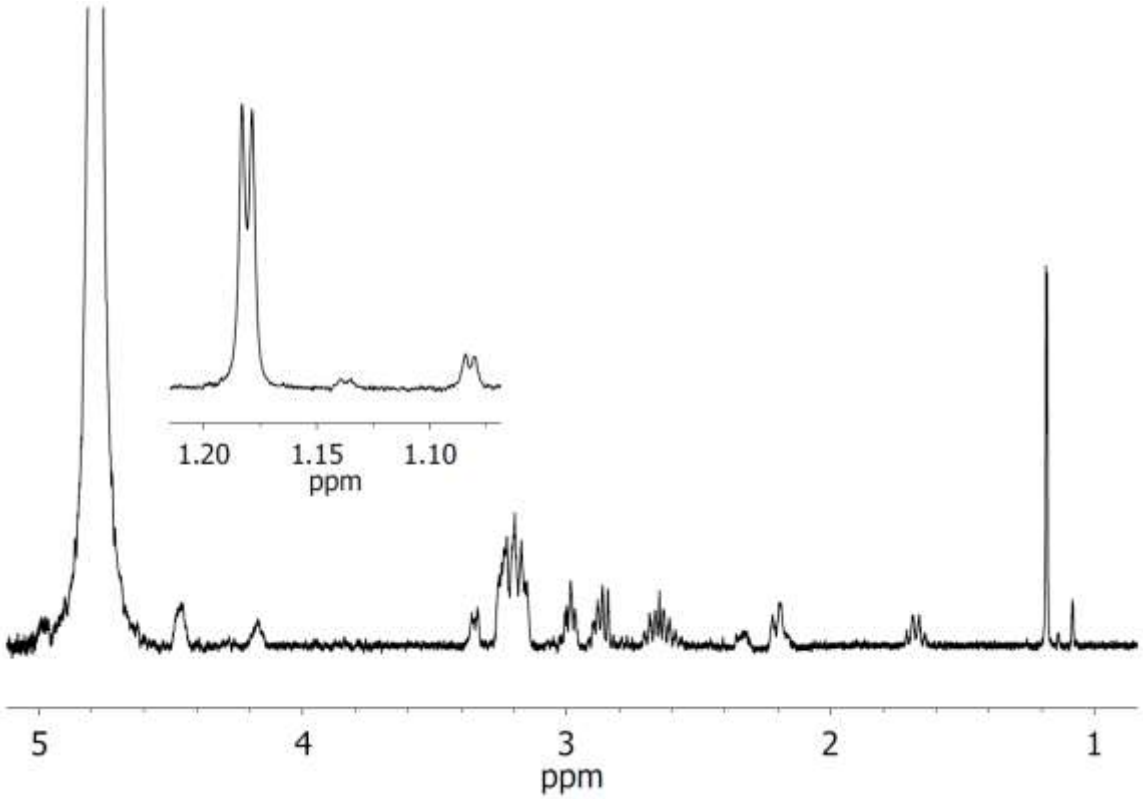

Figure 4. ^{1}H NMR of $L^{1}RhCH_3^{2+}$, 600 MHz, D_2O. Inset: Rh-$\underline{CH_3}$ isomers 1.18 ppm, 1.14 ppm, and 1.08 ppm. $^{2}J[Rh,H] = 2.4$ Hz

the two alkanes was somewhat dependent on absolute concentrations of the reagents, and on the length of time that $L(H_2O)RhH^{2+}$ was photolyzed to generate $L(H_2O)Rh^{2+}$. The observed gaseous products were most likely formed by radical dimerization (eq 3) and hydrogen abstraction from $L(H_2O)RhH^{2+}$ [20] (eq 4) and/or from $CH_3C(CH_3)_2OOH$ (eq 5).[21]

$$2^{\bullet}CH_3 \rightarrow C_2H_6 \qquad (3)$$

$$^{\bullet}CH_3 + L(H_2O)RhH^{2+} \rightarrow CH_4 + L(H_2O)Rh^{2+} \qquad (4)$$

$$^{\bullet}CH_3 + CH_3C(CH_3)_2OOH \rightarrow CH_4 + CH_3C(CH_3)_2O^{\bullet} \qquad (5)$$

The reaction of $L^1(H_2O)Rh^{2+}$ with $C_2H_5C(CH_3)_2OOH$ exhibited an approximate 3 : 1 stoichiometry. Ethane, ethylene and traces of butane were formed in addition to $L^1(H_2O)RhC_2H_5^{2+}$. The ratio, $[C_2H_6] : [C_2H_4] : [C_4H_{10}] = 1 : 0.3 : 0.004$, differs greatly from that expected for ethyl radical self-reaction (1 : 1 : 0.35).[22] The source of ethane is again believed to be hydrogen atom abstraction from rhodium hydride and/or the hydroperoxide, analogous to the reactions of methyl radicals in eq 4 and 5. Hydrogen atom transfer in the opposite direction, *i.e.*, from ethyl radicals to $L^1(H_2O)Rh^{2+}$, eq 6, is the most plausible source of C_2H_4. This reaction regenerates the hydride which reenters the equivalent of reaction 4. Hydrogen atom abstraction from a coordinated ethyl in $(dmgH)_2(H_2O)CoC_2H_5$ to generate $L^1(H_2O)RhH^{2+}$ and ethylene has been demonstrated in our recent work,[10] and adds credibility to the proposed reaction 6. Also, radical self-reactions are shown to be unimportant by finding only negligible amounts of butane. Similarly, the $L^1(H_2O)Rh^{2+}$ / $PhCH_2C(CH_3)_2OOH$ reaction yielded no bibenzyl, the main product of the self-reaction of benzyl radicals.

$$^{\bullet}C_2H_5 + L^1(H_2O)Rh^{2+} \rightarrow C_2H_4 + L^1(H_2O)RhH^{2+} \quad (6)$$

Reactions of $L(H_2O)Rh^{2+}$ with Cobalt Alkyls

Yellow solutions of submillimolar $(dmgH)_2(H_2O)CoCH_3$ turned colorless immediately upon mixing with equimolar amounts of $L^1(H_2O)Rh^{2+}$. This color change is associated with rapid methyl group transfer from cobalt to $L^1(H_2O)Rh^{2+}$, eq 7.[10] The 1:1 stoichiometry was determined from the absorbance decrease at the 440 nm maximum of $(dmgH)_2(H_2O)CoCH_3$.

Product solutions exhibited shoulders near 300 nm and 340 nm, and intense absorption below 300 nm attributable to free $dmgH_2$ formed by dissociation from Co(II), eq 8. As shown in the reactions with alkyl hydroperoxides, the shoulder at 300 nm is associated with the Rh-alkyl bond. The 340 nm feature is characteristic for a species generated from $L^1(H_2O)Rh^{2+}$ and $dmgH_2$ in a slow step following methyl transfer in experiments with excess $L^1(H_2O)Rh^{2+}$.[10] This was confirmed in direct experiments with genuine $dmgH_2$ and $L^1(H_2O)Rh^{2+}$. The 340 nm species is extremely stable both thermally and photochemically, and did not interfere with any of the chemistry in this work.

$$L^1(H_2O)Rh^{2+} + (dmgH)_2(H_2O)CoCH_3 \rightarrow L^1(H_2O)RhCH_3^{2+} + (dmgH)_2(H_2O)Co \quad (7)$$

$$(dmgH)_2(H_2O)Co + 2H^+ + 5H_2O \rightarrow Co(H_2O)_6^{2+} + 2dmgH_2 \quad \text{fast} \quad (8)$$

In some experiments, $(dmgH)_2(H_2O)CoCH_3$ was replaced with $(dmgBF_2)_2(H_2O)CoCH_3$.[23] Alkyl transfer from the latter generates $(dmgBF_2)_2Co(H_2O)_2$ which does not dissociate dioxime ligands and was therefore expected to generate products free of the 340 nm species. Still, small amounts of this species were again observed. In subsequent preparations, the $(dmgBF_2)_2(H_2O)_2Co$ product was removed by

filtration as soon as the reaction was over to minimize its availability in follow-up chemistry.

Benzylcobaloxime also reacts with $L^1(H_2O)Rh^{2+}$ by alkyl group transfer, but the reaction is quite slow. Owing to long reaction times (about 18 hours for millimolar concentrations of both reactants) and extreme air-sensitivity of small concentrations of $L^1(H_2O)Rh^{2+}$, the yields of $L^1(H_2O)RhCH_2Ph^{2+}$ were poor (17 %).

Reactions of $L^1(H_2O)Rh^{2+}$ with ethyl, isopropyl, and isobutyl cobaloximes were completed in several minutes or less, but did not produce alkyl rhodium complexes. As described elsewhere,[10] those reactions take place by hydrogen atom transfer from the alkyl group and produce rhodium hydride and α-olefins.

^{1}H NMR

The methyl group of $L^1(H_2O)RhCH_3^{2+}$ appears as a doublet at 1.18 ppm, Figure 4. There are also two weak doublets at 1.08 ppm and 1.13 ppm that persist through multiple recrystallizations of the perchlorate salt and do not change even after prolonged aging of the NMR solutions. We associate these signals with small amounts of isomeric methylrhodium complexes containing the macrocyclic ligand in different conformations.[24-26] The change in stereochemistry around nitrogen most likely takes place at rhodium(II) stage, similar to other cases of conformational changes that occur at labile metal centers.[27,28] The parent hydride exhibits only one doublet in the hydride region, confirming the presence of a single, RRSS conformer,[29] Figure S7.

The aliphatic region in ^{1}H NMR of $L^2(H_2O)RhCH_3^{2+}$, Figure S5, is similar to that of L^2RhH^{2+} shown in Figure S6. The signal for Rh-*CH*$_3$ is at 1.33 ppm and coincides with the signal for one of the six L^2 methyl groups as deduced from integration data. Also, the

entire 1.19 – 2.35 ppm region integrates to 18 H for $L^2(H_2O)RhH^{2+}$, and 21 H for $L^2(H_2O)RhCH_3^{2+}$.

The resonances for ethyl group in $L^1(H_2O)RhC_2H_5^{2+}$ are found at 0.73 ppm (t, $^3J[H,H]$ = 7.8 Hz, CH_3), and 1.98 ppm (br, CH_2), Figure S2. The weak resonance at 0.68 ppm is again attributed to an isomeric ethyl rhodium species. In the related ethyl rhodoxime, the ethyl signals are found at 0.59 ppm (3H) and 1.24 ppm (2 H)[5], shifted upfield relative to L^1 complexes in the present work owing to unsaturation in the oxime ligand.

^{1}H NMR of $L^1RhCH_2Ph^{2+}$ is shown in Figure 5. The *CH*$_2$-Ph signals appear as two sets of doublets at 3.41 and 3.33 ppm. This assignment is confirmed by the cross peaks in HSQC spectra, Figure S4. The observation of two signals indicates hindered rotation around either Rh-C or C-C bond resulting in nonequivalency of the two methylene hydrogens. The signal from each hydrogen is split by the geminal proton, $^2J[H,H]$ = 9 Hz, and by the rhodium, $^2J[Rh,H]$ = 3.6 Hz. Similar splitting patterns have been observed at low temperatures in various substituted cobaloximes[30,31] and at room temperature for more sterically encumbered *ortho*-xylyl bridged dicobaloximes.[32] However, the benzyl rhodium in this work differs from the cobalt examples in that there is no unsaturation in the macrocyclic L^1 ligand that might result in π - π interactions with the benzene ring,[31] and there are no substituents on the ring that should lead to hindered rotation around the C-C bond.[31,33] It appears that the nonequivalency of the two hydrogens stems from steric features of the highly ruffled, saturated L^1 ligand and its interactions with the benzyl group. The severity of steric interactions in the analogous

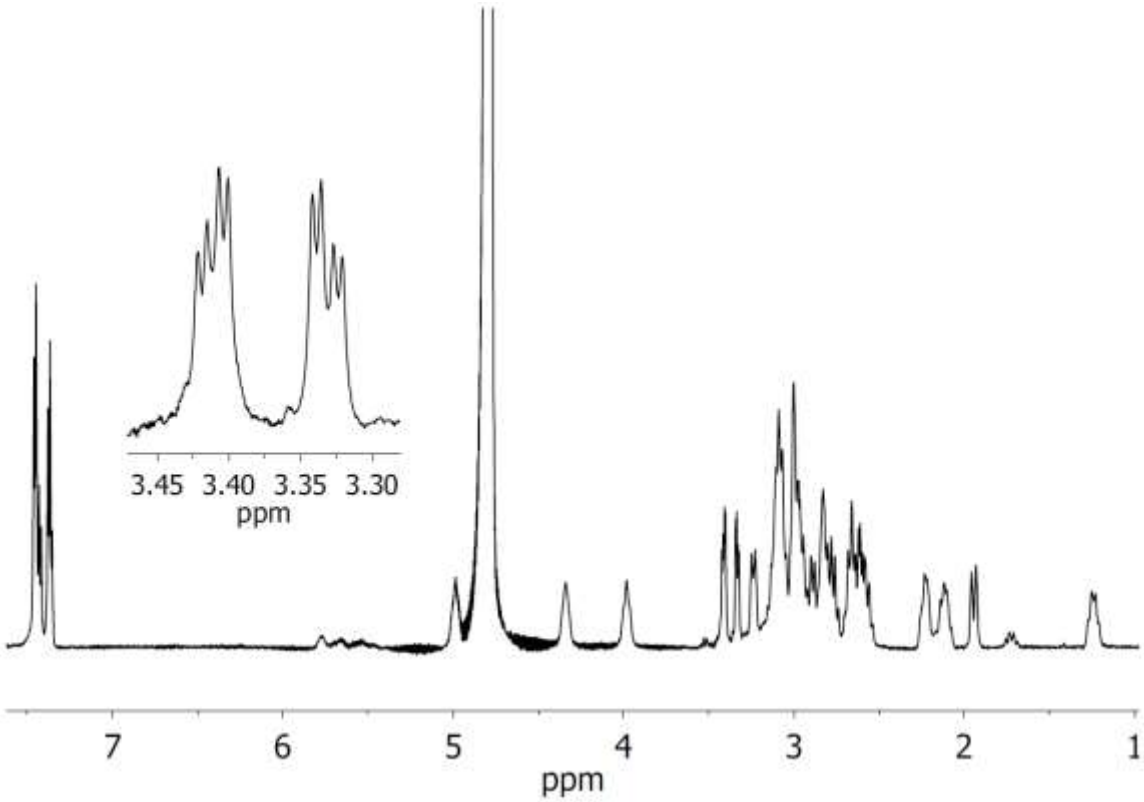

Figure 5. ^{1}H NMR of $L^{1}RhCH_2Ph^{2+}$, 600 MHz, D_2O. Inset: 2 dd signals for nonequivalent Rh-$\underline{CH_2}$-Ph, $^{2}J[Rh,H] = 3.6$ Hz, $^{2}J[H,H] = 9$ Hz

cobalt complex $L^1(H_2O)CoCH_2Ph^{2+}$ is clearly demonstrated by ready homolysis of the Co-C bond.[8]

Reactivity of $L(H_2O)RhR^{2+}$

UV-Vis spectra of $L(H_2O)RhR^{2+}$ solutions remained unchanged over at least several days at room temperature, or several months in a refrigerator, in either argon or oxygen atmosphere in the dark. During this time there was also no indication of even trace amounts of gaseous products by GC. Several minutes of irradiation of air-free solutions of sub-millimolar $L^1(H_2O)RhCH_3^{2+}$ at 313 nm also produced virtually no change in the UV-Vis spectrum, but when the photolysis was conducted in an oxygen atmosphere, large amounts of $L^1(H_2O)RhOO^{2+}$ (λ_{max} = 267 nm, $\varepsilon = 9 \times 10^3$ $M^{-1}cm^{-1}$)[34] were formed. These results clearly identify the photochemical reaction as Rh-C bond homolysis as in eq 9. In the absence of scavengers the two fragments combine to regenerate $L^1(H_2O)RhCH_3^{2+}$, but under aerobic conditions, $L^1(H_2O)Rh^{2+}$ and $^{\bullet}CH_3$ are rapidly converted to $L^1(H_2O)RhOO^{2+}$ and non-absorbing short-lived $CH_3OO^{\bullet}$, respectively.

$$L^1RhCH_3^{2+} \overset{h\nu}{\rightleftharpoons} L^1Rh^{2+} + {}^{\bullet}CH_3 \xrightarrow{O_2,\text{fast}} L^1RhOO^{2+} + CH_3OO^{\bullet} \rightarrow \text{Prod.} \quad (9)$$

The photolysis of $L^1(H_2O)RhR^{2+}$ (R = ethyl, benzyl) under Ar in the presence of a large excess of $Cr(H_2O)_6^{2+}$ produced the respective alkyl chromium complexes, $(H_2O)_5CrC_2H_5^{2+}$ and $(H_2O)_5CrCH_2Ph^{2+}$.[19] These data again support the homolysis followed by rapid capture of alkyl radicals by $Cr(H_2O)_6^{2+}$, eq 10.

$$L^1RhR^{2+} \overset{h\nu}{\rightleftharpoons} L^1Rh^{2+} + {}^{\bullet}R \overset{Cr^{2+}}{\underset{\text{fast}}{\rightarrow}} (H_2O)_5CrR^{2+} \qquad (R = C_2H_5, PhCH_2) \quad (10)$$

However, for R = CH_3, no net loss of the alkylrhodium was observed. This result is easily explained by the initial formation of $(H_2O)_5CrCH_3^{2+}$ in the photochemical step as in eq 10 followed by rapid[10] methyl group transfer back to rhodium in a thermal reaction to regenerate starting materials as shown in eq 11. We have shown recently that the $(H_2O)_5CrCH_3^{2+}$ / $L^1(H_2O)Rh^{2+}$ reaction, *i.e.*, the last step in eq 11, is fast ($k > 10^3$ M^{-1} s^{-1})[10] and yields $L^1RhCH_3^{2+}$. In contrast, the transfer of benzyl is slow ($k \sim 0.1$ M^{-1} s^{-1}), and $(H_2O)_5CrC_2H_5^{2+}$ exhibits intermediate kinetics ($k = 30$ M^{-1} s^{-1}) but yields predominantly $L^1(H_2O)RhH^{2+}$ and ethylene. These data explain the observation of the alkyl chromium product in reaction 10 for R = Et and $PhCH_2$, and the sequence described by eq 11 for R = CH_3.

$$L^1RhCH_3^{2+} \xrightarrow{h\nu,\, Cr^{2+}} L^1Rh^{2+} + CrCH_3^{2+} \xrightarrow{\text{fast}} L^1RhCH_3^{2+} + Cr^{2+} \quad (11)$$

Conclusions

Several novel alkyl complexes of macrocyclic rhodium(III) have been prepared and characterized. Aqueous solutions of these complexes are stable for months in a refrigerator in the absence of light, but UV photolysis readily cleaves the Rh-C bond. The new alkylrhodium compounds represent a potentially useful new class of photochemical radical precursors. This is especially true for the benzyl complex owing to thermal instability and short lifetime of the cobalt analog.

Acknowledgment

We are grateful to Dr. Veysey for help with elemental analysis, Dr. Cady for assistance with HSQC experiments, J. Berry and Dr. Houk for help with ICP experiments, and Dr. Pestovsky for helpful discussions. This research is supported by the

U.S. Department of Energy, Office of Basic Energy Sciences, Division of Chemical Sciences, Geosciences, and Biosciences through the Ames Laboratory. The Ames Laboratory is operated for the U.S. Department of Energy by Iowa State University under Contract DE-AC02-07CH11358.

Supplemental Information

Crystallographic information and UV-Vis and NMR spectra of alkylrhodium complexes are shown in Appendix A.

References

(1) Bounsall, E. J.; Koprich, S. R. *Can. J. Chem.* **1970**, *48*, 1481-1491.
(2) Enemark, J. H.; Feltham, R. D. *Coord. Chem. Rev.* **1974**, *13*, 339-406.
(3) Kristian, K. E.; Song, W.; Ellern, A.; Guzei, I. A.; Bakac, A. *Inorg. Chem.* **2010**, *49*, 7182-7187.
(4) Szajna-Fuller, E.; Bakac, A. *Inorg. Chem.* **2007**, *46*, 10907-10912.
(5) Asaro, F.; Costa, G.; Dreos, R.; Pellizer, G.; von Philipsborn, W. *J. Organomet. Chem.* **1996**, *513*, 193-200.
(6) Giese, B.; Kesselheim, C.; Hartung, J.; Lindner, H. J.; Svoboda, I. *Chem. Ber.* **1993**, *126*, 1193-1200.
(7) Bakac, A.; Espenson, J. H. *Inorg. Chem.* **1989**, *28*, 3901-3904.
(8) Bakac, A.; Espenson, J. H. *Inorg. Chem.* **1987**, *26*, 4305-4307.
(9) Bakac, A.; Espenson, J. H. *Inorg. Chem.* **1987**, *26*, 4353-4355.
(10) Carraher, J. M.; Bakac, A. *Chem. Commun. (London)* **2013**, *49*, 6099-6101.
(11) Bakac, A.; Thomas, L. M. *Inorg. Chem.* **1996**, *35*, 5880-5884.
(12) Schrauzer, G. N.; Windgassen, R. J. *J. Am. Chem. Soc.* **1966**, *88*, 3738-3743.
(13) Milas, N. A.; Surgenor, D. M. *J. Am. Chem. Soc.* **1946**, *68*, 643-644.
(14) Carraher, J. M.; Pestovsky, O.; Bakac, A. *Dalton Transactions* **2012**, *41*, 5974-5980.
(15) Blessing, R. H. *Acta Cryst.* **1995**, *A 51*, 33-38.
(16) Sheldrick, G. M. *Acta Cryst.* **2008**, *A64*, 112-122.
(17) APEX2 Version 4.1 (Bruker AXS Inc.,Madison WI, 2013)
(18) Kochi, J. K. *Organometallic Mechanisms and Catalysis, Chapter 4*; Academic Press: New York, 1978.
(19) Hyde, M. R.; Espenson, J. H. *J. Am. Chem. Soc.* **1976**, *98*, 4463-4469.
(20) Bakac, A. *Inorg. Chem.* **1998**, *37*, 3548-3552.
(21) Bakac, A. *Inorg. React. Mech.* **1998**, *1*, 65.
(22) Bakac, A.; Espenson, J. H. *J. Phys. Chem* **1986**, *90*, 325-327.
(23) Gjerde, H. B.; Espenson, J. H. *Organometallics* **1982**, *1*, 435-440.
(24) Bosnich, B.; Poon, C. K.; Tobe, M. L. *Inorg. Chem.* **1965**, *4*, 1102-1108.

(25) Curtis, N. F. *Coord. Chem. Rev.* **2012**, *256*, 878-895.
(26) Barefield, E. K.; Bianchi, A.; Billo, E. J.; Connolly, P. J.; Paoletti, P.; Summers, J. S.; Van, D. D. G. *Inorg. Chem.* **1986**, *25*, 4197-4202.
(27) Moore, P.; Sachinidis, J.; Willey, G. R. *J. Chem. Soc., Chem. Commun.* **1983**, 522-523.
(28) Bakac, A.; Espenson, J. H. *J. Am. Chem. Soc.* **1986**, *108*, 713-719.
(29) Lemma, K.; Ellern, A.; Bakac, A. *Inorg. Chem.* **2003**, *42*, 3662-3669.
(30) Gupta, B. D.; Vijaikanth, V.; Singh, V. *Organometallics* **2004**, *23*, 2069-2079.
(31) Mandal, D.; Gupta, B. D. *Organometallics* **2006**, *25*, 3305-3307.
(32) Vijaikanth, V.; Gupta, B. D.; Mandal, D.; Shekhar, S. *Organometallics* **2005**, *24*, 4454-4460.
(33) Mandal, D.; Gupta, B. D. *Organometallics* **2007**, *26*, 658-670.
(34) Bakac, A. *J. Am. Chem. Soc.* **1997**, *119*, 10726-10731.

CHAPTER 3

ALKYL GROUP VERSUS HYDROGEN ATOM TRANSFER FROM METAL ALKYLS TO MACROCYCLIC RHODIUM COMPLEXES

Jack M. Carraher and Andreja Bakac

A paper published in *Chemical Communications*[*]

Abstract

Macrocyclic rhodium(II) complexes $LRh(H_2O)^{2+}$ react with $(dmgH)_2(H_2O)CoR$ and with $(H_2O)_5CrR^{2+}$ by alkyl transfer for R = CH_3 to generate $L(H_2O)RhCH_3^{2+}$. When R = C_2H_5, C_3H_7 or C_4H_9, the reaction takes place by hydrogen atom abstraction from the coordinated alkyl and produces $L(H_2O)RhH^{2+}$ and an α-olefin.

Introduction

Hydrogen atom and alkyl group transfer from metal alkyls to appropriate acceptors are frequently involved in catalytic reactions of both industrial and biological significance.[1-8] Mechanistically, the atom or group transfer can be an intramolecular process, such as β-hydrogen elimination or metal-alkyl bond homolysis followed by radical capture. Another possibility is intermolecular transfer of (formally) alkyl anions (S_E2), radicals (S_H2) or cations (S_N2).[1] In several careful mechanistic studies of such alkyl abstraction reactions from transition metal complexes to various acceptors, the

[*] Carraher, Jack M.; Bakac, Andreja *Chem. Commun.,* **2013**, *49*, 6099-6101

reaction has been shown to take place by back-side attack at the alpha carbon leading to inversion of configuration at carbon.[9-13] Predictably, steric effects play a major role and become quite dramatic when both of the reactants are penta- or hexacoordinated transition metal complexes, and access to alpha carbon is severely limited,[1,13-15] although in one instance an unusually small rate variation has been observed for alkyl group exchange between organocobalt(III) porphyrins and cobalt(II) complexes.[13]

In-depth studies of such reactions often involve cobalt, but known examples include a number of other metals including chromium, rhodium, platinum, nickel, palladium and others.[13] Significant reactivity is typically observed only for methyl and primary alkyls, the latter exhibiting rates that are several orders of magnitude lower than those for methyl.

The transfer of groups with even more branching at the coordinated carbon is accompanied by further major rate decrease, but bimolecular substitution persists, and there seem to be no reports of the change-over to hydrogen atom abstraction (HAT) from the alkyl group, although such a path has been suggested in a reaction between a methylrhodium complex and rhodium(II).[16] In contrast, HAT from a coordinated alkyl group is common in interactions between metal alkyls and other hydrogen atom acceptors, such as radicals or strong electrophiles. For example, thiyl radicals react with ethyl complexes of chromium(III) and cobalt(III) macrocycles by β-hydrogen abstraction to generate ethylene and metal(II) macrocycle.[17] Carbon radicals react with metal alkyls by abstraction of an alkyl group or hydrogen atom.[1] Hydrogen transfer from alkyl radicals to reduced metal complexes to generate metal hydride is one of the key steps in chain transfer catalysis in free radical polymerization of olefins.[18,19] Similarly,

hydrogen atom and alkyl group transfers are competitive in the reactions of boranes with main group organometallics and with dialkyl zinc compounds,[20] although there is some evidence that in the latter case hydrogen transfer may be intramolecular.

To gain better insight into factors governing the onset of hydrogen abstraction from metal alkyls, we initiated a study of the reactions of macrocyclic rhodium(II) complexes $L(H_2O)Rh^{2+}$ (L = cyclam (L^1) and *meso*-hexamethylcyclam (L^2)) with cobalt(III) and chromium(III) alkyls. Rhodium(II) complexes were chosen as alkyl / hydrogen acceptors to assure favourable thermodynamics for both potential paths.

Results

Yellow solutions of sub-millimolar $(dmgH)_2(H_2O)CoCH_3$ turned colourless immediately upon mixing with equimolar amounts of $L^1(H_2O)Rh^{2+}$. This colour change is associated with rapid methyl group transfer from cobalt to $L^1(H_2O)Rh^{2+}$ which takes place with a 1 : 1 stoichiometry, eq 1, as determined by spectrophotometric titration. The product solutions exhibited shoulders near 300 nm and 340 nm,‡ and intense absorption below 300 nm attributable to free $dmgH_2$ formed by rapid dissociation from Co(II), eq 2. The shoulder at 300 nm is associated with the Rh-alkyl bond.[21]

$$L^1(H_2O)Rh^{2+} + (dmgH)_2(H_2O)CoCH_3 \rightarrow L^1(H_2O)RhCH_3^{2+} + Co(dmgH)_2 \quad (1)$$

$$Co(dmgH)_2 + 2H^+ + 6H_2O \rightarrow Co(H_2O)_6^{2+} + 2dmgH_2 \quad (2)$$

In a typical example, a solution of 9 mL of 5.6 mM $(dmgH)_2(H_2O)CoCH_3$ (50 μmol) was mixed with 20 mL of 2.3 mM $L^1(H_2O)Rh^{2+}$ (46 μmol) and the mixture allowed to react for a few minutes. The rhodium products were separated from free $dmgH_2$ and unreacted $(dmgH)_2(H_2O)CoCH_3$ by cation exchange and quantified

spectrophotometrically. The yield of $L^1(H_2O)RhCH_3^{2+}$ was 45 μmol. A summary of product data for all of the reactions in this work is provided in Table 1.

Table 1. Kinetics and Products of Reactions of Metal Alkyls (MR) with $L(H_2O)Rh^{2+}$ [a]

L	MR[b]	k / $M^{-1}s^{-1}$ [c]	Products
L^1	$(Co)CH_3$	$\geq 10^3$	$L^1RhCH_3^{2+}$
L^2	$(Co)CH_3$	900 ± 30	$L^2RhCH_3^{2+}$
L^2	$(Co)CD_3$	940 ± 60	$L^2RhCD_3^{2+}$
L^1	$(Co)C_2H_5$	30 ± 4	$\{L^1RhH^{2+} + L^1RhC_2H_5^{2+}\}$,[d] C_2H_4
L^1	$(Co)C_2D_5$	5 ± 2	$\{L^1RhD^{2+} + L^1RhC_2D_5^{2+}\}$,[e] C_2D_4
L^1	$(Co)CH(CH_3)_2$	34 ± 4	L^1RhH^{2+}, C_3H_6
L^1	$(Co)CH(CH_3)C_2H_5$	9 ± 2	$H_2C{=}CHC_2H_5$[f]
L^1	$(Co)CH_2Ph$	~ 0.1	$L^1RhCH_2Ph^{2+}$
L^1	$Cr(H_2O)_5CH_3^{2+}$	$\geq 10^3$	$L^1RhCH_3^{2+}$
L^2	$Cr(H_2O)_5CH_3^{2+}$	~ 10^4	$L^2RhCH_3^{2+}$
L^1	$Cr(H_2O)_5C_2H_5^{2+}$	720 ± 60	$\{L^1RhH^{2+} + L^1RhC_2H_5^{2+}\}$,[d] C_2H_4

[a] In 0.1 M $HClO_4$ or CF_3SO_3H. [b] (Co) = $Co(dmgH)_2(H_2O)$. [c] Obtained with either reagent in excess, 50 μM ≤ [excess reagent] ≤ 30 mM, 10 μM ≤ [limiting reagent] ≤ 0.5 mM. [d] In 10/1 ratio. [e] In 1/5 ratio. [f] Metal-derived products not determined.

Methylrhodium complexes were produced in every reaction involving a methyl group donor in Table 1. The identity of the products was determined from UV-Vis spectra of spent reaction mixtures and of individual fractions obtained by separation by cation exchange. Also, the photolysis of purified fractions led to the formation of methane and ethane, clearly generated in the self-reactions of photochemically produced methyl radicals. Finally, the $L^2(H_2O)Rh^{2+}$ / $(dmgH)_2(H_2O)CoCH_3$ reaction was run on a larger scale, and the product $L^2(H_2O)RhCH_3^{2+}$ was isolated and crystallized as a trifluoromethane sulfonate salt. The crystal structure was determined by X-ray analysis.[21]

Benzylcobaloxime also reacts with $L^1(H_2O)Rh^{2+}$ by alkyl group transfer, but the reaction is quite slow with an estimated rate constant of ~ 0.1 M^{-1} s^{-1}. Such a decrease from methyl to benzyl is consistent with an S_H2 reaction.[14,22] Owing to the long reaction

times (about 18 hours for millimolar concentrations of both reactants) and extreme air-sensitivity of small concentrations of $L^1(H_2O)Rh^{2+}$, the yields of $L^1(H_2O)RhCH_2Ph^{2+}$ were poor (17 %). No $L^1(H_2O)RhH^{2+}$ was produced.

In the same range of concentrations, the reactions of $L^1(H_2O)Rh^{2+}$ with ethyl, isopropyl, and isobutyl cobaloximes were completed in several minutes. In every case, the product was $L^1(H_2O)RhH^{2+}$ (not determined for R = isobutyl) and the corresponding terminal alkene, Table 1. In the case of $(dmgH)_2(H_2O)CoC_2H_5$, small amounts (< 10 %) of ethylrhodium were also observed. These data provide evidence for hydrogen atom transfer from the coordinated alkyl groups to rhodium(II) as in eq 3. In addition, a parallel minor alkyl transfer path operates for R = C_2H_5.

$$L^1Rh^{2+} + (dmgH)_2CoC_2H_5 \rightarrow L^1RhH^{2+} + C_2H_4 + Co(dmgH)_2 \qquad (3)$$

The amount of ethylene decreased to 20 % in the reaction of perdeuterio derivative $(dmgH)_2(H_2O)CoC_2D_5$, yielding a product-based kinetic isotope effect of ~ 4.5 for the HAT path.

Reactions with alkylchromium complexes[23] are somewhat faster than those of cobalt alkyls, but the products and overall reactivity pattern are comparable. As shown in Table 1, the methylchromium reacts with both rhodium(II) complexes by alkyl transfer, eq 4. Ethylchromium, on the other hand, reacts with $L^1(H_2O)Rh^{2+}$ to give large amounts of rhodium hydride and ethylene, and some $L^1(H_2O)RhC_2H_5^{2+}$ (~ 10 % of total products) in an experiment having 1.3 mM $L^1(H_2O)Rh^{2+}$ and 1.5 mM $(H_2O)_5CrC_2H_5^{2+}$. [The gas phase also contained alkanes generated by acidolysis of alkyl chromium complexes which were typically used in excess over $L^1(H_2O)Rh^{2+}$. Control experiments in the absence of rhodium confirmed the acidolysis to be the source of alkanes.] No reaction

was observed between $(H_2O)_5CrC_2H_5^{2+}$ and sterically more encumbered $L^2(H_2O)Rh^{2+}$ during the rather short lifetime of $(H_2O)_5CrC_2H_5^{2+}$ in 0.1 M CF_3SO_3H ($t_{1/2}$ ~ 30 minutes).

$$(H_2O)_5CrCH_3^{2+} + LRh^{2+} + H_2O \rightarrow LRhCH_3^{2+} + Cr(H_2O)_6^{2+} \quad (4)$$

The kinetic data for $L(H_2O)Rh^{2+}$ / alkylmetal reactions were obtained from absorbance vs. time data at 25 °C with either reagent in pseudo-first order excess. An example of the plot of k_{obs} against the concentration of excess reagent is shown in Figure 1 for the $L^1(H_2O)Rh^{2+}$ / $(dmgH)_2(H_2O)CoCH(CH_3)_2$ reaction. The linear fit through all of the points agrees with the experimentally determined 1:1 stoichiometry. Similar plots for other reactions are shown in Figures S1 - S6.[†] Kinetic data are summarized in Table 1. The key feature is the large difference in rate constants between methyl and ethyl complexes, both in the cobalt and chromium series. The remaining alkylcobaloximes (R = iso-propyl, isobutyl) react with rate constants (34 and 9 M^{-1} s^{-1}, respectively) that are comparable or somewhat smaller than that for ethyl (30 M^{-1} s^{-1} in the cobaloxime series). This kinetic pattern follows closely the change in products from alkylrhodium for R = methyl to {rhodium hydride + olefin} for the rest of the compounds in Table 1.

The reaction of $L^1(H_2O)Rh^{2+}$ with $(dmgH)_2(H_2O)CoC_2D_5$ has $k_{C2D5} = 5 \pm 2$ M^{-1} s^{-1}, much lower than that for the protio complex (30 ± 4 M^{-1} s^{-1}), consistent with HAT as the major path. In contrast, there is no measureable kie for the $L^2(H_2O)Rh^{2+}$ / $(dmgH)_2(H_2O)CoCH(D)_3$ reaction which is assigned as alkyl transfer.

[†] Electronic Supplementary Information (ESI) available: Experimental detail, spectroscopic data and kinetic plots

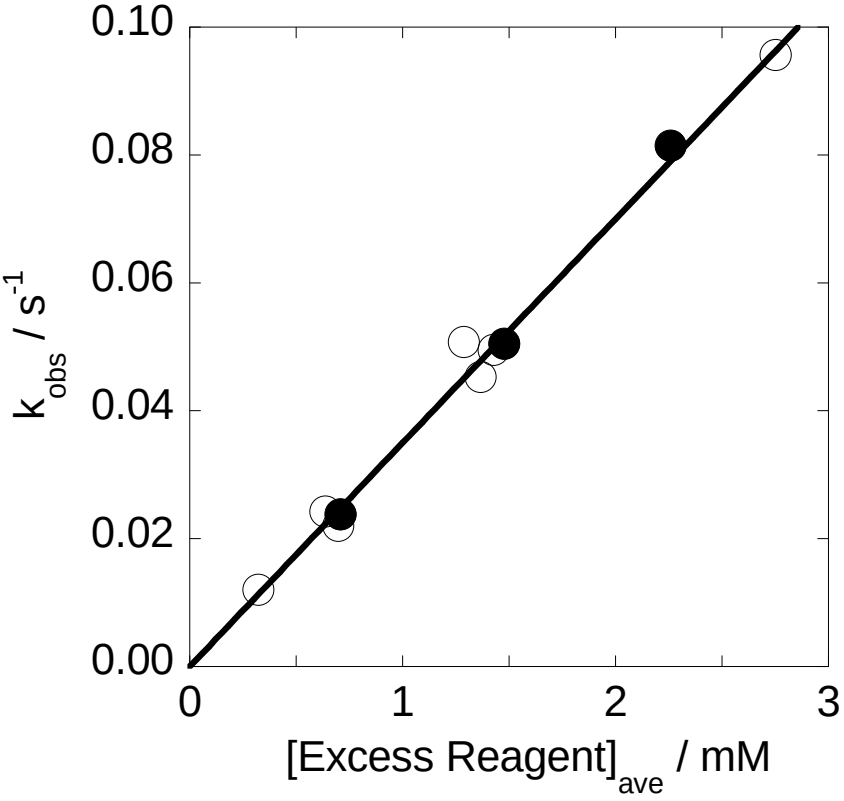

Figure 1. Plot of k_{obs} vs concentration of excess $L^1(H_2O)Rh^{2+}$ (filled circles) or $(dmgH)_2(H_2O)CoCH(CH_3)_2$ (open circles) for hydrogen atom transfer from the alkyl group. The concentration of $L^1(H_2O)Rh^{2+}$ has an associated standard deviation of ± 5 %.

Discussion and Conclusions

Precise thermodynamic data are not available to determine whether the outcome of the above reactions is controlled by kinetics or thermodynamics. In general, the bond dissociation energy (BDE ≡ ΔH^0) of Rh(III)-H bonds is greater than that of Rh(III)-C bonds. The difference is even greater on the BDFE scale, and especially in aqueous solvents owing to the hydrophobicity of alkyl groups and the entropy increase that accompanies release of an alkyl radical. In a detailed thermodynamic study of alkyl and hydrido Rh(III) porphyrins,[24] Fu and Wayland calculated BDFE = 60 kcal/mol for (TSPP)Rh-H^{4-} (TSPP = tetra-*para*-sulfonatophenyl porphyrin) and 36 kcal/mol for (TSPP)Rh-$C_2H_4D^{4-}$ in H_2O. These values lead to ΔG^0 = -8.9 kcal/mol for ethylene insertion into the hydride. The thermodynamics clearly favor Rh-C_2H_5 over (Rh-H + C_2H_4). Similarly, styrene inserts into the Rh-H bond of (omp)RhH (omp = octamethoxy porphyrinate anion) in benzene with only a slight excess of styrene, indicating that thermodynamics again favor alkylrhodium.[25]

Ethylene insertion into the rhodium-hydrogen bond of $(NH_3)_4(H_2O)RhH^{2+}$ also occurs readily.[26] The equilibrium constant has not been obtained, but the facility with which the reaction takes place, and lack of the reverse process of beta elimination again demonstrate that ethylene insertion is thermodynamically favoured. Macrocyclic complexes in the present work are kinetically much more inert; neither beta-elimination from $L^1(H_2O)RhC_2H_5^{2+}$ nor ethylene insertion into $L^1(H_2O)RhH^{2+}$ under 1 atm C_2H_4 were observed over long periods of time which prevented us from determining the relative stabilities of $L^1(H_2O)RhC_2H_5^{2+}$ vs. ($L^1(H_2O)RhH^{2+}$ + C_2H_4). None the less, the data for the porphyrins and for the spectrally and chemically closely related[26,27] ammine

complexes discussed above strongly suggest $L^1(H_2O)RhC_2H_5^{2+}$ to be thermodynamically preferred over ($L^1(H_2O)RhH^{2+}$ + C_2H_4). Thus, ethyl group transfer to $L(H_2O)Rh^{2+}$ appears to be thermodynamically more favourable than hydrogen abstraction. The predominance of the latter process for ethyl, and the complete lack of alkyl transfer for larger groups are thus controlled by steric factors. In previous studies that utilized mainly first-row transition metals[10,22,28] the thermodynamic bias toward metal alkyl apparently could not be overcome by kinetically more favourable hydrogen atom abstraction from beta carbon to generate {metal hydride + olefin}.

Acknowledgment

This research was supported by the U.S. Department of Energy, Office of Basic Energy Sciences, Chemical Sciences, Geosciences, and Biosciences Division through the Ames Laboratory. The Ames Laboratory is operated for the U.S. Department of Energy by Iowa State University under Contract No. DE-AC02-07CH11358.

Notes

The feature at 340 nm is a combination of the 352 nm band of $L^1(H_2O)Rh^{3+}$ and the 340 nm band of a new species generated in a slow follow-up step from $L^1(H_2O)Rh^{2+}$ and $dmgH_2$ as confirmed in control experiments with $L^1(H_2O)Rh^{2+}$ and genuine $dmgH_2$. Detailed studies were not carried out, but the thermal and photochemical inertness of the new species suggests that it is a rhodium(III) complex of modified $dmgH_2$. To avoid spectral interference from this species, the remainder of the experiments were run with a slight (10 %) excess of $(dmgH)_2(H_2O)CoCH_3$.

Supplemental Information

Experimental procedures, instrumentation, spectral features of MR^{n+}, and plots of k_{obs} vs. $[MR^{n+}]$ are shown in Appendix B.

References

(1) Kochi, J. K. *Organometallic Mechanisms and Catalysis*; Academic Press: New York, 1978; Vol. Volume 5
(2) Eisch, J. J.; Adeosun, A. A.; Dutta, S.; Fregene, P. O. *Eur. J. Org. Chem.* **2005**, *2005*, 2657-2670
(3) Yamada, K.-i.; Tomioka, K. *Chem. Rev.* **2008**, *108*, 2874-2886
(4) Simoes, J. A. M.; Beauchamp, J. L. *Chem. Rev.* **1990**, *90*, 629-688
(5) Peng, C.-H.; Scricco, J.; Li, S.; Fryd, M.; Wayland, B. B. *Macromolecules (Washington, DC, U. S.)* **2008**, *41*, 2368-2373
(6) Li, S.; Bruin, B. d.; Peng, C.-H.; Fryd, M.; Wayland, B. B. *J. Am. Chem. Soc.* **2008**, *130*, 13373-13381
(7) Papish, E. T.; Magee, M. P.; Norton, J. R.; Elsevier Science B.V.: 2001, p 39-74.
(8) Hirner, A. V. *Anal. Bioanal. Chem.* **2006**, *385*, 555-567
(9) Chrzastowski, J. Z.; Cooksey, C. J.; Johnson, M. D.; Lockman, B. L.; Steggles, P. N. *J. Am. Chem. Soc.* **1975**, *97*, 932-934
(10) Johnson, M. D. *Acc. Chem. Res.* **1983**, *16*, 343-349
(11) Fritz, H. L.; Espenson, J. H.; Williams, D. A.; Molander, G. A. *J. Amer. Chem. Soc.* **1974**, *96*, 2378-2381
(12) Jensen, F. R.; Madan, V.; Buchanan, D. H. *J. Amer. Chem. Soc.* **1971**, *93*, 5283-5284
(13) Stolzenberg, A. M.; Cao, Y. *J. Am. Chem. Soc.* **2001**, *123*, 9078-9090
(14) Samuels, G. J.; Espenson, J. H. *Inorg. Chem.* **1980**, *19*, 233-235
(15) Lee, S.; Ku, T. Y. *Polyhedron* **2007**, *26*, 2901-2905
(16) Zhang, L.; Chan, K. S. *J. Organomet. Chem.* **2007**, *692*, 2021-2027
(17) Huston, P.; Espenson, J. H.; Bakac, A. *Organometallics* **1992**, *11*, 3165-3166
(18) Woska, D. C.; Xie, Z. D.; Gridnev, A. A.; Ittel, S. D.; Fryd, M.; Wayland, B. B. *J. Am. Chem. Soc.* **1996**, *118*, 9102-9109
(19) Gridnev, A. A.; Ittel, S. D.; Fryd, M.; Wayland, B. B. *Organometallics* **1996**, *15*, 222-235
(20) Zhu, J.; Mukherjee, D.; Sadow, A. D. *Chem Commun (Camb)* **2012**, *48*, 464-466, and references therein.
(21) Carraher, J. M.; Ellern, A.; Bakac , A. *Submitted* **2013**
(22) Dodd, D.; Johnson, M. D.; Lockman, B. L. *J. Am. Chem. Soc.* **1977**, *99*, 3664-3673
(23) Hyde, M. R.; Espenson, J. H. *J. Am. Chem. Soc.* **1976**, *98*, 4463-4469
(24) Fu, X.; Wayland, B. B. *J. Am. Chem. Soc.* **2005**, *127*, 16460-16467
(25) Feng, M.; Chan, K. S. *J. Organomet. Chem.* **1999**, *584*, 235-239
(26) Thomas, K.; Osborn, J. A.; Powell, A. R.; Wilkinson, G. *J. Chem. Soc., A* **1968**, 1801-1806

(27) Bakac, A.; Thomas, L. M. *Inorg. Chem.* **1996**, *35*, 5880-5884
(28) Espenson, J. H.; Shveima, J. S. *J. Am. Chem. Soc.* **1973**, *95*, 4468-4469

CHAPTER 4

TRANSITION METAL ION-ASSISTED PHOTOCHEMICAL GENERATION OF ALKYL HALIDES AND HYDROCARBONS FROM CARBOXYLIC ACIDS

Jack M. Carraher, Oleg Pestovsky, and Andreja Bakac

A paper published in *Dalton Transactions*[*]

Abstract

Near-UV photolysis of aqueous solutions of propionic acid and aqueous Fe^{3+} in the absence of oxygen generates a mixture of hydrocarbons (ethane, ethylene and butane), carbon dioxide, and Fe^{2+}. The reaction becomes mildly catalytic (about five turnovers) in the presence of oxygen which converts a portion of alkyl radicals to oxidizing intermediates that reoxidize Fe^{2+}. The photochemistry in the presence of halide ions (X^- = Cl^-, Br^-) generates ethyl halides via halogen atom abstraction from FeX_n^{3-n} by ethyl radicals. Near-quantitative yields of C_2H_5X are obtained at $\geq$ 0.05 M X^-. Competition experiments with $Co(NH_3)_5Br^{2+}$ provided kinetic data for the reaction of ethyl radicals with $FeCl^{2+}$ ($k = 4.0 (\pm 0.5) \times 10^6$ $M^{-1}s^{-1}$) and with $FeBr^{2+}$ ($k = 3.0 (\pm 0.5) \times 10^7$ $M^{-1}s^{-1}$). Photochemical decarboxylation of propionic acid in the presence of Cu^{2+} generates ethylene and Cu^+. Longer-chain acids also yield alpha olefins as exclusive

[*] Carraher, Jack M.; Pestovsky, Oleg; Bakac, Andreja *Dalton Trans.*, **2012**, *41*, 5974-5980

products. These reactions become catalytic under constant purge with oxygen which plays a dual role. It reoxidizes Cu^{+} to Cu^{2+}, and removes gaseous olefins to prevent accumulation of Cu^{+}(olefin) complexes and depletion of Cu^{2+}. The results underscore the profound effect that the choice of metal ions, the medium, and reaction conditions exert on the photochemistry of carboxylic acids.

Introduction

Decarboxylation of carboxylic acids and metal carboxylates is an important step in a number of transformations[1] that lead to C-C and C-N bond formation as in Heck-type olefination,[2] decarboxylative cross-coupling,[3-8] metal-catalyzed reductions via metal hydrides,[9] various other transformations of benzoic acids,[10] and preparation of enantiomerically pure compounds in enzyme-catalyzed processes.[11]

Photochemistry provides a powerful approach to decarboxylation and has found utility in chemical synthesis through addition of radicals to electron deficient alkenes[12], deuterium exchange with a carboxyl group in D_2O in the presence of thiols,[13] synthesis of metal alkyls,[14] or as a controlled source of radicals to initiate polymerization of vinyl acetate.[15] Photochemical decarboxylation of formic acid has seen great advances in recent years and promises to become an important source of hydrogen as fuel.[16,17]

Another energy-related area that would greatly benefit from novel and efficient approaches to decarboxylation is the conversion of biomass to fuels and chemicals.[18-20] Deoxygenation and decarboxylation of fatty acid methyl esters, known as biodiesel, generate ‘green’ diesel which closely resembles petroleum-derived hydrocarbons and could replace them as fuels.[21,22] Unfortunately, most of the current processes for decarboxylation of biodiesel utilize hydrogenation at elevated temperatures and pressures

in the presence of various metal-based catalysts.[23-25] More energy-efficient decarboxylation methods, especially those not requiring hydrogen would represent a major improvement.

These and related issues prompted us to examine iron(III) and copper(II) salts as reagents and potential catalysts for photochemical conversion of carboxylic acids to hydrocarbons and functionalized derivatives. Metal ion-assisted decarboxylation, especially with iron compounds, has already received some attention,[26-29] but work with copper has been quite limited.[29,30] Several groups demonstrated increased photoreactivity of carboxylic acids in the presence of iron(III). In the proposed mechanism, the photochemical cleavage of carboxylato iron complexes generates carboxyalkyl radicals followed by rapid thermal decarboxylation.[26,27,29] This conclusion was recently questioned in a study of Fe(III)-assisted decarboxylation of glyoxalic, tartaric, pyruvic, and lactic acids by Glebov et al.[31] These authors invoked a persistent radical complex [Fe^{II}••••OC(O)R] that dissociates into R(O)CO• and Fe(II) on a millisecond time scale.

Photochemical decarboxylation of acetic, propionic, and butyric acids in the presence of Fe^{3+}, UO_2^{2+}, an Fe^{3+}-Cu^{2+} couple, TiO_2, and Pt/TiO_2 was found to generate alkanes, alkenes, CO_2, and in some cases H_2, leading to the conclusion that the nature of both the metal and carboxylic acid determines the outcome.[29] Chlorinated products were observed when succinic, glutaric, and adipic acids were photochemically decarboxylated in the presence of $FeCl_3$.[28]

Here we report the results of our work on some novel aspects of metal-assisted photochemical transformations of carboxylic acids. The majority of work was done with

propionic acid owing to its solubility in water, but our mechanistic conclusions should be applicable to longer-chain acids as well.

Throughout the manuscript, the ions $Fe(H_2O)_6^{3+}$, $Fe(H_2O)_6^{2+}$ and $Cu(H_2O)_6^{2+}$ are abbreviated as Fe^{3+}, Fe^{2+} and Cu^{2+}. The more general notation, Fe(III) and Fe(II), is used when the precise nature of the complex is not known, or when the metal ion exists in more than one form under experimental conditions.

Experimental

Materials

Iron(III) perchlorate hydrate, iron(II) perchlorate hydrate, titanium(IV) oxy sulfate, sodium propionate, deuterium oxide (99.9 % D), 1,10-phenanthroline, 2-methylhexanoic acid, pentanoic acid (all Sigma Aldrich), perchloric acid (70 %), dimethylsulfoxide, sodium hydroxide, glacial acetic acid (all Fisher Scientific), vanadium(IV) oxy sulfate (Alfa Aesar), sodium acetate and barium chloride (both Baker) were of the best quality available and were used as received. Barium(II) perchlorate was obtained from $BaCl_2$ and vanadium(IV) perchlorate from the sulfate, both by ion exchange on Sephadex C-25 and elution with 0.5 M $HClO_4$. Solutions of copper(II) perchlorate were prepared from solid hydrated perchlorate salt and standardized iodometrically. Bromopentaaminecobalt(III) perchlorate[32] was prepared as described in the literature.

Methods and Instrumentation

Photolyses were performed in standard 1-cm square fluorescence quartz cells. Experiments requiring large head space utilized home-made quartz cells with a total volume of 6 mL. Standard mixtures of ethane, ethylene and butane[33] in aqueous solutions

for GC calibration were prepared by the reaction of *tert*-amyl hydroperoxide and excess Fe^{2+}. After shaking the solution for 30 seconds to expel the gases into the headspace, 100 μL of the headspace was injected into the GC. The total peak area (C_2H_4 + C_2H_6 + C_4H_{10}) was then related to the known initial concentration of *tert*-amyl hydroperoxide. The concentrations of gaseous products in Tables 1, 2, and 4 are thus the actual solution concentrations. The concentration of unreacted propionic acid was determined by ^1H NMR. For this purpose, the experiments were performed in D_2O followed by the removal of cationic metal species on a column of Sephadex C-25 resin. Known concentrations of dimethylsulfoxide were added to the sample as internal standard. Iron(II) was quantified with phenanthroline. A correction for Fe(III) was applied as described previously.[34]

Irradiations were carried out at 313 nm (Luzchem LZC-5 photoreactor) and 575 nm (Rayonet). Gaseous products were analyzed with an Agilent Technologies 7890A gas chromatograph equipped with an FID detector and a 0.320 mm I.D. capillary column (GS-GASPRO part # 113-4312, 15 m long). Nitrogen flow rate was 25 cm^3/s. The split injector (1:40) and FID detector were both held at 200^0 C. Initial oven temperature was 40^0 C, increased by 10^0 C/min, and held at a final temperature of 200^0 C for 1 min. Prior to GCMS analysis, reaction solutions were shaken vigorously for 30 seconds, and 100 μL of the headspace was injected into an Agilent 6890 gas chromatograph equipped with a split/splitless injector (10:1 split ratio) and an Agilent HP-PLOT/Q column.

Waters GCT accurate mass time-of-flight mass spectrometer in positive EI mode (70 EV) with a scan rate of 0.3 s per scan and a mass range of 10–200 Daltons was used to detect hydrocarbon products and CO_2. Waters MassLynx 4.0 software was used to acquire and process GC-MS data (average of 3–5 runs). UV-vis spectra were taken with a

Shimadzu UV-3101PC spectrophotometer, and ^{1}H NMR spectra with a Varian 300 MHz NMR (VXR-300). pH measurements were made with an Accumet AP71 pH meter (Fisher) equipped with an Accumet 13-620-AP55 electrode. Water was purified with a Barnstead EASYpure III UV UF system.

Results and Discussion

Photolysis of Fe(III) / Propionic Acid Solutions

Addition of propionic acid to aqueous solutions of Fe(III) caused the appearance of a new band in the UV-Vis spectrum around 300 nm, Figure 1, signaling the formation of Fe(III)-propionate complex(es). Irradiation of such solutions with 313 nm light under argon produced ethane, ethylene and butane as observed and quantified by GC, Table 1. No other products were detected in either GC or NMR. Carbon dioxide was detected by GCMS, but it was not quantified. The results are similar to those reported previously by Bideau et al. except that no butane was observed in that work which utilized much larger concentrations of both propionic acid (1 M) and Fe^{3+} (0.01 – 0.1 M).[30]

Table 1. Products of Photolysis of $Fe^{3+}/C_2H_5CO_2H$[a]

						Gaseous Products		
	$[Fe(III)]_0$	$[Fe^{2+}]_0$	pH	$[EtCO_2H]_0$	$[Fe^{2+}]_\infty$	$[C_2H_6]$	$[C_2H_4]$	$[C_4H_{10}]$
1	6.5	0	1.85	52	6.5	2.4	0.7	0.8
2	7.2	6.8	2.20	55	13.9	1.3	0.3	0.5
3	7.2	6.8	2.19	220	14.9	2.4	0.6	1.0
4	6.3	3.5	1.95	442	8.1	5.1	0.7	0.8
5	2.4	13.6	1.79	55	15	1.7	0.3	0.9
6	27.2[b]	500	1.7	10	[c]	0.01	0.4	0

[a] Under argon, 30 min irradiation, λ_{irr} 313 nm. All concentrations, including those of gaseous products, are given in mM. [b] Irradiated for 20 min, pH ~ 1.7. [c] Not determined.

The best yields of hydrocarbons were obtained at $1.7 \leq pH \leq 2.3$. Outside of this range the yields decreased significantly, most obviously owing to the acid/base equilibria

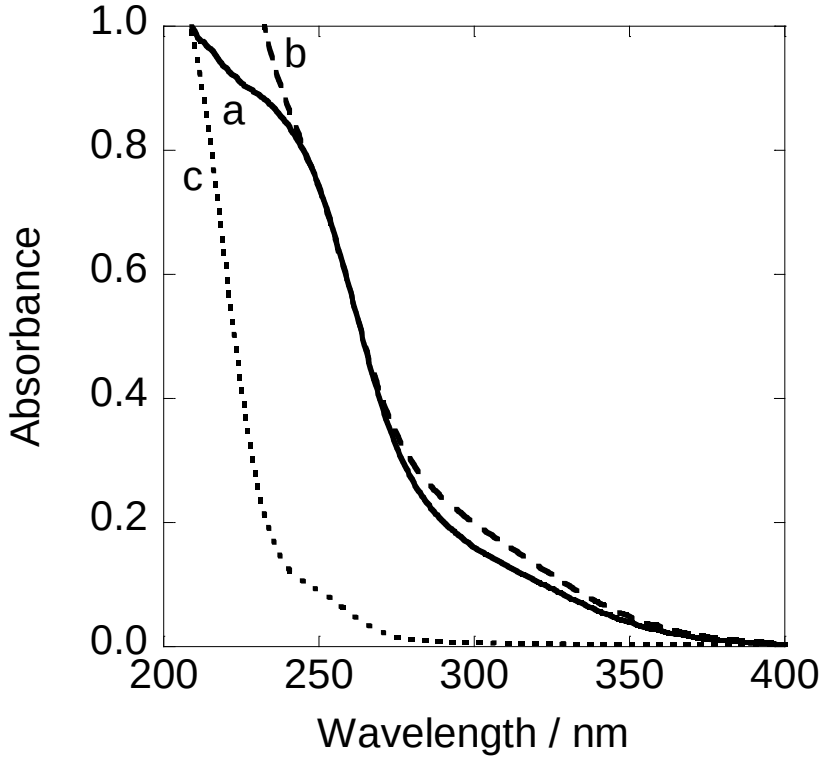

Figure 1. UV-visible absorption spectra of 0.19 mM Fe^{3+} in the absence (a) and presence (b) of 55 mM propionic acid at pH 2.3. Spectrum (c) was obtained after 40 min of photolysis of (b) at 313 nm.

of C_2H_5COOH / $C_2H_5COO^-$ (pK_a = 4.86)[35] and $Fe(H_2O)_6^{3+}$ / $Fe(H_2O)_5(OH)^{2+}$ (pK_a = 2.8),[36] as well as the dimerization of $Fe(H_2O)_5(OH)^{2+}$.[36] The observed optimum pH range is consistent with $C_2H_5COO^-$ and Fe^{3+} as key species involved in the formation of iron propionate complex, in agreement with literature data.[37]

The 300 nm feature decreased, and finally disappeared, during the photolysis, Figure 1, spectrum *c*. At this point all of Fe(III) has been reduced to Fe(II), and the formation of gaseous products ceased. In total, less than one equivalent of hydrocarbon products were generated per mole of Fe^{3+}. No products were detected in control experiments in which Fe^{3+} was omitted or replaced with Fe^{2+}.

The observed hydrocarbon products are indicative of the involvement of ethyl radicals, and suggest the decarboxylation mechanism[38] shown in eq 1 - 3, where K_1 = 2.8 × 10^3 M^{-1} at 1 M ionic strength.[37] Similar conclusions have been reached in earlier studies.[12,13,15,39,40] However, large proportions of ethane in experiments 1 - 5 rule out bimolecular self-reactions of ethyl radicals, eq 4, as a major product-generating path. The self-reactions would generate more butane than C_2 products with an expected ratio of ethane : ethylene : butane = 1 : 1 : 3.[33] Admittedly, the standard error on absolute concentrations of the three products (about 50 %) and even on relative yields (30 %) is large, but the consistent dominance of ethane over ethylene and butane is firmly established and outside the experimental error.

$$Fe^{3+} + C_2H_5CO_2^- \rightleftharpoons FeOC(O)C_2H_5^{2+} \qquad K_1 \qquad (1)$$

$$FeOC(O)C_2H_5^{2+} \xrightarrow{h\nu} Fe^{2+} + C_2H_5CO_2^{\bullet} \qquad (2)$$

$$C_2H_5CO_2^{\bullet} \xrightarrow{\text{fast}} {}^{\bullet}C_2H_5 + CO_2 \qquad (3)$$

$$2^{\bullet}C_2H_5 \rightarrow \{C_2H_4 + C_2H_6 + C_4H_{10}\} \quad (4)$$

$$^{\bullet}C_2H_5 + C_2H_5CO_2H/\ FeOC(O)C_2H_5^{2+} \rightarrow C_2H_6 + \text{products} \quad (5)$$

$$^{\bullet}C_2H_5 + Fe^{3+} \rightarrow C_2H_4 + Fe^{2+} + H^{+} \quad (6)$$

In the series of experiments 2 - 4 in Table 1, the yields of gaseous products increased with increasing concentrations of propionic acid. This is believed to be caused in part by larger concentrations of the photoactive propionate complexes which led to a faster reaction and smaller losses of hydrocarbon products during photolysis. The increased amounts of ethane over ethylene and butane at the highest concentration of $C_2H_5CO_2H$ (0.44 M, entry 4) suggest that ethyl radicals also react, albeit slowly, with free[38,41] and/or coordinated propionic acid as in eq 5. No attempt was made to unravel the kinetics of these reactions because the proportions of various iron species, especially the higher propionate complexes, almost certainly change with the concentration of propionic acid/propionate.

Butane is believed to be formed mainly by dimerization of ethyl radicals, in which case the associated concentration of ethylene should be about one third of [butane]. The observed yields of ethylene are larger, and comparable to those of butane at $[Fe^{3+}]_0 \sim 0.7$ mM, entries 1 - 4. Thus an additional ethylene-generating step is required. It seems most plausible that a portion of the radicals are oxidized by Fe^{3+} as in eq 6. When Fe(III) (27 mM) was used in large excess over propionic acid (10 mM), 98 % of the product was ethylene, entry 6.

Additional experiments were performed to estimate the rate constant for reaction 6. Radicals were generated in a thermal reaction between Fe^{2+} and *tert*-amyl

hydroperoxide, eq 7. Table 2 summarizes the results. The product ratio [C_2H_6] : [C_2H_4] : [C_4H_{10}] in the absence of added substrates deviated somewhat from that expected for

$$Fe^{2+} + C_2H_5C(CH_3)_2OOH \rightarrow FeOH^{2+} + (CH_3)_2CO + {}^{\bullet}C_2H_5 \qquad (7)$$

radical self-reactions. Specifically, in experiments that had comparable concentrations of Fe^{2+} and hydroperoxide, ethane was produced in larger amounts than ethylene, Table 2, entry 1. We rationalize the extra ethane by the reaction of ethyl radicals with the hydroperoxide, most likely by hydrogen atom abstraction from the hydroperoxo group, in analogy to the known reaction of methyl radicals with *tert*-BuOOH for which $k = 1.9 \times 10^4$ M^{-1} s^{-1}.[42] Our previous hypothesis that extra ethane in Fe(II) / hydroperoxide reactions comes from the slow reduction of alkyl radicals by Fe(II)[33] may be incorrect, given that added Fe^{2+} failed to increase the proportion of ethane in photochemical experiments with propionate. On the other hand, the multiple equilibria in Fe(II) / Fe(III) / propionate solutions[43] alter the concentrations of aqua metal ions and of free propionic acid/propionate, as well as the resulting steady-state concentrations of the radicals. The complexity of these solutions complicates the assignment of specific reactivity, or a lack thereof, to individual species. Thus, we cannot completely rule out a reaction between Fe^{2+} and ${}^{\bullet}C_2H_5$ in a propionate-free environment.

The product distribution in entry 5 more closely resembles that of ethyl radical self-reaction (1 : 1 : 3) than does entry 1. This result is rationalized by the higher steady state concentration of ethyl radicals which favors the self-reaction, eq 4, over H-atom abstraction from the hydroperoxide.

Table 2: Products of Reactions of Ethyl Radicals with Fe(III) and with Propionic Acid[a]

Entry	$[Fe(III)]_0$	[Fe(II)]	$[ROOH]_0$[b]	$[C_2H_5CO_2H]_0$	$[C_2H_6]$ / $[C_2H_4]$ / $[C_4H_{10}]$
1	0.1	1.2	0.7	0	0.11 / 0.06 / 0.27
2	33.6	1.2	0.7	0	0.10 / 0.08 / 0.27
3	68.2	1.2	0.7	0	0.08 / 0.12 / 0.25
4	103	1.2	0.7	0	0.08 / 0.15 / 0.25
5	1.5	44.9	1.5	0	0.17 / 0.16 / 0.59
6[c]	1.3	45.2	1.5	40	0.31 / 0.26 / 0.46

[a] Radicals generated in the $Fe^{2+}/C_2H_5C(CH_3)_2OOH$ reaction under argon, pH 1. All concentrations in mM. [b] ROOH = $C_2H_5C(CH_3)_2OOH$. [c] pH = 2.

When the Fe^{2+} / $C_2H_5C(CH_3)_2OOH$ reaction in 0.1 M $HClO_4$ was run in the presence of large concentrations of Fe^{3+}, there was a mild increase in the proportions of ethylene, Table 2, entries 2 - 4. At 0.1 M Fe^{3+}, the yield of ethylene was twice as large as that of ethane. From the effect of Fe^{3+} on the yield of ethylene in Table 2, we estimate $k_6 = 400 \pm 200\ M^{-1}\ s^{-1}$.

In search of evidence for a reaction between Fe(II) propionate complex(es) with ethyl radicals, the Fe^{2+} / $C_2H_5C(CH_3)_2OOH$ reaction was also run under conditions of excess Fe^{2+} (45.2 mM) and propionic acid (40 mM), Table 2, entry 6. Fe(III) was not added deliberately, but small amounts, no larger than those generated in the course of the reaction, were present in solutions of Fe(II). Assuming that the stability constants for $Fe^{II}(O_2CC_2H_5)^+$ and higher complexes are comparable to those of iron(II)-acetate complexes,[43] significant concentrations of both free $C_2H_5CO_2H$ (37 mM) and $Fe^{II}(O_2CC_2H_5)_x^{2-x}$ (2.7 mM) were present in solution. As shown in Table 2, the yield of C_2 products increased somewhat, and that of butane showed a corresponding decrease but the changes were small and this lead was not pursued further.

The decarboxylation in eq 1 - 3 could be made catalytic by introducing an additional step to regenerate Fe^{3+}. In a most desirable scenario, the initially formed Fe^{2+} and ethyl radicals would react with each other as in eq 8 to form ethane and Fe^{3+}. Unfortunately, this reaction does not appear to be significant under the conditions of this work as judged by the failure of even large amounts of externally added Fe^{2+} to increase the yields of ethane as shown in Table 1 and commented above.

$$^{\bullet}C_2H_5 + Fe^{2+} + H^+ \rightarrow C_2H_6 + Fe^{3+} \qquad \text{very slow} \qquad (8)$$

Next, we considered the use of sacrificial oxidants to regenerate Fe^{3+}. Even though Fe^{2+} does not react directly with O_2 under our conditions, several experiments were performed in an oxygen atmosphere. The oxidation was expected to take place by an indirect mechanism shown in eq 9 in which O_2 converts a portion of ethyl radicals to ethylperoxyl radicals[44] followed by oxidation of Fe^{2+} and regeneration of up to three equivalents of Fe^{3+}.[45]

$$^{\bullet}C_2H_5 \xrightarrow{O_2} {}^{\bullet}OOC_2H_5 \xrightarrow[-Fe^{3+}]{Fe^{2+},\,H^+} HOOC_2H_5 \xrightarrow[-Fe^{3+}]{Fe^{2+},\,H^+} {}^{\bullet}OC_2H_5 \xrightarrow[-Fe^{3+}]{Fe^{2+},\,H^+} HOC_2H_5 \qquad (9)$$

Indeed, an experiment under O_2 resulted in consumption of five equivalents of propionic acid per mole of Fe^{3+} as determined from the difference in NMR spectra before and after the photolysis. These experiments required longer irradiation times and a larger, O_2-filled head space which made quantitative determinations of gaseous products unreliable. None the less, gas chromatograms clearly showed that ethane, ethylene, and butane were formed in large amounts and in ratios comparable to those seen under argon, suggesting that the main decarboxylation route in eq 1 - 6 continues in parallel with O_2 chemistry that regenerates Fe^{3+}. Surprisingly, a large excess of Fe^{2+} (10 mM) led to

ethylene as the main product. It appears that other oxidizing species, in addition to those in eq 9, are involved. No ethanol was detected, but a signal for acetic acid appeared at 1.9 ppm after long irradiation times, consistent with ethanol as an intermediate.

Photolysis of Fe(III) /Propionic Acid / Halide Ions

Addition of NaBr to Fe^{3+} / propionic acid solutions caused an increase in absorbance around 417 nm, signaling the presence of iron bromide complex(es), but the absorbance change at the irradiation wavelength (313 nm) was negligibly small, Figure S2. The effect of 0.05 - 0.1 M NaCl on the 313 nm absorbance was more significant, Figure S3, owing to the larger stability constant for $FeCl^{2+}$.[43] We suspect that some photolysis of $FeCl^{2+}$ [46] took place under our conditions to generate small amounts of chlorine atoms followed by rapid reaction with chloride to produce $Cl_2^{\bullet-}$. The most likely fate of $Cl_2^{\bullet-}$ is reduction by Fe^{2+}, $k = 1.4 \times 10^7$ M^{-1} s^{-1},[47,48] with minor contribution from $Cl_2^{\bullet-}$ self-reaction and/or reaction with ethyl radicals. These side reactions did not seem to have a measurable effect on the productive photochemistry described below as judged by the similarity of results with those obtained in bromide solutions that exhibited no absorbance at the irradiation wavelength.

The photolysis of Fe(III) / propionate / halide solutions generated ethyl halides, C_2H_5X (X = Cl, Br). The yields increased with increasing concentrations of halide ions and reached 89 % of total products in the head space at $[X^-] = 0.10$ M, Table 3. The remaining products were C_2H_4, C_2H_6, and C_4H_{10}. In view of the much lower volatility of alkyl halides compared to hydrocarbon products, the actual yields of RX in solution are estimated to be nearly quantitative at $[X^-] = 0.10$ M.

The reaction is believed to involve FeX^{2+} (X = Cl, Br) as the active oxidant as shown for $FeCl^{2+}$ in eq 10 - 11, similar to the previously reported reaction of methyl radicals with $FeBr^{2+}$.[49] The concentrations of FeX^{2+} in Table 3 were calculated from the total concentrations of X^- and Fe(III) and the known stability constants[43] (K_{FeCl} = 4.2 M^{-1}, K_{FeBr} = 0.5 M^{-1} at μ = 1 M). Corrections were made for ionic strength (K_{FeCl} = 4.4 M^{-1} at μ = 0.45 M, K_{FeBr} = 0.75 M^{-1} at μ = 0.2 M) based on the relationship determined by Rabinowitch and Stockmayer for $FeCl^{2+}$.[50]

$$Fe^{3+} + Cl^- \rightleftharpoons FeCl^{2+} \qquad K_{FeCl} \qquad (10)$$

$$^{\bullet}C_2H_5 + FeCl^{2+} \rightarrow C_2H_5Cl + Fe^{2+} \qquad (11)$$

Table 3. Products of Photolysis of $Fe^{3+}/C_2H_5CO_2H/X^-$[a]

$[Br^-]_0$	$[Cl^-]_0$	$[FeX^{2+}]_0$[b]	$[C_2H_5X] / [C_2H_6] / [C_2H_4] / [C_4H_{10}]$[c]
5	-	0.03	2.29 / 1.92 / 0.60 / 1.93
10	-	0.06	3.17 / 1.68 / 0.33 / 1.04
50	-	0.30	3.56 / 0.66 / 0.05 / 0.09
100	-	0.57	3.90 / 0.43 / 0.03 / 0.03
-	5	0.23	2.89 / 1.94 / 0.74 / 0.14
-	10	0.44	3.40 / 1.58 / 0.46 / 0.60
-	50	1.78	3.59 / 0.57 / 0.20 / 0.06
-	100	2.80	4.77 / 0.36 / 0.19 / 0.06

[a] Under argon, pH 1.9 ± 0.3, λ_{irr} 313 nm, irradiation time 30 min, $[propionic\ acid]_0$ = 55 mM, $[Fe(III)]_0$ = 7.1 mM. All concentrations of solution species in mM. [b] Initial concentrations of $FeBr^{2+}$ and $FeCl^{2+}$ were calculated from $[Fe(III)]_{tot}$ and $[X^-]$ using literature equilibrium constants, see text. [c] Ratio of GC peak areas for head space samples.

Kinetics of $^{\bullet}C_2H_5$ / FeX^{2+} Reactions

Rate constants for the reactions of ethyl radicals with FeX^{2+} (X = Br, Cl) were determined in competition experiments with $(NH_3)_5CoBr^{2+}$ for which k_{12} = 3.0 (± 0.2) × 10^6 M^{-1} s^{-1}.[51] The reactions of FeX^{2+} are shown in eq 11 (X = Cl) and eq 13 (X = Br). These experiments utilized small concentrations of $C_2H_5C(CH_3)_2OOH$ (0.20 – 0.51 mM)

and a slight excess of Fe^{2+} (0.54 – 0.99 mM) to keep steady-state concentrations of ethyl radicals low and thus to minimize losses in radical self-reactions. The concentrations of Fe(III) (10 - 151 mM), halides (10 - 25 mM Br^-, 5 - 10 mM Cl^-), and $(NH_3)_5CoBr^{2+}$ (0.5 - 10 mM) were large and essentially constant for the duration of each run. The largest change in the concentration of excess reagents was 20%, but typically it was much less than 10%. For the calculations of rate constants, the concentrations of excess reagents were averaged over the course of each experiment.

$$^{\bullet}C_2H_5 + (NH_3)_5CoBr^{2+} + (5H^+) \rightarrow C_2H_5Br + Co^{2+} + 5NH_4^+ \quad (12)$$

$$^{\bullet}C_2H_5 + FeBr^{2+} \rightarrow C_2H_5Br + Fe^{2+} \quad (13)$$

Expressions in eq 14 and 15 describe the relationship between the concentrations of alkyl halides generated in individual steps and the products of relevant rate constants and concentrations of the competing substrates. In these equations, $[C_2H_5Br]_{12}$ and $[C_2H_5Br]_{13}$ denote the yields of C_2H_5Br in reactions 12 and 13.

The required product ratios were calculated from the experimentally determined concentrations of Fe^{2+} at the beginning and end of each run under the assumption that ethyl radicals react only in reactions 11 and 12 or 12 and 13. This assumption is justified by our calculations which show that radical self-reactions and the reaction with Fe^{3+} consume less than 1% of ethyl radicals.

Fe^{2+} is consumed in the radical-generating step 7, and is regenerated in the $^{\bullet}C_2H_5$ / FeX^{2+} reactions, eq 11 or 13. When X = Cl, eq 11, C_2H_5Cl is also produced. If all of the ethyl radicals reacted with $FeCl^{2+}$, then Fe^{2+} would be fully recovered, *i.e.*, $[Fe^{2+}]_0 - [Fe^{2+}]_\infty = \Delta[Fe^{2+}] = 0$. When $^{\bullet}C_2H_5$ reacts with $(NH_3)_5CoBr^{2+}$, eq 12, an equivalent of C_2H_5Br is formed, and no Fe^{2+} is regenerated. In the extreme when $Rate_{12} >> Rate_{11}$, the

difference $\Delta[Fe^{2+}] = [C_2H_5C(CH_3)_2OOH]_0$. Under actual experimental conditions both $(NH_3)_5CoBr^{2+}$ and $FeCl^{2+}$ compete for $^{\bullet}C_2H_5$. Therefore, $\Delta[Fe^{2+}]$ lies between the two extremes, and the ratio $[C_2H_5Cl]$ / $[C_2H_5Br]_{12}$ in eq 14 can be replaced by $([C_2H_5C(CH_3)_2OOH] - \Delta[Fe^{2+}])$ / □□$\Delta[Fe^{2+}]$. The same is true for the ratio $[C_2H_5Br]_{13}$ / $[C_2H_5Br]_{12}$ in eq 15 which applies when $FeBr^{2+}$ and $(NH_3)_5CoBr^{2+}$ compete for ethyl radicals, eq 12 - 13.

$$\frac{[C_2H_5Cl]}{[C_2H_5Br]_{12}} = \frac{[C_2H_5C(CH_3)_2OOH]_0 - \Delta[Fe^{2+}]}{\Delta[Fe^{2+}]} = \frac{k_{11}[FeCl^{2+}]}{k_{12}[Co(NH_3)_5Br^{2+}]} \quad (14)$$

$$\frac{[C_2H_5Br]_{13}}{[C_2H_5Br]_{12}} = \frac{[C_2H_5C(CH_3)_2OOH]_0 - \Delta[Fe^{2+}]}{\Delta[Fe^{2+}]} = \frac{k_{13}[FeBr^{2+}]}{k_{12}[Co(NH_3)_5Br^{2+}]} \quad (15)$$

Plots according to eq 14 and 15 are shown in Figure 2. The slopes of the lines yielded ratios of the corresponding rate constants $k_{11} / k_{12} = 1.32 \pm 0.08$ and $k_{13} / k_{12} = 10.4 \pm 0.5$. From these values, and the previously determined k_{12},[51] one obtains $k_{11} = 4.0$ $(\pm 0.6) \times 10^6$ M^{-1} s^{-1} and $k_{13} = 3.0$ $(\pm 0.5) \times 10^7$ M^{-1} s^{-1}. These rate constants follow the trend expected for S_H2 reactions,[52,53] *i.e.*, $FeBr^{2+}$ reacts faster than $FeCl^{2+}$, and methyl radicals react faster than ethyl radicals. The rate constant for the reaction of methyl radicals with $FeBr^{2+}$, $k_{16} > 10^8$ M^{-1} s^{-1}, was estimated in our earlier work.[49]

$$^{\bullet}CH_3 + FeBr^{2+} \rightarrow CH_3Br + Fe^{2+} \quad (16)$$

The competition ratio for methyl radicals, $k_{16} / k_{17,}$ was determined in experiments analogous to those described above for ethyl radicals, except that *tert*-amyl hydroperoxide in the radical-generating step of eq 7 was replaced by *tert*-butyl hydroperoxide.

$$^{\bullet}CH_3 + (NH_3)_5CoBr^{2+} (+5H^+) \rightarrow CH_3Br + Co^{2+} + 5NH_4^+ \quad (17)$$

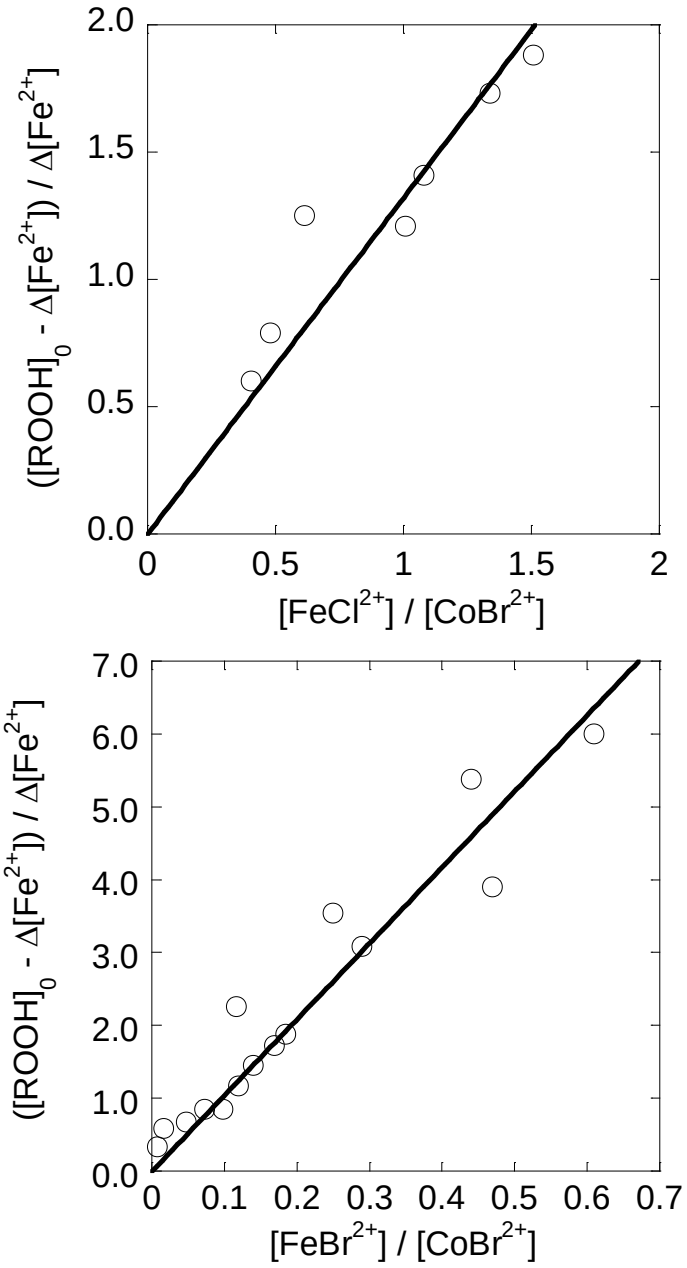

Figure 2. Plots according to eq 14 (top) and eq 15 (bottom). R = $C_2H_5C(CH_3)_2$. Concentrations: 0.54 – 0.99 mM Fe^{2+}, 0.20 – 0.51 mM ROOH, 0.9 – 3.8 mM $FeCl^{2+}$, 0.08 – 0.27 mM $FeBr^{2+}$, and 0.5 – 10 mM $(NH_3)_5CoBr^{2+}$. The plotted concentrations of $FeBr^{2+}$, $FeCl^{2+}$, and $(NH_3)_5CoBr^{2+}$ are the averages for each run.

The plot of ($[(CH_3)_3COOH]_0$ - $\Delta[Fe^{2+}]$)□□ / $\Delta[Fe^{2+}]$ against the ratio $[FeBr^{2+}]$ / $[(NH_3)_5CoBr^{2+}]$ yielded the ratio $k_{16} / k_{17} = 6.0 \pm 0.6$, Figure S1, which leads to $k_{17} > 10^7$ M^{-1} s^{-1}.

Photolysis of Cu(II) / Propionate Solutions

Addition of propionic acid to solutions of Cu^{2+} causes an increase in absorbance in the 550 – 800 nm range and a shift of the 800 nm maximum to 770 nm. Also, the UV intensity is significantly increased, Figure 3, signaling the formation of a copper propionate complex, K = 170 M^{-1}.[43]

Irradiation of solutions containing Cu^{2+} and $C_2H_5CO_2H$ (λ_{irr} = 313 nm or 575 nm) yielded ethylene as the sole gaseous product, even in the presence of a large excess (0.05 M) of sodium chloride or bromide. The yield of ethylene was much smaller at pH 2.9 (0.03 mM) than at pH 6.9 (1.2 mM) where the concentration of the propionate complex is greater, Table 4. Under air-free conditions, the reaction also produced Cu^0, most likely by disproportionation of initially formed Cu^+ as in eq 18 - 20.

$$Cu^{II}(O_2CC_2H_5)^+ \xrightarrow{h\nu} Cu^+ + CO_2 + {}^\bullet C_2H_5 \quad (18)$$

$$Cu^{2+} + {}^\bullet C_2H_5 \rightarrow Cu^+ + C_2H_4 + H^+ \quad (19)$$

$$2Cu^+ \rightarrow Cu^{2+} + Cu^0 \quad (20)$$

Table 4. Products of Photolysis of $Cu^{2+}/C_2H_5CO_2H$[a]

	Atmosphere	pH	$[C_2H_5CO_2H]_0$	$[C_2H_4]$
1	Ar	6.9	55.0	1.2
2	Ar	2.9	55.0	0.03
3	10% air[b]	6.5	55.0	1.4
4	Air	6.9	58.3	2.9
5	O_2	6.0	26.8	2.8

[a] $[Cu^{2+}]_0$ = 7.0 mM. All concentrations in mM. [b] 90% argon.

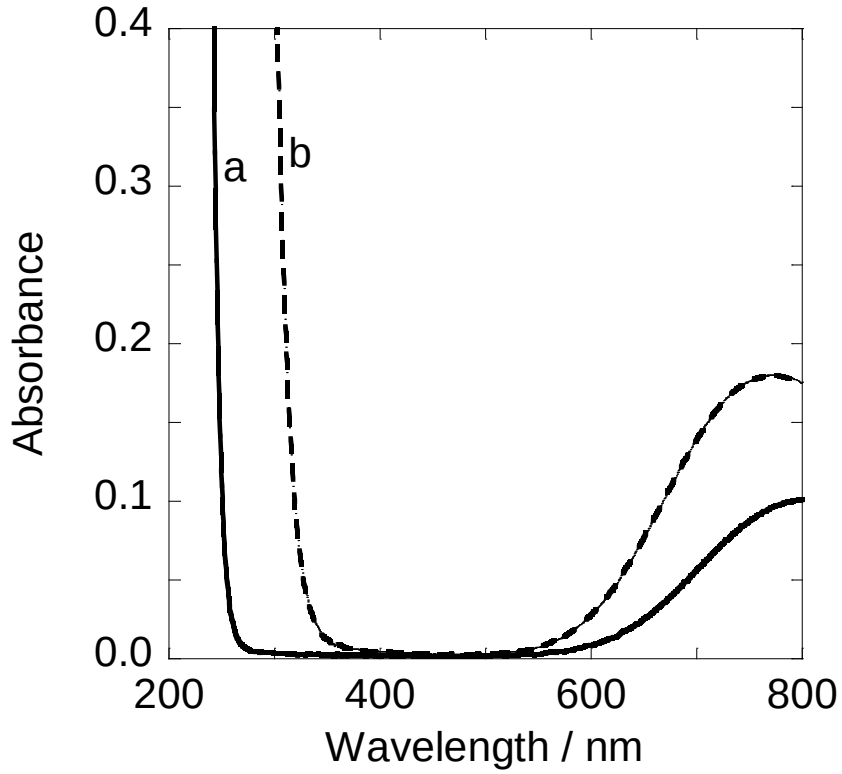

Figure 3. UV-visible absorption spectra of 7 mM Cu^{2+} (a), and mixture of 7 mM Cu^{2+} and 27 mM propionate at pH 6 (b).

Next, the photolysis was performed in an oxygen atmosphere in order to reoxidize Cu^+ and prevent disproportionation. As expected, Cu^0 was not observed under such conditions, but the production of ethylene stopped long before all of the propionic acid was exhausted. A new maximum was observed in the UV difference spectrum at 270 nm, diagnostic of the Cu(I)-ethylene complex[54] for which $K_{21} = 2.2 \times 10^5\ M^{-1}$.

$$Cu^+ + C_2H_4 \rightleftharpoons Cu(C_2H_4)^+ \qquad (21)$$

Nearly complete consumption of propionic acid could be accomplished only under continuous purge with O_2 to remove ethylene and reoxidize Cu^+. Only traces of unreacted propionic acid were observed by ^1H NMR after a 6 hour irradiation of a solution containing 2.8 mM Cu^{2+} and 38 mM propionic acid (pH 7) at 575 nm.

The successful photolysis with the 575 nm light prompted us to attempt photolysis with sunlight to take advantage of the more intense band in the 700 - 800 nm region, Figure 3. For this purpose, 15 mL of O_2-saturated solution of Cu^{2+} (1 mM) and sodium propionate (105 mM) in D_2O in a 10 cm cylindrical quartz cell was exposed to daylight on a windowsill for one week. The 15 mL head space was filled with O_2. After one week, the concentration of propionic acid decreased by 15 mM as determined by ^1H NMR. Ethylene (91 %) and ethane (9 %) were detected in the headspace. The source of ethane may be the reaction between ethyl radicals and propionic acid, eq 5, which could contribute only after the majority of Cu^{2+} was reduced to Cu^+ and removed as $Cu(C_2H_4)^+$. No further decrease in propionic acid was observed after an additional week of photolysis, confirming that large amounts of ethylene in solution effectively halt the catalytic process.

Longer-Chain Acids

Irradiation of solutions containing 2-methyl-hexanoic acid and Fe^{3+} under argon yielded hexane, 1-hexene, 2-*cis*-hexene, and 2-*trans*-hexene. Under O_2, a mixture of C_1 - C_6 hydrocarbons was generated. Similarly, pentanoic acid under argon produced mainly octane and small amounts of butane and butene.

2-Methyl-hexanoic acid in the presence of Cu^{2+} under argon yielded 1-hexene, 2-*cis*-hexene, and 2-*trans*-hexene. Pentanoic acid produced 1-butene, and octanoic acid produced 1-heptene. In every case the UV difference spectra exhibited bands around 270 nm indicative of Cu(I)-olefin complexes.[54] These solutions were turbid owing to the lower solubility of these longer-chain acids and their copper complexes. The reduced reactivity of Cu^+ toward O_2 in mixed H_2O:CH_3CN solvents[55] limited the photochemical conversion to a single turnover.[56]

Octanoic and oleic acids were successfully solubilized in water with Triton X-100,[57] but the photolysis in the presence of Fe^{3+} generated disproportionately large amounts of alkanes, most likely a result of hydrogen atom abstraction by the radicals from Triton X-100.

Acknowledgment

We are thankful to Dr. Stephen Veysey for his assistance with GCMS experiments. This manuscript has been authored under Contract No. DE-AC02-07CH11358 with the U.S. Department of Energy.

Supplemental Information

Figures S1 – S3 are shown in Appendix C.

References

(1) Gooßen, L. J.; Rodríguez, N.; Gooßen, K. *Angew. Chem. Int. Ed.* **2008**, *47*, 3100-3120.
(2) Myers, A. G.; Tanaka, D.; Mannion, M. R. *J. Am. Chem. Soc.* **2002**, *124*, 11250-11251.
(3) Gooßen, L. J.; Lange, P. P.; Rodríguez, N.; Linder, C. *Chemistry – A European Journal* **2010**, *16*, 3906-3909.
(4) Gooßen, L. J.; Rudolphi, F.; Oppel, C.; Rodríguez, N. *Angew. Chem. Int. Ed.* **2008**, *47*, 3043-3045.
(5) Rudolphi, F.; Song, B.; Gooßen, L. J. *Adv. Synth. Catal.* **2011**, *353*, 337-342.
(6) Zhang, F.; Greaney, M. F. *Org. Lett.* **2010**, *12*, 4745-4747.
(7) Zhang, M.; Zhou, J.; Kan, J.; Wang, M.; Su, W.; Hong, M. *Chem. Commun.* **2010**, *46*, 5455-5457.
(8) Zhao, D.; Gao, C.; Su, X.; He, Y.; You, J.; Xue, Y. *Chem. Commun.* **2010**, *46*, 9049-9051.
(9) Casey, C. P.; Singer, S. W.; Powell, D. R. *Can. J. Chem.* **2001**, *79*, 1002-1011.
(10) Gooßen, L. J.; Collet, F.; Gooßen, K. *Isr. J. Chem.* **2010**, *50*, 617-629.
(11) Ward, O. P.; Singh, A. *Curr. Opin. Biotechnol.* **2000**, *11*, 520-526.
(12) Horvat, M.; Mlinaric-Majerski, K.; Griesbeck, A. G.; Basaric, N. *Photochem. Photobiolog. Sci.* **2011**, *10*, 610-617.
(13) Itou, T.; Yoshimi, Y.; Nishikawa, K.; Morita, T.; Okada, Y.; Ichinose, N.; Hatanaka, M. *Chem. Commun.* **2010**, *46*, 6177-6179.
(14) Roche, T. S.; Endicott, J. F. *J. Am. Chem. Soc.* **1972**, *94*, 8622-8623.
(15) Yang, D.; Ni, X.; Chen, W.; Weng, Z. *J. Photochem. Photobiol. A: Chem.* **2008**, *195*, 323-329.
(16) Boddien, A.; Gärtner, F.; Federsel, C.; Sponholz, P.; Mellmann, D.; Jackstell, R.; Junge, H.; Beller, M. *Angew. Chem. Int. Ed.* **2011**, *50*, 6411-6414.
(17) Boddien, A.; Mellmann, D.; Gärtner, F.; Jackstell, R.; Junge, H.; Dyson, P. J.; Laurenczy, G.; Ludwig, R.; Beller, M. *Science* **2011**, *333*, 1733-1736.
(18) Kalnes, T. M., Terry; and Shonnard, David R. *Int. J. Chem. React. Eng.* **2007**, *5*, A48.
(19) Savage, P. E. *Preprints of Symposia - Amer. Chem. Soc., Division of Fuel Chemistry* **2010**, *55*, 245-246.
(20) Serrano-Ruiz, J. C.; Braden, D. J.; West, R. M.; Dumesic, J. A. *Applied Cat. B: Environ.* **2010**, *100*, 184-189.
(21) Kubičková, I.; Kubička, D. *Waste and Biomass Valorization* **2010**, *1*, 293-308.
(22) Smith, B.; Greenwell, H. C.; Whiting, A. *Energy & Environ. Sci.* **2009**, *2*, 262-271.
(23) Han, J.; Sun, H.; Duan, J.; Ding, Y.; Lou, H.; Zheng, X. *Adv. Synth. Catal.* **2010**, *352*, 1805-1809.
(24) Kunkes, E. L.; Simonetti, D. A.; West, R. M.; Serrano-Ruiz, J. C.; Gärtner, C. A.; Dumesic, J. A. *Science* **2008**, *322*, 417-421.
(25) Yakovlev, V. A.; Khromova, S. A.; Sherstyuk, O. V.; Dundich, V. O.; Ermakov, D. Y.; Novopashina, V. M.; Lebedev, M. Y.; Bulavchenko, O.; Parmon, V. N. *Catal. Today* **2009**, *144*, 362-366.

(26) Gilbert, B. C.; Hodges, G. R.; Lindsay, S. J. R.; MacFaul, P.; Taylor, P. *J. Chem. Soc., Perkin Trans. 2* **1996**, 519-524.
(27) Gilbert, B. C.; Lindsay, S. J. R.; Parsons, A. F.; Setchell, P. K. *J. Chem. Soc., Perkin Trans. 2* **1997**, 1065-1073.
(28) Kuhnle, J. A.; Lundin, R. E.; Waiss, A. C., Jr. *J. Chem. Soc., Chem. Commun.* **1972**, 287-288.
(29) Bideau, M.; Claudel, B.; Faure, L.; Rachimoellah, M. *J. Photochem.* **1987**, *39*, 107-128.
(30) Bideau, M.; Claudel, B.; Faure, L.; Kazouan, H. *J. Photochem. Photobiol. A:* **1992**, *67*, 337-348.
(31) Glebov, E. M.; Pozdnyakov, I. P.; Grivin, V. P.; Plyusnin, V. F.; Zhang, X.; Wu, F.; Deng, N. *Photochem. Photobiol. Sci.* **2011**, *10*, 425-430.
(32) Haim, A.; Taube, H. *Inorg. Chem.* **1963**, *2*, 1199-1203.
(33) Bakac, A.; Espenson, J. H. *J. Phys. Chem* **1986**, *90*, 325-327.
(34) Pestovsky, O.; Bakac, A. *Inorg. Chem.* **2005**, *45*, 814-820.
(35) *CRC Handbook of Chemistry and Physics*; 89th ed.; Haynes, W. M., Ed.; CRC Press: Boca Raton, FL, 2008-2009.
(36) Margerum, D. W.; Sommer, B. A. *Inorg. Chem.* **1970**, *9*, 2517-2521.
(37) Perrin, D. D. *J. Chem. Soc.* **1959**, 1710-1717.
(38) Davies, M. J.; Gilbert, B. C.; Thomas, C. B.; Young, J. *J. Chem. Soc., Perkin Trans. 2* **1985**, 1199-1204.
(39) Funke, A.; Ziegler, F. *Biofuels, Bioproducts and Biorefining* **2010**, *4*, 160-177.
(40) Matsubara, S.; Yokota, Y.; Oshima, K. *Org. Lett.* **2004**, *6*, 2071-2073.
(41) Neta, P.; Grodkowski, J.; Ross, A. B. *J. Phys. Chem. Ref. Data* **1996**, *25*.
(42) Bakac, A.; Wang, W.-D. *Inorg. React. Mech.* **1998**, *1*, 65-73.
(43) Sillen, L. G., Martell, A. E. *Stability Constants of Metal-Ion Complexes*; 2nd ed.; The Chemical Society, Burlington House: London, England, 1964.
(44) Slagle, I. R.; Feng, Q.; Gutman, D. *J. Phys. Chem* **1984**, *88*, 3648-3653.
(45) Bakac, A. *Inorg. React. Mech.* **1998**, *1*, 65.
(46) Nadtochenko, V. A.; Kiwi, J. *Inorg. Chem.* **1998**, *37*, 5233-5238.
(47) Thornton, A. T.; Laurence, G. S. *J. Chem. Soc., Dalton Trans.* **1973**, 804-813.
(48) Jayson, G. G.; Parsons, B. J.; Swallow, A. J. *J. Chem. Soc., Faraday Trans. 1* **1973**, *69*, 1597-1607.
(49) Bakac, A. *Croat. Chem. Acta* **2001**, *74*, 633-640.
(50) Rabinowitch, E.; Stockmayer, W. H. *J. Am. Chem. Soc.* **1942**, *64*, 335-347.
(51) Kelley, D. G.; Espenson, J. H.; Bakac, A. *Inorg. Chem.* **1990**, *29*, 4996-5000.
(52) Beckwith, A. L. J.; Pigou, P. E. *Aust. J. Chem.* **1986**, *39*, 77-87.
(53) Beckwith, A. L. J.; Pigou, P. E. *Aust. J. Chem.* **1986**, *39*, 1151-1155.
(54) Buxton, G. V. G., John C.; Sellers, Robin M. *J. Chem. Soc., Dalton Trans.* **1976**, 2160-2165.
(55) Wakisaka, A.; Shimizu, Y.; Nishi, N.; Tokumaru, K.; Sakuragi, H. *J. Chem. Soc., Faraday Trans.* **1992**, *88*, 1129-1135.
(56) Senanayake, G.; Muir, D. *Metallurgical and Materials Transactions B* **1990**, *21*, 439-448.
(57) Ruiz, F.-J.; Rubio, S.; Pérez-Bendito, D. *Anal. Chem.* **2007**, *79*, 7473-7484.

CHAPTER 5

GENERATION OF FREE OXYGEN ATOMS O(^{3}P) IN SOLUTION via PHOTOLYSIS OF 4-BENZOYLPYRIDINE N-OXIDE:

MECHANISTIC INSIGHT FROM TIME RESOLVED PHOTOLYSIS

Jack M. Carraher and Andreja Bakac

A manuscript in preparation

Abstract

Photolysis of 4-benzoylpyridine N-oxide (BPyO) in the presence of quenchers of the triplet excited state (^{3}BPyO*) produces up to 41 % O(^{3}P). In the absence of ^{3}BPyO* quenchers a maximum of 13 % O(^{3}P) relative to consumed BPyO is obtained. The remaining products are hydroxylated-4-benzoylpyridine and 4-benzoylpyridine. ^{3}BPyO* exhibits maxima at 380 nm and 490 nm ($\varepsilon_{380\ nm} = 3.5 \times 10^4\ M^{-1}\ cm^{-1}$ and $\varepsilon_{490\ nm} = 1.05 \times 10^4\ M^{-1}\ cm^{-1}$), and reacts readily with O_2 ($k = 1.4 \times 10^9\ M^{-1}\ s^{-1}$). Additionally, the rate of BPyO consumption (as determined by UV-vis) decreases in the presence of ^{3}BPyO* quenching agents. Second order rate constants for ^{3}BPyO* quenching were determined. The radical anion ($BPyO^{\bullet-}$) was generated upon reduction of ^{3}BPyO* by Fe^{2+} or $ABTS^{2-}$. $BPyO^{\bullet-}$ exhibits a maximum at 510 nm ($\varepsilon_{510\ nm} = 2200\ M^{-1}\ cm^{-1}$), and is relatively unreactive. When generated from ^{3}BPyO* and $ABTS^{2-}$; back electron transfer ($ABTS^{\bullet-}$ +

BPyO$^{\bullet-}$) is observed ($k = 1.7 \times 10^9$ M^{-1} s^{-1}). A mechanism for photochemical deoxygenation of BPyO is proposed on the basis of kinetic data and product distribution under various conditions. Additionally, comparisons are made between the observed intermediates and similar triplet excited states and radical anions.

Introduction

The reactivity of triplet oxygen atom, O(^{3}P), has been widely studied in the gas phase[1-10] for its significance in atmospheric chemistry.[4-6,11,12] It is relevant not only because of its own chemistry, but for the formation of other photoactive species, which can in turn generate other reactive oxygen species.[5,13] For instance, photolysis of tropospheric N_2O leads to the formation of O(^{3}P).[11] O(^{3}P) can react with O_2 and generate ozone.[5,14] Photolysis of O_3 generates O(^{3}P)[5] and other reactive species like O(^{1}D) and $^{\bullet}$OH.[5] Generation of these highly reactive species in the presence of pollutants can lead to acid rain.[13] Direct reactions of O(^{3}P) have also been examined in the context of materials degradation in spacecraft.[7,15] To the contrary, substantially less is known about O(^{3}P) reactions in solution.

Recent work by McCulla et al. suggests that there is a great deal of biological significance in the solution phase chemistry of O(^{3}P). The results in this work suggest that O(^{3}P) can selectively target cysteine residues for oxidation due to its thiophilicity. In this study McCulla supports the assertion that the chemistry observed is due to O(^{3}P) based on the different reactivity expected for other reactive oxygen species.[16] O(^{3}P) has the potential to be significant in an industrial setting. O(^{3}P) is known to react with aromatic hydrocarbons[2,3] and alkanes[8,17] yielding alcohols, and with olefins[4,9,10,18-21] to yield epoxides, ketones, and aldehydes. Compared to other reactive oxygen species,

$O(^3P)$ is quite selective. For instance, O_3 is known to react with olefins to produce aldehyde/ketone and carboxylic acid.[13,22] Hydroxyl and superoxide radicals can get involved in radical chain reactions. Additionally, they are less selective due to their high reactivity, $k_{\bullet OH + organics}$ typically $10^8 - 10^9$ M^{-1} s^{-1}.[23-25] $^1O_2$ is reported to yield ketones, aldehydes, and alcohols in reactions with olefins, but no epoxides.[26] $O(^1D)$ is too short lived to be useful in aqueous solutions, and readily inserts into O-H bonds of water yielding "hot" (energetically excited) H_2O_2.[27] The O-O bond of "hot" H_2O_2 cleaves yielding 2 $^\bullet$OH.[27] $O(^1D)$ not consumed by solvent molecules will relax to $O(^3P)$.[5,13]

Despite the unique reactivity of $O(^3P)$, its implementation as a synthetic tool is hampered by methods for its generation. Unfortunately, current methods for $O(^3P)$ generation have low yields and produce other reactive oxygen species.[14,18,20,28-30] Microwave discharge,[19] for instance, is reported to generate $O(^1D)$, $^1O_2$, and O_3 in addition to $O(^3P)$.[18] Other methods like the photolysis of heterocyclic N-oxides [28,29,31,32] and S-oxides[33-35] typically have low yields of $O(^3P)$. Additionally, the formation of $O(^3P)$ is often assumed on the basis of deoxygenated reactant and oxidized solvent.[36,37] There is a great deal of disagreement when it comes to the mechanistic details of $O(^3P)$ generation from photolysis of compounds containing N-oxide and S-oxide functionalities. The excited triplet state of heterocyclic N-oxides has been suggested to be responsible for photo-deoxygenation, while O migration and ring cleavage are attributed to the excited singlet.[31,38,39] This hypothesis is supported by an apparent correlation between the degree to which the triplet is formed in substituted pyridine N-oxides and the extent of deoxygenation.[28,31,37,40] Additionally, introduction of O_2 (a known triplet quencher)[41-43] results in a decrease in the efficiency of deoxygenation.[38,40] To the contrary, recent

reports from de Lucas et al.[44] and Jenks[45] suggest that the observed triplet does not result in ejection of $O(^3P)$. De Lucas et al. bases this conclusion on the observation that generation of the triplet excited state of a thiophene S-oxide *via* energy transfer from triplet excited benzophenone did not result in deoxygenation of a the S-oxide.[44] Likewise, Jenks' calculations suggest that the observed triplet excited state of thiophene S-oxide is too low in energy for deoxygenation.[45] A third possibility that has been suggested is that free $O(^3P)$ is never formed. The resulting chemistry is attributed to an oxaziridine intermediate.[46-48] In one example the oxaziridine intermediate is believed to have been trapped by *para*-anisidine in a study in which DNA was cleaved as a result of photolysis of 3-amino-1,2,4-benzotriazine 1,4-dioxide.[46] Though the above mentioned publications offer a great deal of insight into the photolysis of N- and S-oxides; the mechanisms and roles of intermediates involved in $O(^3P)$ generation remain unclear.

In the current study, the intermediates and products of photolysis of 4-benzoylpyridine N-oxide (BPyO) are identified and characterized. Mechanistic details are gleaned from experimental data, and a more complete picture of pyridine N-oxide photochemistry emerges. The molecule BPyO was chosen for this study, because early studies have suggested an 80 % yield of 4-benzoylpyridine (BPy) (*i.e.*, 80 % deoxygenation).[37] The author attributed the efficiency of deoxygenation to the fast intersystem crossing ($k_{isc} \sim 10^{11}$ s^{-1}); 'forcing' the molecule into the triplet manifold, and thereby minimizing the reactivity of the excited singlet.[37] Additionally, we reason that the benzophenone-like character of BPyO is expected to yield a triplet excited state (^{3}BPyO*) with a relatively long lifetime that we can observe by laser flash photolysis

(LFP). Direct observation of ^{3}BPyO* in tandem with product analysis offer a great deal of insight into the photochemical deoxygenation process of BPyO.

Experimental

Materials

The following items were of the best available quality, and were used as received. Iron(III) perchlorate hydrate, iron(II) perchlorate hydrate, palladium(II) acetate, nickel(II) perchlorate hydrate, manganese(II) perchlorate hydrate, 2,2′-azino-bis(3-ethylbenzothiazoline-6-sulfonic acid) diammonium salt, deuterium oxide (99.9 % D), 4-benzoylpyridine, 1,10-phenanthroline, methanol, 2-propanol, chromotropic acid (all Sigma Aldrich), perchloric acid (70 %), phosphoric acid (85 %), benzophenone, trifluoroacetic acid, dimethylsulfoxide, sodium iodide, sodium bromide, sodium chloride (all Fisher Scientific), silver(I) nitrate, potassium chromate (both Baker), acetonitrile (Honeywell), and acetonitrile-d3 (99.8 % D) (Cambridge Isotopes). Solutions of copper(II) perchlorate were prepared from solid hydrated perchlorate salt and standardized iodometrically. 4-Benzoylpyridine N-oxide,[49] *trans*-cyclam chromium(III) dicyano triflate (cyclam = 1,4,8,11-tetraazacyclotetradecane),[50] and perchlorate salts of cyclam nickel(II) ((cyclam)Ni^{2+}),[51] *meso*-5,5,7,12,12,14-hexamethylcyclam nickel(II) ((Me_6-cyclam)Ni^{2+}),[52] (lR,4S,8R,11S)-1,4,8,11-tetramethylcyclam nickel(II) ((Me_4-cyclam)Ni^{2+}),[53] (1R,4R,8S,11S)-C-meso-1,4,5,5,7,8,11,12,12,14-decamethylcyclam nickel(II) ((Me_{10}-cyclam)Ni^{2+}),[54] and UO_2^{2+} [55] were available in our laboratory from earlier studies.

Instrumentation

UV-vis spectra were collected with a Shimadzu UV-3101PC spectrophotometer, NMR spectra with a Bruker AVIII-600 (600 MHz) and analyzed with MestReNova version 8.1 software. GCMS data was collected with an Agilent 6890 gas chromatograph equipped with a split/splitless injector (10:1 split ratio). An Agilent HP-PLOT/Q column attached to a Waters GCT accurate mass time-of-flight mass spectrometer in positive EI mode (70 EV) with a scan rate of 0.3 s per scan and a mass range of 10–200 Daltons. Waters MassLynx 4.0 software was used to acquire and process GC-MS data (average of 3–5 runs). Laser-flash photolysis (LFP) was carried out with a Lambda Physik Excimer Pro 2 xenon chloride excimer laser and an Applied Photophysics monitoring system.[56] Quenching of $*UO_2^{2+}$ emission by BPyO was observed by LFP experiments which utilized a Phasar dye laser system with LD 490 dye from Exciton.[57] Steady-state photolysis was carried out at 313 nm in a Luzchem LZC-5 photoreactor. KaleidaGraph 4.0 software was used for data analysis and processing. Water was purified with a Barnstead EASYpure III UV UF system.

Methods

LFP irradiations were carried out in 1 cm square quartz fluorescence cells with Chromres Puresep T 7/16" septa. Unless otherwise stated, all experiments utilized the 308 nm Excimer laser. UV-vis spectra were collected before and after LFP. Typical LFP experiments were carried out in degassed solutions containing 50 – 100 μM BPyO, and were monitored at 490 nm. Concentrations of substrate, when present, ranged from 10^{-6} to 10^{-1} M. Kinetic traces obtained by LFP were fit to appropriate rate equations (typically

1st order) using the software native to the Applied Photophysics monitoring system, or further analyzed with KaleidaGraph data processing software.

313 nm irradiations utilizing the Luzchem LCZ-5 photoreactor required the implementation of a set of filters to block photons of undesired wavelengths. The filter set was comprised of a 30 mL beaker containing an aqueous solution of 1 mM K_2CrO_4 that was placed in the center of another 100 mL beaker containing a 0.33 M aqueous solution of $CuSO_4$. The sample was placed in the center of the inner beaker, and the levels of the filter solutions were brought up to the bottom of the screw cap on the spectrophotometric cells. A composite UV-vis spectrum of the two filters (1 cm path length each) is shown in the SI, Figure S1, and exhibits an absorption of 2 at 302 nm and 340 nm. The progress of sample irradiation was monitored by UV-vis, $\Delta\varepsilon_{292\ nm}$ = 15,000 M^{-1} cm^{-1} in H_2O and $\Delta\varepsilon_{322\ nm}$ = 20,000 M^{-1} cm^{-1} in MeCN. Samples were irradiated to 50 – 90 % consumption of BPyO. ^{1}H NMR data were collected after photolysis of 0.6 mL solutions of 1 mM BPyO. These samples were irradiated in a 0.1 cm quartz cell, and ^{i}PrOH internal standards were added prior to ^{1}H NMR data collection. As a control 1 mM solutions of BPyO in 0.1 cm cells were irradiated *via* 500 laser shots and analyzed by ^{1}H NMR. The ^{1}H NMR data collected after LFP irradiation were identical to the data collected after irradiation by the photoreactor method.

Molar absorptivities of BPyO were determined from UV-vis spectra after dissolution of a known mass of solid BPyO in either H_2O, $\varepsilon_{292\ nm}$ = 19,700 M^{-1} cm^{-1}, or MeCN, $\varepsilon_{322\ nm}$ = 21,200 M^{-1} cm^{-1}. The molar absorptivity of the aqueous solution determined in this work is consistent with the previously reported literature value.[58]

The K_a of $BPyOH^+$ in water was determined spectrophotometrically. UV-vis spectra were collected of solutions containing 38 μM BPyO and 0 - 6 M $HClO_4$ (6 M ionic strength, $NaClO_4$). The absorbance at 292 nm was plotted as a function of -log[$HClO_4$] and fit to eq S6. The absorbance at 292 nm decreases only slightly above 3 M $HClO_4$, and nearly all BPyO is assumed to be in the form $BPyOH^+$ at 6 M $HClO_4$. Full protonation of BPyO is not observed at 1 M ionic strength; therefore, more data was collected at 6 M ionic strength. The absorbance due to BPyO at 292 nm was the same in the presence of 1 M as 6 M $NaClO_4$ solutions, but absorbance at 292 nm in the presence of 1 M $HClO_4$ varied slightly with ionic strength ($Abs_{292\ nm}$ = 0.5 and 0.6 for μ = 6 M and 1 M, respectively). The absorbance at 292 nm was plotted as a function of –log[$HClO_4$]. K_a (1.2 ± 0.5 M^{-1}) was determined from the fit of equation S6 to the plot. The UV-vis spectra, Figure S2, plot of $Abs_{292\ nm}$ vs. -log[$HClO_4$], Figure S3, and derivation of eq S6 are shown in the SI.

The K_a of $BPyOH^+$ in acetonitrile ($K_a^{BPyOH^+} = 4 \pm 4 \times 10^{-13}$ M^{-1}) was determined by a method similar to that described for aqueous solutions. The K_a of $PyOH^+$ compounds in MeCN is known to vary widely with [H_2O];[59] BPyO was found to be no exception. For this reason, CF_3CO_2H was chosen instead of $HClO_4$ to avoid addition of H_2O with the acid (no special precautions were taken to dry MeCN in this work). Solutions containing 1.09 mM BPyO and 0 - 94 mM CF_3CO_2H were prepared in 0.1 cm cells, and spectra were collected. No further decrease in absorbance at 322 nm was observed at CF_3CO_2H concentrations above 94 mM. Unlike $HClO_4$, which dissociates completely in water, the K_a of CF_3CO_2H in MeCN (pK_a = 12.65 ± 1.38)[60] is relevant to

the calculation of K_a for $BPyOH^+$ in MeCN. The spectrum of BPyO with no added CF_3CO_2H is assumed to contain only BPyO. The spectrum in which 94 mM CF_3CO_2H and BPyO are present is assumed to contain only $BPyOH^+$ on the basis of UV-vis spectra containing $[CF_3CO_2H] > 94$ mM. The difference in molar absorptivity was determined ($\Delta\varepsilon_{322\ nm} = 19{,}700\ M^{-1}\ cm^{-1}$) from these two extremes. The change in absorbance at 322 nm relative to BPyO with no added CF_3CO_2H was used to calculate $[BPyOH^+]$. The K_a of $BPyOH^+$ in MeCN was determined for each spectrum and averaged.

The molar absorptivity of ^{3}BPyO* in water ($\varepsilon_{417\ nm} = 19{,}000 \pm 500\ M^{-1}\ cm^{-1}$) was determined by monitoring the formation of $ABTS^{\bullet-}$ ($\varepsilon_{417\ nm} = 3.47\times 10^4\ M^{-1}\ cm^{-1}$),[61] a product resulting from reduction of ^{3}BPyO* by $ABTS^{2-}$, eq 5, during LFP ($\lambda_{mon} = 417$ nm) of a degassed solution containing 40 μM BPyO and 50 μM $ABTS^{2-}$. Accurate determination of the molar absorptivity of ^{3}BPyO* by this method requires the following be true: (i) all ^{3}BPyO* observed reacts with $ABTS^{2-}$ to generate $BPyO^{\bullet-}$ and $ABTS^{\bullet-}$, (ii) the amount of absorbance of $BPyO^{\bullet-}$ (relative to $ABTS^{\bullet-}$) is negligible at 417 nm, (iii) any decay of $ABTS^{\bullet-}$ signal must be sufficiently separated in time from its formation, and (iv) direct irradiation of $ABTS^{2-}$ must not generate $ABTS^{\bullet-}$ on the time scale of LFP. These criteria are met under the experimental conditions: (i) the maximum $Abs_{417\ nm}$ due to $ABTS^{\bullet-}$ formation relative to initial absorbance from ^{3}BPyO* does not change with $[ABTS^{2-}]$. (ii) The absorbance at due to $ABTS^{\bullet-}$ formation at the peak of the kinetic trace is ~ 3 times greater than the initial absorbance due to ^{3}BPyO*, Figure 7, AND formation of $BPyO^{\bullet-}$ by reduction of ^{3}BPyO* with Fe^{2+}, eq 4, yields $BPyO^{\bullet-}$ absorbance that is roughly one quarter of the absorbance observed for ^{3}BPyO* at 490 nm, Figure 5; and one

tenth at 417 nm. Therefore the ratio of $\varepsilon_{ABTS^{\bullet-}}$ / $\varepsilon_{BPyO^{\bullet-}}$ at 417 nm is ~ 30 : 1. Experiments with Fe^{2+} and ^{3}BPyO* yield a ratio of 35 : 1 at 417 nm ($BPyO^{\bullet-}$ $\varepsilon_{417\ nm} \sim 1 \times 10^3\ M^{-1}\ cm^{-1}$ vs. $ABTS^{\bullet-}$, $\varepsilon_{417\ nm} = 3.47 \times 10^4\ M^{-1}\ cm^{-1}$).[61] (iii) The amount of absorbance due to $ABTS^{\bullet-}$ formation is independent of the rate of back electron transfer, eq 6, at all concentrations of $ABTS^{\bullet-}$ examined (that is, formation and decay or $ABTS^{\bullet-}$ are well separated in time). (iv) No change in absorbance at 417 nm was observed upon LFP of $ABTS^{2-}$. All of the above mentioned chemistry is described in more detail in the **Results** section.

The **quantum yield for ^{3}BPyO* formation in water** was determined by 308 nm LFP of standard solutions of $Ru(bpy)_3^{2+}$. A degassed solution of 6.6 μM BPyO ($Abs_{308\ nm}$ = 0.092) in a 1 cm square fluorescence cell was subjected to a 308 nm laser flash. The absorbance due to ^{3}BPyO* formation (λ_{mon} = 380 nm, $\Delta\varepsilon_{380\ nm} = 35{,}200\ M^{-1}\ cm^{-1}$)[62] was observed immediately following the laser flash, [^{3}BPyO*] = 1.3 μM. A solution of $Ru(bpy)_3^{2+}$ ($Abs_{308\ nm}$ = 0.091) was flashed in the same fashion to generate $Ru(bpy)_3^{2+}$* (Φ = 1, $\Delta\varepsilon_{380\ nm} = 8700\ M^{-1}\ cm^{-1}$).[63,64] The experiment generated 5.6 μM $Ru(bpy)_3^{2+}$*, from which we obtained a quantum yield of 0.2 for formation of ^{3}BPyO* in H_2O.

The molar absorptivity of ^{3}BPyO* in MeCN could not be determined by $ABTS^{\bullet-}$ as described for aqueous solutions, due to low solubility of $(NH_4)_2ABTS$ in MeCN. Therefore, a lower limit ($\varepsilon_{490\ nm} \geq 4300 \pm 900\ M^{-1}\ cm^{-1}$) was determined by $Ru(bpy)_3^{2+}$ actinometry (Φ = 1, $\Delta\varepsilon_{380\ nm} = 11{,}000\ M^{-1}\ cm^{-1}$).[64-66] The quantum yield for ^{3}BPyO* formation in MeCN is unknown, and the lower limit of ε was obtained by using $\Phi_{^3BPyO^*}$ = 1 in calculations. Absorbance of the two solutions, BPyO and $Ru(bpy)_3^{2+}$, at

the excitation wavelength, 308 nm, was 0.1. A spectrum of ^{3}BPyO* was collected by monitoring LFP at several wavelengths, Figure S6.

The molar absorptivity of BPyO$^{\bullet-}$ in water was determined by LFP (λ_{mon} = 490 nm) of 40 μM BPyO in the presence of 10 mM Fe^{2+} in 0.1 M $HClO_4$. A spectrum of BPyO$^{\bullet-}$ was collected and is shown in Figure 6. ^{3}BPyO* was generated immediately following the laser flash. Over the next 3 μs the signal due to ^{3}BPyO* decreased to roughly one quarter its initial intensity due to reduction by Fe^{2+} (forming BPyO$^{\bullet-}$), eq 4. The BPyO$^{\bullet-}$ signal decayed over 200 μs. The entire kinetic trace is described in detail in the **Results** section and can be seen in Figure 5. The concentration of ^{3}BPyO* was calculated from the absorbance immediately following the laser flash ($\varepsilon_{490\ nm}$ = 1.05 × 10^4 M^{-1} cm^{-1}). All ^{3}BPyO* was assumed to have been converted to BPyO$^{\bullet-}$ within the first 3 μs following the laser flash ($[^3BPyO^*]_o = \Delta[BPyO^{\bullet-}]$). The absorbance 3 μs after the laser flash yielded $\varepsilon_{490\ nm}$ = 1950 ± 50 M^{-1} cm^{-1} for BPyO$^{\bullet-}$. The same criteria as those described above (^{3}BPyO*/$ABTS^{2-}$) are met under the experimental conditions. (i) The amount of absorbance due to reduction ^{3}BPyO* is independent of [Fe^{2+}], *i.e.*, all ^{3}BPyO* reacts with Fe^{2+} to yield BPyO$^{\bullet-}$. (ii) Aqueous Fe^{3+} does not absorb at 490 nm. (iii) The formation and decay of absorbance due to BPyO$^{\bullet-}$ are sufficiently separated in time. (iv) Fe^{2+} does not absorb at 308 nm and is therefore unable to be excited by the 308 nm laser flash.

Results

Laser Flash Photolysis of BPyO

LFP of degassed aqueous solutions of 50 μM BPyO, Figure 1, spectrum a, yielded a long lived transient which decayed with k_{obs} = 1.2 × 10^5 s^{-1}. This transient exhibits absorption maxima at 380 nm, 3.5 (± 0.1) × 10^4 M^{-1} cm^{-1} and 490 nm, 1.05 (± 0.02) × 10^4 M^{-1} cm^{-1}, Figure 2. A plot of k_{obs} vs. [BPyO], Figure 3, indicates that ^{3}BPyO* decays unimolecularly, eq 1, with k_1 = 3.3 (± 0.9) × 10^4 s^{-1}, and through quenching by ground state BPyO, eq 2 k_2 = 1.5 (± 0.2) × 10^9 M^{-1} s^{-1}. The transient reacted rapidly with O_2, eq 3, and a plot of k_{obs} vs. [O_2], Figure 4, is linear with slope = 1.4 (± 0.1) × 10^9 M^{-1} s^{-1} and y-intercept = 1.2 × 10^5 s^{-1}. The y-intercept is consistent with the observed signal decay in degassed solutions. The large second order rate constant in the reaction with O_2 suggests that the transient absorbing species is most likely a triplet,[42,43,67] and is therefore concluded to be the lowest triplet excited state of BPyO.

^{3}BPyO* → Products (1)

^{3}BPyO* + BPyO → Products (2)

^{3}BPyO* + $^3O_2$ → Products (1)

The lifetime of ^{3}BPyO* was not affected by pH or deuteration of the solvent. ^{3}BPyO* signal intensity decreased with increasing [H^+]. In the extreme of 6 M $HClO_4$, where $BPyOH^+$ is dominant, no photochemistry was observed.

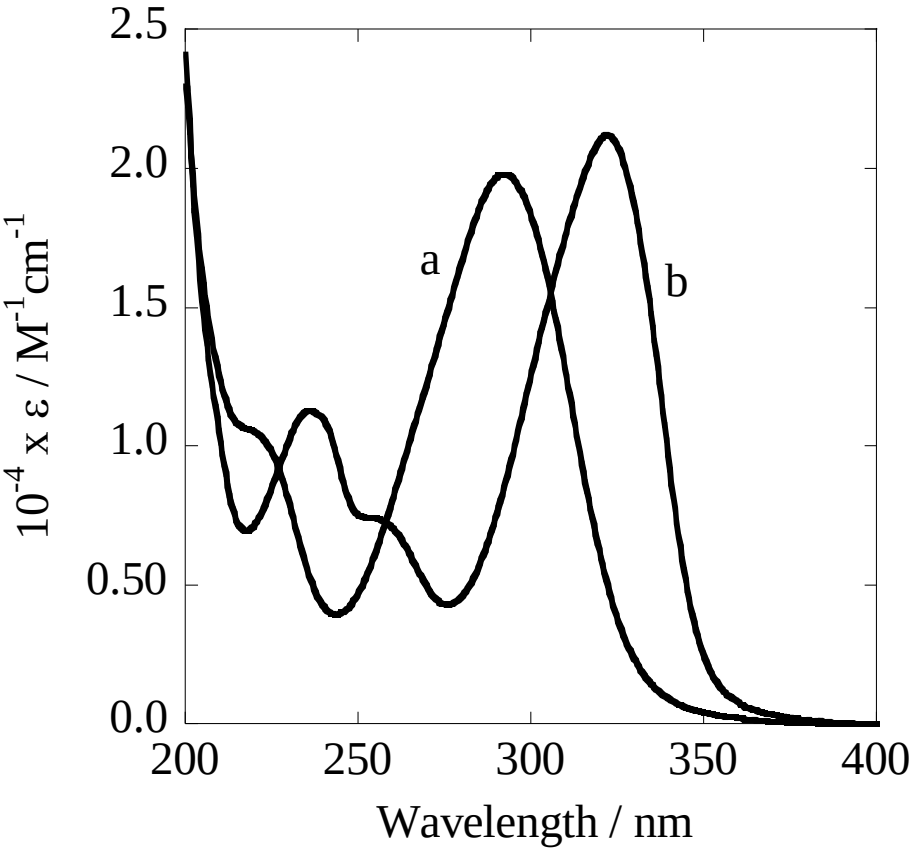

Figure 1. UV-vis spectra of BPyO in water (a) and acetonitrile (b)

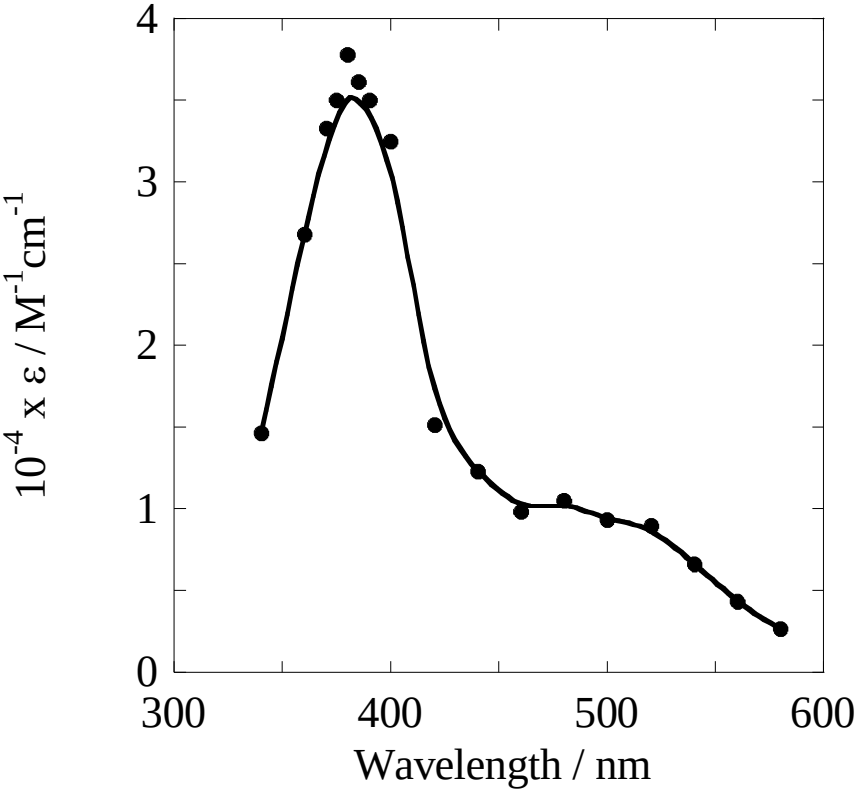

Figure 2. Transient absorption spectrum of ^{3}BPyO* in water obtained from 308 nm LFP of degassed solutions

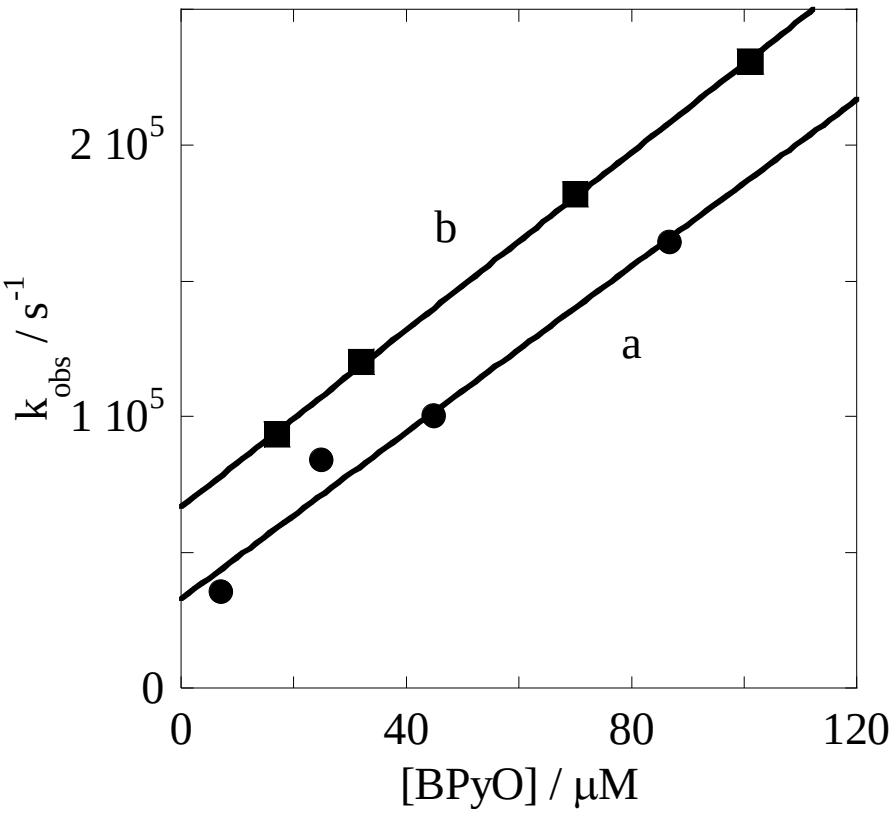

Figure 3. Plot of k_{obs} vs. [BPyO] obtained from 308 nm LFP of degassed solutions of BPyO, λ_{mon} = 490 nm, in water (a) and in acetonitrile (b)

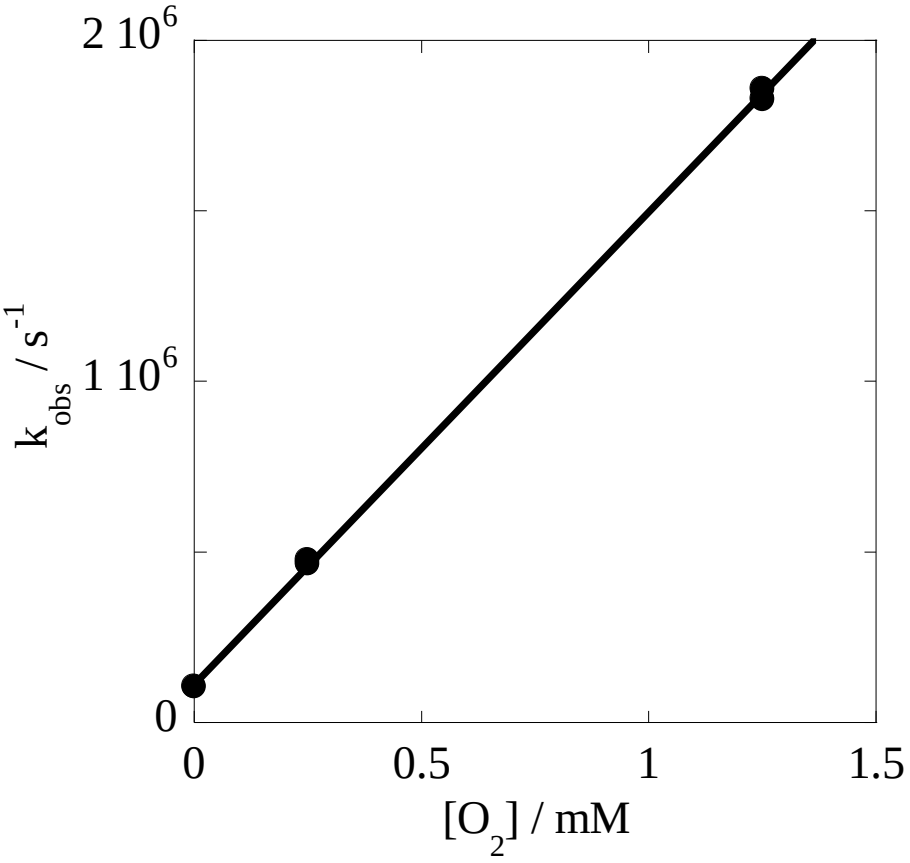

Figure 4. Plot k_{obs} vs. $[O_2]$ for quenching of ^{3}BPyO*

Laser Flash Photolysis of BPyO and Triplet Quenchers

The quenching of ^{3}BPyO* by several compounds was studied by LFP, and second order rate constants were determined. All plots of k_{obs} vs. [Q] are linear and exhibit y-intercept consistent with ^{3}BPyO* decay in the absence of quenchers (~ 1×10^5 s^{-1}). The results are summarized in Table 1. The compound *trans*-dicyano(cyclam)-chromium(III) ((cyclam)$Cr(CN)_2^+$), Table 1, was chosen because its excited state is known to emit at 720 nm.[68,69] Quenching of ^{3}BPyO* by (cyclam)$Cr(CN)_2^+$ was expected to yield (cyclam)$Cr(CN)_2^+$* and result in observable emission. Quenching of ^{3}BPyO* was observed by LFP absorption measurements (λ_{mon} = 490 nm), but emission at 720 nm due to (cyclam)$Cr(CN)_2^+$* was not. Quenching of *UO_2^{2+} emission at 495 nm[70] by BPyO was observed upon LFP (λ_{ex} = 490 nm) of degassed aqueous solutions containing 3 mM UO_2^{2+}, 0.5 M H_3PO_4, and 50 – 149 μM BPyO, Table 1. None of the quenching agents listed in Table 1 yielded observable products of electron transfer with the exceptions of Fe^{2+}, entries 16 – 17, and $ABTS^{2-}$, entry 19. MeOH and ^{i}PrOH had no effect on the lifetime of ^{3}BPyO*.

Table 1. Second order rate constants for quenching of ^{3}BPyO* by various compounds [a]

Substrate	k / M^{-1} s^{-1}
Ag^{+} [b]	5.8 (± 0.1) × 10^6
Mn^{2+} [b]	2.3 (± 0.1) × 10^7
Ni^{2+}	6.5 (± 0.1) × 10^7
(Me_{10}-cyclam)Ni^{2+} [c]	7.5 (± 0.4) × 10^7
Fe^{2+} [b,d]	1.2 (± 0.1) × 10^8
Fe^{2+} [e,d]	1.3 (± 0.1) × 10^8
Fe^{2+} [f]	1.3 (± 0.1) × 10^8
(Me_4-cyclam)Ni^{2+} [g]	1.6 (± 0.1) × 10^8
Cu^{2+} [h]	1.7 (± 0.1) × 10^8
Fe^{3+} [h]	2.5 (± 0.1) × 10^8
(cyclam)$Cr(CN)_2^+$ [i]	4.0 (± 0.1) × 10^8
(Me_6-cyclam)Ni^{2+} [j]	4.4 (± 0.1) × 10^8
(cyclam)Ni^{2+} [i]	1.7 (± 0.1) × 10^9

Table 1. (continued)

Substrate	k / $M^{-1} s^{-1}$
$*UO_2^{2+}$ [k]	2.5 (± 0.3) × 10^9
Pd^{2+} [b]	4.8 (± 0.1) × 10^9
O_2 [l]	1.4 (± 0.1) × 10^9
I^- [m]	2.2 (± 0.1) × 10^9
I^-	5.0 (± 0.1) × 10^9
$ABTS^{2-}$ [n]	4.1 (± 0.1) × 10^9
	1.7 (± 0.3) × 10^9 [o]

[a] All LFP (λ_{ex} = 308 nm, λ_{mon} = 510 nm) was carried out under Ar in aqueous solutions containing 50 μM BPyO, and no added $HClO_4$ unless otherwise stated. Metal ions shown without specific ligands are aqua-species. [b] 0.1 M $HClO_4$. [c] Me_{10}-cyclam = (1R,4R,8S,11S)-C-meso-1,4,5,5,7,8,11,12,12,14-decamethyl-1,4,8,11-tetraazacyclotetradecane. [d] $^3BPyO^* + Fe^{2+} \rightarrow BPyO^{\bullet-} + Fe^{3+}$. [e] 1.0 M $HClO_4$. [f] 5 mM $HClO_4$. [g] Me_4-cyclam = (1R,4S,8R,11S)-1,4,8,11-tetramethyl-1,4,8,11-tetraazacyclotetradecane. [h] 1 M $HClO_4$. [i] cyclam = 1,4,8,11-tetraazacyclotetradecane. [j] Me_6-cyclam = meso-5,5,7,12,12,14-hexamethyl-1,4,8,11-tetraazacyclotetradecane. [k] $*UO_2^{2+} + BPyO \rightarrow UO_2^{2+} + {}^3BPyO^*$. [l] Taking $[O_2]$ = 10 mM in O_2-sat. MeCN;[71] then $k_{O2,MeCN} \sim 2 \times 10^9\ M^{-1}\ s^{-1}$. [m] Acetonitrile solvent. [n] λ_{mon} = 417 nm. [o] $BPyO^{\bullet-} + ABTS^{\bullet-}$ back electron transfer dependent on $[ABTS^{\bullet-}]$, eq 6.

Reduction of ^{3}BPyO* to BPyO$^{\bullet-}$

$BPyO^{\bullet-}$ was observed as a result of $^3BPyO^*$ reduction by Fe^{2+} or $ABTS^{2-}$. Kinetic traces obtained from LFP of BPyO in the presence of Fe^{2+} are shown in Figure 5. These traces consist of three distinctly separate chemical events that are outlined in eq 4. First, the formation of $^3BPyO^*$ is observed immediately following the laser flash (a jump in absorbance from 0 to ~ 0.08). Then reduction of $^3BPyO^*$ by Fe^{2+} yielding $BPyO^{\bullet-}$ and Fe^{3+} is indicated by the absorbance decreasing to ~ 0.02. Finally, the kinetic trace shows the decay of $BPyO^{\bullet-}$. The reduction of $^3BPyO^*$ with Fe^{2+} is first order with respect to $[Fe^{2+}]$ and has no dependence on $[HClO_4]$, Table 1.

The final absorbance due to $BPyO^{\bullet-}$ formation is independent of $[Fe^{2+}]$ at pH 0 and 1, Figure 5 (right), but no absorbance due to $BPyO^{\bullet-}$ was observed at low $[HClO_4]$ (5

mM), Figure 5 (left) trace (e). The rate of $BPyO^{\bullet-}$ decomposition at pH 0 and 1 is independent of $[Fe^{2+}]$, and increases dramatically with ionic strength ($k_{obs} = 1 \times 10^4\ s^{-1}$ at $\mu = 0.1$ M and $k_{obs} = 1 \times 10^5\ s^{-1}$ at $\mu = 0.4$ M).

$$BPyO \xrightarrow{h\nu} {}^3BPyO^* \underset{-Fe^{3+}}{\xrightarrow{Fe^{2+}}} BPyO^{\bullet-} \rightarrow \text{Products} \qquad (4)$$

Unfortunately, the formation of Fe^{3+} could not be confirmed in these experiments due to the substantial absorbance already present in the UV, where Fe^{3+} absorbs $\varepsilon_{240\ nm} = 4160\ M^{-1}\ cm^{-1}$.[72] Nor could Fe^{3+} production be inferred from the changes in $[Fe^{2+}]$ by phenanthroline test[73] due to small $\Delta[Fe^{2+}]$ relative to large $[Fe^{2+}]_o$. It was also not possible to study the possible back electron transfer reaction ($BPyO^{\bullet-} + Fe^{3+} \rightarrow BPyO + Fe^{2+}$) due to rapid quenching of ${}^3BPyO^*$ by Fe^{3+}, $k = 2.5\ (\pm 0.1) \times 10^8\ M^{-1}\ s^{-1}$. Spectra of $BPyO^{\bullet-}$ obtained by photochemical reduction (${}^3BPyO^* + Fe^{2+}$) and by thermal reduction ($BPyO + {}^{\bullet}C(CH_3)_2OH$) exhibit a maximum at 510 nm ($\varepsilon_{510\ nm} = 2.2 \pm 0.2 \times 10^3\ M^{-1}\ cm^{-1}$), Figure 6. The thermal reduction of BPyO is described in detail in the section *Independent generation of $BPyO^{\bullet-}$*.

Formation of $BPyO^{\bullet-}$ during LFP of BPyO in the presence of $ABTS^{2-}$ is implied by exponential growth of $ABTS^{\bullet-}$ signal, eq 5. Kinetic traces for these reactions are qualitatively similar to those observed during LFP of BPyO and Fe^{2+}, Figure 7. Again, three distinct chemical events are observed: (i) generation of ${}^3BPyO^*$ by the laser flash, (ii) reduction of ${}^3BPyO^*$ by $ABTS^{2-}$, and (iii) decay of $BPyO^{\bullet-}$. However, $ABTS^{2-}$ and Fe^{2+} differ in two ways. First, the formation of $BPyO^{\bullet-}$ is not directly observed;

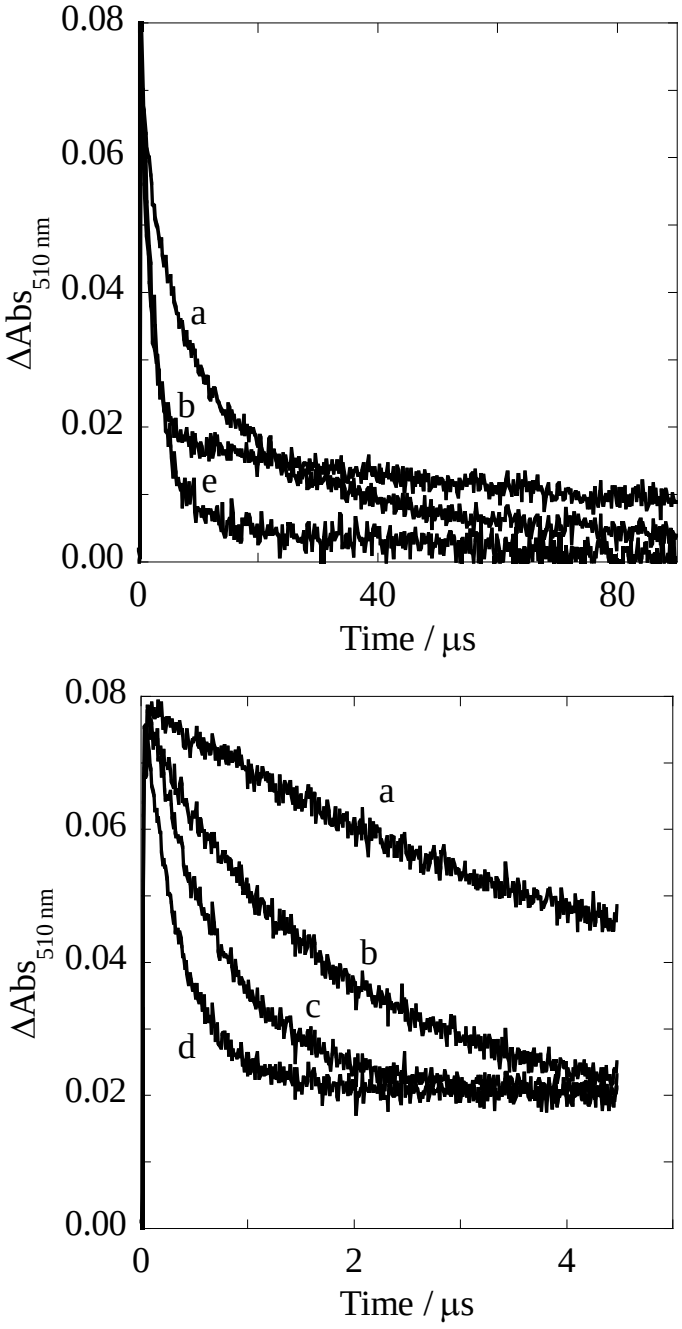

Figure 5. LFP kinetic traces λ_{ex} = 308 nm, λ_{mon} = 510 nm, of degassed solutions of 43 μM BPyO, 0.1 M $HClO_4$, containing 0 mM (a), 3 mM (b), 9 mM (c), and 18 mM (d) Fe^{2+}. Kinetic trace (e) contains 5 mM Fe^{2+} and 5 mM $HClO_4$. Entire kinetic traces (*top*). First 4.5 μs (*bottom*).

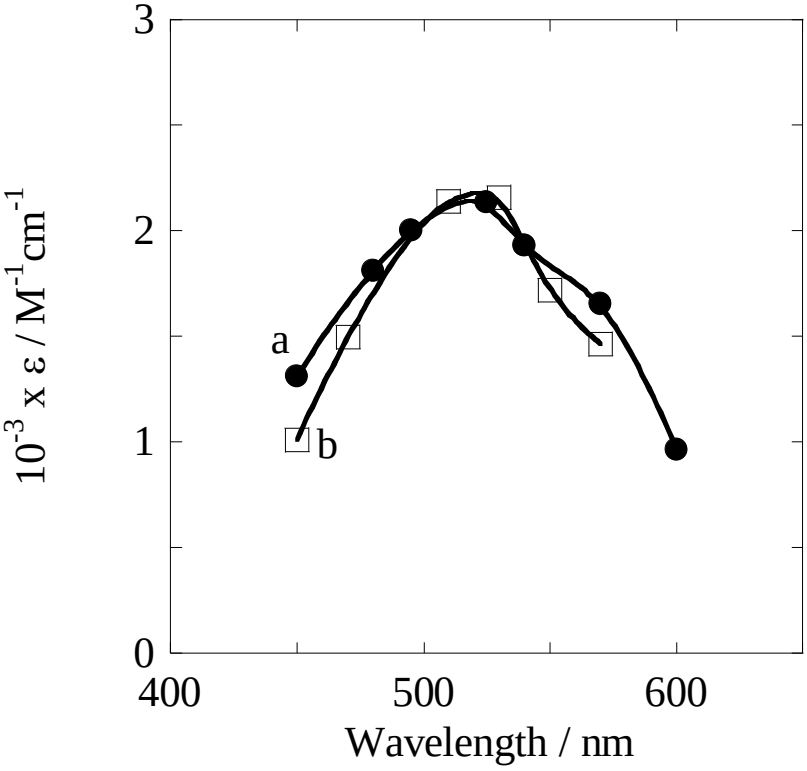

Figure 6. Absorbance spectrum of $BPyO^{\bullet-}$ generated by 308 nm LFP of a solution containing 9 mM Fe^{2+}, 50 μM BPyO, and 0.1 M $HClO_4$ (a) and 1 mM UO_2^{2+}, 0.5 M $^{i}PrOH$, 0.5 M H_3PO_4, and 70 μM BPyO (b). *Spectrum b multiplied by 1.5 to account for loss of $^{\bullet}C(CH_3)_2OH$ in side reactions with $^{\bullet}C(CH_3)_2OH$ and UO_2^{2+}, see Independent generation of $BPyO^{\bullet-}$.*

formation of $ABTS^{\bullet-}$ is observed, as shown in eq 5. Second, the decay of the $ABTS^{\bullet-}$ signal fits a second order rate equation, $k_6 = 3\ (\pm\ 2) \times 10^9\ M^{-1}\ s^{-1}$, which suggests back electron transfer, eq 6. UV-vis before and after LFP indicate that $[ABTS^{2-}]$ and $[ABTS^{\bullet-}]$ remain unchanged by LFP; consistent with back electron transfer. The rate constant for formation of $ABTS^{\bullet-}$ signal, $k_5 = 4.1\ (\pm\ 0.1) \times 10^9\ M^{-1}\ s^{-1}$, was determined by LFP of solutions containing 40 μM BPyO and 30 – 90 μM $ABTS^{2-}$, Figure S6. The amount of absorbance due to ^{3}BPyO* formation decreased as $[ABTS^{2-}]$ increased. This is a result of $ABTS^{2-}$ acting as an internal filter ($\varepsilon_{308\ nm} = 22{,}000\ M^{-1}\ cm^{-1}$).[61] Higher concentrations of $ABTS^{2-}$ result in fewer photons being absorbed by BPyO, and consequently, less ^{3}BPyO* is formed in the flash. This effect can be seen in traces a and b in Figure 7. Independent LFP of $ABTS^{2-}$ in the absence of BPyO does not generate $ABTS^{\bullet-}$ on the time scale of the experiment, Figure 7, trace c. The final reaction in the sequence (back electron transfer, eq 6) was studied by LFP of solutions containing 40 μM BPyO, 50 μM $ABTS^{2-}$, and 7 – 22 μM $ABTS^{\bullet-}$. The plot of $k_{6\ obs}$ vs. $[ABTS^{\bullet-}]$, Figure S7, is linear with an intercept at $8\ (\pm\ 6) \times 10^3\ s^{-1}$ and slope = $k_6 = 1.7\ (\pm\ 0.3) \times 10^9\ M^{-1}\ s^{-1}$, Table 1. The intercept, having no dependence on $[ABTS^{\bullet-}]$, is in good agreement with k_{obs} for $BPyO^{\bullet-}$ decay when generated from Fe^{2+}. Also, the 2nd order rate constant obtained by this method is in good agreement with the k_6 obtained from fitting to a 2nd order rate equation when no $ABTS^{\bullet-}$ was added prior to LFP. LFP of BPyO and $ABTS^{\bullet-}$ in the absence of $ABTS^{2-}$ does not result in quenching of ^{3}BPyO*.

Qualitatively similar results were obtained from LFP of a solution containing benzophenone (BP) and $ABTS^{2-}$, however, the limited solubility of BP in water hindered further investigation.

$$^{3}BPyO^{*} + ABTS^{2-} \rightarrow BPyO^{\bullet-} + ABTS^{\bullet-} \quad (5)$$

$$BPyO^{\bullet-} + ABTS^{\bullet-} \rightarrow BPyO + ABTS^{2-} \quad (6)$$

Reduction of BPyO to $BPyO^{\bullet-}$

$BPyO^{\bullet-}$ was generated *via* reduction of ground state BPyO by 2-hydroxy-2-propyl radical, eq 7. The radical was generated through the known chemistry between $^{*}UO_2^{2+}$ and $^{i}PrOH$, eq 8.[74] A degassed solution containing 1 mM UO_2^{2+}, 0.5 M H_3PO_4, 70 μM BPyO, and 0.5 M $^{i}PrOH$ was irradiated by 308 nm LFP. The concentration of $^{*}UO_2^{2+}$ was determined by its absorption at 580 nm[75] during LFP of an identical solution without $^{i}PrOH$. The spectrum of $BPyO^{\bullet-}$ obtained from these experiments, Figure 6, spectrum b, required correction by a factor of 1.5 due to loss of $^{\bullet}C(CH_3)_2OH$ in side reactions 9 and 10. Such a correction is reasonable given the pseudo first order rate constants for these reactions under the given conditions ($k_9 = 1 \times 10^4\ s^{-1}$ and $k_{10} = 8 \times 10^4\ s^{-1)}$. Simulations with KINSIM[76] suggest $k_7 \sim 2 \times 10^9\ M^{-1}\ s^{-1} \Rightarrow k_{7\ pseudo} \sim 1.4 \times 10^5\ s^{-1}$.

$$BPyO + {}^{\bullet}C(CH_3)_2OH \rightarrow BPyO^{\bullet-} + (CH_3)_2C{=}O + H^{+} \quad (7)$$

$$^{*}UO_2^{2+} + HC(CH_3)_2OH \rightarrow UO_2H^{2+} + {}^{\bullet}C(CH_3)_2OH \quad (8)$$

$$2\,{}^{\bullet}C(CH_3)_2OH \rightarrow \text{Products} \quad (9)$$

$$^{\bullet}C(CH_3)_2OH + UO_2^{2+} \rightarrow (CH_3)_2C{=}O + UO_2^{+} + H^{+} \quad (10)$$

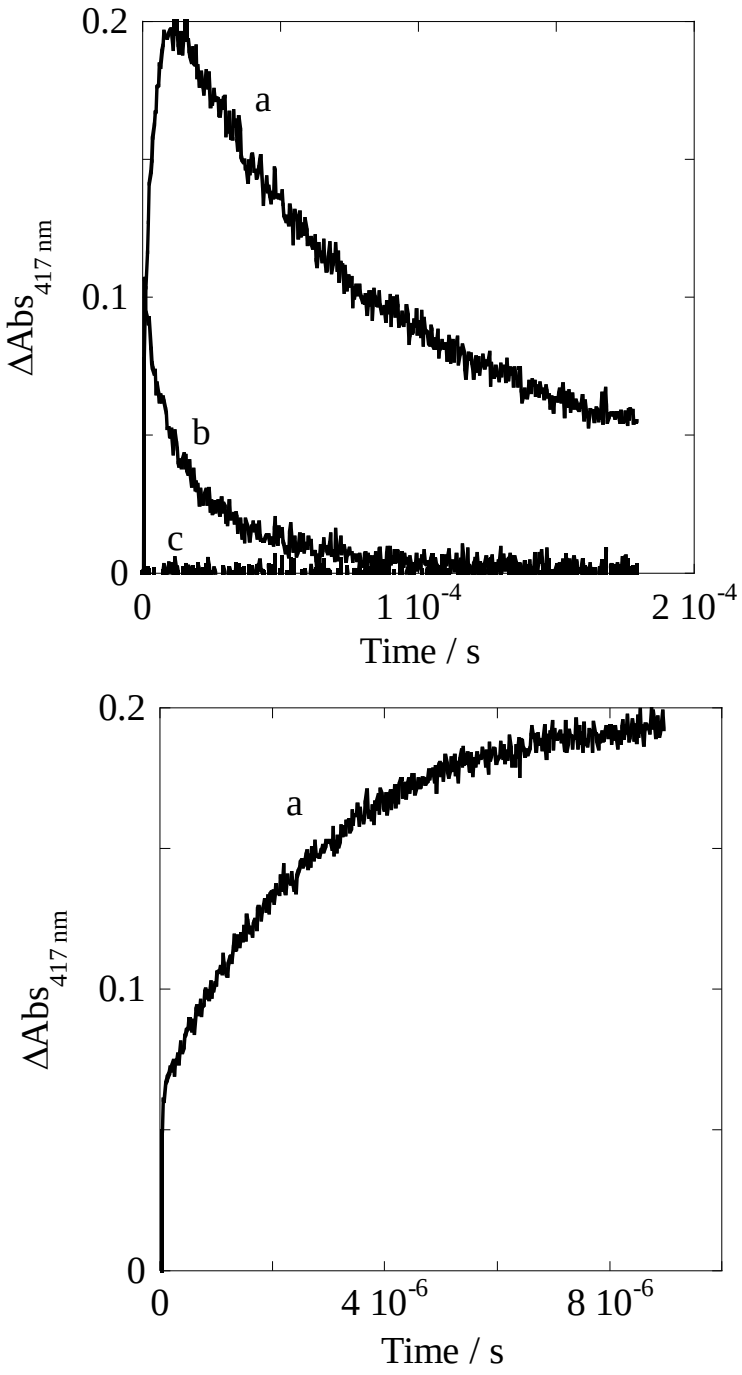

Figure 7. LFP (λ_{ex} = 308 nm, λ_{mon} = 417 nm) of degassed aqueous solutions containing 40 μM BPyO, 50 μM $ABTS^{2-}$ (a) 40 μM BPyO (b) 50 μM $ABTS^{2-}$ (c) (*top*). First 9 μs after the laser flash for solution a, eq 5 (*bottom*).

Laser Flash Photolysis of BPyO in MeCN

Results of LFP of BPyO in MeCN were similar to those obtained in aqueous solutions. ^{3}BPyO* was generated, Figure S8, and decayed with a rate constant dependent on [BPyO], Figure 2 ($k_1 = 6.7 \times 10^4$ s^{-1}, $k_2 = 1.5 \times 10^9$ M^{-1} s^{-1}). As in aqueous solutions, ^{3}BPyO* was quenched by O_2 ($k_{air\text{-}sat} = 3.0 \times 10^6$ s^{-1} and $k_{O2\text{-}sat} = 1.5 \times 10^7$ s^{-1}) and I^-, entry 15 in Table 1. Qualitatively similar results were obtained from LFP of solutions containing BPyO and $ABTS^{2-}$, but the investigation was hindered by the limited solubility of $(NH_4)_2$ABTS in MeCN, ~ 28 μM.[62] An attempt was made to view reduction of ^{3}BPyO* by tetramethylbenzidine,[77] but TMB was found to be photoactive.

Product Analysis

The products of BPyO irradiation were determined by UV-vis, GCMS, and ^{1}H NMR. The UV-vis spectra collected before and after irradiation of BPyO, Figures 8 and S9, bear striking resemblance to genuine BPy, Figure S10 (*i.e.*, irradiated BPyO in aqueous solution exhibits a maximum near 260 nm with molar absorptivity on the order of 10^4 M^{-1} cm^{-1}). GCMS analyses of irradiated solutions of BPyO (both in H_2O and MeCN) indicate formation of 5 new isomers of BPyO (parent mass: 199.20 g/mol) which eluted at 15.78, 15.85, 16.73, 17.04, and 17.46 minutes. Un-reacted BPyO eluted at 18.32 minutes and trace amounts of BPy (183.20 g/mol) at 15.32 minutes were also observed. ^{1}H NMR collected after irradiation (85 % consumption) of a degassed aqueous solution of 1.3 mM BPyO supports a substantial amount of BPyO conversion to the isomers observed by GCMS. The following chemical shifts (in ppm) were obtained: 8.77 d, 8.49 d, 8.46 s, 7.97 d, 7.87 t, 7.79 t, 7.74 d, 7.62 q, 7.48 t, Figure 9. Several of these chemical

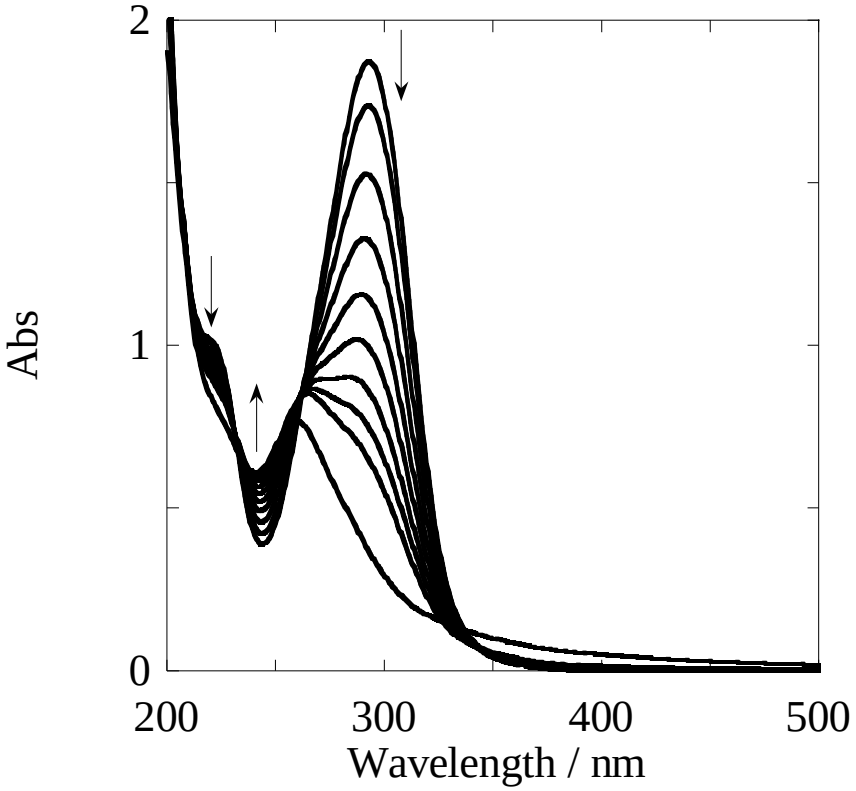

Figure 8. UV-vis spectra (1 cm path length) of degassed aqueous solutions of 95 μM BPyO collected at 30 second intervals during irradiation through $CuSO_4/K_2CrO_4$ dual filter. Final spectrum collected after an additional 10 minutes of irradiation. Method of irradiation utilized the Luzchem photoreactor

shifts overlap those of BPyO and/or BPy. The signals at 8.49, 7.97, 7.87, and 7.62 ppm are consistent with BPyO, Figure S11a. Also, the downfield portion of the 7.62 ppm quartet is consistent with both BPyO and BPy. Two signals (8.77 and 7.48 ppm) are slightly shifted (by + 0.1 and - 0.07 ppm respectively) from those expected for BPy, Figure S11b. Two new signals at 8.46 and 7.74 ppm are assigned as aromatic C-*H*'s of a hydroxylated ring. Integration of the signal at 7.48 ppm suggests a maximum of 3 – 4 % of the irradiated BPyO could have been cleanly deoxygenated to BPy under these conditions. The ^{1}H NMR data collected after irradiation (65 % consumption) of a degassed MeCN-d3 solution containing 2 mM BPyO, Figure 10, is more informative than in D_2O because O-*H* chemical shifts are observable. Like in D_2O, several of the chemical shifts overlap BPyO and/or BPy. The chemical shifts that can be attributed to BPyO, Figure S12a, are doublets at 8.19 and 7.79 ppm; BPy, Figure S12b, doublets at 8.79 and 7.83 ppm; or both with a triplet at 7.68 ppm and quartet at 7.56 ppm. The remaining signals are assigned as C-*H* signals on OH-substituted aromatic rings: 7.76 d, 7.62 d, and 7.51 t; or as O-*H* singlets: 9.67, 6.48, 6.46, 6.41, 6.10, and 3.97 ppm which upon addition of D_2O are no longer visible. The signal at 9.67 ppm is assigned as an O-*H* on the carbon *ortho* to BPy nitrogen. The signal at 3.97 ppm is consistent with the methanolic O-*H* on Ph-CHO*H*-Py (4.03 ppm d), Figure S13. Formation of Ph-CHOH-Py has been ruled out, because (i) the ^{1}H NMR spectrum of irradiated BPyO lacks the Ph-C*H*OH-Py doublet at 5.77 ppm; (ii) the signal at 3.97 ppm in the irradiated BPyO solution is a singlet and not a doublet; (iii) the aromatic region of C_6H_5-CHOH-C_5H_4N is shifted to up field to 7.2 – 7.4 ppm; and (iv) GCMS does not indicate any products with a mass greater than 199.20 g/mol. The methanolic OH is therefore concluded to be the result of H-bonding.

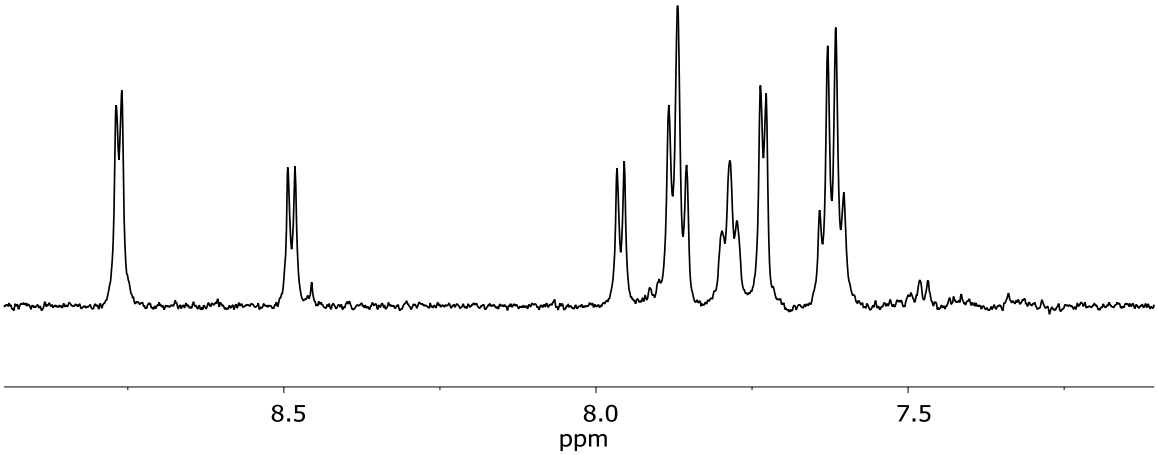

Figure 9. ^{1}H NMR spectrum after air-free irradiation of 1.3 mM BPyO in D_2O. Δ[BPyO] ~ -1.1 mM

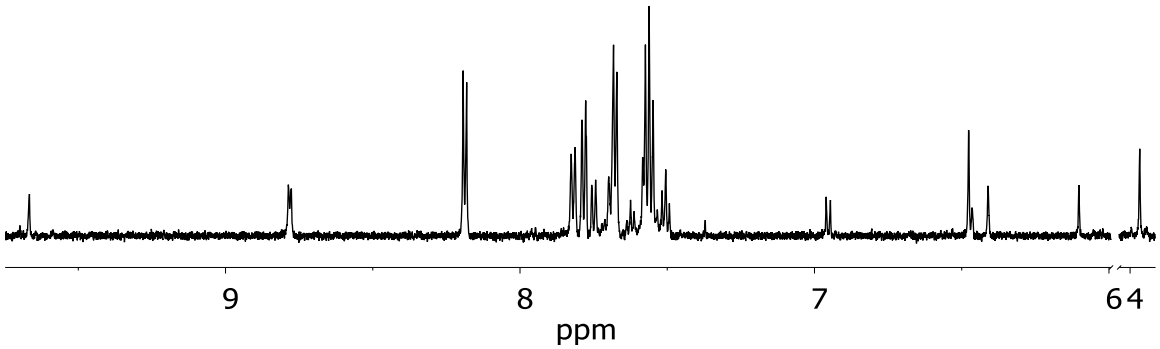

Figure 10. ^{1}H NMR spectrum after air-free irradiation of 2.0 mM BPyO in CD_3CN. Δ[BPyO] ~ -1.3 mM

^{1}H NMR spectra after irradiation of air- and O_2-saturated solutions in both solvents are very similar to those obtained under Ar.

Note: Irradiations of mM concentrations of BPyO are expected to be dominated by equations 2 and 3; O_2 is expected to have little effect on the ^{1}H NMR.

Formation of a yellow product, $\lambda_{max} \sim 400$ nm, in Ar purged MeCN was observed several minutes after irradiation had ceased. The formation of color was more rapid in the presence of O_2 and ambient light. ^{1}H NMR spectra were no different when extra precautions were taken to keep the samples air-free and in the dark. The yellow product was not observable by ^{1}H NMR, and is therefore concluded to be produced in concentrations below the detection limit. The molar absorptivity of this unidentified species is calculated to be $\varepsilon_{400\ nm} \geq 10^4\ M^{-1}\ cm^{-1}$.

Rate of BPyO Consumption in the Presence of Triplet Quenchers

Quenching of ^{3}BPyO* retards consumption of BPyO; provided [Q] is sufficiently high to compete with reactions 1and 2 The relative rates of consumption are related to the slopes of the lines drawn through the initial data points acquired under each set of conditions, Figure 11. Each line intersects the y-axis at the origin. The slope is 6.4 in the absence of triplet quenchers, 0.9 under O_2-saturated conditions, and 3.5 in the presence of 0.2 mM I^-. The difference in slopes in the presence of quenchers is qualitatively consistent with the relative pseudo first order rate constants for ^{3}BPyO* quenching under each set of experimental conditions ($k_{O2} = 1.8 \times 10^6\ s^{-1}$ and $k_{I^-} = 1 \times 10^6\ s^{-1}$) and the loss of ^{3}BPyO* through reactions 1and 2 ($k_{1+2} = 1.3 \times 10^5\ s^{-1}$). 1.26 mM O_2 is twice as efficient at quenching ^{3}BPyO* than 0.2 mM I^- ($k_{O2} / k_{I^-} = 1.8$); the slope under O_2 should be at least a factor of 2 smaller than I^-. The larger ratio of the slopes than expected from

rate constants for ^{3}BPyO* quenching suggests that BPyO is consumed through chemistry of ^{3}BPyO*, but not exclusively. Another pathway that does not involve ^{3}BPyO* also consumes BPyO.

Note: No I_3^- formation was observed under these conditions. Irradiation of BPyO in the presence of DMSO resulted in faster consumption of BPyO, *discussed below*.

Cyclopentene as O(^{3}P) Scavenger

Irradiation of aqueous solutions containing BPyO and cyclopentene, a molecule known to react with O(^{3}P) to yield C_2H_4 with 24 % efficiency,[1,30] eq 11, produced C_2H_4, indicating formation of O(^{3}P). LFP of 65 μM BPyO in the absence and presence of 5.6 mM *c*-C_5H_8 resulted in identical rate constants for ^{3}BPyO* signal decay (1.6×10^5 s^{-1}).

$$O(^3P) + c\text{-}C_5H_8 \rightarrow C_2H_4 + C_3H_4O \quad 24\ \% \qquad (11)$$

The % C_2H_4 produced decreased linearly with increasing [BPyO] in the range 10 – 160 μM, Figure 12. Simple competition between *c*-C_5H_8 and BPyO for O(^{3}P) does not explain this decrease in relative yield; $k_{BPyO\ +O(3P)}$ would have to be 6×10^{11} M^{-1} s^{-1}. That is 3 orders of magnitude larger than Scaiano's work suggests for O(^{3}P) + C_6H_6 or C_6H_5N.[28,29] Interestingly, the linear trend observed under Ar is also observed in the presence of O_2 and 0.5 mM I^-, and the slopes are equal. The decrease in % C_2H_4 is likely the result of ^{3}BPyO* by the ground state, eq 2. Perhaps the most glaring differences in relative yield of C_2H_4 obtained under each set of conditions are the y-intercepts in Figure 12. The y-intercept obtained under each set of conditions is directly related to the ratio of rate constants (O_2 or I^- versus *c*-C_5H_8) in competition for O(^{3}P). Consider irradiations in the presence of O_2; 0.25 mM and 1.26 mM O_2 react with O(^{3}P) with the rate constants k_{pseudo}= 0.1×10^7 s^{-1} and 0.5×10^7 s^{-1}, respectively. Compared to 5.6 mM *c*-C_5H_8,

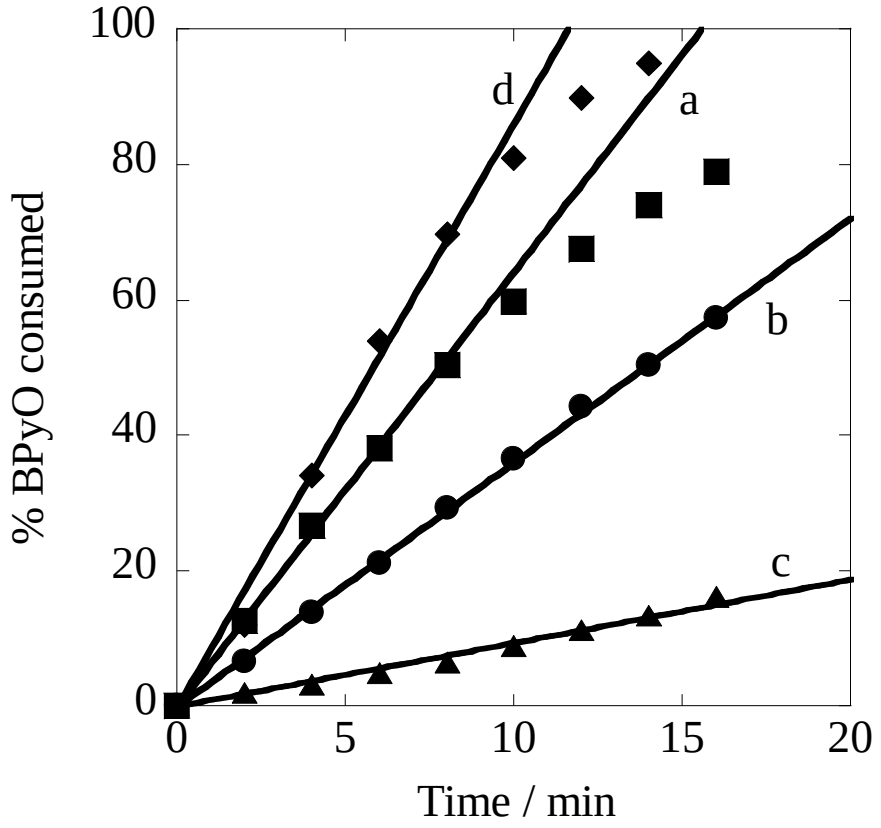

Figure 11. Plot of % BPyO consumed (determined by $\Delta Abs_{292\ nm}$) vs. irradiation time of 62 μM BPyO in the absence of substrate (a) and in the presence of 0.2 mM I^- (b), 1.26 mM O_2 (c), and 50 mM DMSO (d).

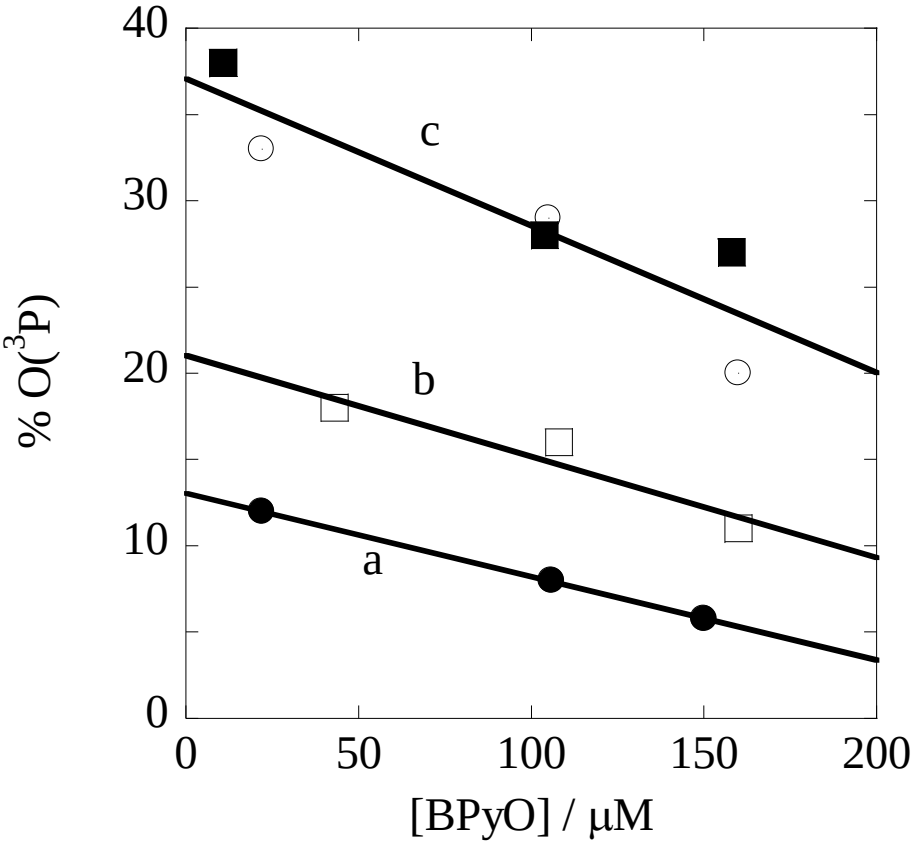

Figure 12. Plot of % $O(^3P)$ vs. [BPyO]. % $O(^3P)$ determined from C_2H_4 production after irradiation of BPyO in the presence of 5.6 mM *c*-C_5H_8 relative to consumption of BPyO as determined by UV-vis. Solutions contained varying concentrations of BPyO, 5.6 mM *c*-C_5H_8, and Ar (a), 0.5 mM I^- (b), and air-saturated ■ and O_2-saturated ○ (c)

$k = 9.0 \times 10^7\ s^{-1}$, only a minute fraction of $O(^3P)$ is lost to O_2. This also explains why the data for air-saturated and O_2-saturated conditions overlap (the amount of $O(^3P)$ reacting with *c*-C_5H_8 under air- vs. O_2-saturated conditions are 99 % and 95 %, respectively). Competition with 0.5 mM I^-, on the other hand, is expected to be more comparable. Iodide is expected to exhibit diffusion controlled reactivity with $O(^3P)$ similar to Br^-, $k = 200 \times 10^9\ M^{-1}\ s^{-1}$.[29] Therefore, at 0.5 mM I^- the pseudo first order rate constant is $1 \times 10^8\ s^{-1}$ for $I^- + O(^3P)$. Under these conditions I^- competes with *c*-C_5H_8 at a ratio of nearly 1 : 1. Indeed, the amount of C_2H_4 observed in the presence of 0.5 mM I^- is consistent with this ratio (*i.e.*, half as much C_2H_4 is observed in the presence of 0.5 mM I^- than under air-saturated conditions). The differences in y-intercepts strongly imply formation of $O(^3P)$ on the basis of relative yields of C_2H_4 and direct correlation of those yields with rate constants for reactions with $O(^3P)$; and suggest that decay of ^{3}BPyO* in reaction 1 consumes BPyO. The small slope obtained from each of these series relative to the large difference in y-intercept also suggests that BPyO quenching of ^{3}BPyO*, eq 2, likely occurs through a combination of non-destructive energy transfer and oxygen transfer.

Note: In the presence of 0.5 mM I^- and no added acid, I_3^- is not expected to form in any appreciable concentration due to unfavorable conditions for hydrolysis. The most likely fate of IO^- would involve a reaction with cyclopentene (the bulk reactive species). Additionally, the change to [*c*-C_5H_8] as a result of these reactions is negligible, and therefore k_{pseudo} is expected to remain constant. Making a small correction for ^{3}BPyO* decay at each [BPyO] and competition for $O(^3P)$ by either O_2 or I^- yields slopes closer to zero and suggests formation of up to 41 % $O(^3P)$.

Other Attempts to Scavenge O(^{3}P)

Irradiation in the presence of other O(^{3}P) acceptors was attempted with I^-, Br^-, and Cl^- at pH 2. The expected chemistry is shown in reactions 12 – 14. The system was limited by K_{14}[78] for Br^- and Cl^- and the known photochemistry of all X_3^-.[79,80] Formation of I_3^- and Br_3^- was observed, but could not be accurately quantified due to the aforementioned photochemistry and subsequent reactions involving X_3^-. Interestingly, I^- was the only halide that had an effect on k_{obs} for ^{3}BPyO* decay. An attempt was made to observe H_3PO_3 by oxidation of H_3PO_2 with O(^{3}P) due to its thermodynamic favorability, $\Delta H \sim -350$ kJ/mol,[81] however, no H_3PO_3 was observed. It is possible that the lack of an open coordination site on the phosphorous atom provided a kinetic barrier that was too high given the parallel reactions in which O(^{3}P) could have participated. Addition of O(^{3}P) to triphenylphosphine was problematic due to the direct photolysis of triphenylphosphine.

$$O(^3P) + X^- \rightarrow XO^- \quad (12)$$

$$XO^- + 2H^+ + X^- \rightarrow X_2 + H_2O \quad (13)$$

$$X_2 + X^- \rightleftarrows X_3^- \quad (14)$$

Irradiation of BPyO with DMSO

Irradiation of solutions of BPyO and DMSO resulted in faster consumption of BPyO as determined by UV-vis, Figure 11. The presence of DMSO was also found to decrease k_{obs} for ^{3}BPyO* decay from 9.5 ($\pm$ 0.2) $\times 10^4$ s^{-1} in its absence to 7.1 ($\pm$ 0.2) $\times 10^4$ s^{-1} at 50 mM DMSO. No further decrease in k_{obs} was observed when [DMSO] $\geq$ 50 mM was used, Figure S5. A decrease in k_{obs} was also observed when DMSO was present

during LFP of BPyO in MeCN. Up to 20 % $DMSO_2$ was generated as a result of BPyO photolysis in the presence DMSO in degassed MeCN-d3. Up to 3.4 % $DMSO_2$ was observed by ^1H NMR after irradiation of millimolar BPyO in degassed D_2O, Figure 13. Sulfinic and sulfonic acids were also observed in yields that increased linearly with [DMSO]. The majority of $DMSO_2$ was generated before 50 % consumption of BPyO (determined by UV-vis) during serial irradiations of 1.6 mM BPyO and 0.2 M DMSO. Sulfinic and sulfonic acids were detected only after 50 % of the BPyO had been consumed, Table 2. GC/FID analysis of the headspace after irradiation of BPyO in the presence of DMSO indicates formation of CH_4 and C_2H_6. The ^1H NMR and GC/FID data strongly suggest the formation of $^{\bullet}OH$ after prolonged irradiation; sulfinic and sulfonic acids, CH_4, and C_2H_6 are known products of reactions between $^{\bullet}OH$ and DMSO.[82] Photolysis of hydroxypyridine N-oxides is known to generate $^{\bullet}OH$,[83] and $^{\bullet}OH$ have been suggested in the photodegradation of hydroxypyridines.[84] Formation of sulfinic and sulfonic acids after 50 % consumption of BPyO suggests that $^{\bullet}OH$ is a product resulting from irradiation of (OH)BPy. To investigate; 1.5 mM BPyO was irradiated to 35 % consumption, and then 0.2 M DMSO was added. The new solution was irradiated further (75 % consumption), and analyzed by ^1H NMR. Product analysis indicates the formation of mostly sulfinic and sulfonic acids with very little $DMSO_2$, Table 2 below the line.

Note: The absolute concentrations of $DMSO_2$, CH_3SO_2H, and CH_3SO_3H only increased with irradiation time. The apparent decrease in yield shown in Table 2 is a direct result of BPyO consumption by pathways which do not yield DMSO derived products at prolonged irradiation times.

Table 2. DMSO derived products as a function of BPyO consumption (irradiation time).

% BPyO Consumed [a]	% $DMSO_2$	% CH_3SO_2H	% CH_3SO_3H
18	5	0	0
50	4	0	0
68	3	5	5
95	3	3	4
75 [b]	2	4	2

[a] Irradiation of degassed solution of 1.5 mM BPyO with 0.2 M DMSO in D_2O by photoreactor method. [BPyO] consumed determined by UV-vis and [DMSO derived product] determined by ^{1}H NMR vs. ^{i}PrOH internal standard. [b] 1.5 mM BPyO irradiated to 35 % consumption, then 0.2 M DMSO added and solution irradiated to 75 % BPyO consumption.

Photolysis of BPyO/DMSO solutions under air- or O_2-saturated conditions selectively produced $DMSO_2$ in yields that increased linearly with [DMSO], Figure 13. The systems were more complicated due to direct irradiation of DMSO in O_2-saturated solutions producing $DMSO_2$.

A spectrophotometrically unobservable complex (BPyO•DMSO) is believed to be responsible for the more rapid consumption of BPyO, Figure 11 d, and smaller k_{obs} for ^{3}BPyO* decay in the presence of DMSO. This chemistry was not investigated further.

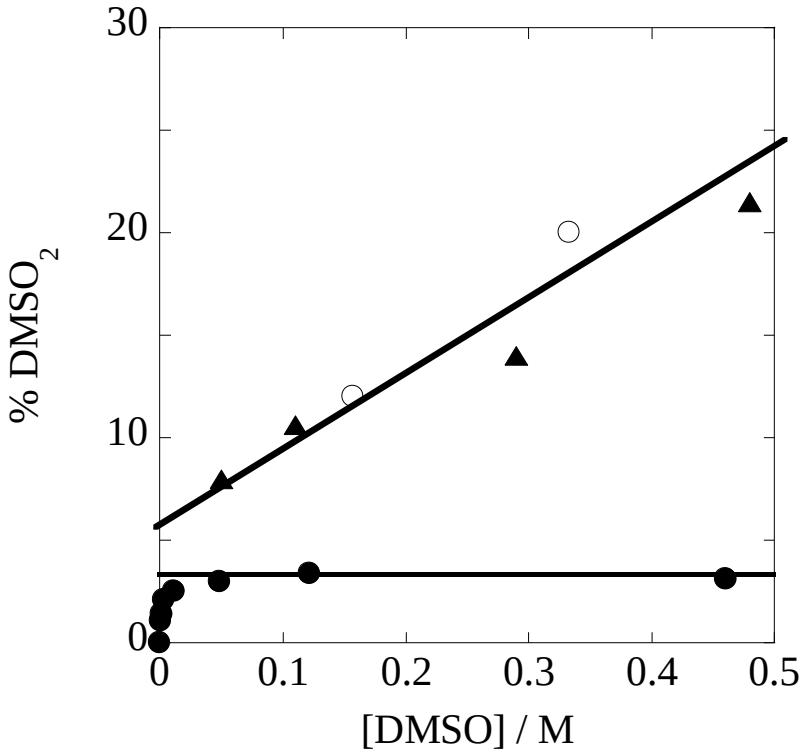

Figure 13. Plot of % $DMSO_2$ vs. [DMSO] after irradiation of 1.2 mM BPyO (0.1 cm path length) in D_2O. Data was collected under Ar ●, air-saturated ○, and O_2-saturated ▲. % $DMSO_2$ relative to consumed BPyO (determined by UV-vis). Solutions were irradiated to 70 % consumption of BPyO.

Discussion

Mechanism

The mechanism for photolysis of BPyO is described in Scheme 1. Absorption of a photon excites BPyO to ^{1}BPyO*. ^{1}BPyO* (i) cleaves the N-O bond yielding O(^{3}P), (ii) rearranges to (OH)BPy, or (iii) undergoes intersystem crossing to ^{3}BPyO*. Once formed ^{3}BPyO* (iv) undergoes self-decay yielding (OH)BPy and may relax to ground state BPyO, (v) reacts with BPyO generating (OH)BPy or by energy transfer, or (vi) is quenched, typically returning ^{3}BPyO* to BPyO. The quenching reaction may or may not involve electron transfer. This scheme is consistent with the above described results: (i) The production of C_2H_4 in the presence of ^{3}BPyO* quenchers and lack of effect on ^{3}BPyO* decay by the presence of *c*-C_5H_8 leave no doubt that ^{3}BPyO* is not the excited state from which O(^{3}P) is ejected. Therefore, O(^{3}P) is concluded to be a product of ^{1}BPyO*. (ii) Parallel unimolecular rearrangement and/or ring cleavage from ^{1}BPyO* cannot be ruled out. (iii) ^{3}BPyO* is the first observed intermediate formed. The quantum yield suggests that no less than 20 % of ^{1}BPyO* undergoes intersystem crossing to ^{3}BPyO* under the conditions studied. UV-vis and % O(^{3}P) experiments suggest that ^{3}BPyO* chemistry, eq 1 – 2, consumes BPyO. More specifically (iv) the large differences in y-intercepts in Figure 12 observed in the presence and absence of ^{3}BPyO* quenchers suggest that reaction 1 results in some consumption of BPyO, and (v) the steady decrease in % O(^{3}P) with increasing [BPyO] suggests that reaction 2 consumes BPyO. (vi) The relative rates of BPyO quenching in the presence and absence of quenchers (shown in Figure 11) indicate that the quenching agents studied return ^{3}BPyO* to the ground state. The same mechanism is expected to hold in MeCN, though the yields of O(^{3}P) may be

different. Prolonged irradiation of BPyO solutions produces •OH, presumably through photolysis of (OH)BPy.

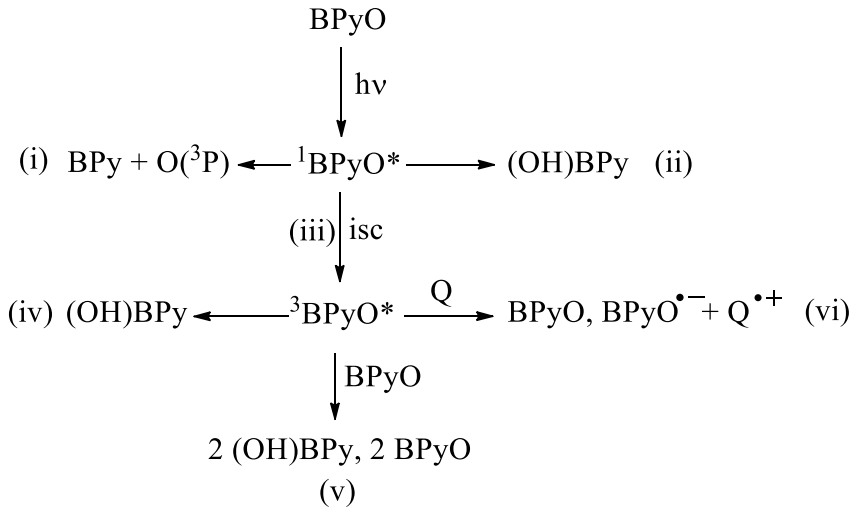

Scheme 1. Photochemical mechanism for O(^{3}P) production and decay of BPyO

^{3}BPyO* Relative to Other Triplet Excited Ketones

^{3}BPyO* has a life-time,[43,85] absorbance spectrum,[43,86] and reactivity with molecular oxygen[43] that is similar to ^{3}BP* and ^{3}BPy*, but is relatively unreactive.[85,86] Both ^{3}BP*[87-89] and ^{3}BPy*[86] react readily with alcohols by H-atom abstraction. The presence of up to 3 M MeOH has no effect ^{3}BPyO* signal decay. The oxide functionality in ^{3}BPyO* appears to be the source of the diminished reactivity; which is consistent with the correlation drawn by Scaiano et al. between the electronic effects on rates for HAT from 2-propanol in substituted benzophenones.[88] Like ^{3}BP*[90,91], ^{3}BPyO* is quenched by transition metal species and iodide. Most of these reactions are believed to be energy transfer because they yield no observable products. However, reduction of the excited state followed by rapid back electron transfer with no observable intermediates, as proposed by Jammoul et al. in iodide quenching of ^{3}BP*,[91] cannot be ruled out. The electron transfer reactions that were unquestionably observed in this work allow the

assignment of a lower limit for the reduction potential of ^{3}BPyO* (^{3}BPyO*/BPyO$^{\bullet-}$ ≥ 0.77 V).[81] This explains the above mentioned lack of reactivity with alcohols. ^{3}BP* is known to oxidize water[85] (1.35 V at pH 7)[92] and produce hydroxylated-benzophenones in degassed aqueous solutions.[43]

BPyO$^{\bullet-}$ Relative to Other Photochemically Generated Radical Anions

BPyO$^{\bullet-}$ is spectroscopically similar to BP$^{\bullet-}$,[85] BPy$^{\bullet-}$,[86,93] and Py$_2$CO$^{\bullet-}$[67,86] (λ_{max} ~ 490 ± 30 nm). However, the reactivity of these ketyl radicals is quite different. The presence of O_2 has no effect on the decay of BPyO$^{\bullet-}$.[94] BP$^{\bullet-}$ has been used in the purification of organic solvents because of its reactivity with H_2O and O_2.[95,96] [95,96] The back electron transfer reaction observed with ABTS$^{\bullet-}$ suggests that redox potential of BPyO$^{\bullet-}$, like ^{3}BPyO*, is also fairly weak (BPyO / BPyO$^{\bullet-}$ ≥ 0.67 V based on ABTS$^{\bullet-}$ / ABTS^{2-} couple).[61] The dependence of the rate of BPyO$^{\bullet-}$ decay on ionic strength (10^4 s^{-1} at μ = 0.1 M and 10^5 s^{-1} at μ = 0.4 M) suggests a bimolecular pathway involving two BPyO$^{\bullet-}$ molecules. The presence of Fe^{2+} and the high acid concentration necessary for the longevity of *UO_2^{2+} limit product analysis for BPyO$^{\bullet-}$ decay by ^{1}H NMR, the relatively large molar absorptivity of ABTS^{2-} limits the concentrations for photochemical reasons. We can therefore only speculate as to the identity of the products of the bimolecular BPyO$^{\bullet-}$ reaction. Electron transfer to yield BPyO and B(OH)PyO and dimerization analogous to BP$^{\bullet-}$[89] are both plausible. So is deoxygenation of one or both molecules.

Attempts to observe the intermediate reported by Scaiano et al. at 325 nm (reported to be CH_3CNO)[28] upon LFP of BPyO were unsuccessful; nor was it observed upon LFP of PyNO.

Conclusions

This work provides evidence for the formation of up to 41 % $O(^3P)$ during the photolysis of 4-benzoylpyridine N-oxide in the presence of ^{3}BPyO* quenching agents. This not only rules out ^{3}BPyO* as the source of $O(^3P)$, but shows that its chemistry is responsible for substantially diminished yields of $O(^3P)$ due to consumption of BPyO in non-deoxygenation pathways. These results suggest that one must be careful in choosing conditions when deoxygenation is the desired reaction.

Acknowledgment

This research was supported by the U.S. Department of Energy, Office of Basic Energy Sciences, Chemical Sciences, Geosciences, and Biosciences Division through the Ames Laboratory. The Ames Laboratory is operated for the U.S. Department of Energy by Iowa State University under Contract No. DE-AC02-07CH11358.

Supplemental Information

Figures S1 – S13 and derivations of equations S6 and S10 are shown in appendix D.

References:

(1) Cvetanovic, R. J.; Ring, D. F.; Doyle, L. C. *J. Phys. Chem* **1971**, *75*, 3056.

(2) Nicovich, J. M.; Gump, C. A.; Ravishankara, A. R. *J. Phys. Chem* **1982**, *86*, 1684.

(3) Nicovich, J. M.; Gump, C. A.; Ravishankara, A. R. *J. Phys. Chem* **1982**, *86*, 1690.

(4) Gaffney, J. S.; Atkinson, R.; Pitts, J. N. *J. Am. Chem. Soc.* **1975**, *97*, 5049.

(5) Hewitt, C. N.; Harrison, R. M. *Atmospheric Environment (1967)* **1985**, *19*, 545.

(6) Blanco, M. B.; Taccone, R. A.; Lane, S. I.; Teruel, M. A. *The Journal of Physical Chemistry A* **2006**, *110*, 11091.

(7) Garton, D. J.; Minton, T. K.; Troya, D.; Pascual, R.; Schatz, G. C. *The Journal of Physical Chemistry A* **2003**, *107*, 4583.

(8) Cvetanović, R. J. *J. Phys. Chem. Ref. Data* **1987**, *16*, 261.

(9) Upadhyaya, H. P.; Naik, P. D.; Pavanaja, U. B.; Kumar, A.; Vatsa, R. K.; Sapre, A. V.; Mittal, J. P. *Chem. Phys. Lett.* **1997**, *274*, 383.

(10) Sun Young, L.; Hee Soo, Y.; Wee Kyung, K.; Jung, K.-H. *Chem. Phys. Lett.* **1996**, *257*, 415.

(11) Nishida, S.; Takahashi, K.; Matsumi, Y.; Taniguchi, N.; Hayashida, S. *The Journal of Physical Chemistry A* **2004**, *108*, 2451.

(12) Jenkin, M. E.; Clemitshaw, K. C. *Atmos. Environ.* **2000**, *34*, 2499.

(13) Paulson, S. E.; Orlando, J. J. *Geophysical Research Letters* **1996**, *23*, 3727.

(14) Amichai, O.; Treinin, A. *Chem. Phys. Lett.* **1969**, *3*, 611.

(15) Gindulyte, A.; Massa, L.; Banks, B.; Miller, S. R. In *Protection of Materials and Structures from Space Environment*; Kleiman, J., Iskanderova, Z., Eds.; Springer Netherlands: 2003; Vol. 5, p 299.

(16) Zhang, M.; Ravilious, G. E.; Hicks, L. M.; Jez, J. M.; McCulla, R. D. *J. Am. Chem. Soc.* **2012**, *134*, 16979.

(17) Lucien, E.; Greer, A. *The Journal of Organic Chemistry* **2001**, *66*, 4576.

(18) Zadok, E.; Rubinraut, S.; Mazur, Y. *The Journal of Organic Chemistry* **1987**, *52*, 385.

(19) Tanner, D. D.; Kandanarachchi, P.; Das, N. C.; Brausen, M.; Vo, C. T.; Camaioni, D. M.; Franz, J. A. *The Journal of Organic Chemistry* **1998**, *63*, 4587.

(20) Thomas, K. B.; Greer, A. *The Journal of Organic Chemistry* **2003**, *68*, 1886.

(21) Gibson, K. D.; Sibener, S. J. *Surf. Sci.* **2006**, *600*, L76.

(22) Bailey, P. S. *Ozonation in organic chemistry / Philip S. Bailey ; editorial advisor, Walter Trahanovsky*; Academic Press: New York, 1978.

(23) Byczkowski, J. Z.; Gessner, T. *Int. J. Biochem.* **1988**, *20*, 569.

(24) Buxton, G. V.; Greenstock, C. L.; Helman, W. P.; Ross, A. B. *J. Phys. Chem. Ref. Data* **1988**, *17*, 513.

(25) Ervens, B.; Gligorovski, S.; Herrmann, H. *PCCP* **2003**, *5*, 1811.

(26) Frimer, A. A. *Chem. Rev.* **1979**, *79*, 359.

(27) Reisz, E.; Schmidt, W.; Schuchmann, H.-P.; von Sonntag, C. *Environmental Science & Technology* **2003**, *37*, 1941.

(28) Bucher, G.; Scaiano, J. C. *J. Phys. Chem* **1994**, *98*, 12471.

(29) Scaiano, J. C.; Bucher, G.; Barra, M.; Weldon, D.; Sinta, R. *Journal of Photochemistry and Photobiology A: Chemistry* **1996**, *102*, 7.

(30) Brown, W. G.; Hart, E. J. *J. Phys. Chem* **1978**, *82*, 2539.

(31) Albini, A.; Alpegiani, M. *Chem. Rev.* **1984**, *84*, 43.

(32) Kurasawa, Y.; Takada, A.; Kim, H. S. *J. Heterocycl. Chem.* **1995**, *32*, 1085.

(33) Gurria, G. M.; Posner, G. H. *The Journal of Organic Chemistry* **1973**, *38*, 2419.

(34) Still, I. W. J.; Arora, P. C.; Chauhan, M. S.; Kwan, M. H.; Thomas, M. T. *Can. J. Chem.* **1976**, *54*, 455.

(35) Still, I. W. J.; Arora, P. C.; Hasan, S. K.; Kutney, G. W.; Lo, L. Y. T.; Turnbull, K. *Can. J. Chem.* **1981**, *59*, 199.

(36) McCulla, R. D.; Jenks, W. S. *J. Am. Chem. Soc.* **2004**, *126*, 16058.

(37) Albini, A.; Fasani, E.; Frattini, V. *Journal of Photochemistry* **1987**, *37*, 355.

(38) Lin, S.-K. *Journal of Photochemistry* **1987**, *37*, 363.

(39) Tokumura, K.; Matsushita, Y. *Journal of Photochemistry and Photobiology A: Chemistry* **2001**, *140*, 27.

(40) Bellamy, F.; Barragan, L. G. R.; Streith, J. *Journal of the Chemical Society D: Chemical Communications* **1971**, 456.

(41) Foote, C. S. *Photochem. Photobiol.* **1991**, *54*, 659.

(42) Grewer, C.; Brauer, H.-D. *J. Phys. Chem* **1994**, *98*, 4230.

(43) Ledger, M. B.; Porter, G. *Journal of the Chemical Society, Faraday Transactions 1: Physical Chemistry in Condensed Phases* **1972**, *68*, 539.

(44) de Lucas, N. C.; Albuquerque, A. C. C.; Santos, A. C. A. S.; Garden, S. J.; Nicodem, D. E. *Journal of Photochemistry and Photobiology A: Chemistry* **2007**, *188*, 293.

(45) Stoffregen, S. A.; Lee, S. Y.; Dickerson, P.; Jenks, W. S. *Photochemical & Photobiological Sciences* **2014**, *13*, 431.

(46) Daniels, J. S.; Chatterji, T.; MacGillivray, L. R.; Gates, K. S. *The Journal of Organic Chemistry* **1998**, *63*, 10027.

(47) Cordes, T.; Regner, N.; Heinz, B.; Borysova, E.; Ryseck, G.; Gilch, P. *Journal of Photochemistry and Photobiology A: Chemistry* **2009**, *206*, 10.

(48) Orf, H. W.; Dolphin, D. *Proceedings of the National Academy of Sciences* **1974**, *71*, 2646.

(49) Muth, C. W.; Darlak, R. S.; Patton, J. C. *J. Heterocycl. Chem.* **1972**, *9*, 1003.

(50) Kane-Maguire, N. A. P.; Bennett, J. A.; Miller, P. K. *Inorg. Chim. Acta* **1983**, *76*, L123.

(51) Macartney, D. H.; McAuley, A. *Inorg. Chem.* **1983**, *22*, 2062.

(52) Curtis, N. F. *Coord. Chem. Rev.* **1968**, *3*, 3.

(53) Barefield, E. K.; Wagner, F. *Inorg. Chem.* **1973**, *12*, 2435.
(54) Wagner, F.; Barefield, E. K. *Inorg. Chem.* **1976**, *15*, 408.
(55) Mao, Y.; Bakac, A. *The Journal of Physical Chemistry A* **1997**, *101*, 7929.
(56) Song, W.; Kristian, K. E.; Bakac, A. *Chemistry – A European Journal* **2011**, *17*, 4513.
(57) Connolly, P.; Espenson, J. H.; Bakac, A. *Inorg. Chem.* **1986**, *25*, 2169.
(58) Cheng, M.; Bakac, A. *Dalton Transactions* **2007**, 2077.
(59) Chmurzynski, L. *Molecules* **1997**, *2*, 169.
(60) Eckert, F.; Leito, I.; Kaljurand, I.; Kütt, A.; Klamt, A.; Diedenhofen, M. *J. Comput. Chem.* **2009**, *30*, 799.
(61) Scott, S. L.; Chen, W. J.; Bakac, A.; Espenson, J. H. *J. Phys. Chem* **1993**, *97*, 6710.
(62) this; work.
(63) Sutin, N.; Creutz, C. In *Inorganic and Organometallic Photochemistry*; AMERICAN CHEMICAL SOCIETY: 1978; Vol. 168, p 1.
(64) Navon, G.; Sutin, N. *Inorg. Chem.* **1974**, *13*, 2159.
(65) Caspar, J. V.; Meyer, T. J. *J. Am. Chem. Soc.* **1983**, *105*, 5583.
(66) Yuasa, J.; Fukuzumi, S. *Chem. Commun.* **2006**, 561.
(67) Elisei, F.; Favaro, G.; Romani, A. *Chem. Phys.* **1990**, *144*, 107.
(68) Kane-Maguire, N. A. P.; Crippen, W. S.; Miller, P. K. *Inorg. Chem.* **1983**, *22*, 696.
(69) Bakac, A.; Espenson, J. H. *J. Phys. Chem* **1993**, *97*, 12249.
(70) Darmanyan, A. P.; Khudyakov, I. V. *Photochem. Photobiol.* **1990**, *52*, 293.
(71) Che, Y.; Tokuda, K.; Ohsaka, T. *Bull. Chem. Soc. Jpn.* **1998**, *71*, 651.
(72) Margerum, D. W.; Sommer, B. A. *Inorg. Chem.* **1970**, *9*, 2517.
(73) Pestovsky, O.; Bakac, A. *Inorg. Chem.* **2005**, *45*, 814.
(74) Sergeeva, G.; Chibisov, A.; Levshin, L.; Karyakin, A. *J. Chem. Soc., Chem. Commun.* **1974**, 159.
(75) Andreja Bakac, H. D. B. *Appl. Spectrosc.* **1997**, *51*, 1916.
(76) Barshop, B. A.; Wrenn, R. F.; Frieden, C. *Anal. Biochem.* **1983**, *130*, 134.
(77) Ewa Szajna-Fuller, Y. H., Jennifer L. Rapp, Gezahegn Chaka, Victor S. Y. Lin, Marek Pruski, Andreja Bakac *Dalton Transactions* **2009**, 3237.
(78) Wang, T. X.; Kelley, M. D.; Cooper, J. N.; Beckwith, R. C.; Margerum, D. W. *Inorg. Chem.* **1994**, *33*, 5872.
(79) Grossweiner, L. I.; Matheson, M. S. *J. Phys. Chem* **1957**, *61*, 1089.
(80) Kalmar, J.; Doka, E.; Lente, G.; Fabian, I. *Dalton Transactions* **2014**, *43*, 4862.
(81) *Standard Potentials in Aqueous Solution*; Allen J, B.; Parsons, R.; Jordan, J., Eds.; CRC Press: Ney York, 1985; Vol. 1.
(82) Veltwisch, D.; Janata, E.; Asmus, K.-D. *Journal of the Chemical Society, Perkin Transactions 2* **1980**, 146.
(83) Tobin, D.; Arvanitidis, M.; Bisby, R. H. *Biochem. Biophys. Res. Commun.* **2002**, *299*, 155.

(84) Stapleton, D. R.; Konstantinou, I. K.; Karakitsou, A.; Hela, D. G.; Papadaki, M. *Chemosphere* **2009**, *77*, 1099.

(85) Bensasson, R. V.; Gramain, J.-C. *Journal of the Chemical Society, Faraday Transactions 1: Physical Chemistry in Condensed Phases* **1980**, *76*, 1801.

(86) Görner, H. *Chem. Phys.* **2008**, *344*, 264.

(87) Silva, R. S.; Nicodem, D. E. *Journal of Photochemistry and Photobiology A: Chemistry* **2008**, *194*, 76.

(88) Wagner, P. J.; Truman, R. J.; Scaiano, J. C. *J. Am. Chem. Soc.* **1985**, *107*, 7093.

(89) Beckett, A.; Porter, G. *Transactions of the Faraday Society* **1963**, *59*, 2038.

(90) Hammond, G. S.; Foss, R. P. *J. Phys. Chem* **1964**, *68*, 3739.

(91) Jammoul, A.; Dumas, S.; D'Anna, B.; George, C. *Atmospheric Chemical Physics* **2009**, *9*, 4229.

(92) Wood, P. M. *Biochem. J.* **1988**, *253*, 287.

(93) Nelson, D. A.; Hayon, E. *J. Phys. Chem* **1972**, *76*, 3200.

(94) Janzen, E. G.; Happ, J. W. *J. Phys. Chem* **1969**, *73*, 2335.

(95) *Purification of Laboratory Chemicals*; 5 ed.; Chai, C.; Armarego, W. L. F., Eds.; Butterworth-Heinemann: Oxford, 2003.

(96) *Experimental Organic Chemistry*; 2 ed.; Harwood, L. M.; Moody, C. J.; Percy, J. M., Eds.; Blackwell Science, Inc.: Malden, MA, 1999.

GENERAL CONCLUSIONS

The above described work offers mechanistic detail for the formation of several reactive intermediates on the basis of kinetics experiments and product analysis. A pathway to carcinogenic forms of chromium from 'inert' chromium (III) was found. Novel macrocyclic rhodium(III) alkyl complexes (thermally stable photochemical precursors for alkyl radicals) were successfully synthesized and characterized. The first mechanistic shift (kinetics versus thermodynamics) in group transfer reactions between coordinatively saturated transition metal complexes was investigated. A novel method for 'green' production of functionalized alkanes utilizing inexpensive transition metals and oxygen was developed. Definitive evidence for $O(^3P)$ generation in solution via photolysis of a pyridine N-oxide was found, and mechanism proposed.

Biologically "Inert" Chromium(III)?

While trace amounts of chromium(III) are believed to be necessary for the enhancement of insulin activity,[1-3] it is known that high-valent chromium (IV, V, VI) species are carcinogenic.[4,5] Previous work[2,6-8] suggests that there are several routes to formation of hydroperoxido-chromium(III) in biological systems either by substitution or redox reactions with Cr(III). The work described in chapter 1 supports our earlier assertion that the mechanism for decay of $CrOOH^{2+}$ involves high-valent chromium species.[9,10] The relative amount of high-valent chromium generated during the decomposition of $CrOOH^{2+}$ decomposition is higher as pH nears the biologically relevant

range. In light of these and other findings[2,7,8] perhaps its use as a dietary supplement and use for weight loss[11,12] should be more carefully considered.

Thermally Stable Photochemical Precursors to Alkyl Radicals

Novel macrocyclic rhodium alkyl complexes have been prepared by two methods. The group transfer method is more atom economical with respect to rhodium, but is inefficient at transferring ethyl and incapable of transferring isopropyl groups due to a mechanistic shift from group transfer to hydrogen atom abstraction. The hydroperoxide method is more efficient for synthesis of $LRhR^{2+}$ complexes in which R contains β-hydrogen. In general, the bond dissociation energy of Rh-H complexes is larger than that for Rh-C complexes;[13] however, several Rh-H complexes insert olefins into the Rh-H bond; suggesting the Rh-R is thermodynamically preferred to Rh-H.[13-15] Therefore, we conclude that a mechanistic shift from thermodynamically favored Rh-R to kinetically favored Rh-H occurs in the reaction between $M\text{-}R^{n+}$ and LRh^{2+} on the basis of kinetics experiments and product analysis. The resulting $LRhR^{2+}$ complexes exhibit resistance to thermal decomposition in solution at elevated temperature and in the presence of oxygen or strongly reducing metals.

Tunable 'Green' Method for Deoxygenation of Biomass-Derived Fatty Acids

Deoxygenation of potentially biomass derived acids was achieved by metal-assisted photochemical decarboxylation. Decarboxylation by this method generates alkyl radicals; the products of which can be tuned depending on their environment. Alkyl halides, alkanes, and olefins have been generated by this method. Copper(II) salts were the most promising for catalytic production of α-olefins (utilizing atmospheric O_2 to regenerate Cu^{2+}).

Free Oxygen Atoms in Solution!

The energetic species responsible for deoxygenation upon irradiation of N- and S-oxides has been long debated.[16-26] Photolysis of 4-benzoylpyridine N-oxide generates a triplet excited state that is observable by Laser Flash Photolysis. ^{3}BPyO* was readily quenched by O_2, I^-, and several transition metal complexes. Additionally, the rate of BPyO consumption was severely retarded by the presence of triplet quenchers. Photolysis in the presence of cyclopentene (known to react with O(^{3}P) to yield C_2H_4) strongly suggests formation of free O(^{3}P) in yields that decrease with increasing [BPyO]. An analogous set of experiments in the presence of triplet quenchers revealed that not only is ^{3}BPyO* not responsible for formation of free O(^{3}P), but is a major pathway for non-deoxygenative consumption of BPyO yielding mainly hydroxylated-BPy. ^{1}BPyO* appears to be the most likely source of O(^{3}P).

References

(1) Wiernsperger, N.; Rapin, J. *Diabetology & Metabolic Syndrome* **2010**, *2*, 70.
(2) Vincent, J. B. *Acc. Chem. Res.* **2000**, *33*, 503.
(3) Kotaś, J.; Stasicka, Z. *Environ. Pollut.* **2000**, *107*, 263.
(4) Norseth, T. *Environ. Health Perspect.* **1981**, *40*, 121.
(5) Little, L. G.; Sugden, K. D. In *Metal Complex–DNA Interactions*; John Wiley & Sons, Ltd: 2009, p 463.
(6) Song, W.; Bakac, A. *Inorg. Chem.* **2009**, *49*, 150.
(7) Levina, A.; Lay, P. A. *Coord. Chem. Rev.* **2005**, *249*, 281.
(8) Codd, R.; Dillon, C. T.; Levina, A.; Lay, P. A. *Coord. Chem. Rev.* **2001**, *216–217*, 537.
(9) Bakac, A. *Coord. Chem. Rev.* **2006**, *250*, 2046.
(10) Wang, W. D.; Bakac, A.; Espenson, J. H. *Inorg. Chem.* **1993**, *32*, 5034.
(11) Lau, F.; Bagchi, M.; Sen, C.; Bagchi, D. *Mol. Cell. Biochem.* **2008**, *317*, 1.
(12) Bagchi, M.; Bagchi, D.; Preuss, H. G. *Chromium (III) in promoting weight loss and lean body mass*

Obesity : Epidemiology, Pathophysiology, and Prevention, 2007.
(13) Fu, X.; Wayland, B. B. *J. Am. Chem. Soc.* **2005**, *127*, 16460.
(14) Feng, M.; Chan, K. S. *J. Organomet. Chem.* **1999**, *584*, 235.
(15) Thomas, K.; Osborn, J. A.; Powell, A. R.; Wilkinson, G. *J. Chem. Soc. A* **1968**, 1801.
(16) Albini, A.; Alpegiani, M. *Chem. Rev.* **1984**, *84*, 43.
(17) Albini, A.; Fasani, E.; Frattini, V. *Journal of Photochemistry* **1987**, *37*, 355.
(18) Lin, S.-K. *Journal of Photochemistry* **1987**, *37*, 363.
(19) Tokumura, K.; Matsushita, Y. *Journal of Photochemistry and Photobiology A: Chemistry* **2001**, *140*, 27.
(20) Bucher, G.; Scaiano, J. C. *J. Phys. Chem* **1994**, *98*, 12471.
(21) Bellamy, F.; Barragan, L. G. R.; Streith, J. *Journal of the Chemical Society D: Chemical Communications* **1971**, 456.
(22) de Lucas, N. C.; Albuquerque, A. C. C.; Santos, A. C. A. S.; Garden, S. J.; Nicodem, D. E. *Journal of Photochemistry and Photobiology A: Chemistry* **2007**, *188*, 293.
(23) Stoffregen, S. A.; Lee, S. Y.; Dickerson, P.; Jenks, W. S. *Photochemical & Photobiological Sciences* **2014**, *13*, 431.
(24) Daniels, J. S.; Chatterji, T.; MacGillivray, L. R.; Gates, K. S. *The Journal of Organic Chemistry* **1998**, *63*, 10027.
(25) Cordes, T.; Regner, N.; Heinz, B.; Borysova, E.; Ryseck, G.; Gilch, P. *Journal of Photochemistry and Photobiology A: Chemistry* **2009**, *206*, 10.
(26) Orf, H. W.; Dolphin, D. *Proceedings of the National Academy of Sciences* **1974**, *71*, 2646.

ACKNOWLEDGEMENTS

I would like to thank my committee chair, Dr. Andreja Bakac, for her guidance, encouragement, and friendship; and my committee members for sharing their wisdom and experience and offering their friendship and advice.

I would also like to thank the faculty of Iowa State University, Department of Chemistry for their encouragement, friendship, and the occasion translation of journal articles written in foreign languages. Additionally, my fellow group members have proven invaluable to my education. They have taught me the intricacies of various techniques, offered insightful thoughts in discussions, and provided sanity breaks.

I am extremely grateful for support from family and friends during my academic pursuit. My wife, Sarah, has kept me grounded, and has offered an immeasurable amount of loving support and understanding. My parents, Mike and June, and my in-laws, Tom and Linda, who have supported us on the home front, and kept us going when things got difficult.

The work was supported by grant CHE 0602183 from the Nation Science Foundation (Chapter 1), Graduate Assistance in Areas of National Need (GAANN),[*] U.S. Department of Education (Chapter 4), and the U.S. Department of Energy under contract number DE-AC02-07CH11358 (Chapters 2, 3, & 5). All work was performed at the Ames Laboratory with the U.S. Department of Energy. The document number assigned to this thesis/dissertation is IS-T 3118.

[*] This program provides fellowships, through academic departments and programs of IHEs, to assist graduate students with excellent records who demonstrate financial need and plan to pursue the highest degree available in their course study at the institution in a field designated as an area of national need.

APPENDIX A

PREPARATION AND REACTIVITY OF MACROCYCLIC RHODIUM(III) ALKYL COMPLEXES

Table of Contents

Table S1. Structure refinement data for *trans*-$[L^2(H_2O)RhCH_3]^{2+}$ and *trans*-$[L^1(H_2O)RhCH_2Ph]^{2+}$

	$[L^2(H_2O)RhCH_3]^{2+}$	$[L^1(H_2O)RhCH_2Ph]^{2+}$
empirical formula	$C_{17}H_{37}Cl_2N_4O_9Rh$	$C_{34}H_{54}Cl_4N_8O_{18}Rh_2$
formula weight	615.32	1210.47
temperature	173(2) K	173(2) K
wavelength	0.71073 Å	0.71073 Å
cryst. syst., sp.group	monoclinic, $P2_1/c$	monoclinic, $P2_1/c$
unit cell dimensions	a = 7.9942(12) Å b = 15.505(2) Å c = 10.2975(15)Å β = 102.377(2)°	a = 16.7567(9) Å b = 18.9758(10) Å c = 15.5961(8) Å β = 104.6980(10)°
volume	1246.7(3) $Å^3$	4796.8(4) $Å^3$
Z, calculated density	2, 1.639 Mg/m^3	4, 1.676 Mg/m^3
absorption coefficient	0.952 mm^{-1}	0.989 mm^{-1}
F(000)	636	2464
crystal size	0.21 x 0.19 x 0.16 mm^3	0.25 x 0.22 x 0.11 mm^3
θ range for data collection	2.4136 to 28.8515	1.26 to 28.13 °
limiting indices	$-10 \le h \le 10$ $-20 \le k \le 20$ $-13 \le l \le 13$	$-22 \le h \le 2$ $-25 \le k \le 25$ $-20 \le l \le 20$
reflections collected/unique	13211/3271 [R(int) = 0.0285]	48895 /11734 [R(int) = 0.0392]
completeness to θ_{max}	99.8 %	99.9 %
absorption correction	multi-scan	multi-scan
max and min transmission	0.86 and 0.75	0.90 and 0.79
data/restraints/parameters	3271/48/193	11734/432/595
goodness-of-fit on F^2	1.152	1.082
final R indices [I > 2σ(I)]	R1 = 0.0380 wR2 = 0.0929	R1 = 0.0822 wR2 = 0.2196
R indices (all data)	R1 = 0.0450 wR2 = 0.0963	R1 = 0.1079 wR2 = 0.2418
largest diff. peak and hole	1.121 and -0.620 e $Å^{-3}$	2.126 and -1.033e $Å^{-3}$

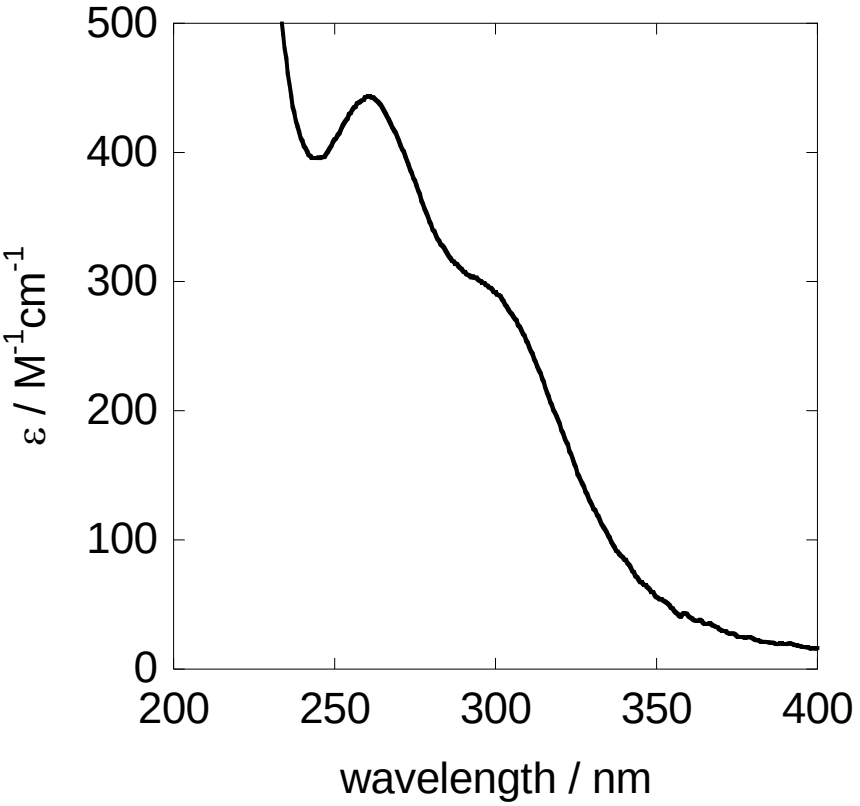

Figure S1. UV spectrum of $L^1(H_2O)RhC_2H_5^{2+}$ in acidic aqueous solution.

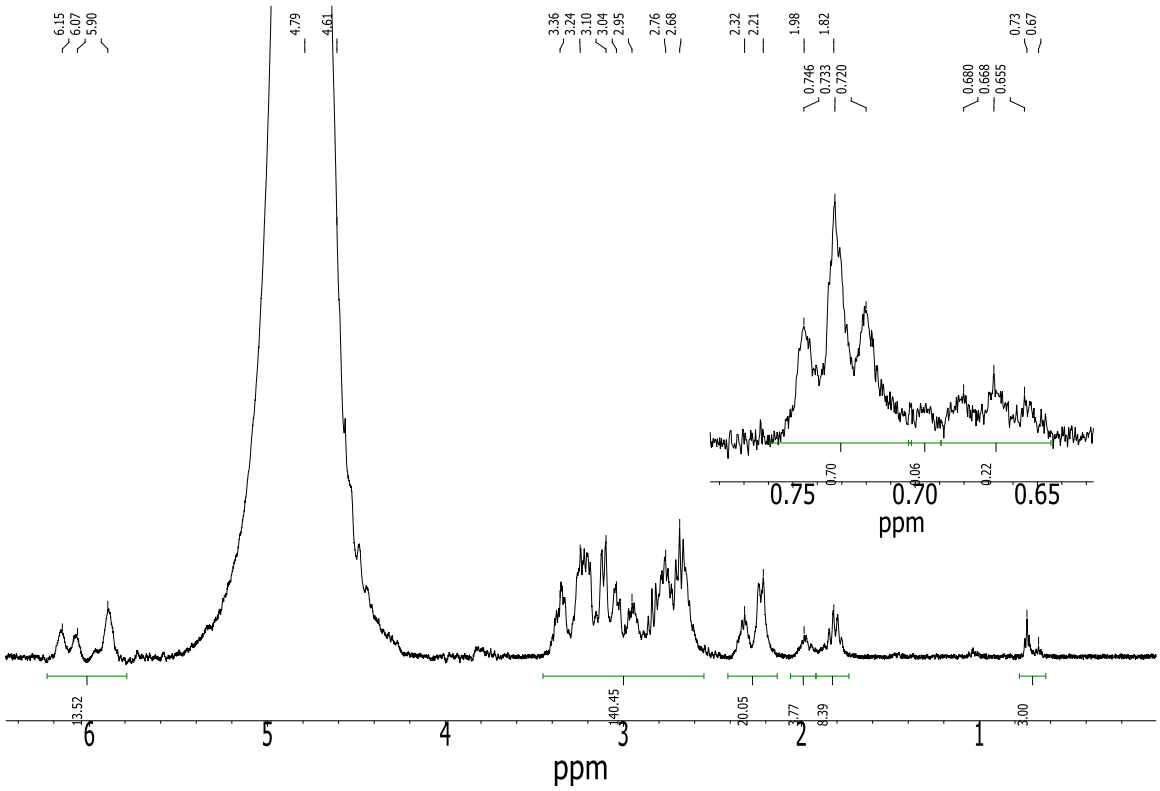

Figure S2. ^{1}H NMR of $L^{1}(H_2O)RhCH_2CH_3^{2+}$, 600 MHz, D_2O, after reaction between $L^{1}(H_2O)Rh^{2+}$ and $C_2H_5C(CH_3)_2OOH$. The solution contains approximately equimolar amount of $L^{1}(H_2O)_2Rh^{3+}$. The signals at 1.98 ppm (Rh-$\underline{CH_2}$-CH_3, ^{2}J[Rh,H] = 3 Hz), 0.73 ppm and 0.67 ppm (Rh-CH_2-$\underline{CH_3}$) disappear upon UV photolysis under O_2.

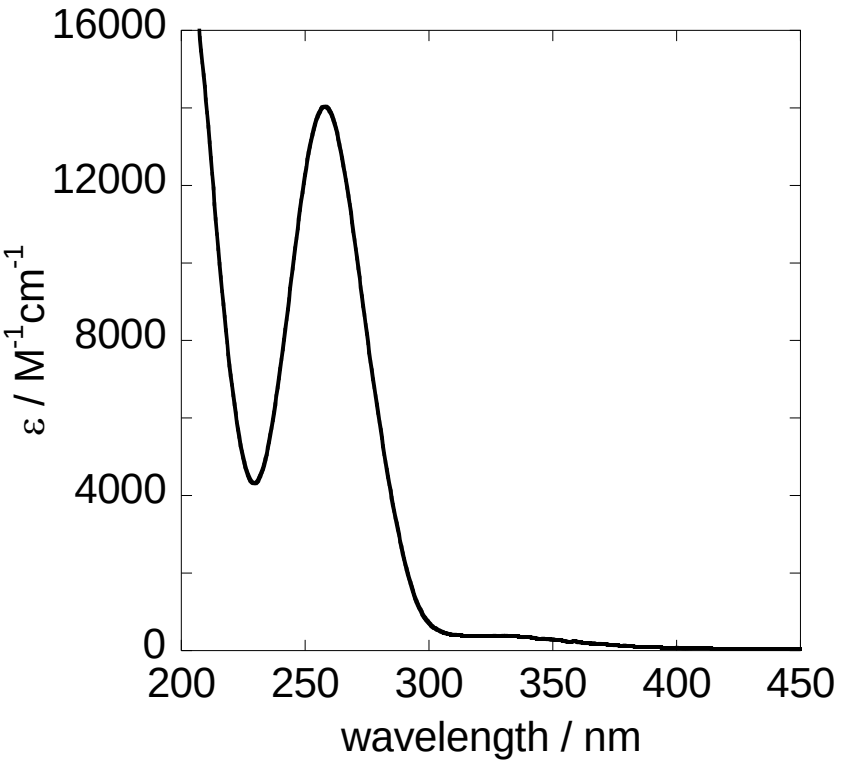

Figure S3. UV spectrum of $L^1(H_2O)RhCH_2C_6H_5^{2+}$ in acidic aqueous solution.

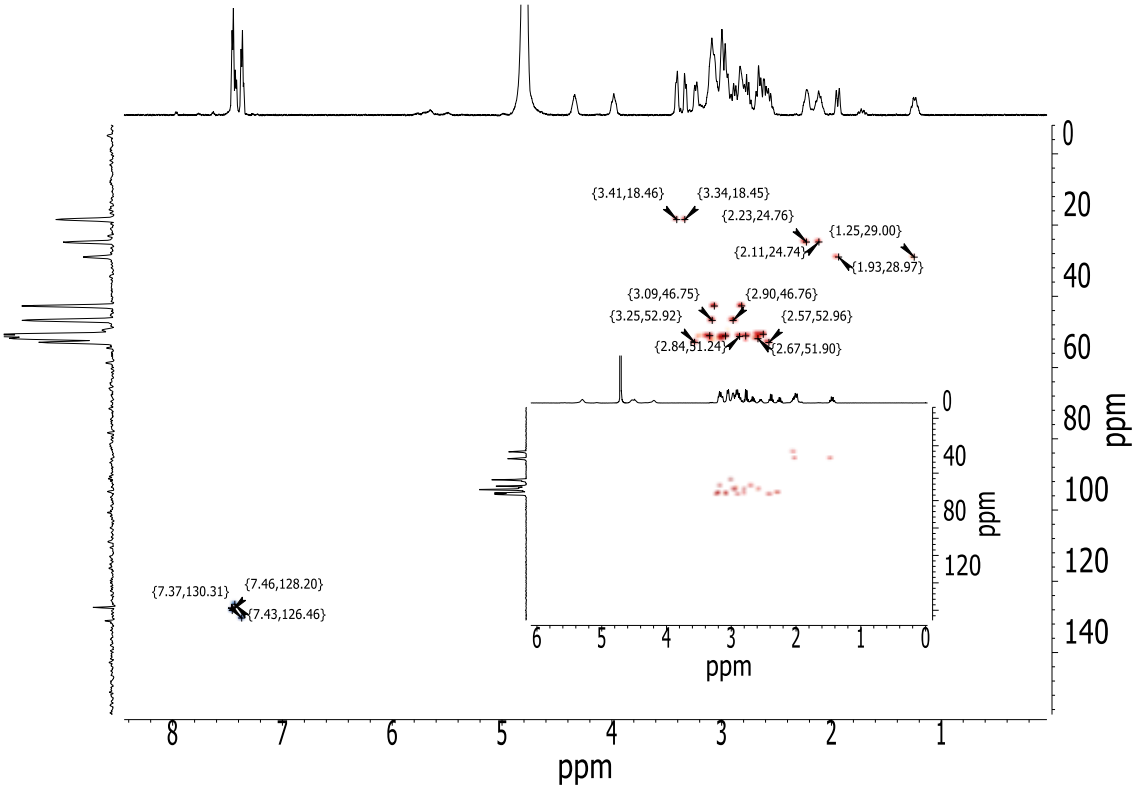

Figure S4. HSQC spectrum of of $L^1(H_2O)RhCH_2Ph^{2+}$, 600 MHz, D_2O. ^1H NMR (horizontal), ^{13}C projection (vertical). Rh-$\underline{CH_2}$-Ph signals: ^1H 3.34, 3.41 ppm, ^{13}C 18.45 ppm. Rh-CH_2-$\underline{Ph}$ signals: ^1H 7.37-7.46 ppm, ^{13}C 126.46 – 130.31 ppm. Inset: HSQC spectrum of $L^1(H_2O)RhH^{2+}$.

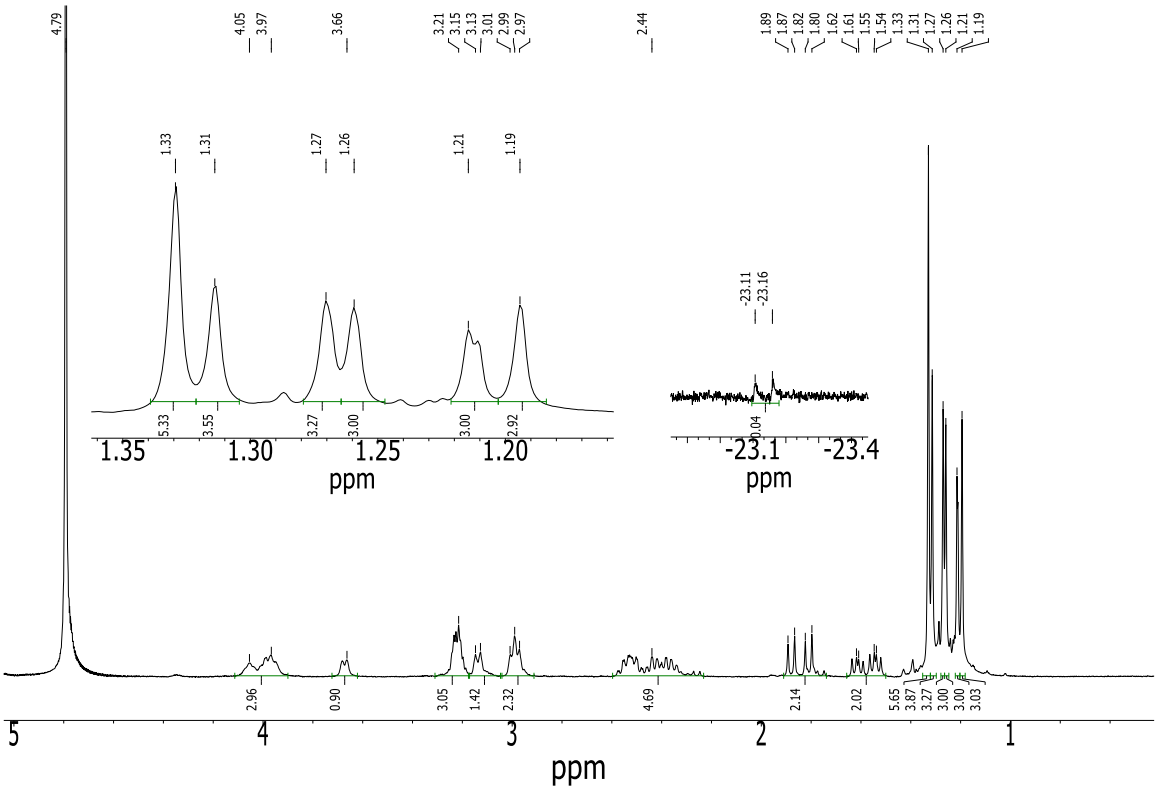

Figure S5. ^{1}H NMR of $L^{2}(H_2O)RhCH_3^{2+}$, 600 MHz, D_2O. Left inset: Ligand-CH_3 groups + Rh-CH_3 (1.33 ppm). There are 21 hydrogens in the 1.20 – 1.35 ppm region for $L^{2}(H_2O)RhCH_3^{2+}$, and 18 in the same region for $L^{2}(H_2O)RhH^{2+}$, Figure S8. Right inset: Rh-H region shows traces of remaining $L^{2}(H_2O)RhH^{2+}$ that was used as a starting material in the prep of the methyl complex, see Experimental.

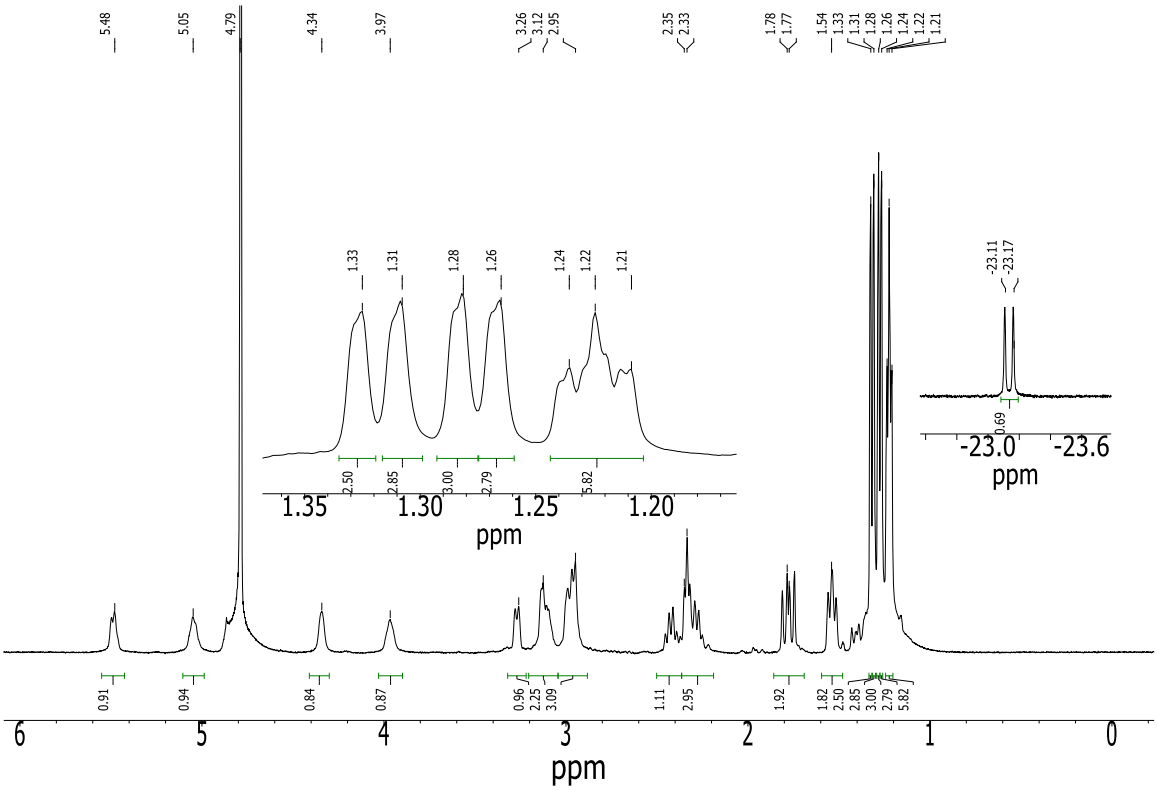

Figure S6. ^{1}H NMR of $L^{2}(H_2O)RhH^{2+}$, 600 MHz, D_2O. Left inset: ligand-CH_3 groups. Right inset: Rh-H signal. Signals at 5.05 ppm and 5.48 ppm are for exchangeable N-H protons.

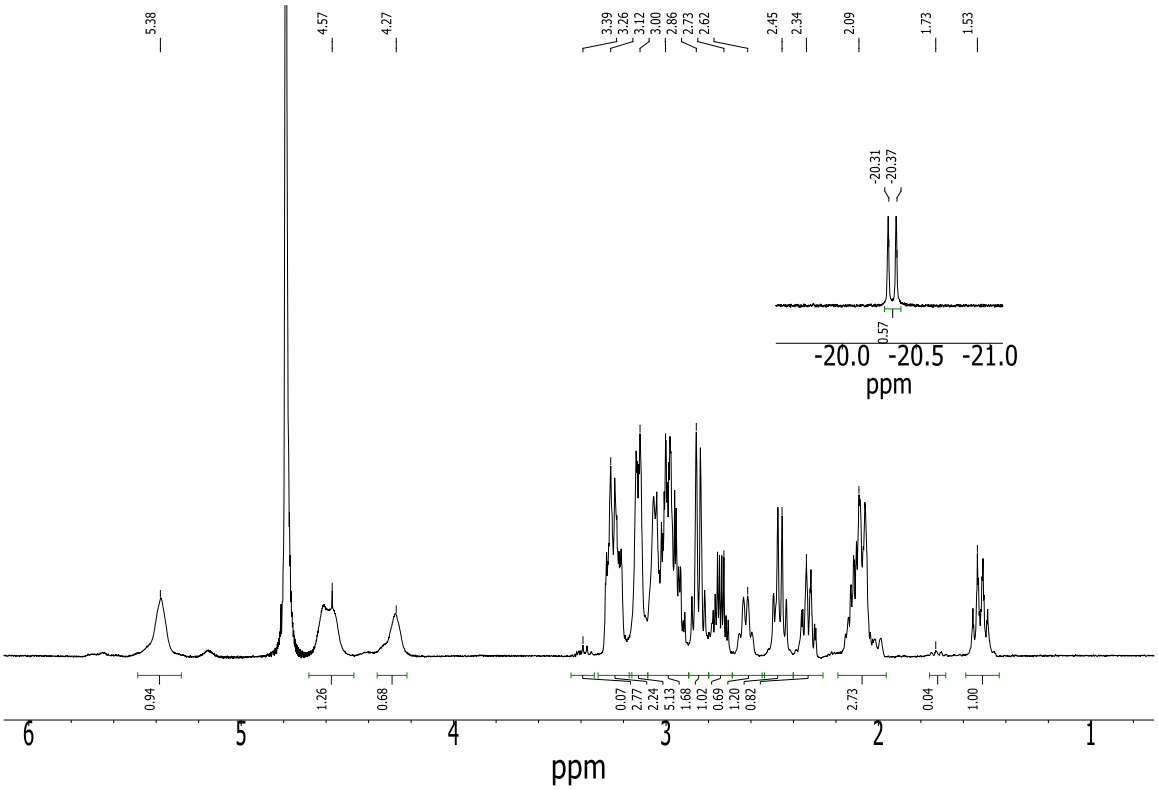

Figure S7. ^{1}H NMR of $L^{1}RhH^{2+}$, 600 MHz, D_2O.

APPENDIX B

ALKYL GROUP VERSUS HYDROGEN ATOM TRANSFER FROM METAL ALKYLS TO MACROCYCLIC RHODIUM COMPLEXES

Table of Contents

Experimental

Acidic aqueous solutions of $L(H_2O)Rh^{2+}$ complexes (L = L^1, L^2) were generated by photolysis of the corresponding hydrides $L(H_2O)RhH^{2+}$.[1] Solid perchlorate and trifluoromethanesulfonate salts of $L(H_2O)RhH^{2+}$ were prepared as described previously.[1] Alkyl cobalt complexes $(dmgH)_2(H_2O)CoR$ ($dmgH_2$ = dimethylglyoxime)[2] and solutions of alkyl chromium complexes[3] $(H_2O)_5CrR^{2+}$ were prepared by published procedures.

Instrumentation

Photolyses were performed in standard 1-cm square fluorescence quartz cells in Luzchem LZC-5 photoreactor at 313 nm. Gaseous products were analyzed with an Agilent Technologies 7890A gas chromatograph equipped with an FID detector and a 0.320 mm I.D. capillary column (GS-GASPRO 113-4312, 15 m). Nitrogen flow rate was 25 cm^3/s. The split injector (1:40) was kept at 200 °C and FID detector at 350 °C. Initial oven temperature was 40 °C, increased by 10 °C/min, and held at a final temperature of 200 °C for 1 min. UV-Vis spectra and kinetic data were collected with a Shimadzu UV-3101PC spectrophotometer. Kinetic data were fitted with KaleidaGraph 4.0 software.

Spectrophotometric titrations and kinetics were monitored at the absorbance maxima of cobalt, chromium or rhodium complexes, as appropriate. The specific wavelengths and associated molar absorptivities are summarized in Table S1. The identity and concentrations of the rhodium products were determined spectrophotometrically on samples purified by ion exchange. Owing to spectral similarity of the alkyl and hydrido complexes, and their similar behavior on Sephadex, a portion of the purified solutions was also photolyzed under argon followed by GC analysis to confirm the identity of the axial group. In every case the results, as judged by

the presence or lack of the products of alkyl radical self-reactions, agreed with the spectrophotometric assignment.

The kinetics of the reactions with alkyl cobalt complexes were determined in the presence of large excess of one or the other reactant, and the data were fit to an expression for first order kinetics. The pseudo-first order rate constants so obtained were plotted against the concentration of excess reagent to obtain second-order rate constants, Figures S1 - S6. Kinetic traces for reaction involving alkylchromium complexes exhibited some tailing at longer times, caused by the slow background decay of the excess alkylchromium complex. Kinetic traces were fitted to an expression for {first + linear} kinetics, and the exponential part was used to determine the second-order rate constants for the reactions with rhodium(II) complexes.

Table S1. Summary of Spectral Data for Alkyl Complexes of Cobalt and Chromium[a]

Alkyl donor (conc/10^{-4} M)[b]	λ_{max} / nm	ε / M^{-1} cm^{-1}
$(dmgH)_2(H_2O)CoCH_3$ (0.4 - 2.2)	440	1525
$(H_2O)_5CrCH_3^{2+}$ (0.1 - 0.3)	258	2400
$(dmgH)_2(H_2O)CoCH_2CH_3$ (0.5 - 9.1)	451	1480
$(H_2O)_5CrCH_2CH_3^{2+}$ (0.4 - 1.3)	278	2400
$(dmgH)_2(H_2O)CoCH(CH_3)_2$ (3.0 - 30)	463	1340
$(dmgH)_2(H_2O)CoCH(CH_3)CH_2CH_3$ (3.9 - 9.2)	454	1430

[a] Source: References [2,4-6]. [b] Concentration range in kinetic experiments.

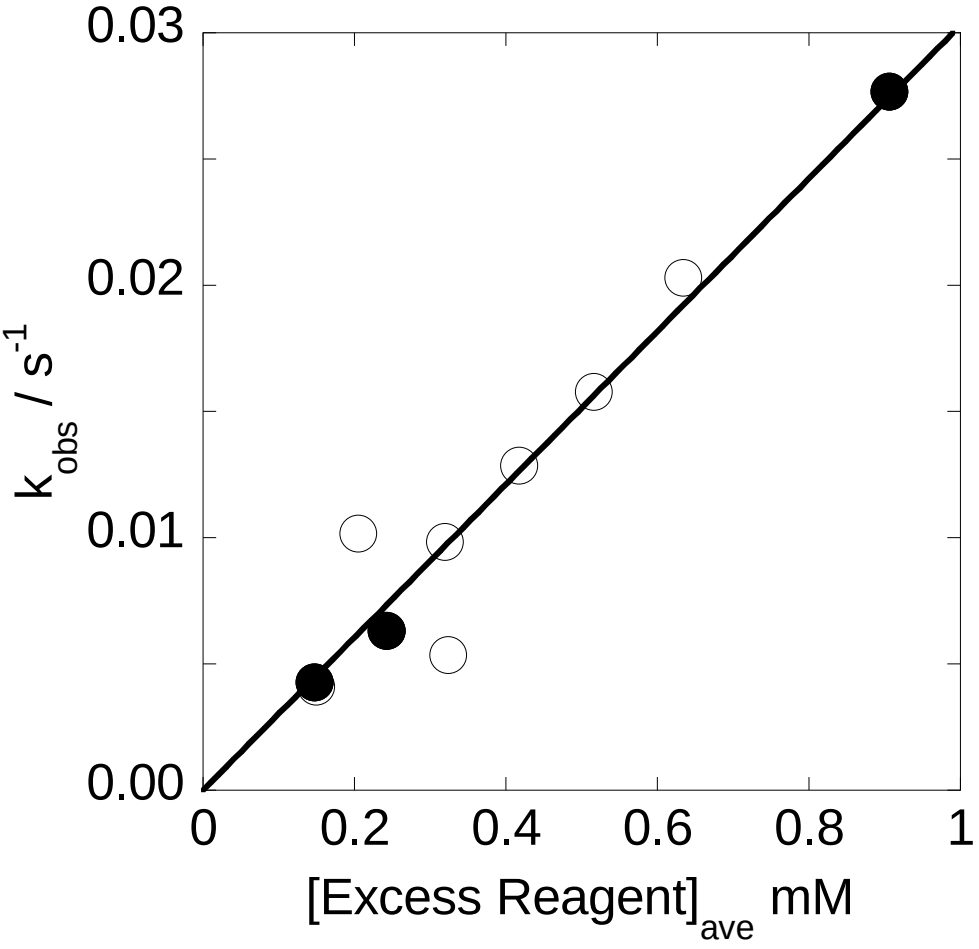

Figure S1. Plot of k_{obs} vs [Excess Reagent] for the reaction between $L^1(H_2O)Rh^{2+}$ and $(dmgH)_2(H_2O)CoCH_2CH_3$. • $[L^1(H_2O)Rh^{2+}]$ in excess. ○ $[(dmgH)_2(H_2O)CoCH_2CH_3]$ in excess.

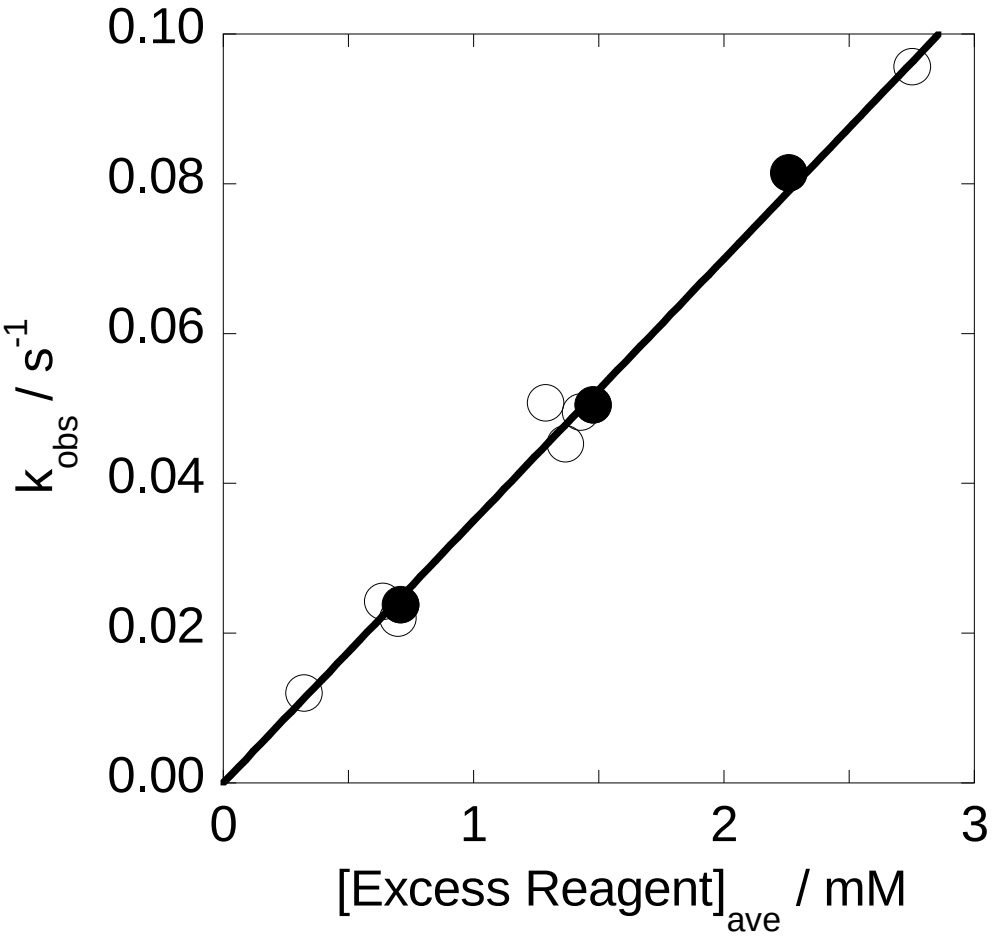

Figure S2. Plot of k_{obs} vs [Excess Reagent] for the reaction between $L^1(H_2O)Rh^{2+}$ and $(dmgH)_2(H_2O)CoCH(CH_3)_2$ • $[L^1(H_2O)Rh^{2+}]$ in excess. ○ $[(dmgH)_2(H_2O)CoCH(CH_3)_2]$ in excess.

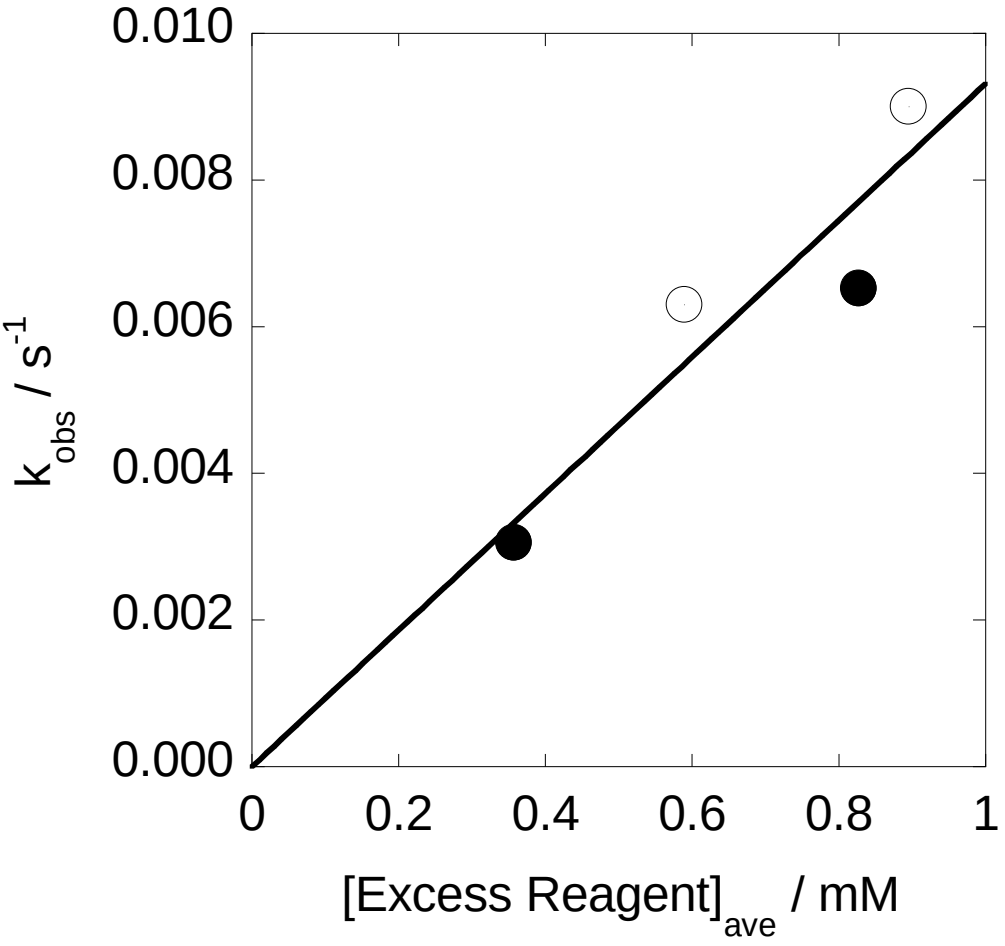

Figure S3. Plot of k_{obs} vs [Excess Reagent] for the reaction between $L^1(H_2O)Rh^{2+}$ and $(dmgH)_2(H_2O)CoCH(CH_3)CH_2CH_3$. • $[L^1(H_2O)Rh^{2+}]$ in excess. ○ $[(dmgH)_2(H_2O)Co$-$CH(CH_3)CH_2CH_3]$ in excess.

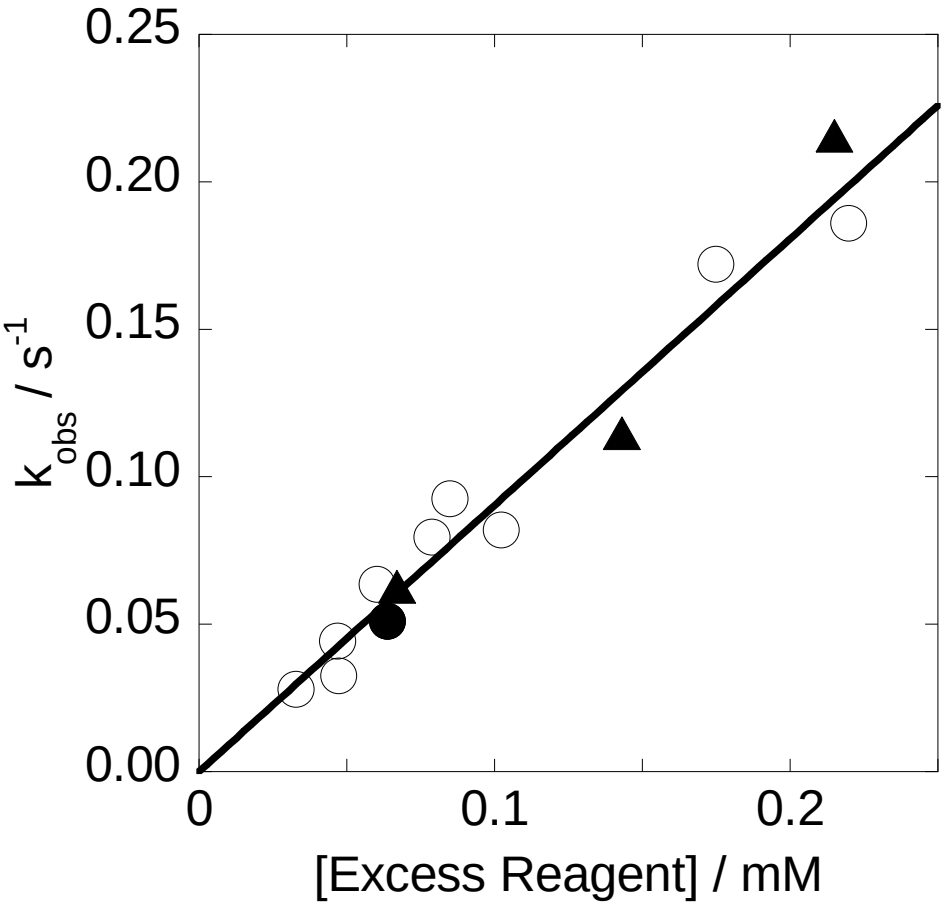

Figure S4. Plot of k_{obs} vs [Excess Reagent] for the reaction between $L^2(H_2O)Rh^{2+}$ and $(dmgH)_2(H_2O)CoCH_3$. •[$L^2(H_2O)Rh^{2+}$] in excess. ○[$(dmgH)_2(H_2O)CoCH_3$] in excess. ▲ [$(dmgH)_2(H_2O)CoCD_3$] in excess.

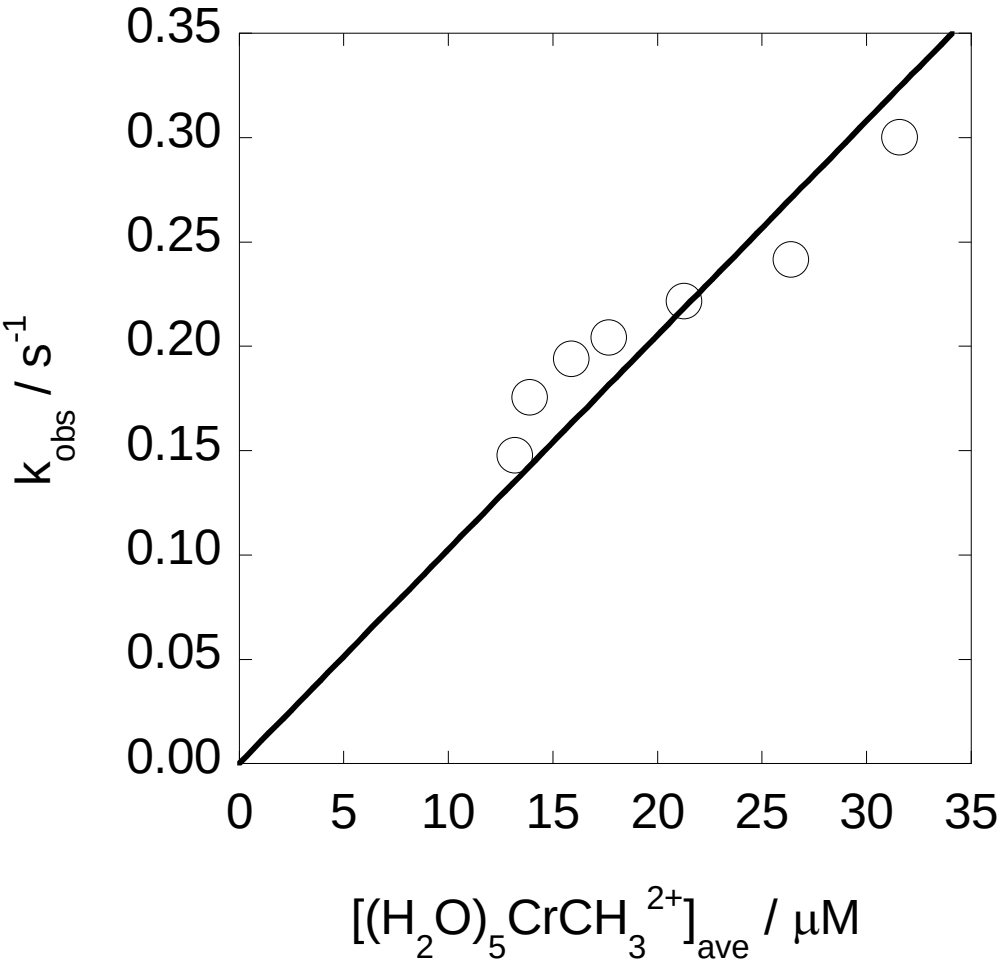

Figure S5. Plot of k_{obs} vs $[(H_2O)_5CrCH_3^{2+}]$ for the reaction between $L^2(H_2O)Rh^{2+}$ and $(H_2O)_5CrCH_3^{2+}$.

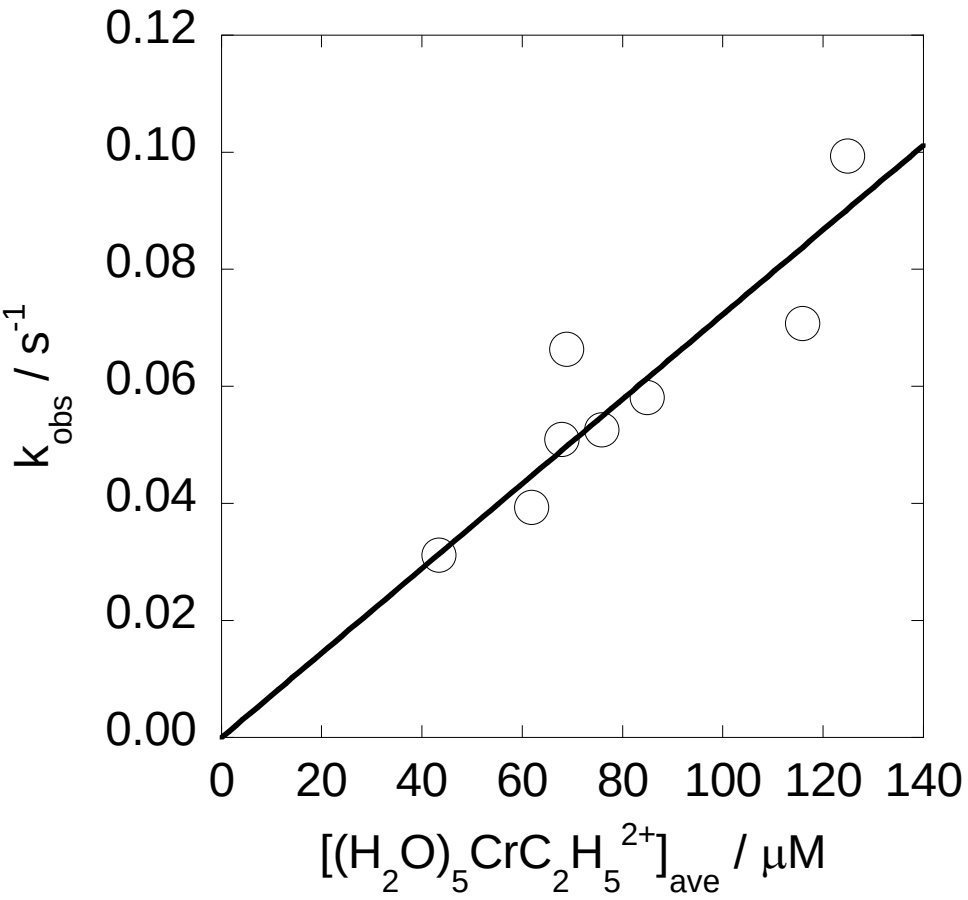

Figure S6. Plot of k_{obs} vs $[(H_2O)_5CrCH_2CH_3^{2+}]$ for the reaction between $L^1(H_2O)Rh^{2+}$ and $(H_2O)_5CrCH_2CH_3^{2+}$.

References

(1) Bakac, A.; Thomas, L. M. *Inorg. Chem.* 1996, *35*, 5880-5884.
(2) Schrauzer, G. N.; Windgassen, R. J. *J. Am. Chem. Soc.* 1966, *88*, 3738-3743.
(3) Hyde, M. R.; Espenson, J. H. *J. Am. Chem. Soc.* 1976, *98*, 4463-4469.
(4) Bakac, A.; Espenson, J. H. *J. Am. Chem. Soc.* 1984, *106*, 5197-5202.
(5) Dodd, D.; Johnson, M. D. *J. Organomet. Chem.* 1973, *52*, 1-232.
(6) Espenson, J. H.; Shveima, J. S. *J. Am. Chem. Soc.* 1973, *95*, 4468-4469.

APPENDIX C

TRANSITION METAL ION-ASSISTED PHOTOCHEMICAL GENERATION OF ALKYL HALIDES AND HYDROCARBONS FROM CARBOXYLIC ACIDS

Table of Contents

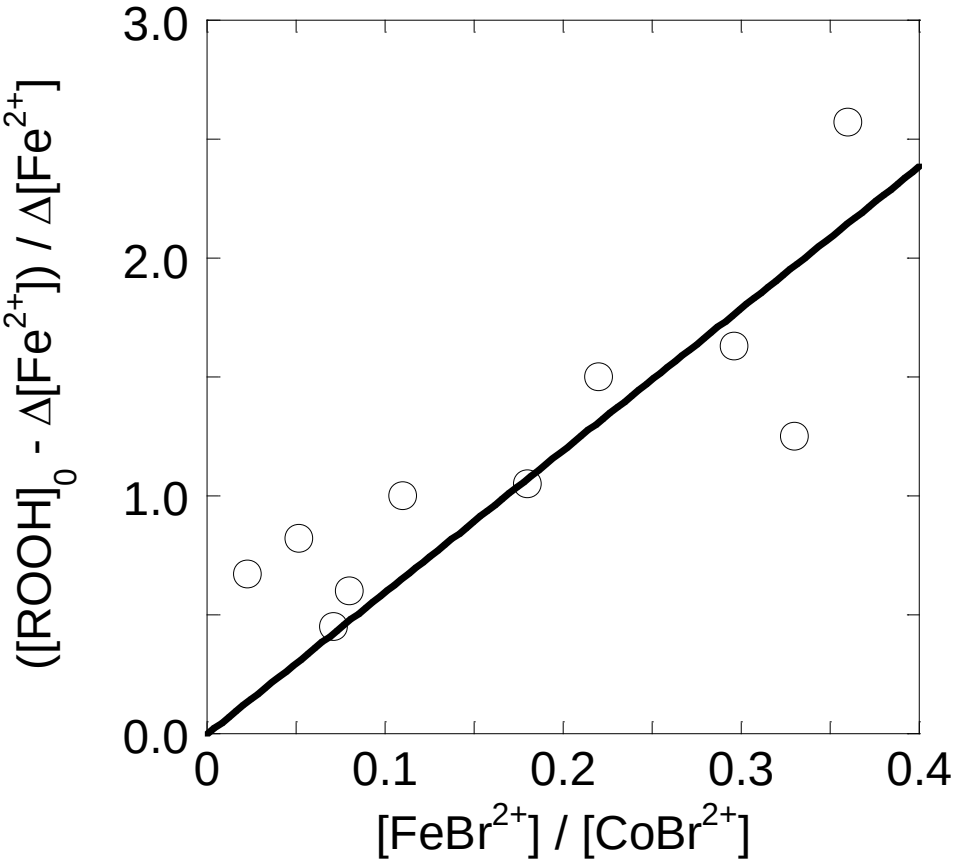

Figure S1. Plot of product ratios $[ROOH]_0$ - $\Delta[Fe^{2+}]$ / $\Delta[Fe^{2+}]$ vs. $[FeBr^{2+}]$ / $[(NH_3)_5CoBr^{2+}]$ according to eq 15. R = $(CH_3)_3C$. Concentrations: 0.57 – 0.62 mM Fe^{2+}, 0.47 – 0.50 mM $(CH_3)_3COOH$, 0.10 – 0.23 mM $FeBr^{2+}$, and 0.5 – 2.2 mM $(NH_3)_5CoBr^{2+}$. The plotted concentrations of $FeBr^{2+}$ and $(NH_3)_5CoBr^{2+}$ are the averages for each run.

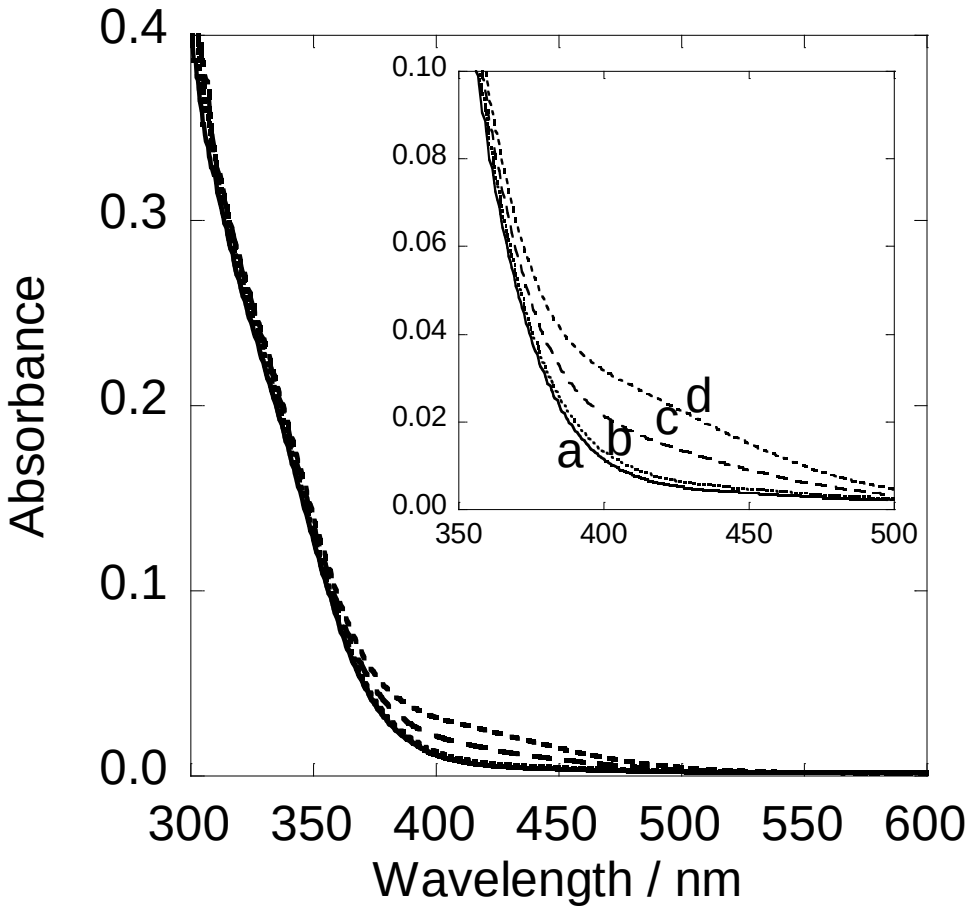

Figure S2. UV-vis absorption spectra (0.1 cm path length) of 7.1 mM Fe^{3+} + 55 mM propionic acid + 5 mM Br^- (a), + 10 mM Br^- (b), + 50 mM Br^- (c), 100 mM Br^- (d). pH = 1.85 at pH = 1.85 and μ = 0.2 M.

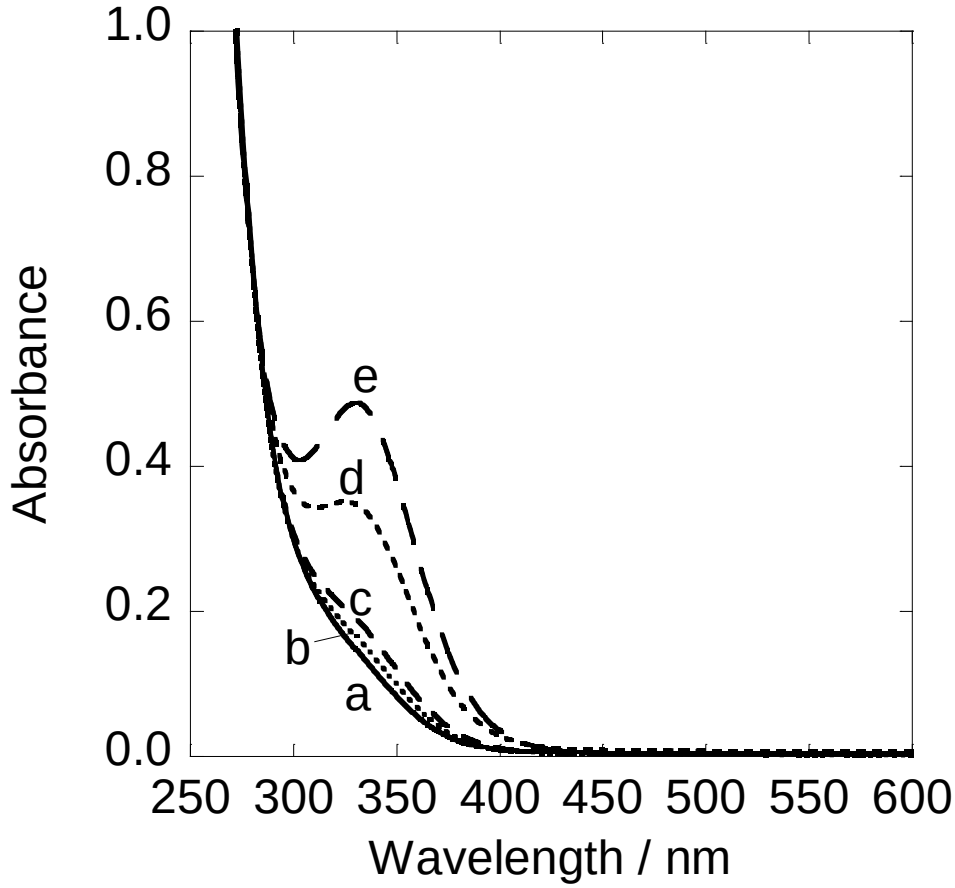

Figure S3. UV-vis absorption spectra (0.1 cm path length) of 7.1 mM Fe^{3+} + 55 mM propionic acid (a), + 5 mM Cl^- (b), + 10 mM Cl^- (c), + 50 mM Cl^- (d), and 100 mM Cl^- (e) at pH = 1.85 and μ = 0.2 M.

APPENDIX D

Supplementary Information for

Generation of Free Oxygen Atoms O(^{3}P) in Solution *via* Photolysis of 4-Benzoylpyridine N-oxide: Mechanistic Insight from Time Resolved Photolysis

Table of Contents

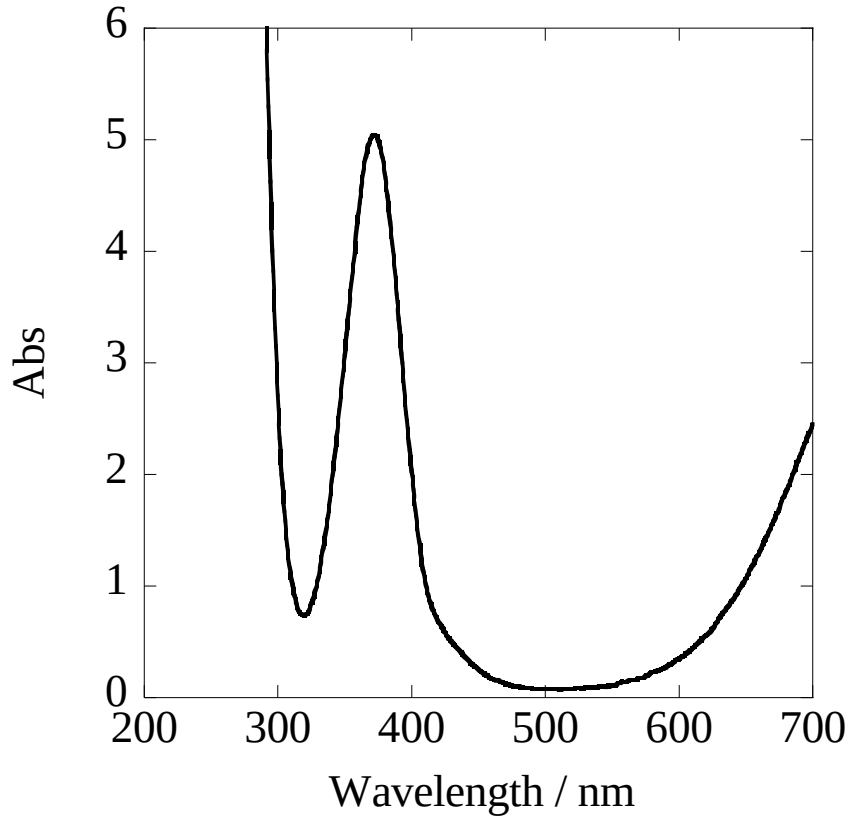

Figure S1. Composite UV-vis spectrum of 1 mM K_2CrO_4 inner filter bath + 0.33 M $CuSO_4$ outer filter bath. Spectra collected in 1 cm cells and added in KaleidaGraph

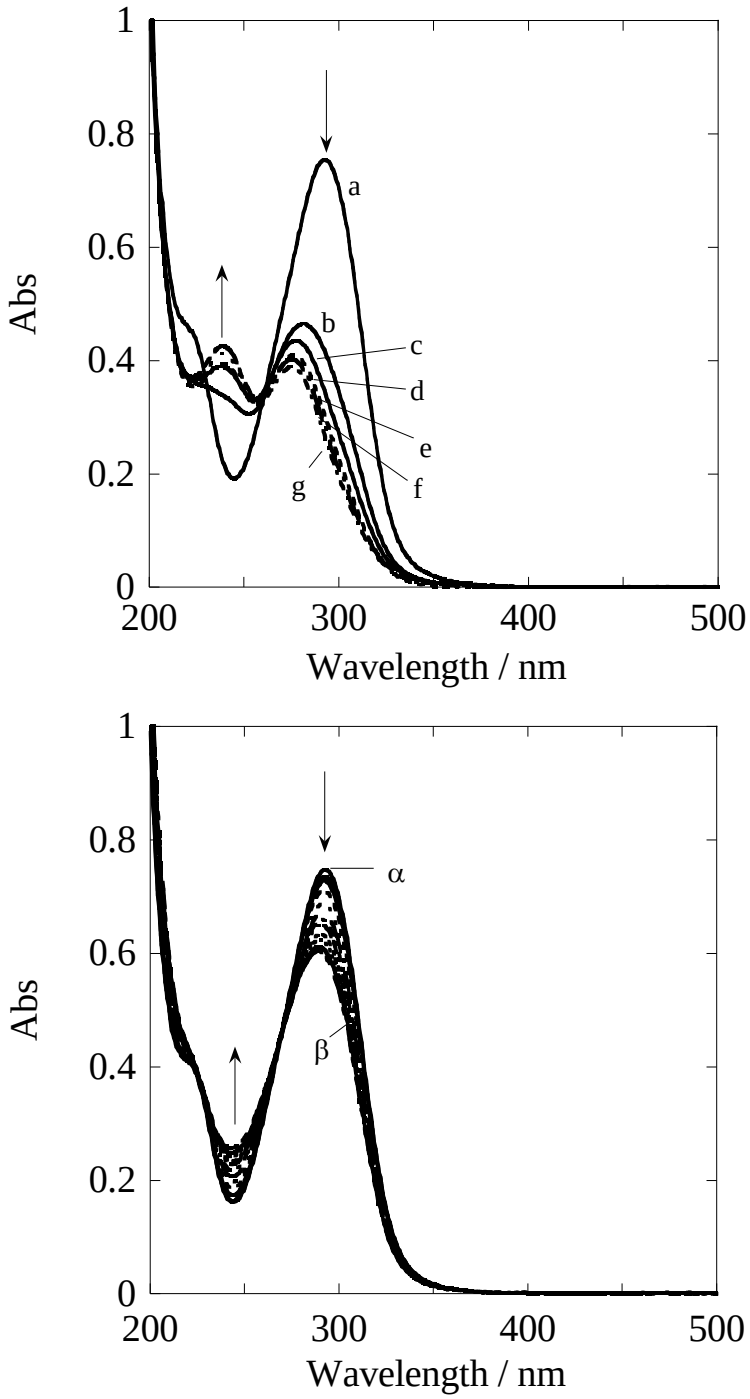

Figure S2. UV-vis spectra of 38 μM BPyO in water at 0 M (a), 0.98 M (b), 1.95 M (c), 2.93 M (d), 3.90 M (e), 4.88 M (f), and 5.85 M (g) $HClO_4$ at 6 M ionic strength (top); and 0 M (α), 9.7 mM, 0.098 M, 0.20 M, 0.29 M, 0.39 M, 0.49 M, 0.59 M, 0.69 M, 0.78 M, 0.88 M, 0.98 M (β) at 1 M ionic strength (bottom) *for clarity only 0 M and 0.98 M are denoted in the figure*

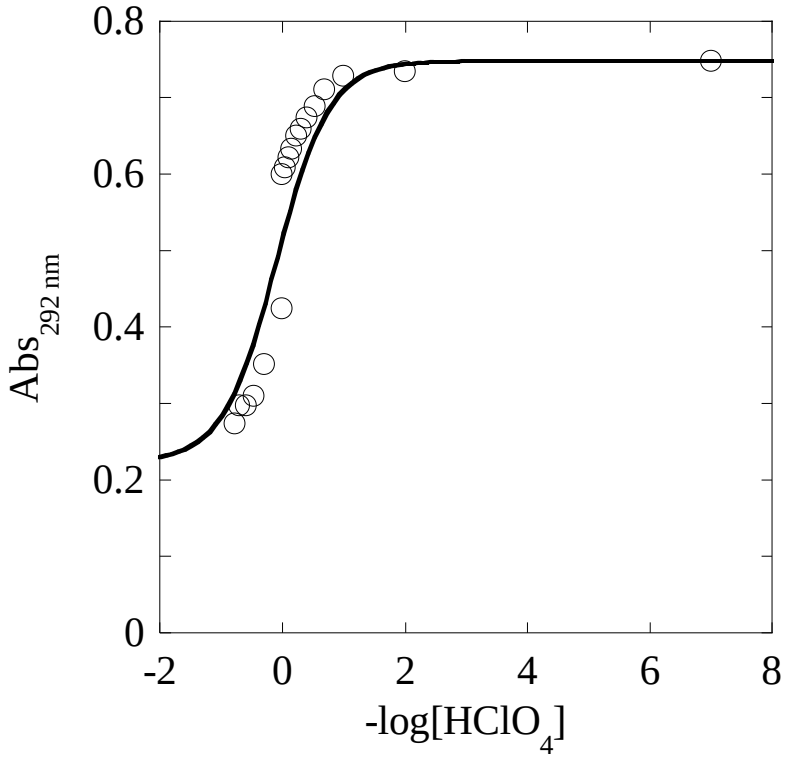

Figure S3. Plot of $Abs_{292\ nm}$ vs $-\log([HClO_4])$. Plots are fit to equation S6. $[BPyO]_{tot}$ = 38 μM, $\varepsilon_{292nm}^{BPyO}$ = 19,700 M^{-1} cm^{-1},[1] $\varepsilon_{292nm}^{BPyOH^+}$ = 5,900 M^{-1} cm^{-1} (from UV-vis spectrum at 5.85 M $HClO_4$, Figure S2). The fit yields $K_a = 1.2 \pm 0.2$

Derivation of equation fit to absorbance as a function of $HClO_4$ concentration for the determination of the K_a of $BPyOH^+$ in water.

$$[BPyO]_{tot} = [BPyO] + [BPyOH^+] \quad \& \quad K_a = [BPyO]\,[H^+] / [BPyOH^+] \qquad (S1)$$

$$Abs_{292\ nm} = Abs_{292nm}^{BPyO} + Abs_{292nm}^{BPyOH^+} = [BPyO]\,\varepsilon_{292nm}^{BPyO} + [BPyOH^+]\,\varepsilon_{292nm}^{BPyOH^+} \qquad (S2)$$

$$Abs_{292\ nm} = [BPyO]\,\varepsilon_{292nm}^{BPyO} + ([BPyO]_{tot} - [BPyO])\,\varepsilon_{292nm}^{BPyOH^+} \qquad (S3)$$

$$[BPyO]_{tot} = [BPyO] + ([BPyO]\,[H^+]) / K_a \Rightarrow [BPyO] = [BPyO]_{tot}(K_a / ([H^+] + K_a)) \qquad (S4)$$

$$Abs_{292\ nm} = [BPyO]_{tot}\,(K_a\,\varepsilon_{292nm}^{BPyO} + [H^+]\,\varepsilon_{292nm}^{BPyOH^+}) / (K_a + [H^+]) \qquad (S5)$$

$$Abs_{292\ nm} = [BPyO]_{tot}\,(K_a\,\varepsilon_{292nm}^{BPyO} + 10^{-\log[HClO_4]}\,\varepsilon_{292nm}^{BPyOH^+}) / (K_a + 10^{-\log[HClO_4]}) \qquad (S6)$$

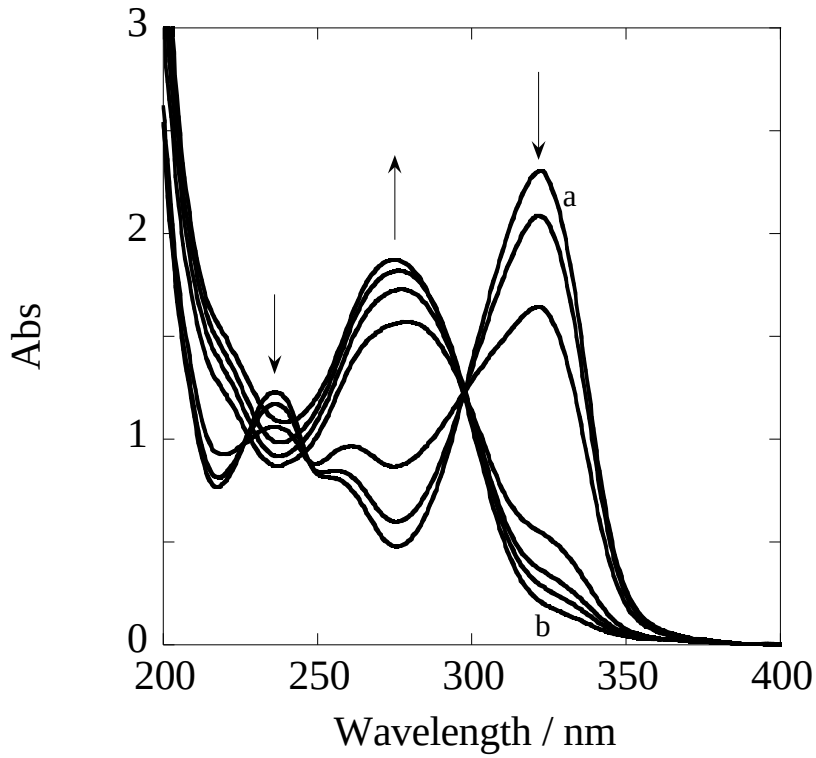

Figure S4. UV-vis spectra (1 mm path length) of 1.09 mM BPyO in AN in the presence of 0 mM (a), 0.94 mM, 3.75 mM, 30.1 mM, 53.7 mM, 74.8 mM, and 94.0 mM (b) CF_3CO_2H. The difference in spectrum (a) and (b) yielded $\Delta\varepsilon_{322\ nm}$ = 19,700 M^{-1} cm^{-1}.

Derivation of $BPyOH^+$ in AN as determined by UV-vis spectra of 1.7 mM BPyO in the presence of CF_3CO_2H.

$$BPyO + H^+ \rightleftharpoons BPyOH^+ \qquad 1/K_a^{BPyOH^+} \;\&\; CF_3CO_2H \rightleftharpoons CF_3CO_2^- + H^+ \quad K_a^{TFA} \quad (S7)$$

$$BPyO + CF_3CO_2H \rightleftharpoons BPyOH^+ + CF_3CO_2^- \quad K_a^{TFA} / K_a^{BPyOH^+} = K \quad (S8)$$

$$K = [BPyOH^+][CF_3CO_2^-] / ([BPyO][CF_3CO_2H]) \qquad (S9)$$

$$K_a^{BPyOH^+} = K_a^{TFA}[BPyO][CF_3CO_2H] / ([BPyOH^+][CF_3CO_2^-]) \qquad (S10)$$

The change in absorbance at 322 nm relative spectrum (a) was used to calculate $[BPyOH^+]$. The concentrations of the remaining species were determined as follows: (assuming CF_3CO_2H : BPyO = 1 : 1) $[BPyOH^+] = [CF_3CO_2^-] = [BPyO]_{total} - \Delta Abs_{322nm}^{BPyO} / \Delta\varepsilon_{322\ nm}$; $[BPyO] = [BPyO]_{total} - [BPyOH^+]$; and $[CF_3CO_2H] = [CF_3CO_2H]_{total} - [CF_3CO_2^-]$. The pK_a for CF_3CO_2H in MeCN in the literature is pK_a = 12.65 ± 1.38.[2]

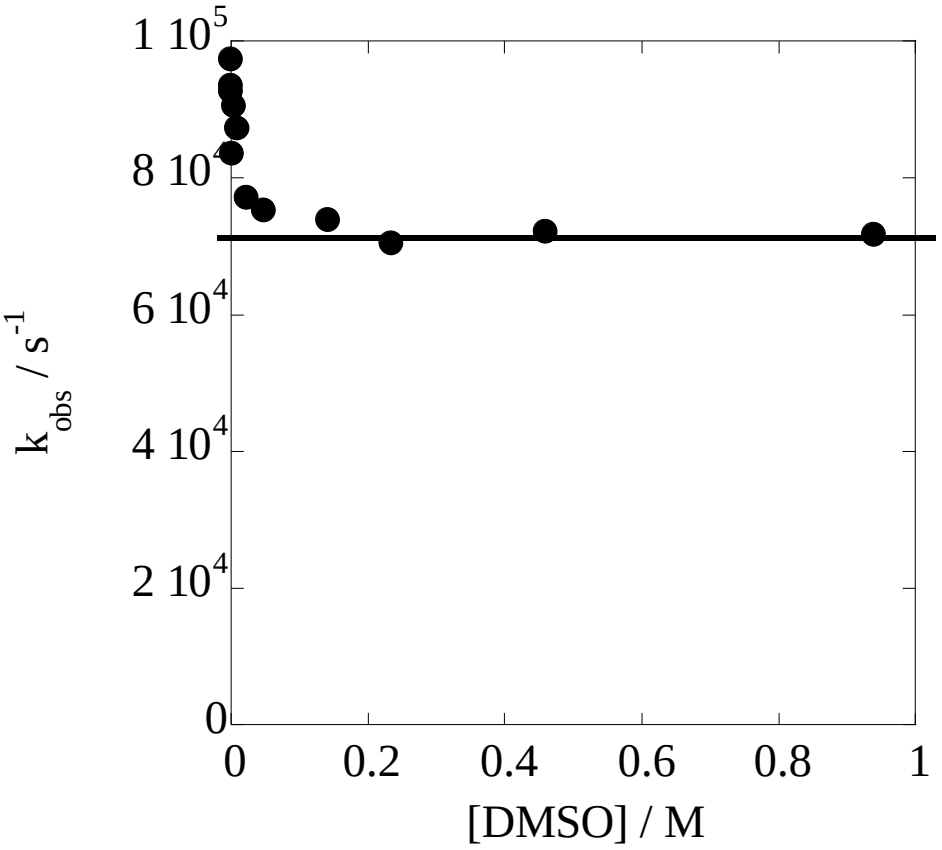

Figure S5. Plot k_{obs} vs [DMSO] upon LFP of 45 μM BPyO in degassed aqueous solutions

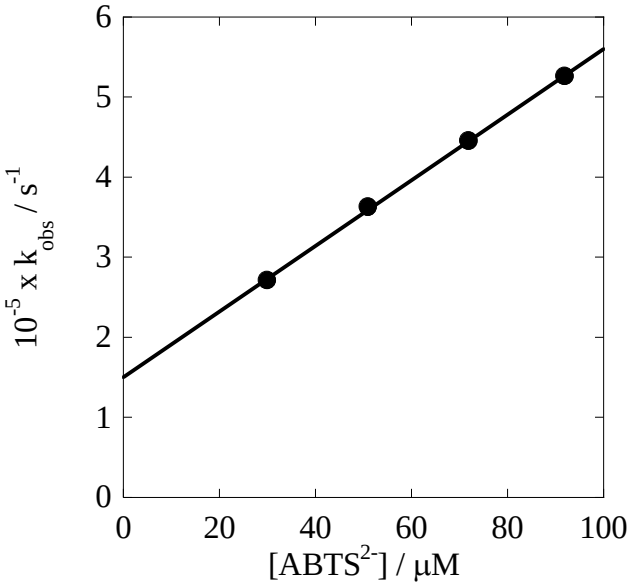

Figure S6. Plot k_{obs} vs [$ABTS^{2-}$] upon 308 nm LFP of degassed aqueous solutions containing 40 μM BPyO in the presence of 30 - 93 μM $ABTS^{2-}$. Kinetic traces monitored at 417 nm (where $ABTS^{\bullet-}$ ε = 34,700 M^{-1} cm^{-1}).

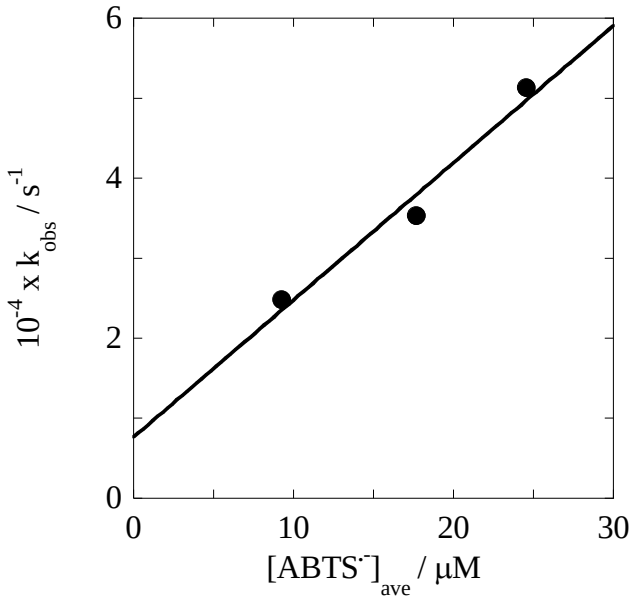

Figure S7. Plot k_{obs} vs $[ABTS^{\bullet-}]$ upon 308 nm LFP of degassed aqueous solutions containing 40 μM BPyO in the presence of 50 μM $ABTS^{2-}$ and 7 – 21 μM $ABTS^{\bullet-}$. Kinetic traces monitored at 417 nm (where $ABTS^{\bullet-}$ ε = 34,700 M^{-1} cm^{-1}).

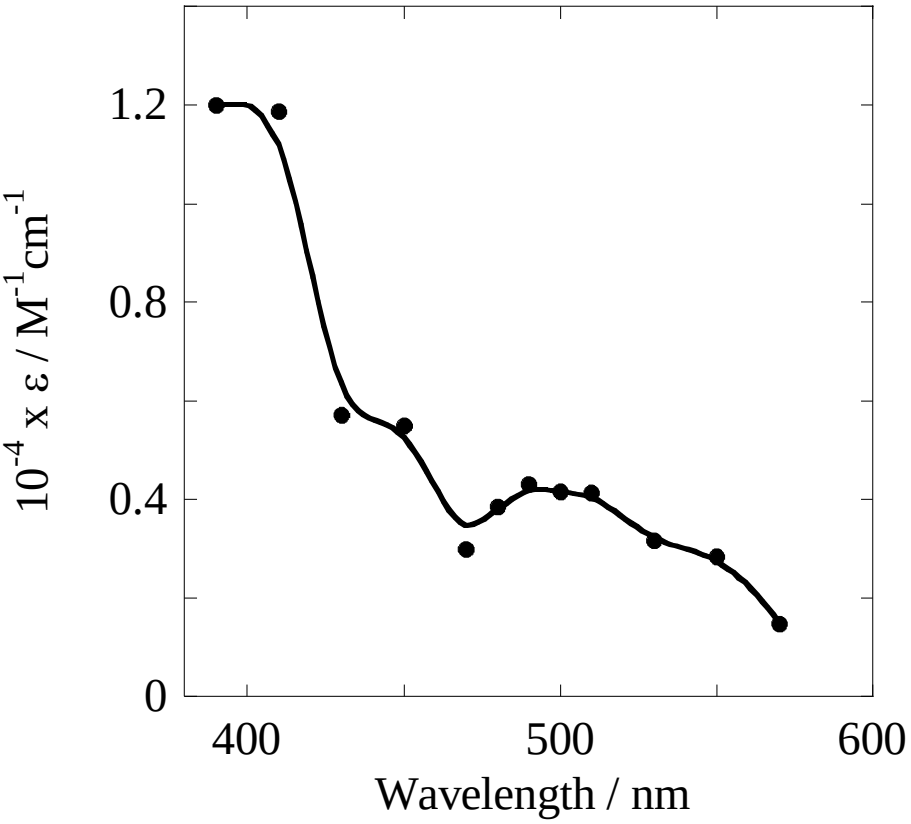

Figure S8. Transient absorption spectrum of ^{3}BPyO* in AN obtained from 308 nm LFP of degassed solutions

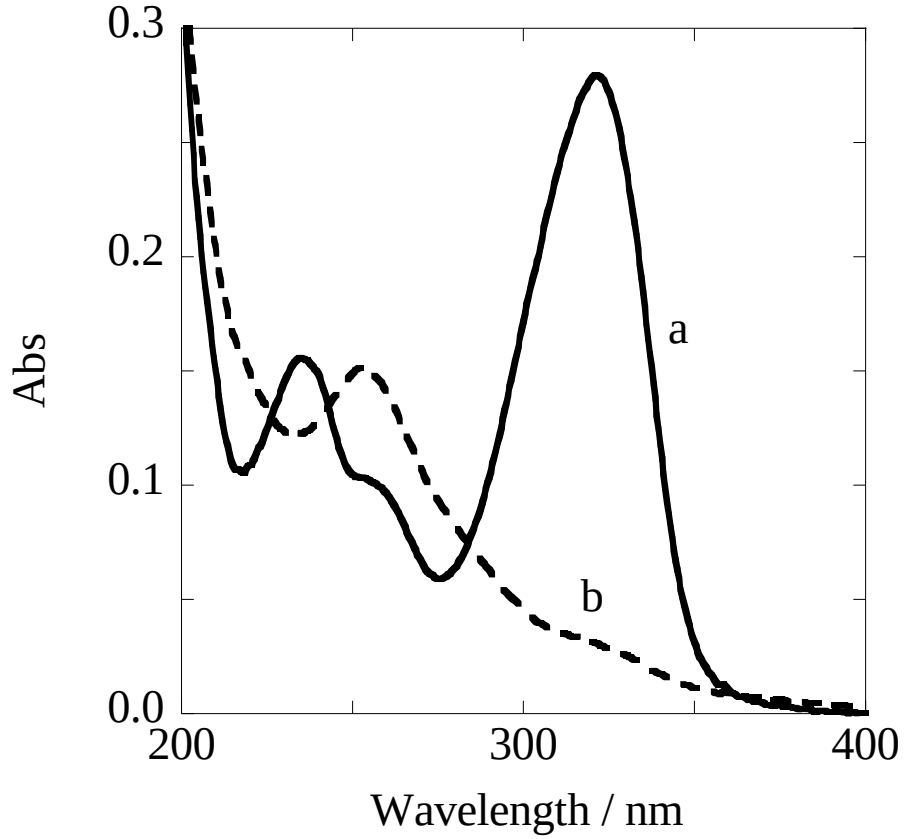

Figure S9. UV-vis spectra (1 mm cell) before (a) and after (b) irradiation (313 nm photoreactor) of 0.13 mM BPyO in an air-free acetonitrile solution

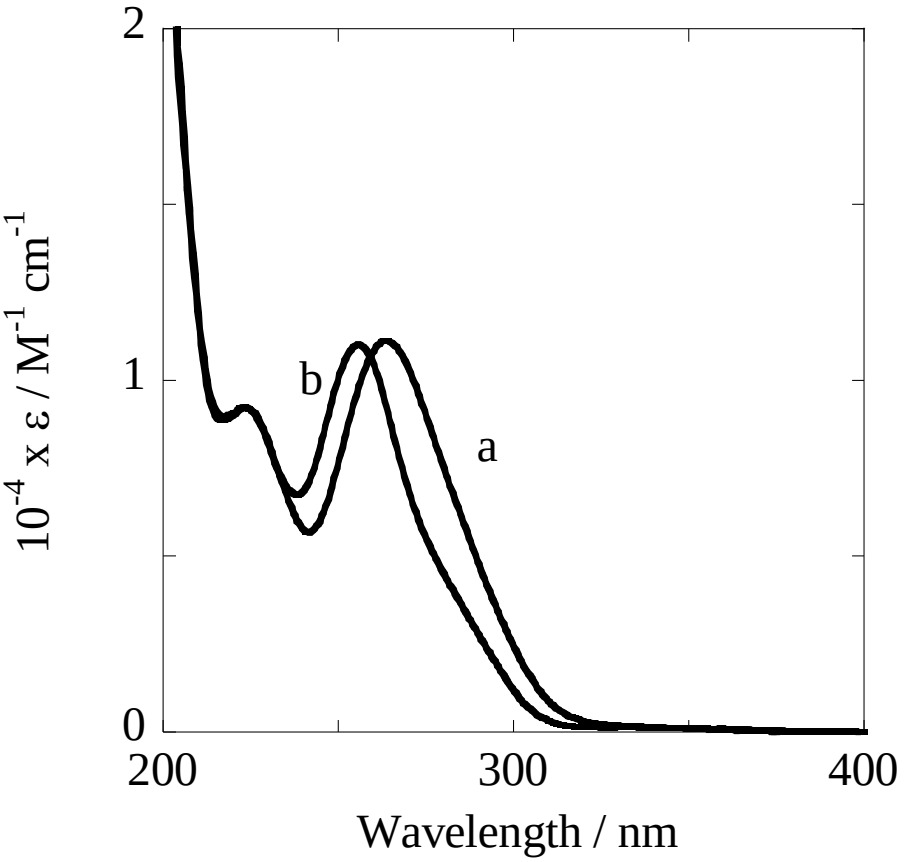

Figure S10. UV-vis spectra of BPy in water (a) and acetonitrile (b)

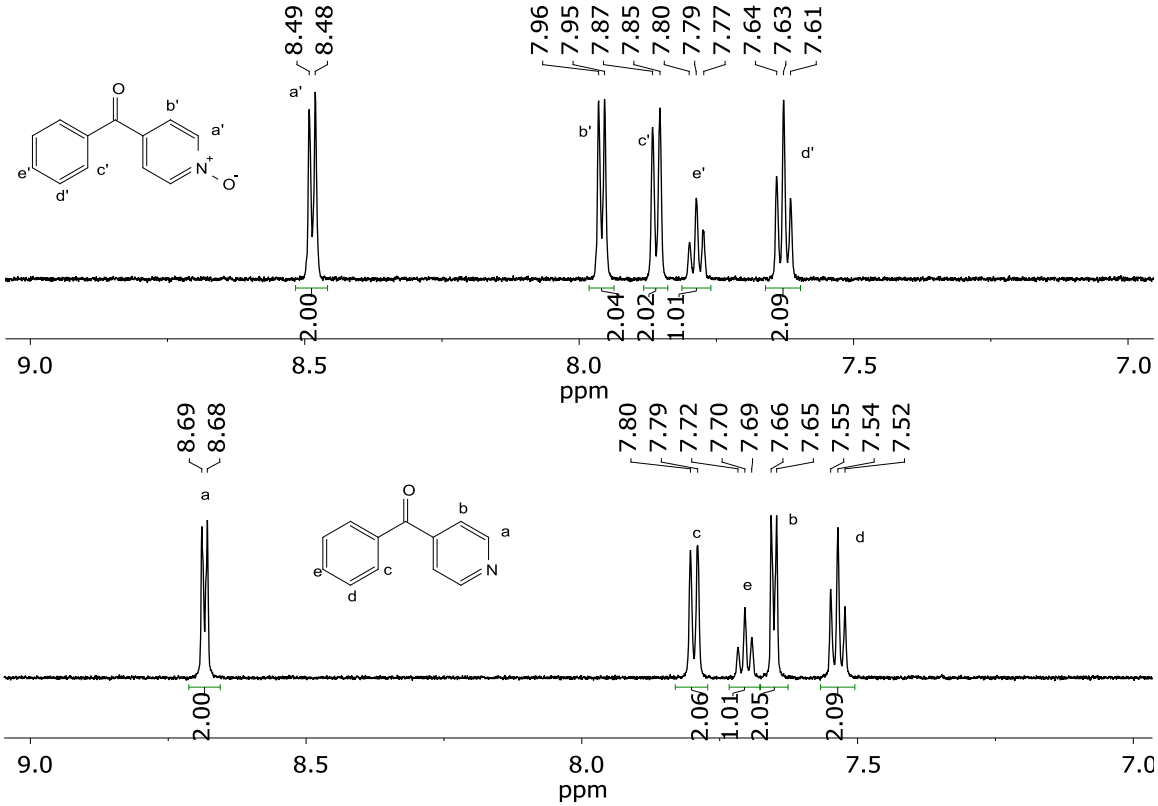

Figure S11. ^{1}H NMR (600 MHz) of BPyO (top) and BPy (bottom) in D_2O

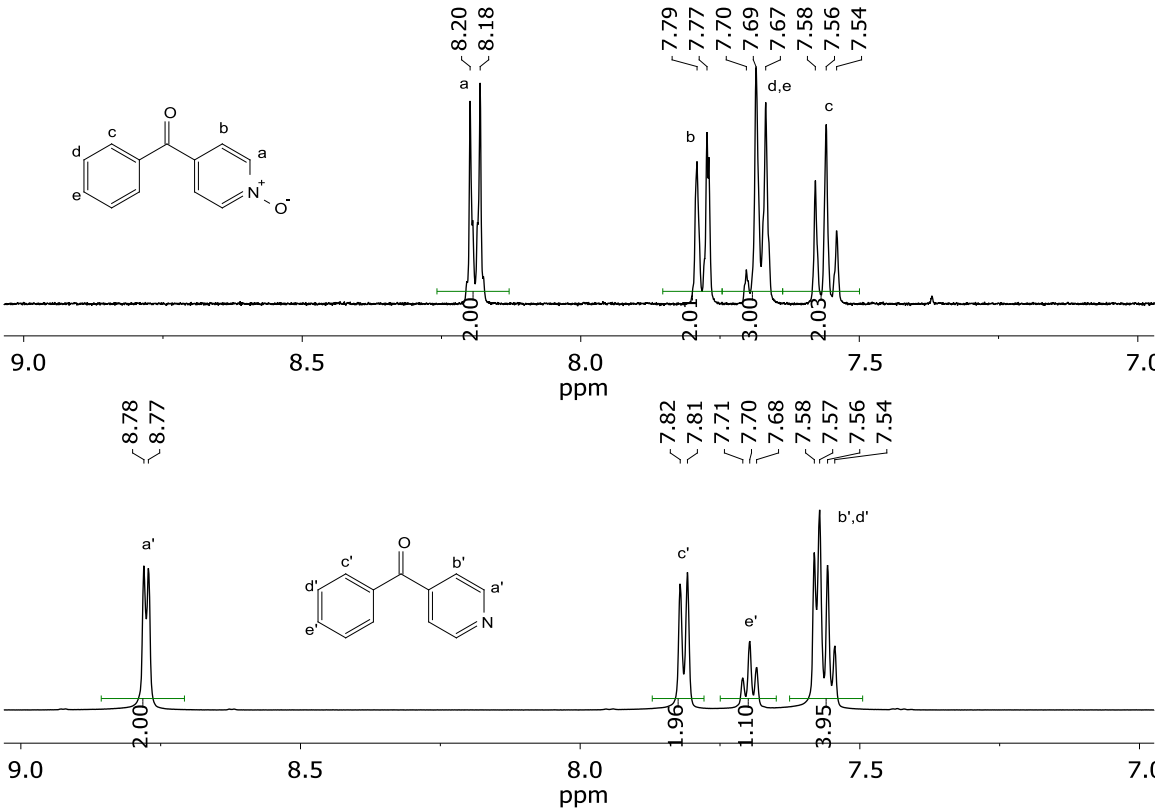

Figure S12. ^{1}H NMR (600 MHz) of BPyO (top) and BPy (bottom) in CD_3CN

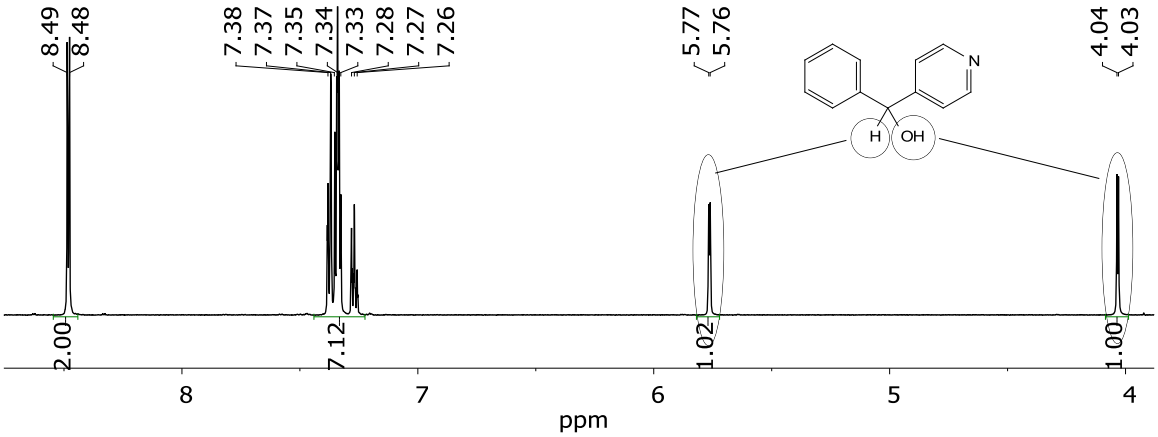

Figure S13. ^{1}H NMR (600 MHz) of B(OH)Py in CD_3CN. Sample prepared from BPy and $NaBH_4$[1]

References

(1) Cheng, M.; Bakac, A. *Dalton Transactions* **2007**, 2077.

(2) Eckert, F.; Leito, I.; Kaljurand, I.; Kütt, A.; Klamt, A.; Diedenhofen, M. *J. Comput. Chem.* **2009**, *30*, 799.